Synthesis of Thalidomide Analogues and Their Potential in Cancer Treatment

By

Sheng (Kelvin) Wang (1081655)

A Thesis

Submitted to the Faculty of Health and Environmental Sciences of

Auckland University of Technology in Fulfillment of the

Requirements for the Degree of

Doctor of Philosophy (Science)

Sept 2017

School of Science, Faculty of Health and Environmental Sciences

Primary Supervisor: A.Prof. Jun Lu

Secondary Supervisor: Prof. Jinghao Fei

Additional Supervisor: Dr. Jack Chen

Synthesis of Thalidomide Analogues and Their Potential in Cancer Treatment

Approved by:

Primary Supervisor: A.Prof. Jun Lu

Signature:_____

Secondary Supervisor: Prof. Jinghao Fei

Signature:_____

Additional Supervisor: Dr. Jack Chen

Signature:_____

Table of Contents

List of Figures

List of Tables

Attestation of Authorship

I hereby declare that this submission is my own work and that, to the best of my knowledge and belief, it contains no materials previously published or written by another person (except where explicitly mentioned in the acknowledgements), no material has been submitted for the award of any other degree or diploma of a university or other institution of higher learning.

Name:_____

Signature:_____

Date: _____

Acknowledgements

After graduated from Bachelor degree of Biomedical Science at Victoria University of Wellington in 2008, I found that I really love to study Organic Chemistry. For my postgraduate work, I preferred to be involved in a research project based on Organic Synthesis. In 2013, after 5 years, my dream came true!

In my PhD study, I am extremely thankful to my primary supervisor A.Prof. Jun Lu for giving me the opportunity to work on this incredibly interesting project highly based on work of organic synthesis. Also, A.Prof Jun Lu is knowledgeable about anti-cancer research. In the course of my work, he has guided me patiently, and given me a lot of good advice, so that I could avoid many detours in my research. He gave me careful and valuable guidance for the data analysis and thesis writing. Not only he helped me in academic area, but he also tried his best to find potential job opportunities for me to give me strong financial support during my study period.

I also need to express my special thanks to my two mentor supervisors Prof. Allan Blackman & Dr. Jack Chen about technical support in organic synthesis study and research chemistry laboratory management. I will never forget the serious problems that happened in 2013 and 2016, and your technical guidance allowed me to progress my project smoothly.

In addition, I would like to thank my additional supervisor Prof. Jinghao Fei & Prof. Ahmed Al-Jumaily for their financial support. Their support and patience to me had given me strength to complete my PhD study.

Special thanks should be given to all my technical advisors in AUT to provide professional assistant during my PhD study. I am particularly grateful to Dr. Yan Li, Dr. Michael Steiner, A.Prof. Dongxu Liu for their professional help on cell culture experiment or instrument work. I also appreciate Laboratory Manager Dr. Sonya Popoff, Ms Yan Wang and Ms. Meie Zou about preparation of laboratory equipment. This strongly contributed to the best experiments result of my research.

I am truly grateful to all research staffs in our team including Loretta White, Jenifer Wu, Cindy Yang, Tinu Odeleye, Reza Nemati, Helen Mok, Teng Ma, Piyush Bugde, Riya Biswas, Yutao Chen and Kally Shi.

Finally, I'd like to thank my parents, Yamin Wang and Rongxin Wang, for their ultimate support and encouragement during my study. I need to thank for my wife, Wei Li, for her contribution to my life and her understanding of my work. My daughter, Zimeng Gloria Wang, although she is too young to know this: Papa, write thesis… Yes! This thesis is for you!

Intellectual Property Rights

Thalidomide & thalidomide analogues have been studied in this research study. Two novel analogue structures have been developed from research study, and have been confirmed by Scifinder Scholar search.

The main sponsors contributed to this Intellectual Properties include Sheng (Kelvin) Wang, A.Prof. Jun Lu, Dr. Jack Chen, but also there is special thanks for contribution of Intellectual Properties including Ahmed Al-Jumaily, Allan Blackman & Jinghao Fei.

Ethics Approval

In this study, health human blood samples were used to determine biological activity for synthetic compounds. The special thanks should be given to NZ Blood Service to provide the human blood samples which contributes to my study. In addition, I need to express the special thanks to Health and Disability Ethics Committees to approval my study.

Abbreviations

ATP: Adenosine-5’-triphosphate

AUT: Auckland University of Technology

Carbon dioxide: CO_2

CDK: Cyclin E-cyclin dependent kinase

EAC: Ehrlich ascites carcinoma

ECM: Extracellular matrix

ENL: Erythema nodosum leprosum

FBS: Fetal bovine serum

FDA: Food and Drug Administration

FGF: fibroblast growth factor

HeLa: Human cervical carcinoma

HIV: Human immunodeficiency virus

HUVECs: Human umbilical vein endothelial cells

HRMS: High resolution mass spectra

hPBMC: human peripheral blood mononuclear cells

HT-29: Human colon carcinoma

IC_{50}: the concentration (μM) of the experimental compounds generating a 50% inhibition in cell growth

ICAM-1: Intercellular cell adhesion molecule-1

IL-6: Interleukin-6

IFN-γ: Interferon-gamma

IMiDs: Thalidomide analogues

Ip: Intra-peritoneal

IR: Inhibition rate

Log: Logarithm

LPS: Lipopolysaccharide

LRMS: Low resolution mass spectra

LSGS: Low serum growth supplement

mg/mL: milligram/milliliter

MM: Multiple myeloma

mM: millimoles per litre

MMPs: Matrix metalloproteinases

MTD: Maximum tolerated dose

MTT: [3-(4, 5-dimethylthiazol-2-yl)-2, 5-diphenyl tetrazolium bromide]

ROS: Reactive oxygen species

PBMCs: Peripheral blood mononuclear cells

PBS: Phosphate buffer saline

PC-3: Human prostate carcinoma

pRb: Retinoblastoma protein

rHuPF-4: Recombinant human PF-4

R_f value: Retardation factor

TCR: T-cell receptor

THP1 cells: TNF-α in promonocytic cell line

TGF-β: Transforming growth factor-β

TLC: Thin-layer chromatography

TNF-α: Tumour necrosis factor-α

µM: micromoles per litre

UV: Ultraviolet

VCAM-1: Vascular cell adhesion molecule-1

VEGF: Vascular endothelial growth factor

VIS: Visible

Abstract

Thalidomide has been used as an effective treatment for multiple myeloma. It is suggested that thalidomide exert its effects via immunomodulation and anti-angiogenesis. Many thalidomide analogues have been developed in order to reduce its adverse effect of teratogenicity and to improve its efficacy or potency.

In this study, I have synthesised two novel thalidomide analogues 3-[(1*R*)-1-hydroxy-1-methyl-3-oxo-1,3-dihydro-2*H*-isoindol-2-yl]piperidine-2,6-dione (compound **3**) and 3-[(1*S*)-1-hydroxy-1-methyl-3-oxo-1,3-dihydro-2*H*-isoindol-2-yl]piperidine-2,6-dione (compound **4**), along with two other phthalimides 2-(2,6-dioxopiperidin-3-yl)-phthalimidine (EM-12) (compound **2**) and 2-(1-Chloromethyl-2,6-dioxopiperidin-3-yl)phthalimidine (compound **5**). The novelty has been confirmed by Scifinder Scholar search. The biological activities of the novel compounds have been tested and compared with thalidomide.

Compounds **3**, **4** and **5** significantly increased TNF-α inhibition rate in lipopolysaccharide-induced human white blood cells compared with thalidomide. Compound **2** showed similar TNF-α inhibition rate as thalidomide. For anti-angiogenic effects, all analogues except compound **5** exhibited inhibition in a dose-dependent manner. Compound **3** and **4** generated significantly higher inhibitory effect compared with thalidomide.

For anti-proliferative effects, compound **2**, **3** and **4** showed no statistical difference compared with thalidomide treatment. Compound **5** showed significant tumour cell growth inhibition with arresting cell cycle in S and G2-M phase, as analysed by flow cytometer.

In conclusion, two novel thalidomide analogues compound 3 and 4 have been successfully synthesised and they possess significantly higher biological activities as compared with the parent compound thalidomide. It is possible to add other chemical groups to those four synthesised compounds to obtain more analogues which may possess better biological activities.

Chapter I: Overall Introduction

1.1 Overview

Thalidomide was synthesized for the first time in the 1950s by a German pharmaceutical company and marketed as a sedative. At that time, a lot of pregnant women tried to use thalidomide as a morning sickness drug to relieve their nausea. However, thalidomide was discovered to have a serious adverse effect which is teratogenic toxicity. It was reported that thalidomide is highly teratogenic, and results in severe malformations in the children of women who took the drug during pregnancy. Consequently, thalidomide was immediately withdrawn from the market in 1961 (McBride; Ward, 1962). Later on, interest in thalidomide has been renewed because it appeared to be promising for the treatment of leprosy. In 1998, the FDA of the United States approved thalidomide in the treatment of erythema nodosum leproum (ENL) (Moreira *et al.*, 1993; Sampaio *et al.*, 1991). It was determined that capability to decrease lipopolysaccharide (LPS)-induced tumour necrosis factor-alpha (TNF-α) production is the most notable effect to thalidomide, so that the clinical efficacy of thalidomide in inflammatory and autoimmune disease has been partly attributed to its ability to inhibit TNF-α. TNF-α is a core cytokine produced by immune cells in the blood stream, and acts as a pro-angiogenic factor. Thalidomide inhibits TNF-α by stimulating the degradation of messenger RNA (mRNA) that are involved in immune responses, the stimulation of inflammation, and the suppression of certain cytokines. In order to increase the efficacy of treatment in the clinic and to minimize side effects, a great deal of interests has arisen to analyze and determine the structural relationship between thalidomide and its biological activities.

Over three decades ago, Folkman introduced the notion that solid tumours cannot grow beyond 2-3 mm^3 without the formation of new blood vessels (Domenico, 2009). Inhibition of angiogenesis has thereafter been perceived as a promising strategy for cancer treatment. D'Amato and co-workers demonstrated that thalidomide inhibits basic fibroblast growth factor (FGF)-induced angiogenesis in the rabbit cornea and tumour growth in rabbits. Subsequently, the anti-tumour activity of thalidomide was evaluated in numerous clinical trials. Partial response, stable disease, or tumour regression have been reported in patients

with multiple myeloma (González-Barca et al., 2016; Rajkumar et al., 2000), AIDS-related Kaposi's sarcoma (Fife *et al.*, 1998), high-grade gliomas (Fine et al., 2000), hepatocellular carcinoma (Lin et al., 2005), renal cell carcinoma (Eisen et al., 2000) and advanced melanoma (Stebbing et al., 2001).

Angiogenesis is a critical regulator of tumour growth and metastasis (Folkman, 1995). Tumour angiogenesis, the development of new blood vessels by the tumour, is regulated by the production of angiogenic stimulators including vascular endothelial growth factor (VEGF). Because VEGF is a key regulatory factor in the prognosis of various cancers, inhibition of VEGF production is a promising therapeutic approach for treating cancer. Breast cancer is a life threatening disease that is geographically the second highest in New Zealand, about 70% of women who are diagnosed with breast cancer and about 80% of women who die from it are 50 years or older (Seneviratne *et al.*, 2016). Commonly, surgery is the first line of treatment for primary breast cancer, and current treatment for metastatic breast cancer includes chemotherapy or radiotherapy used in an adjuvant setting combination with anti-angiogenic drugs such as thalidomide in the treatment (Ali *et al.*, 2011).

In this study, therefore, thalidomide and a number of structural analogues will be synthesized including novel structural analogues. These compounds are then tested in a number of biological assays and their activities assessed. All details will be described in the following section.

1.2 Main Aims of Study

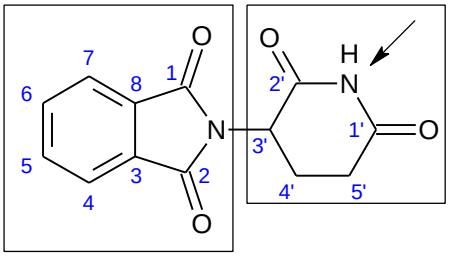

Phthalimide Ring Glutarimide Ring

Figure 1: Structure of thalidomide with structures of two rings; "arrow" indicates imide position of glutarimide ring

Literature about the structural activity relationship of thalidomide analogues suggest that substitution on the phthalimide ring (Figure 1) preserves or even increases the biological activity of the parent compound. Also, it has been reported that analogues of thalidomide with imide *N*-substitution on the glutarimide ring (Figure 1) still retains or improves the parent compound's biological activities such as TNF-α modulation activity. Based on these considerations, the parent compound of thalidomide and its structural analogues will be synthesized, and the biological activities of all of these compounds will be determined and compared.

Angiogenesis contributes to the development of new blood vessels for tumour growth and metastasis, and this process is highly regulated by the production of angiogenic stimulators such as vascular endothelial growth factor (VEGF). In addition, the relationship between TNF-α and VEGF has been proposed and stated that TNF-α can directly activate endothelial cells' migratory pathways through transactivation between the endothelial/epithelial tyrosine kinase Etk and VEGF receptor 2. TNF-α promotes angiogenesis through its ability to synergize VEGF-induced vessel permeability, and TNF-α is also capable of inducing gene expression of proangiogenic molecules such as VEGF and its receptors. In this case, thalidomide or its structural analogues inhibit TNF-α by stimulating the degradation of messenger RNAs (mRNAs) that are involved in the immune response, the stimulation of inflammation, and the suppression of certain cytokines.

Therefore, the first hypothesis of this study becomes: TNF-α modulation activity from thalidomide analogues with substitution on the phthalimide ring or imide *N*-substitution is

not negatively changed compared to the molecular function of the parent compound thalidomide.

The second hypothesis: *in vitro* anti-angiogenic activity of thalidomide analogues with substitution on the phthalimide ring or imide *N*-substitution has no negative change when compared with thalidomide.

In addition to the above, metastatic breast cancer cells were also investigated. The cytotoxic effect of synthesised analogues against cancer cells was determined and compared with the parent compound thalidomide. Also, the basic mechanism of action of the cytotoxic effect in this study was also determined and compared between thalidomide and its structural analogues.

1.3 Design of study

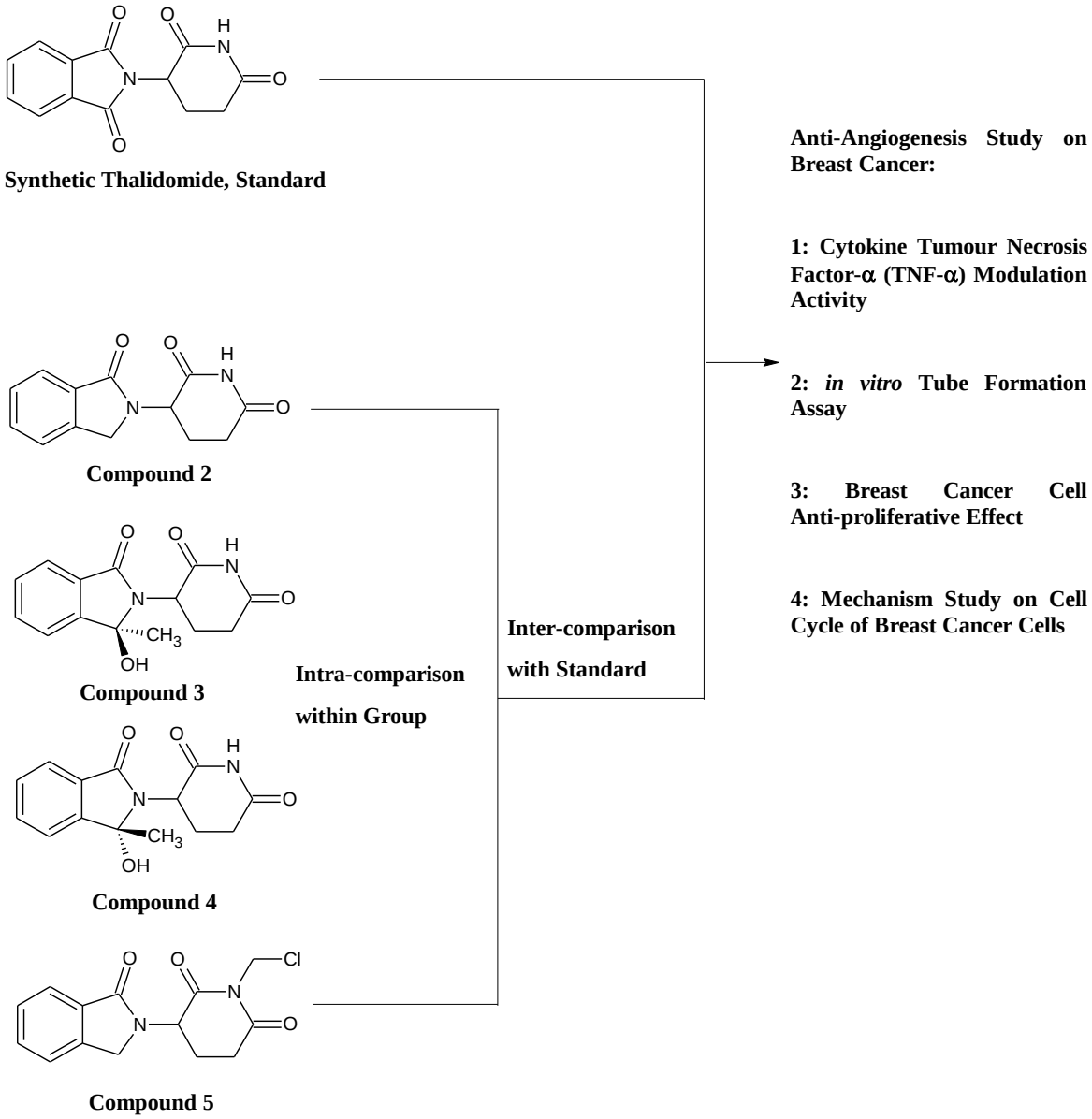

Figure 2: Overall design of study. All compounds (compound **1**: thalidomide as standard; thalidomide analogues: compound **2**, compound **3**, compound **4** & compound **5**). After their synthesis, thalidomide and all analogues were place in anti-angiogenesis studies including 1: TNF-α modulation activity; 2: *in vitro* tube formation sssay; 3, breast cancer cell anti-proliferative effect; & 4, mechanism of cell cycle study. In all studies, all outcomes from *in vitro* anti-angiogenesis breast cancer study compared between thalidomide and all analogues as inter-comparison. Intra-comparison was achieved through outcomes of *in vitro* anti-angiogenesis breast cancer studies from all analogues.

The overall aim of the study (Figure 2) is to compare the efficacy of thalidomide as the standard and its synthetic analoguesin variety of *in vitro* assays. There are two main parts of this thesis, including Chapter 2: organic synthesis for structural development, and Chapter 3: *in vitro* anti-cancer studies on breast cancer. In Chapter 2, the organic synthesis work is described, including two novel compounds that have not been reported before. All synthetic compounds including thalidomide (compound **1**) as the standard and other structural analogues are described. The structural analogues include 2-(2,6-dioxopiperidin-3-yl)-phthalimidine (EM-12) (compound **2**), the isomers 3-[(1*R*)-1-hydroxy-1-methyl-3-oxo-1,3-dihydro-2*H*-isoindol-2-yl]piperidine-2,6-dione (compound **3**) & 3-[(1*S*)-1-hydroxy-1-methyl-3-oxo-1,3-dihydro-2*H*-isoindol-2-yl]piperidine-2,6-dione (compound **4**), and 2-(1-chloromethyl-2,6-dioxopiperidin-3-yl)phthalimidine (compound **5**). Chapter 3 is *in vitro* breast cancer cell treatment with thalidomide and its analogues. In this chapter, a tube formation assay was performed, which describes the ability of endothelial cells to preserve the capability to divide and rapidly migrate in response to certain angiogenic signals. After treatment with thalidomide or its analogues, the amount of tube formations and tube areas contribute to determine the angiogenesis activity in the *in vitro* study. The number of tube formations and their area *vs*. the whole area were the end points for this assay to compare values between thalidomide and all other analogues. TNF-α modulation activity was also determined. In fact, modulation activity of TNF-α is a notable and important biomarker and was applied to determine whether structural modification or imide *N*-substitution with a chain compared to the parent compound of thalidomide would negatively affected the activity. In this study, blood samples from nine healthy volunteers were used in an ELISA assays of TNF-α modulation activity. This data can statistically contribute to determine the efficacy comparison between thalidomide and its analogues. In addition, the cancer cell MDA-MB-231 (a typical type of breast cancer cell) was used to determine and compare the anti-proliferative effects after treatment of thalidomide or its analogues. Also, the mechanism of action was investigated by determining of which phase in the cell cycle was affected by treatment of thalidomide and its analogues.

1.1 Significance of Study

Due to thalidomide's teratogenicity, many thalidomide analogues have been developed to either avoid teratogenicity or increase pharmacological efficacy. This study developed novel thalidomide analogues. Notably, a hydroxide group has been added on the structure, and it has the potential to increase its pharmacological effect. The biological efficacy of new compounds have been compared with the parent compound. If similar effects or a higher effect can be observed, then those novel thalidomide analogues will have the potential to be developed into new anti-cancer treatment and to be patented.

Chapter II: Organic synthesis of thalidomide and its analogues

2.1 Literature review about thalidomide and its analogues

2.1.1 Thalidomide and its history in cancer treatment

Thalidomide (*N*-α-phthalimido-glutarimide), has the chemical formula $C_{13}H_{10}N_2O_4$, with a molecular weight of 258.23 g/mol, and its synthetic name is (±)-2-(2,6-dioxopiperidin-3-yl)-1*H*-isoindole-1,3(2*H*)-dione. Its structure contains a phthalimide ring and a glutarimide ring. Thalidomide is usually formed as a racemic mixture of dextrorotatory (*R*) and levorotatory (*S*) enantiomers (Figure 3) with ratio of 1:1.

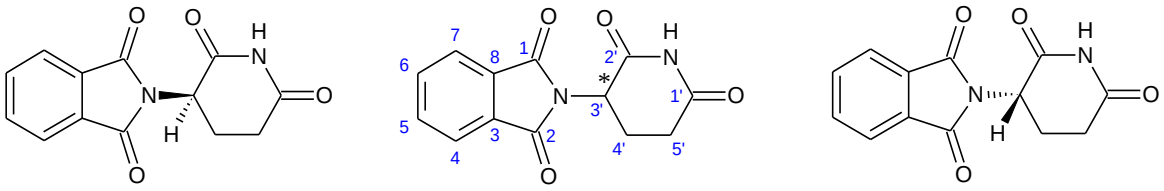

S-thalidomide *R,S* -racemic-thalidomide *R*-thalidomide

Figure 3: Chemical structure of racemic thalidomide and its stereoisomers, * denotes a chiral center.

Thalidomide at physiological pH aqueous conditions undergoes rapid spontaneous (non-enzymatic) degradation (Eriksson *et al.*, 1997; Eriksson *et al.*, 1998; Lyon *et al.*, 1995). Thalidomide is an off-white to white crystalline powder with a melting point of 275-277 °C (Goosen *et al.*, 2002; Schumacher *et al.*, 1965). Thalidomide is poorly soluble in water and ethanol with a maximum aqueous solubility of around 50 μg/mL (Silva et al., 2013). Thalidomide was first synthesized in 1953 by the Swiss pharmaceutical company Ciba, who did not continue with its development because of apparent lack of pharmacologic effects (Ribatti *et al.*, 2005). Thalidomide was initially intended for use as an anti-convulsant in epilepsy therapy, but lacked efficacy. However, thalidomide was found to cause deep sleep promptly and without any hangover effects. Nor was any acute toxicity found, even in high

doses (Schützenberger *et al.*, 1979; Somers, 1960). Thalidomide was then remarketed as a sedative and tranquilizer in 1956, and soon became the most widely applied sleeping pill in Germany (Avorn 2011). No significant side effects were observed when thalidomide was tested on rodents, and subsequently 14 pharmaceutical companies were marketing thalidomide in 46 countries. Popular sedatives at the time, such as barbiturates, often exhibited severe addictive properties, and fatal overdoses were not uncommon. Thalidomide at the time was considered a safe replacement for barbiturates as it lacked these properties (Ribatti *et al.*, 2005; Schulz, 2001; Teo *et al.*, 2005). Approval in the United States was delayed however by the Food and Drug Administration (FDA) because of concerns over neuropathy (Xue *et al.*, 2015).

Until 1961, both McBride in Australia (McBride, 1961) and Lenz (Somers, 1962) in Germa independently discovered the horrific teratogenic effects of thalidomide. They described a higher incident rate of birth defects in newborns when their mothers had been taking thalidomide during pregnancy. The most common teratogenic phenotypes induced by the drug were limb malformation, such as complete absence of the limbs (amelia) or absence of certain regions of the limb (phocomelia) (Therapontos *et al.*, 2009; Vargesson, 2013). Other frequently observed phenotypes were ear and eye defects, as well as malformations of internal organs such as kidney and heart (Vargesson, 2015; Vargesson, 2013). Some case about gastrointestinal deformities which cannot be cured was also reported, and this often related to early childhood deaths. After that, thalidomide was quickly withdrawn from the German and other world markets (Zwingenberger, 1995). However, there were more than 10,000 children affected by this accident in the world (Miller *et al.*, 1999).

In 1965, thalidomide was reported to be effective in treatment of erythema nodosum leprosum (ENL), an acute complication associated with leprosy (Sheskin, 1965). At the same time, Thalidomide was the first time involved in cancer study in 1965, and it was demonstrated to reduce the growth the rate of growth of 7,12-dimethylbenzanthracene-induced tumours in Sprague-Dawley rats (Mückter, 1965; Mückter *et al.*, 1969), but the clinical results reported in the same year using thalidomide in cancer patients were inconclusive (Grabstald *et al.*, 1965; Olson *et al.*, 1965). The development of limb bud requires a complex interaction of both angiogenesis and vasculogenesis. Angiogenesis is the formation of new blood vessels from sprouts of pre-existing vessels. Thus, since 1994

thalidomide for cancer treatment was renewed because thalidomide is an inhibitor of angiogenesis. Subsequently, thalidomide has been involved in human clinical trials for the first time with refractory and relapsed multiple myeloma (MM), more than 30 percent of response rate has been found in all patients (Larkin, 1999a; Singhal *et al.*, 2002b). In the subsequent studies, thalidomide was for the first time used in combination chemotherapy with dexamethasone. The response rate was significantly increased to 60-70% because of the synergistic effects of both agents (Alexanian *et al.*, 2003; Dimopoulos *et al.*, 2001a; Palumbo *et al.*, 2001; Weber, 2003). Not just for cancer treatment, thalidomide has been widely researched for a variety of diseases including rheumatoid arthritis (Gutiérrez‐Rodríguez, 1984), Behcet's disease (Hamza, 1986), graft-versus-host diseases (Vogelsang et al., 1992), lupus erythematosus (Atra *et al.*, 1993) and HIV-I (Makonkawkeyoon *et al.*, 1993). Due to the effectiveness of thalidomide in a variety of disease, thalidomide has been widely used in the development of analogues to improve efficacy with low related toxicity such as lenalidomide and pomalidomide. These thalidomide analogues have been developed by the American biopharmaceutical company Celgene.

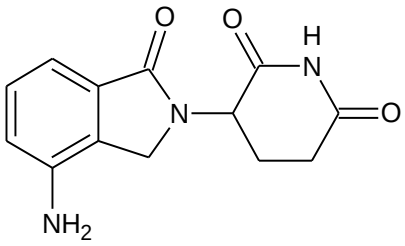

Lenalidomide

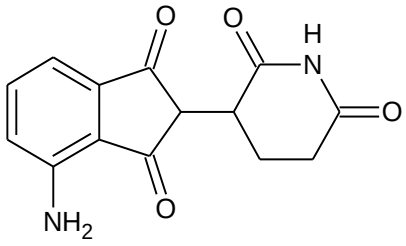

Pomalidomide

Figure 4: Structure of thalidomide analogue including lenalidomide and pomalidomide developed by American biopharmaceutical company Celgene

Thalidomide gained approval by the US FDA in 1998 for ENL treatment, and for multiple myeloma in 2006. Those two thalidomide analogues lenalidomide and pomalidomide (Figure 4) have been approved for treatment of multiple myeloma in 2006 and 2013. Lenalidomide has also had approval from US FDA in treatment of myelodysplastic syndrome, a pre-stage of acute myeloid leukemia (Kortüm *et al.*, 2015; List *et al.*, 2005).

2.1.2 Pharmacodynamics of thalidomide

2.1.2.1 Pre-clinical Studies

Early studies on thalidomide as an anti-cancer agent began following reports that it was a teratogen. Because of its teratogenicity, it was considered to have cytostatic effects and was investigated against many types of animal tumour models, however the results were not encouraging (McBride, 1961; Ward, 1962). After the demonstration by D'Amato and co-workers that thalidomide is an inhibitor of angiogenesis in 1994, the interest of thalidomide in pre-clinical studies was renewed. However, thalidomide does not show any anti-tumour activity as a single agent in the majority of murine and rat tumour models, such as Ching and co-workers to focus on implanted clone 38 tumour in dose of 100 mg/kg (Ching *et al.*, 1995), Gutman worked on implanted B16-F10 melanoma and colon carcinoma cells in mice and Lewis Lung tumour models (Gutman *et al.*, 1996). Not only this, but thalidomide was also shown to promote metastasis of prostate adenocarcinoma in rat models (Pollard, 1996). Therefore, generally thalidomide does not show potent anti-tumour effects in rodents. Based on those findings, combination studies involving thalidomide and other clinical or novel anti-cancer agents were explored and found to be more effective. For example, mice treated with thalidomide combined with cyclophosphamide or adriamycin had significantly smaller tumour that those given those two chemotherapeutic agents alone in mouse model of breast cancer (Nguyen et al., 1997). Also, for implant colon 38 tumour in mice the higher cure rates was found in treatment of thalidomide (100 mg/kg) with 5,6-dimethylsanthenone-4-acetic acid (DMXAA) (Ching *et al.*, 1999).

2.1.2.2 Clinical Studies

2.1.2.2.1 Thalidomide in Solid Tumours

Thalidomide has been evaluated in the treatment of a variety of solid tumours including prostate cancer, breast cancer, renal cancer and Kaposi's sarcoma in HIV positive and negative patients.

Figg and co-workers conducted a phase II study evaluating two dosing regimens of thalidomide (200 mg/d vs 1200 mg/d) in androgen-independent prostate cancer, which has failed to respond to previous therapy (Figg et al., 2001b). They reported that 18% of patients

who took thalidomide 200 mg daily had a decrease of over 50% in prostate specific antigen level, with the overall median survival being 15.8 months (Figg et al., 2001a). Tumour angiogenesis has prognostic value in invasive breast cancer and has been shown to be correlated with metastatic potential. It was only logical that anti-angiogenic agents would be tried in its therapy. In a phase II study, patients with progressive metastatic breast cancer with daily 200 mg of thalidomide or 800 mg to be escalated to 1,200 mg (Baidas et al., 2000). Evaluation of circulating angiogenic factors and pharmacokinetic studies failed to provide insight into the reason for the lack of efficacy. In fact, thalidomide has been demonstrated to reduce microvessel density of tumour in animal model (Kotoh et al., 1999), leading to its clinical trials in solid tumours. In the treatment of renal cell carcinoma, Stebbing and co-workers reported that 2 out of 22 patients (9%) taking thalidomide at 200 mg/day had stable disease for over 12 months, and 5 patients (23%) had stable disease for 6-12 months (Stebbing et al., 2001). Another report showed 16 out of 26 patients (62%) with renal carcinoma had stable disease for 6 months (Motzer et al., 2002). Thalidomide has also been trialed in Kaposi's sarcoma, an oncological condition associated with human immunodeficiency virus (HIV) infection, Fife and co-workers reported that 6 of 17 patients (35%) who took a daily dose of thalidomide at 100 mg achieved a partial response, and 4 (24%) had stable disease (Fife *et al.*, 1998). Since thalidomide alone only produced marginal benefit in many types of solid tumours, more clinical studies tried to combine thalidomide with other anti-cancer agents and the combination therapy showed more effectiveness in treating solid tumours (Bartlett *et al.*, 2004; Wong *et al.*, 2012).

2.1.2.2.2 Thalidomide in Hematological Malignancies

For MM, thalidomide has been demonstrated to increase bone marrow microvascularity which is highly correlated to disease progression (Vacca et al., 1995; Vacca et al., 1999; Vacca et al., 1994), thalidomide was involved in a clinical trial as an anti-angiogenic agent for MM. Singhal and other colleagues were among the first to investigate thalidomide to patients with advanced and refractory MM. Thalidomide was initiated at a daily dose of 200 mg, and the dose was increased by 200 mg every 2 weeks to a maximum of 800 mg/day if tolerated. The rates of total response, event-free survival and overall survival were 32%, 22% and 58%, respectively. There was no statistical difference in bone marrow microvessel density between responders and non-responders, however, responding patients had a

reduction in bone marrow plasmacytosis and serum β2-microglobulin concentrations and an increase in haemoglobin levels (Singhal *et al.*, 2002a). According to this result, several similar clinical trials were conducted to focus on the dose-response of MM treatment and modulation of cytokine activity. The optimal outcome in clinical pharmacology is to determine optimal dose of thalidomide treatment to balance between clinical efficacy and dose-related toxicity. The low-doses (50-400 mg/day) of thalidomide were effective and recorded a 24% response rate in 33 patients (Larkin, 1999b; Yakoub-Agha *et al.*, 2012). In 2003 Wechalekar and other colleagues found thalidomide at a dose of 200 mg/day was an effective higher dose and less toxic in a clinical trials where 43% of 30 patients responded (Weber *et al.*, 2003). For modulation cytokine activity, thalidomide in a dose of 400 mg/day treated 30 patients was reported an overall response rate of 60%, but also concentration of cytokine such as vascular endothelial growth factor (VEGF), basic fibroblast growth factor (bFGF), interleukin-6 (IL-6) and TNF-α, were significantly lower in both bone marrow and peripheral blood in responders after 4-8 weeks of thalidomide treatment (Dmoszyńska *et al.*, 2002). Similarly, Li with other colleagues found VEGF and bFGF levels were higher after treatment than before thalidomide treatment, while intercellular cell adhesion molecule-1 (ICAM-1) and vascular cell adhesion molecule-1 (VCAM-1) were significantly lower after treatment in responders, but were not changed in non-responders (Li *et al.*, 2003).

The clinical benefit of thalidomide increases significantly when it is combined with other agents. Thalidomide in combination with dexamethasone has become one of the most commonly used front-line regimens in the U.S. for patients with MM and was approved by the FDA for this indication in 2006 (Richardson et al., 2007). This combination can improve the overall response rate generally from over 30% to over 50% (Barlogie *et al.*, 2001; Dimopoulos *et al.*, 2001b; Palumbo *et al.*, 2001; Rajkumar *et al.*, 2000; Rajkumar *et al.*, 2002). In a further study, thalidomide or a combined regimen of thalidomide-dexamethasone were combined with other existing anti-cancer agents such as cisplatin, cyclophosphamide, etoposide, doxorubicin, vincristine, melphalan and clarithromycin. It was the first time to combine vincristine with regime of thalidomide-dexamethasone, this combination treatment appeared to be highly effective in previous untreated patients with MM, but this treatment was also associated with a high rate of thrombotic events, polyneuropathy, and neutropenia infections (Schutt et al., 2005). In treatment with MM, some cytotoxic drugs such as

vincristine and doxorubicin with intermittent high-dose dexamethasone showed a response rate of 55% to 85% in patients with newly diagnosed MM. However, this cytotoxic treatment regime did not show advantages in survival rates (Durie *et al.*, 2004; Samson *et al.*, 1989). Thalidomide was given at 50 mg/day orally and the dose increased slowly to a maximum of 400 mg/day. The complete response plus good partial response rate was 49%, with an overall response rate of 87% and 90%. This result suggested the addition of thalidomide to the combination regime significantly improves the response rate and quality of responses compared with pegylated liposomal doxorubicin, vincristine, and decreased-frequency dexamethasone regime alone (Baz et al., 2014). Another combination from a case report for regimen of thalidomide-dexamethasone is bortezomib as proteasome inhibitor, this novel combination therapy showed less dose related toxicity for relapse and refractory IgD MM (Schmielau *et al.*, 2005). E, Terpos with other colleagues studied the efficacy and safety of the combination of bortezomib, melphalan and dexamethasone with intermittent thalidomide in phase II clinical trials to treat relapsed/refractory myeloma. Bortezomib (1.0 mg/m^2) was given on days 1, 4, 8, and 11, oral melphalan (0.15 mg/kg) on day 1-4, whereas thalidomide (100 mg/day) and dexamethasone (12 mg/m^2) were administered day 1-4 and 17-20 of a 28-day cycle, for four cycles. Thalidomide in this study contributed to bone remodelling through regulation of osteoclast and cytokines. The overall response rate was 66%, and the median time to respond was 35 days with 9.3 months for median of progression, it concluded that thalidomide is active (Terpos et al., 2008). Meanwhile, cyclophosphamide as a cytotoxic drug was involved in combination treatment of bortezomib and thalidomide-dexamethasone regimen in clinical phase II. Cyclophosphamide in dose of 150 mg/m^2 was orally administrated on day-1 to day-4 in two cycles of treatment with 70 patients with relapsed or refractory MM. This study showed that the combination treatment as a highly effective salvage therapy with manageable toxicity during the treatment (Kim et al., 2010). To overcome chemoresistance, the curcumin, which is the yellow pigment in turmeric, was applied to increase sensitivity of thalidomide and bortezomib to MM by down-regulating NF-κB and NF-κB-regulated gene products. This study suggested curcumin can enhance the activity of thalidomide and bortezomib in treatment for patients with MM (Sung *et al.*, 2009). The exact mechanism of action of thalidomide in the treatment of MM is still under investigation, and a number of hypotheses as summarized in the next section have been proposed.

2.4.1 Mechanism of Action in Cancer Treatment

2.1.3.1 Anti-angiogenesis

The mechanism of thalidomide's angiogenesis is not fully understood. It is thought thalidomide inhibits the production of angiogenic cytokine, such as bFGF and VEGF, to inhibit endothelial cell proliferation (Kruse *et al.*, 1998). Although thalidomide entered clinical trials for MM as an anti-angiogenic agent (Singhal et al., 1999), a decrease in microvessel density was not observed in patients who were responding to thalidomide therapy (Singhal et al., 1999), suggesting thalidomide may act through other mechanism apart from anti-angiogenesis.

2.1.3.2 Inhibition and stimulation of cytokines

Cytokines are soluble glycoproteins released by cells of immune system, which act non-enzymatically through specific receptors to regulate immune response. Thalidomide can modulate the biosynthesis of several cytokines, which is thought to provide the basis for its biological effects. The most notable effect of thalidomide on cytokine production is that it decreases lipopolysaccharide (LPS)-induced TNF-α production in human monocytes and macrophages *in vitro* (Corral et al., 1996). This inhibition is a result of the increased degradation of TNF-α messenger RNA (mRNA). Thalidomide-bound α1- acid glycoprotein inhibited TNF-α production of human monocytes. Turk and other colleagues suggested the binding of thalidomide to α1- acid glycoprotein caused down-regulation of TNF-α production (Turk *et al.*, 1996). TNF-α is regarded as a survival and proliferation factor for human myeloma cells through activation of the MEK/MAPK and NF-κB signaling pathway (Hideshima *et al.*, 2001), so that inhibition of TNF-α may restrict tumour growth and cause tumour cell death (Hideshima *et al.*, 2001). Furthermore, thalidomide's ability to modulate TNF-α production may have indirect effects on the myeloma/BMSC microenvironment to inhibit the localization and growth of MM cells.

In addition, Hideshima T, and other colleagues in 2001 reported that IL-6 is another important factor to regulate human MM cells, and they demonstrated IL-6 is a growth and anti-apoptotic factor in human MM cells and characterized the signaling cascades mediating several effects (Hideshima *et al.*, 2001). IL-6 induces proliferation of MM cell activation of the Ras/Raf/MEK/MAPK signaling pathway (Ogata et al., 1997), whereas the JAK/STAT3

signaling pathway promotes MM cell survival (Figure 5) (Catlett-Falcone et al., 1999). Thalidomide also has the ability to modulate the production of other cytokines, such as IL-1β, IL-2, IL-4, IL-5, IL-8, IL-10, IL-12, interferon-gamma IFN-γ, bFGF and VEGF (Corral *et al.*, 1999; Dunzendorfer *et al.*, 1999; Hallek *et al.*, 1998; Haslett *et al.*, 1997; Kenyon *et al.*, 1997; Moller *et al.*, 1997; Verbon *et al.*, 2000; Zwingenberger *et al.*, 1995).

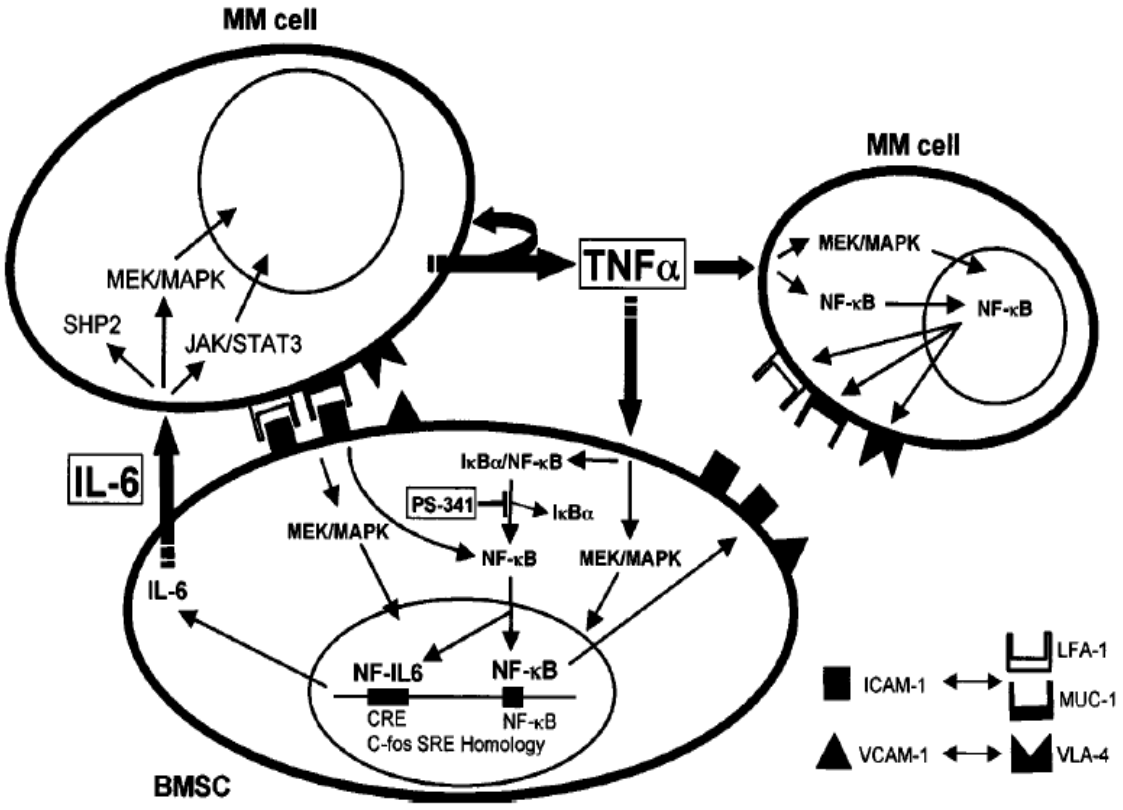

Figure 5: A model for the role of TNF-α in the pathophysiology of MM. TNF-α secreted from MM cells induces modest proliferation, as well as MEK/MAPK and NF-κB activation

2.1.3.3 Stimulation of Lymphocytes and Natural Killer Cells

The immunological adjuvant action of thalidomide therefore stimulates the otherwise ineffectual immune response to tumour antigen enhancing an anti-cancer response. Thalidomide action highly depends on the type of immune cells that are activated and types of stimulus which cell received. *In vitro* study showed thalidomide induced an IL-2-mediated primary T-cell proliferation through the T-cell receptor (TCR) complex with a concomitant increase in IFN-γ production (Catlett-Falcone et al., 1999). This proliferation is greater for

the cytotoxic, rather than helper, T-cell subset, which was supported by observations in thalidomide-treated HIV seropositive patients where was increased the population of cytotoxic T cells and plasma levels of IL-2 receptor, a marker of T-cells activation. The stimulatory property could partially explain anti-inflammatory effects of thalidomide in inflammatory bowel disease in which the activity of cytotoxic T cells is diminished. Thalidomide can significantly increase the lysis of human multiple-myeloma cell lines and patient MM cells after incubation with IL-2-primed peripheral blood mononuclear cells (PBMCs) (Davies et al., 2001). Coupled with clinical observations that thalidomide increased natural killer cell numbers and function in MMPs responding to thalidomide therapy, they suggested that thalidomide could enhance the immune response against tumours by increasing natural killer cell numbers and function in humans (Davies et al., 2001).

2.1.4 Synthesis of Thalidomide Analogues

2.1.4.1 Precursor synthesis

The structure of thalidomide contains two ring systems including the phthalic ring and the glutarimide ring. Based on retrosynthetic analysis (Figure 6), the common route for the synthesis of thalidomide or relative analogues requires phthalic anhydride to be connected with the glutarimide ring. While phthalic anhydride can be easily synthesized to achieve from the corresponding acids, and the glutarimide ring can be easy to reach from a linear structure such as commercially available Boc-protected *L*-glutamine. This pathway can be applied to synthesize thalidomide or relative thalidomide analogues with substitution on the aromatic system of the phthalic ring for cross-coupling reactions. The potential substitution can be a halide or nitro group.

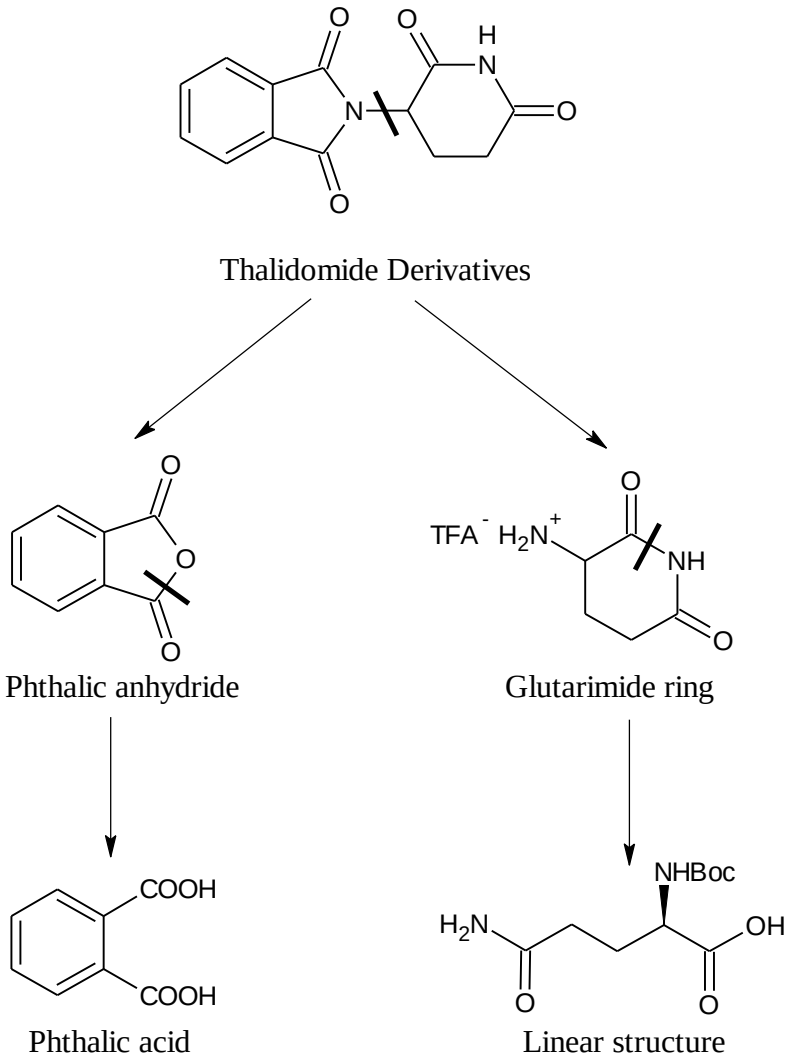

Figure 6: Retrosynthesis pathway to access various thalidomide derivatives

Generally, phthalic acid (diacid) is treated with refluxing acetic anhydride for conversion into the corresponding anhydride with a yield of 75% (Saudi et al., 2016). Then, this phthalic anhydride is ready for coupling reaction with the glutarimide ring. The glutarimide ring at this time is formed as the salt form with trifluoroacetic acid according to the procedure by Lohbeck with co-workers (Lohbeck *et al.*, 2016). A carbonyldiimidazole contributes to cyclisation of Boc-protected *L*-glutamine in tetrahydrofuran at reflux, affording racemic Boc-protected glutarimide ring in around 45% yield. 4-Dimethylaminopyridine also contributes to this cyclisation reaction to increase yield to 77% (Capitosti *et al.*, 2003). Finally, in the

presence of the base triethylamine, phthalic anhydride couples to a glutarimide salt to produce thalidomide.

2.1.4.2 Previous Synthetic Methods of Thalidomide

Thalidomide was disclosed for the first time by Chemie Grunenthal GmbH in Germany. The preparation consists of three simple steps involving a reaction of glutamic acid with phthalic anhydride, followed by ring closure. Namely, *N*-phthaloyl glutamic acid, prepared from glutamic acid and phthalic anhydride in refluxing pyridine, was treated with acetic anhydride to give *N*-phthaloyl glutamic acid anhydride. This was melted with urea at 170 – 180 ℃ for 20 mins to make thalidomide. However, the reaction product requires multiple re-crystallization from 95% ethanol to generate pure thalidomide in a large scale. Another synthetic method was developed based the previous reaction. Chemists at Dainippon Pharmaceutical in Japan reported to a reaction of alpha-aminoglutarimide with phthalic anhydride in refluxing pyridine for 1 hour. Another method for generation of thalidomide is a reaction about bromoglutarimide from piperidine-2,6-dione with potassium phthalimide in *N*,*N*-dimethylformamide (DMF) with heat.

In fact, a lot of synthetic method for thalidomide has been developed. In 1999, Muller with co-workers reported a further improvement of the classical Grunenthal schedule that allows commercial synthesis of thalidomide. The last step in the Grunenthal synthesis involves a high-temperature melt reaction affording crude thalidomide requiring multiple re-crystallizations. While the original synthesis begins with *L*-glutamic acid, crucial to the Celgene development is the finding that thalidomide can be prepared from *L*-glutamine and *N*-carbethoxyphthalimide in water in the presence of sodium carbonate at room temperature to give *N*-phthaloyl-*L*-glutamine. Cyclization of *N*-phthaloyl-*L*-glutamine (Figure 7) to afford thalidomide is accomplished by treatment with *N,N'*-carbonyldiimidazole (CDI) in the presence of a catalytic amount of 4-(diethylamino)pyridine (DMAP) in tetrahydrofuran (THF) with reflux. Although enantiomerically pure *L*-glutamine is the starting material, racemization occurs in this step. THF is a suitable solvent because of the low solubility of thalidomide and the high solubility of the by-product, which provides an easy way for purification of the product. The procedure can be easily used to prepare thalidomide in a 100 g scale in the laboratory, and it was successfully scaled up to the multikilogram scale in a pilot plant.

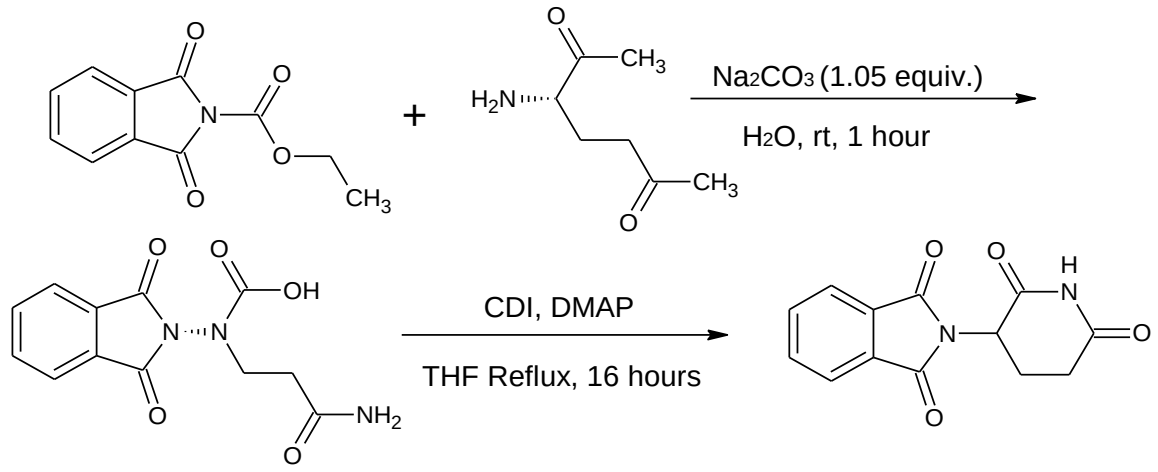

Figure 7: Commercial Synthesis of thalidomide

Not only normal traditional chemistry methods, but also other kinds of techniques have been applied for the synthesis of thalidomide. A microwave technique was introduced during the past decade in organic synthesis and has proved to be highly effective to promote many organic reactions. Since the final step of the original thalidomide preparation requires the formation of the glutarimide ring with urea at high temperature, the microwave irradiation strategy could be considered for improvement of the step. A Spanish group realized the idea of microwave-promoted synthesis of thalidomide. The formation of the glutarimide ring was carried out in 63% yield by microwave irradiation of *N*-phthaloyl-*L*-glutamic acid for 10 mins in the presence of urea. The yield was improved to 85% under microwave irradiation for 15 mins using thiourea instead of urea. The fastest speed by using the microwave technique was reported by Hijji and co-workers. They reported in 2004 that ammonium chloride was found to be an effective source of nitrogen. Namely, phthalic anhydride, glutamic acid, and ammonium chloride were mixed in 1:1:1 ratio with a catalytic amount of DMAP and heated in a conventional microwave oven for 6.5 mins. The mixture melted to a brown liquid. The heating continued for an additional 1 min to give thalidomide in 52% yield in his two-step, one spot reaction after solubilization, precipitation, and re-crystallization.

Solid-phase synthesis of thalidomide and its derivatives is another synthetic method developed by Xiao with co-workers. The method involves a straightforward three-step sequence starting from a resin-linked acid prepared from the coupling of hydroxymethyl

polystyrene with phthalic anhydride in the presence of triethylamine and DMAP in DMF. The acid was then reacted with α-aminoglutarimide in the presence of coupling reagents such as *N,N'*-diisopropylcarbodiimide (DIC) and 1-hydroxybenzotriazole (HOBT) followed by trifluoroacetic acid (TFA) treatment in toluene to form thalidomide with an overall yield of 70%.

Chang with co-workers from 2002 to 2003 developed a series of synthetic methods for thalidomide. This development is quite unique for the glutarimide ring construction and contributes to the final thalidomide synthesis. The mechanism of glutarimide ring formation is through a formal cycloaddition strategy between α-toluenesulfonyl acetamide and unsaturated esters followed by desulfonylation and deprotection reactions. The method can avoid the high temperature melt reaction required in the classical reaction. However, the total yield was quite low, with only 18% in five steps from acrylate (Figure 8) and 30% in three steps from 2-phthalimidoacrylic acid methyl ester (Figure 9).

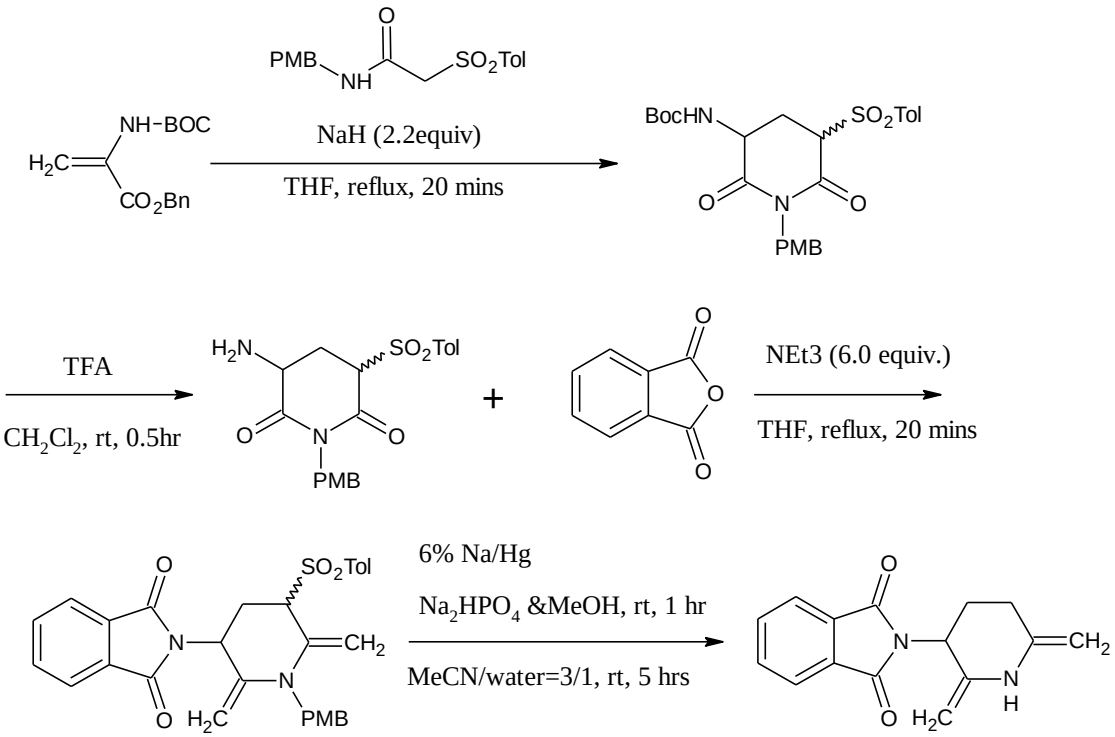

Figure 8: Construction of thalidomide via a formal [3+3] cycloaddition strategy from acrylate

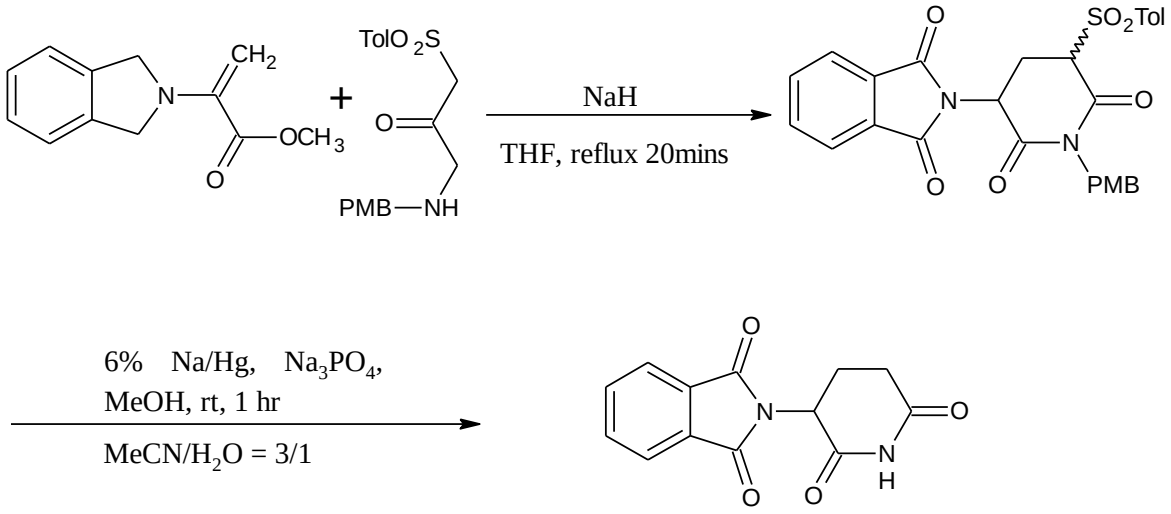

Figure 9: Construction of thalidomide via a formal [3+3] cycloaddition strategy from phthalimidoacrylate

A solid-phase approach was also applied in this strategy (Figure 10), treating an easily accessible polymer-supported with α,β-unsaturated ester. The method may allow the rapid synthesis of thalidomide and its derivatives.

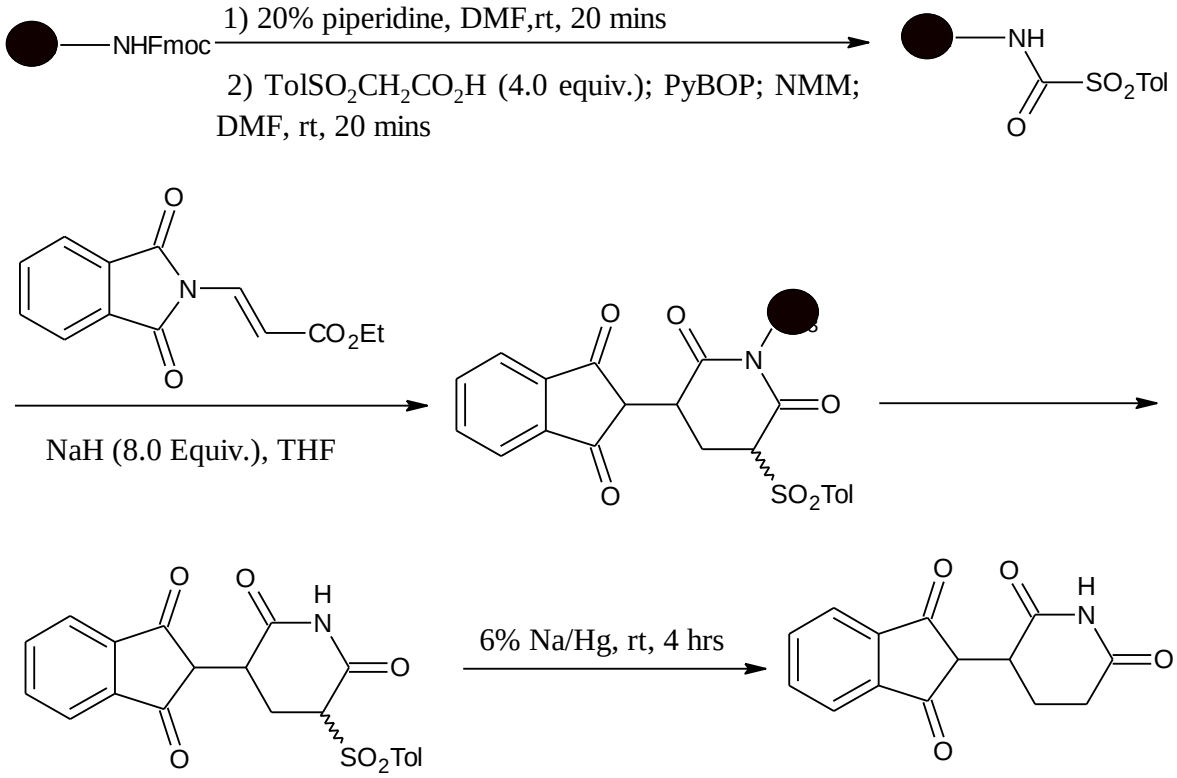

Figure 10: Polymer-supported construction of thalidomide via a formal [3 + 3] cycloaddition strategy

2.1.5 Structure Modification of Thalidomide Analogues

Thalidomide seems to possess a pharmacophoric structure related to its known biological activities as a sedative, anti-malarial, anti-metastatic and anti-androgenic agents (Yuichi, 2002). Thalidomide is composed of two distinct moieties including the phthalimide and glutarimide rings. Based on analysis of structural activity relationships, the glutarimide moiety of thalidomide is related to its sedative/hypnotic and anti-malarial effects and *N*-substituted phthalimide structure possibly relates to immunomodulatory activity through regulation of TNF-α cytokine production.

2.1.5.1 Structural Modification on Phthalimide Ring of Thalidomide

The teratogenic toxicity of thalidomide was found to be mediated by an arene oxide metabolite (Figure 11) of the drug, so that epoxide formation would be prevented if the hydrogen atoms were substituted with electron acceptors such as halogen atoms (Niwayama *et al.*, 1996).

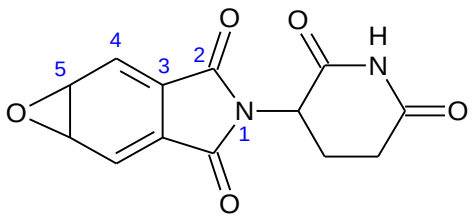

Figure 11: Structure of arene oxide

Based on this, Hashimoto, K and other colleagues in 1994 found tetrafluorophthalimides and tetrachlorophthalimides (Figure 12-a) could enhance TNF-α in promonocytic cell line THP-1 cells, and its inhibitory effect with IC_{50} of 400 nM was to represent over 500-fold compared to treatment of thalidomide (Nishimura *et al.*, 1994). Another method of structural modification was developed an alkylated substitution at *N*-1 of phthalimide with tetrahalothalidomide (Figure 12-b). These structural modifications constantly enhanced TNF-α secretion in the LPS-stimulated human monocytic cell line (THP1 cells).

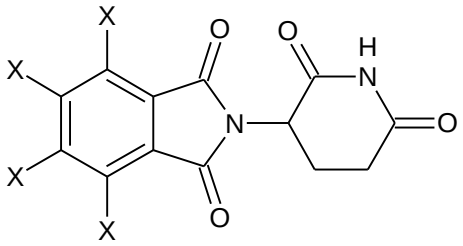

X: Halogen, such as F, Cl, Br

(a)

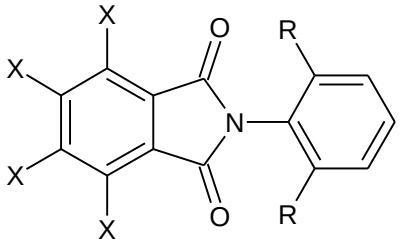

(1) R=R'=H, X=F; (2) R=R'=Me, X=F; (3) R=R'=Et, X=F; (4) R=R'=i-Pr, X=F (5) R=R'=i-Pr, X=F; (6) R=R'=H, X=Cl (7) R=R'=I-Pr, X=Br; (8) R=H, R'=t-Bu, X=F

(b)

Figure 12: Structure of tetrahalophthalimides (a), *N*-phenyltetrafluorophthalimide (b)

Based on the relationships between substitution and TNF-α modulation activity, it was found that introduction of an electron-withdrawing group such as nitro group caused an increase of the TNF-α production-enhancing activity and a decrease of the TNF-α production-inhibition activity (Miyachi et al., 1997). In contrast, introduction of an electron-donating group such as an amino or a hydroxyl group resulted in a decrease of TNF-α production-enhancing activity (Miyachi et al., 1997). This is the main reason that lenalidomide with amino substitution on C-4 phthalimide ring was approved by FDA to be clinically combined with dexamethasone to treatment MM in 2006, and lenalidomide is 50, 000 times more potent than thalidomide in inhibiting TNF-α activity (Awan et al., 2010). S. Périno with others reported the more water-soluble carboxylic acid substitution at the C-5 position (Figure 2) of thalidomide displayed an improvement in (bFGF) growth factor inhibition (Périno *et al.*, 2004). These studies contribute to a relationship between C-4 or C-5 substitution of thalidomide (Figure 2) with the electron-donating group and improvement of clinical effects.

2.2.4.1 Structural Modification on the Glutarimide ring of Thalidomide

To prevent teratogenicity toxicity, a methyl group was structurally developed on the asymmetric carbon atom C-3’ position (Figure 2) to prevent racemization. The methyl group contributes to stabilize the structure of pure enantiomers of thalidomide analogue. The effect

of this small molecular alternation selectively stabilizes thalidomide analogue to formation of (*S*)-enantiomers (Wnendt *et al.*, 1996). Also, this small change contributed to increase the TNF-α inhibitory activity while the reduction of one of the carbonyl-functions in the glutarimide-moiety to a methylene-group decreases activity. H.-W, Man with other colleagues introduced an electrophilic fluorination on the C-3' position (Figure 2) of glutarimide ring of thalidomide analogue. This contributes to chirally stabilize two thalidomide analogues including *α*-fluorothalidomide (Figure 13-a) and α-fluoro-4-aminothalidomide (Figure 13-b). The results from biological determination reported α-fluorothalidomide was found to be cytotoxic and did not inhibit TNF-α production in LPS stimulated human peripheral blood mononuclear cells (hPBMC) at the concentration up to 10 µM, on the other hand, α-fluoro-4-aminothalidomide was non-cytotoxic and was found to be 830-fold more potent than thalidomide as a TNF-α inhibitor (Man *et al.*, 2003).

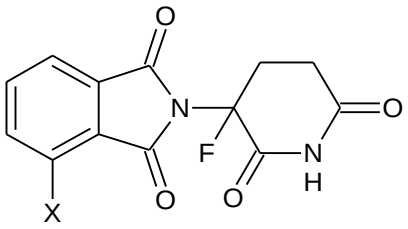

(a) X: H; (b) X: NH_2

Figure 13: (a) *α*-fluorothalidomide; (b) *α*-fluoro-4-aminothalidomide

Another focus of modification on the glutarimide ring is that structure analogues of amonafide and elinafide were reported with a good therapeutic profile (Keller *et al.*, 1956; Ward, 1962). Braña, M.F and other colleagues reported amonafide- (Figure 14-a) and elinafide (Figure 14-b) -related mono and bis-intercalators modified by the introduction of furan or thiophene ring fused to the naphthalimide moiety have shown potent cytotoxic effects to many types of cancer cell lines including human colon carcinoma (HT-29), human cervical carcinoma (HeLa), and human prostate carcinoma (PC-3) (Brana et al., 2004). Especially for substitution of furan, its cytotoxic effect was 2.5-fold more potent that elinafide against human colon carcinoma cells (HT-29) (Brana et al., 2004). In addition, *N*-substituted 3,4 –diphenyl-1H-pyrrole-2,5 diones (Figure 14-c) was suggested to improve the

cytotoxic effects compared to the single glutarimide ring (Brana *et al.*, 1989). Depending on previous efforts, the analysis for combined these structures (Figure 14-d) reported the solubility of basic structure residue which consists of dimethylaminoethyl group substituted at the nitrogen position of glutarimide is very high, but also the polyamine and diamines plays its biological processes within the whole structure.

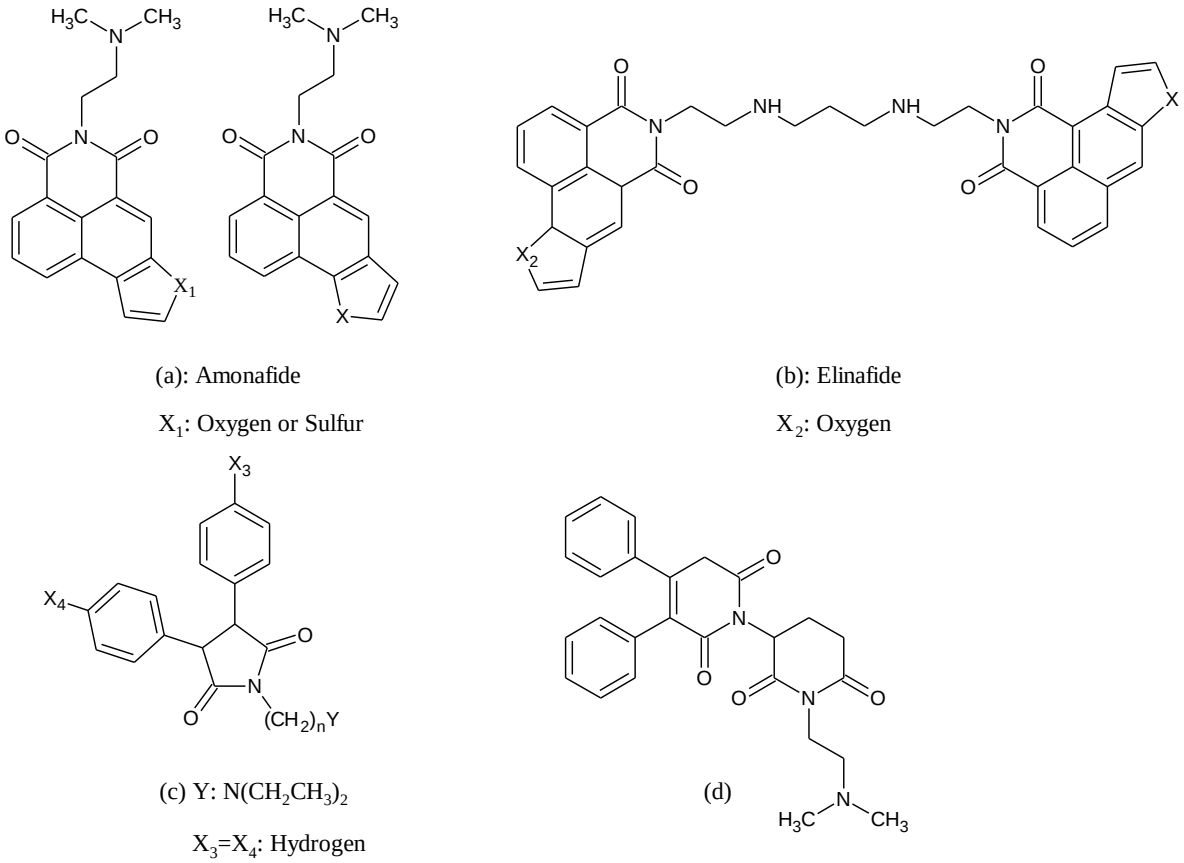

Figure 14: Glutarimide ring structural modification analogues, (a) Amonafide; (b) Elinafide; (c) N-substituted 3,4–diphenyl-1H-pyrrole-2,5 diones; (d) Dimethylaminoethyl group substituted glutarimide ring

Not only just cytotoxicity from *N*-substitution of an amine, the combination of sulphide as an electron donating group with a polyamine structure (Figure 15-a) was another hypothesis that contributed to improve the inhibition effect to TNF-α production. Zahar, M.A.-H with other colleagues reported potent cytotoxic effects to the Ehrlich ascites carcinoma (EAC) cell line could be found in thalidomide sulphur analogues in an *in vitro* study, and the degree of

cytotoxicity and inhibitory effect on TNF-α production were highly attributed to the number of sulphur atoms in the structure of thalidomide analogues (Zahran *et al.*, 2008). In addition, in *in vivo* tumour studies, thalidomide sulfur analogues showed anti-mitotic, apoptotic and necrosis against solid tumours.

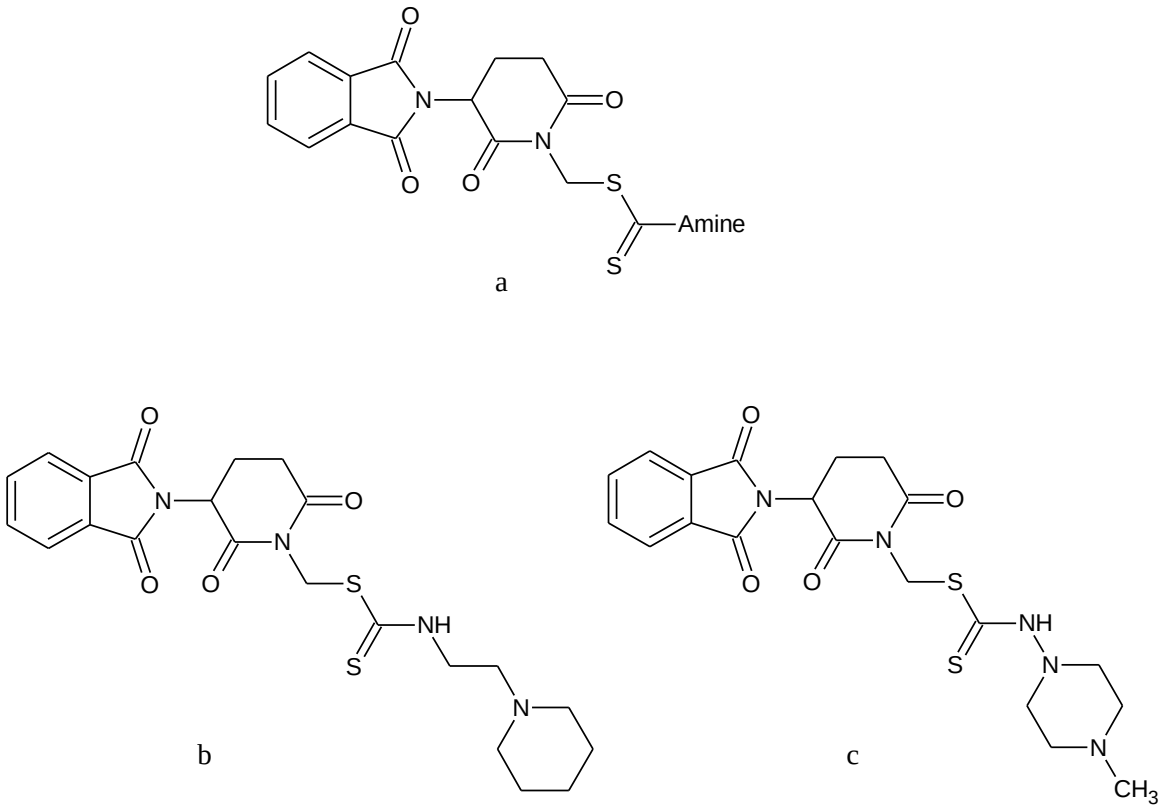

Figure 15: Structure of Thalidomide Sulfur Analogues

Guirgis, A. with other colleagues investigated thalidomide dithiocarbamate analogues (Figure 15-b & 15-c) and focused on changes in the cell adhesion biochemical profile in mice using the model of Ehrlich ascites carcinoma (EAC). In fact, cell adhesion molecules expressed in cancer cells can attract inflammatory cells such as macrophages or lymphocytes, which release trophic factors to enhance cancer cell survival and ease the instability of tumour environments (Aeed *et al.*, 1988; Coussens *et al.*, 2002). This structural development suggested more potent inhibitory effects of dithiocarbamate analogs than thalidomide might be attributed to the presence of sulphur atom in these novel compounds which consequently

lead to increase their suppression effect towards VEGF and βFGF secretion from tumour cells (Guirgis *et al.*, 2010).

2.2 Main Aim of Study in regards to Organic Synthesis

The main aims of the study with regards to organic synthesis are:

(1) Based on synthetic methods published, thalidomide (compound **1**), 2-(2,6-dioxopiperidin-3-yl)-phthalimidine (EM-12) (compound **2**) and *N*-substituted thalidomide analogue 2-(1-chloromethyl-2,6-dioxopiperidin-3-yl)phthalimidine (compound **5**) will be syntheisized

(2) Two novel thalidomide analogues (compound **3** & compound **4**) will be developed by the application of a novel synthetic method.

All thalidomide analogues after synthesis were analyzed by ^{1}H NMR and ^{13}C NMR to confirm their structure. In addition, other analytical characteristics including melting point, IR, and mass spectra were recorded and compared with literature reports. For the two novel compounds, analytical techniques characterisitcs including melting point, optical activity, mass spectra & IR spectra were recorded in detail. All compounds were used in *in vitro* studies.

2.1 Materials and Methods

2.1.2 Materials for Organic Synthesis

All chemical ordering information is shown in the Appendix I.

Other general chemicals were provided by the Chemistry Department of Auckland University of Technology, NZ.

2.1.1 Synthetic Methods & Results

General Details

The synthetic processes for this study were designed to be direct and simple, leading to the highest possible yields for all the final products. Thalidomide (compound **1**), 2-(2,6-dioxopiperidin-3-yl)-phthalimidine (EM-12) (compound **2**) and 2-(1-Chloromethyl-2,6-dioxopiperidin-3-yl) phthalimidine (compound **5**) were individually synthesized by applying the most efficient methods currently published. Also, synthetic methods for two novel compounds, 3-[(1*R*)-1-hydroxy-1-methyl-3-oxo-1,3-dihydro-2*H*-isoindol-2-yl]piperidine-2,6-dione (compound **3**) and 3-[(1*S*)-1-hydroxy-1-methyl-3-oxo-1,3-dihydro-2*H*-isoindol-2-yl]piperidine-2,6-dione (compound **4**) are also described in detail in the following sections.

All reactions were carried out in flame or oven-dried glassware under a dry nitrogen atmosphere. Reactions performed at low temperature were in an ice-water bath to effectively maintain 0 °C. Flash chromatography was carried out using silica gel 60A 40-63u from Fluorochem with the described solvents.

Thin-layer chromatography (TLC) was carried out using Global Science NZ TLC silica gel Alugram sheets using UV light at 254 nm as the visualizing agent, or sheets were developed using staining agents including ammonium molybdate and cerium sulphate in aqueous sulphuric acid. TLC results (R_f value: Retardation factor) were detected with a Spectroline® CM UV-viewing cabinet. Optical rotations were determined using the Perkin Elmer 341 polarimeter, using the sodium-D line (589 nm), with the concentration of the solution measured in gram per 100 mL. High resolution mass spectra (HRMS) were recorded using VG70-SE spectrometer or on a microOTOF-Q mass spectrometer. Low resolution mass spectra (LRMS) were recorded using

Infrared (IR) spectra were recorded using a Nicolet^{TM} iS^{TM} 10 FT-IR Spectrometer with the absorption peaks expressed in wavenumber (cm^{-1}). Melting points for all synthetic solids were carried out with a Kofler bench apparatus, and which is a metal strip with a temperature gradient (ranging from room temperature to 300 °C). NMR spectra were recorded in $CDCl_3$, DMSO-D_6 or methanol-d_4 (CD_3OD) solvent on a Bruker Ascend 400 MHz NMR spectrometer.

Chemical shifts (δ) are reported in parts per million (ppm). Chemical shifts in ^{1}H and ^{13}C spectra were referenced to the residual undeuterated solvent according to Fulmer *et al* (Fulmer et al., 2010). ^{1}H NMR data is reported as chemical shift in ppm, followed by multiplicity: s (singlet), d (doublet), t (triplet), q (quartet), quin (quintet), sext (sextet), oct (octet), dd (doublet of doublets), ddd (doublet of doublet of doublets), dt (doublet of triplets), tt (triplet of triplets); broad signals are labeled with the prefix br; signals of higher order, or signals that are not interpretable due to overlapping are abbreviated with m (multiplet). Coupling constants *J* are reported in hertz (Hz). All compounds are numbered and signal assignments are labeled according (e.g.: 5-H and C-5) where appropriate. In the case of ambiguous assignments, possible nuclei are separated by a forward slash (e.g. C-5/C-7). If signals result from more than one nucleus, the corresponding atoms are separated by a comma (e.g.: C-5, C-7). Diastereotopic protons in CH_2 groups are labeled with the subscripted suffix A or B, where A is the more downfield resonance (e.g.: 4-H_A). Signals which cannot be assigned to any specific atoms are labeled as follows: Ar-H (aromatic proton), Ar-CH (aromatic carbon, proton attached) and Ar-C (quaternary aromatic carbon).

Scheme 1: Synthesis of 2-(2,6-dioxopiperidin-3-yl)isoindole-1,3-dione, thalidomide (Compound 1)

Thaliomide can be directly synthesized from the coupling reaction of a glutarimide ring and a phthalimide ring. Aminoglutarimide (compound **6**) can be formed via intramolecular cyclization from *N*-(*tert*-butoxycarbonyl)-*L*-glutamine. Carbonyldiimidazole as coupling reagent contributes to formation of an amide bond for crosslinking between primary amine and carboxylic acid, so that it contributes the cycliatin reaction to generate aminoglutarimide (compound **6**). To open the five-membered ring in the structure of phthalic anhydride, the

primary amine on the structure of compound **7** acts as a nucleophile to attack either carbonyl group of the phthalic anhydride (which acts as the electrophile). Triethylamine in the reaction acts as a base. Another two electrons on the resulting secondary amine are able to attack the carbonyl group to close the ring within the whole structure. This intramolecular cyclization reaction contributes to formation of the final product (compound **1**).

The thalidomide synthetic method (Figure 16) can be achieved efficiently through a coupling reaction using phthalic anhydride and aminoglutarimide with an appropriate protecting group. The synthetic method of Scheme 1 was performed according to published methodologies (Zhu *et al.*, 2003).

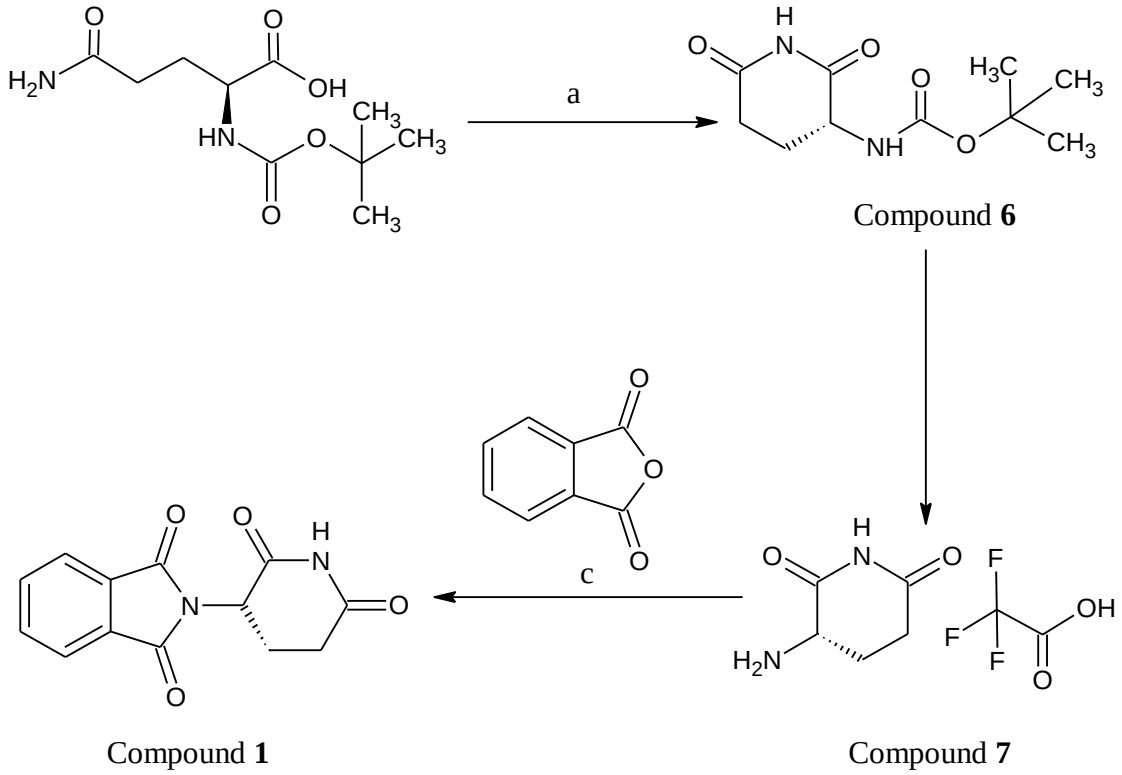

Figure 16: Reagents and conditions: (a) 1, 1'-carbonyldiimidazole (CDI) & tetrahydrofuran (THF), (b) trifluoroacetic acid & dichloromethane, (c) triethylamine & phthalic anhydride

Preparation of 3-(*tert*-butoxycarbonylamino)-2,6-piperidinedione (Compound 6)

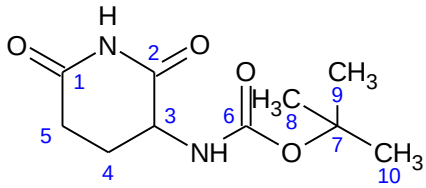

N-(*tert*-butoxycarbonyl)-*L*-glutamine (1.5 g, 6.09 mmol) was added to, and gradually dissolved in tetrahydrofuran (THF) (40 mL) forming a clear solution. 1,1'-Carbonyldiimidazole (CDI) (988 mg, 6.09 mmol) was gradually added to this clear solution. The reaction solution was heated up to reflux for 16 hours. The crude product was obtained after the reaction solution was completely removed. The product was recrystallized from hot ethyl acetate to give compound **6** as white crystal (690 mg, 3.02 mmol, yield: 46%).

Molecular formula: $C_{10}H_{16}N_2O_4$; Molecular weight: 228.24 g/mol

Melting point: 214-216℃

Retention Factor: R_f = 0.67 (ethyl acetate)

IR: 3353 cm^{-1} (-NH-), 3093 cm^{-1} (-CH-), 1727 cm^{-1} & 1678 cm^{-1} (C=O)

^{1}H NMR (DMSO-*d*6) δ = 10.76 (s, 1H, CONHCO), 7.16-7.14 (d, *J* = 8.72 Hz, 1H, RNHCO), 4.26-4.20 (ddd, *J* = 12.4 Hz, 11.7 Hz & 6.6 Hz, 1H, 3-H), 2.76-2.67 (m, 1H, 5-H_A), 2.52-2.34 (m, 2H, 4-H_A, 5-H_B), 1.90-1.88 (m, 1H, 4-H_B), 1.38 ppm (s, 9H, 8-H, 9-H & 10-H);

^{13}C NMR (DMSO-*d*6) δ = 173.4 (C-1), 173.0 (C-2), 155.8 (C-6), 78.6 (C-3), 50.8 (C-7), 31.4 (C-5), 28.6 (C-4), 24.9 (C-8, C-9, C-10) ppm

The spectral data were in accordance with those values reported in relevant literature (Contino-Pépin *et al.*, 2010).

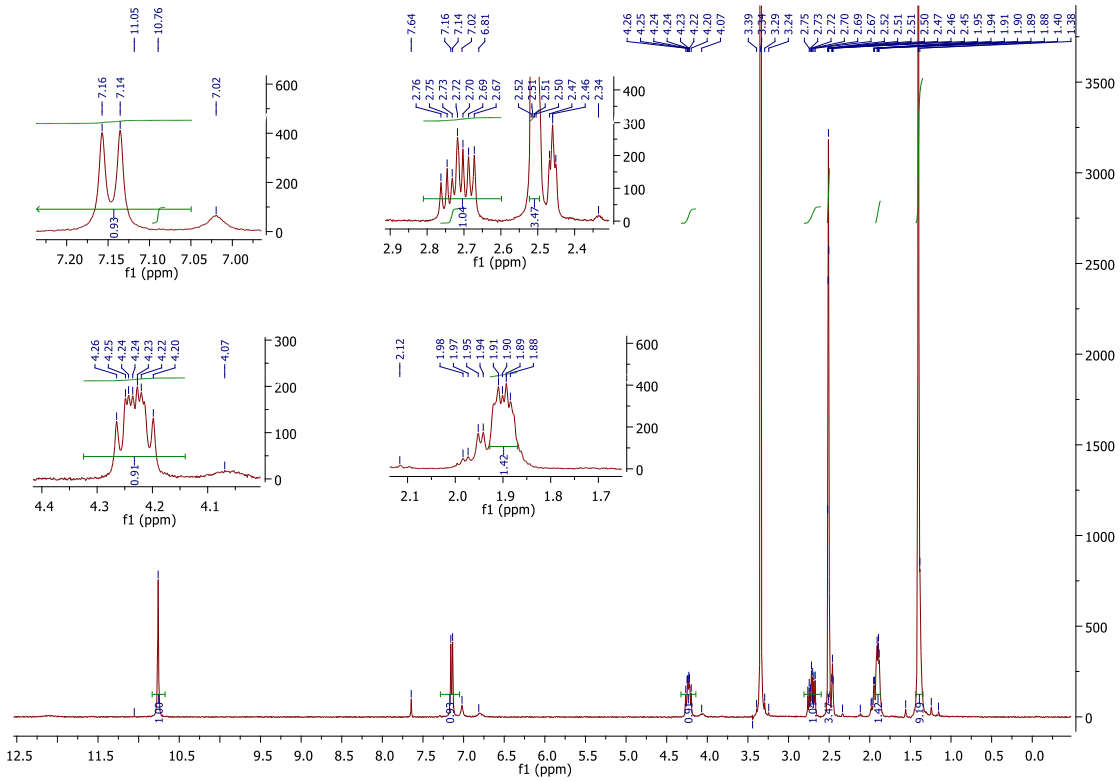

Figure 17: ^{1}H NMR for 3-(tert-butoxycarbonylamino)-2,6-piperidinedione (Compound **6**)

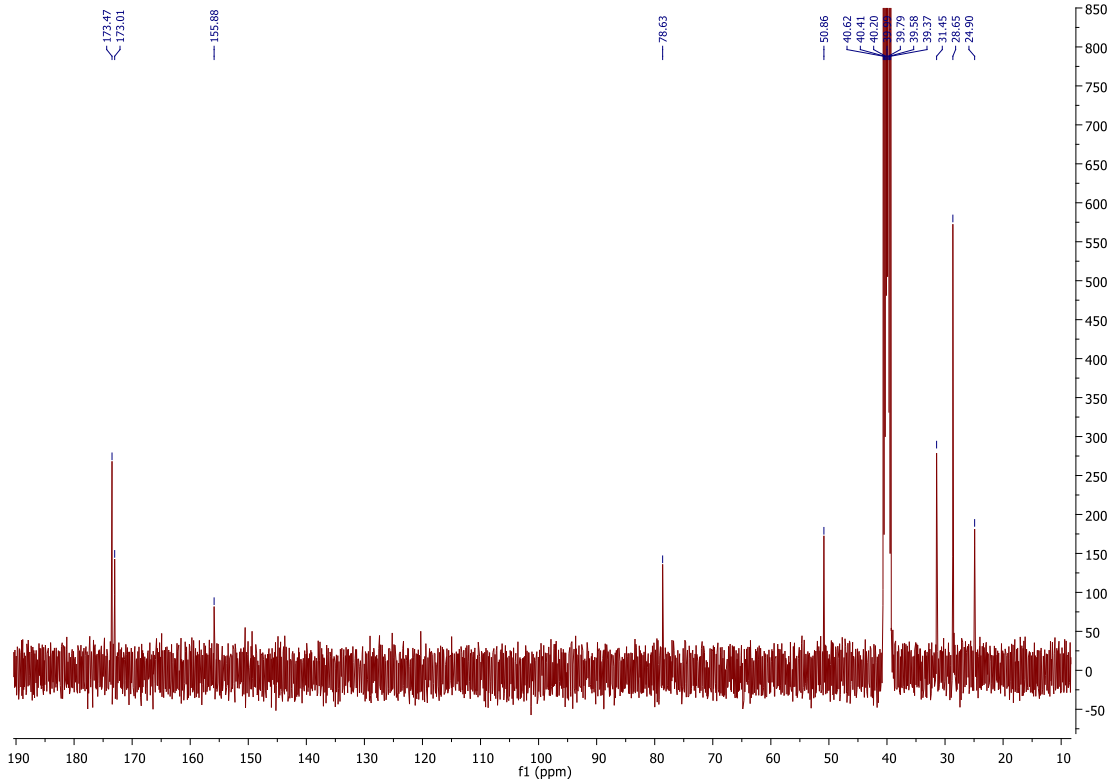

Figure 18: ^{13}C NMR for 3-(tert-butoxycarbonylamino)-2,6-piperidinedione (Compound **6**)

The ^{1}H NMR spectrum (Figure 17) of the compound **6** shows a characteristic singlet in the far downfield region at δ = 10.76 ppm which can be assigned to the acidic glutarimide NH proton. Another downfield region at δ = 7.16 – 7.14 ppm was assigned to the proton of the protected amine as a doublet of doublet with *J* = 8.7 Hz. This effect is due to the proximity of the *N*-methine proton (3-H). The *N*-methine proton (3-H) resonates as a doublet of doublet of doublets at δ = 4.3 – 4.2 ppm, with *J* = 12.4 Hz, 11.7 Hz and 6.6 Hz due to the axial-axial and axial-equatorial couplings with the diastereotopic 4-H protons and the neighboring amide's proton. The two larger coupling constants arise from germinal coupling and axial-axial coupling with one of the adjacent 4-H protons, and the smaller coupling constant is due to axial-equatorial coupling with the second 4-H proton. The complex multiplet at δ = 2.52 – 2.34 ppm and δ = 1.90 – 1.88 ppm were ambiguously assigned as 4-H and 5-H. There was a singlet in the upfield region at δ = 1.38 ppm with an integration ratio calculated at 9:1 compared to a singlet peak in the downfield region of δ = 10.76 ppm. Thus, the protection group was assigned nine protons.

The ^{13}C NMR spectrum (Figure 18) of the compound **6** shows three peaks in the far downfield region (δ = 173.4, 173.0 and 155.8 ppm), typical of carbonyl groups arising from the C-1, C-2 & C-6 nuclei. The peak at δ = 78.6 ppm was ascribed to resonance of the C-3 nuclei due to the presence of a carbonyl group and an amide. A more intense peak was assigned to C-8, C-9 and C-10 (δ = 28.6 ppm), and this was ascribed to resonance of C-8, C-9 and C-10, each having the same chemical environment. Because of the presence of the carbonyl group in its proximity, the peak at δ = 50.8 ppm was determined to be resonance of the ascribed to resonance of the C-5 nuclei. The less intense peak at δ = 24.9 ppm was ascribed to C-7 in the structure because of quaternary carbon. The aliphatic region of the spectrum displays a peak at 31.4 ppm, which was ambiguously ascribed to C-4.

Preparation of 2-(2-oxo-6-thioxo-3piperidinyl)-1*H*-isoindole-1,3(2*H*)-dione (Compound 7)

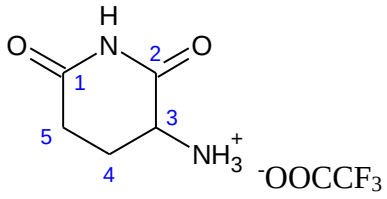

3-(*tert*-Butoxycarbonylamino)-2, 6-piperidinedione (compound **8**) (400 mg, 1.75 mmol) was suspended in dichloromethane (40 mL), forming a white mixture, then trifluoroacetic acid (3.44 mL) was added to the solution in a dropwise fashion. The solution was stirred at the room temperature for 22.5 hours. The solvent was evaporated to give the crude product of compound **7** as light purple solid (380 mg, 1.57 mmol, yield: 95%).

Molecular formula: $C_5H_8N_2O_2.C_2HF_3O_2$; Molecular weight: 242.15 g/mol

IR: 3353 cm^{-1} (-NH-), 3093 cm^{-1} (-CH-), 1727 cm^{-1} & 1678 cm^{-1} (C=O)

^{1}H NMR (DMSO-*d*6) δ = 11.22 (s, 1H, CONHCO), 8.40 (br s, 3H, NH_3^+), 4.16-4,13 (dd, *J* = 8.9 Hz, *J* = 4.94 Hz, 1H, 3-H), 2.68-2.55 (m, 2H, 4-H_A, 5-H_B), 2.10-2.07 (m, 2H, 4-H_B, 5-H_A) ppm;

^{13}C NMR (DMSO-*d*6) δ = 177.7 (C-1), 170.8 (C-2), 158.9 (C-6), 49.5 (C-3), 30.5 (C-5), 22.6 (C-4) ppm

The spectral data were in accordance with those reported in literature (Stewart *et al.*, 2007)

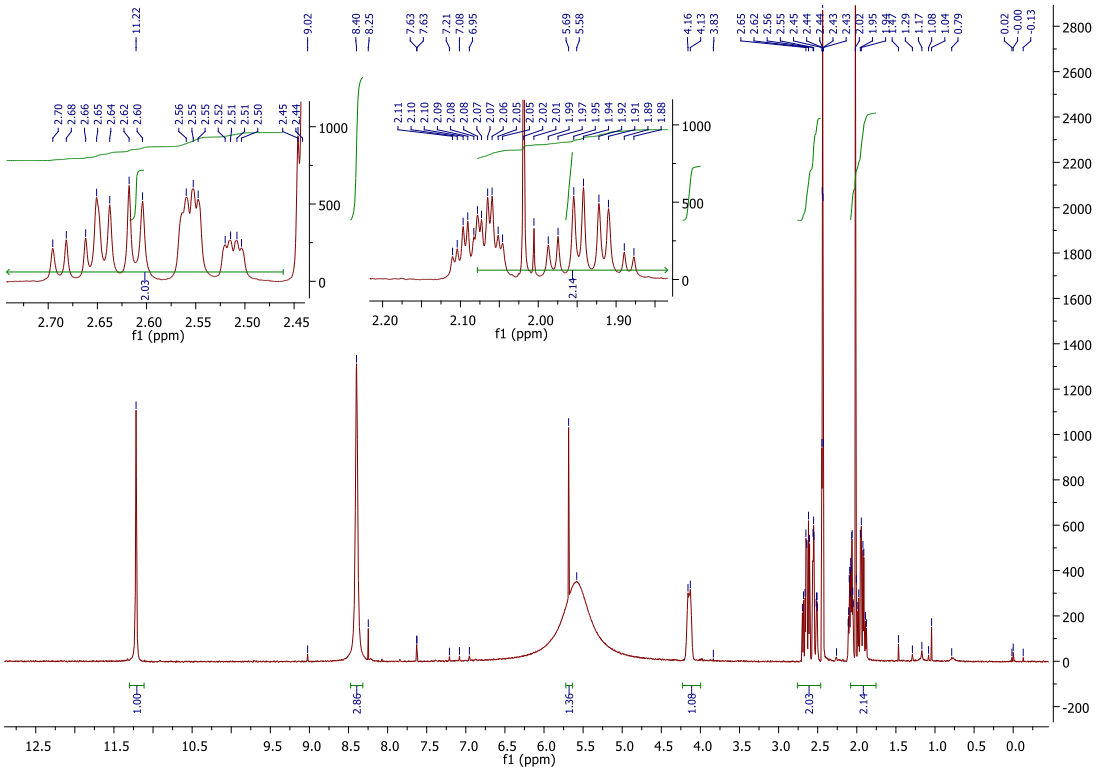

Figure 19: ^{1}H NMR for 2-(2-oxo-6-thioxo-3piperidinyl)-1H-isoindole-1,3(2H)-dione (Compound **7**)

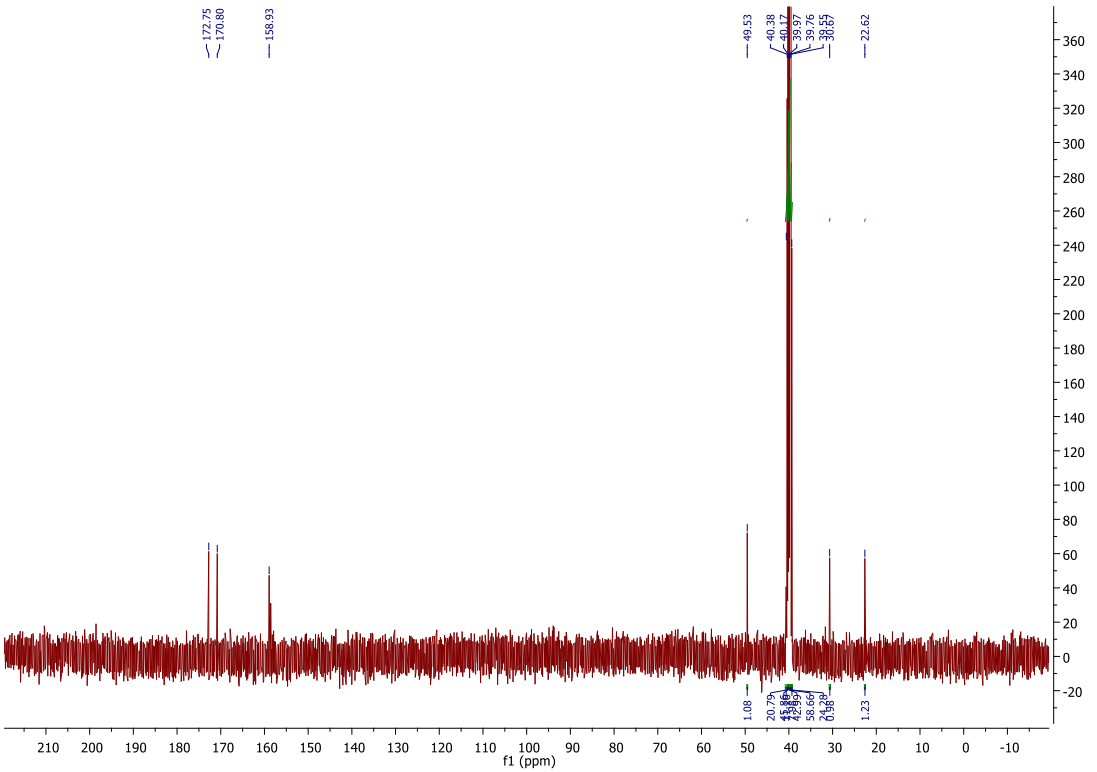

Figure 20: ^{13}C NMR for 2-(2-oxo-6-thioxo-3piperidinyl)-1H-isoindole-1,3(2H)-dione (Compound **7**)

The ^{1}H NMR spectrum (Figure 19) of the compound **7** shows a characteristic singlet in the far downfield region at δ = 11.22 ppm which can be assigned to the acidic glutarimide NH proton. Another downfield region at δ = 8.40 ppm, contains a broad singlet which can be assigned to the proton of the primary amine. The *N*-methine proton (3-H) resonates as a doublet of doublets at δ = 4.16 – 4.13 ppm with *J* = 8.9 Hz & *J* = 4.9 Hz due to the axial-axial and axial-equatorial couplings with the diastereotopic 4-H protons. The complex multiplet at δ = 2.68 – 2.55 ppm and δ = 2.10 – 2.07 ppm were ambiguously assigned as 4-H and 5-H.

The ^{13}C NMR spectrum (Figure 20) of compound **7** shows two peaks in the far downfield region (at δ = 177.7 and 170.8 ppm), typical of a carbonyl group arising from the C-1 & C-2 dual carbonyl system on the glutarimide ring. Another further downfield region at δ = 158.9 ppm is assigned to be a carbonyl group based on the proximity of a CF_3 group. The peak at δ = 49.5 ppm was ascribed to resonance of the C-3 nuclei due to the presence of a carbonyl group and an amide. The aliphatic region of the spectrum displays peaks at δ = 30.5 and 22.62 ppm which were ambiguously ascribed to C-4 and C-5.

Preparation of 2-(2,6-dioxopiperidin-3-yl)isoindole-1,3-dione (thalidomide, Compound 1)

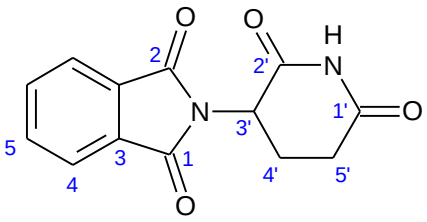

The crude product 2-(2-oxo-6-thioxo-3-piperidinyl)-1*H*-isoindole-1,3(2*H*)-dione (compound **7**) (1.25 g, 5.16 mmol) was completely dissolved in tetrahydrofuran (THF) (70mL). After adding phthalic anhydride (890 mg, 6 mmol), triethylamine (Et_3N) (1.39 mL, 10 mmol) was added to the solution. The reaction solution was refluxed for 2 days. The solvent was completely concentrated to give the crude product, and purified product was re-crystallized

to give final thalidomide product (compound **1**) as white solid (500 mg, 1.94 mmol, yield: 40%).

Molecular formula: $C_{13}H_{10}N_2O_4$; Molecular weight: 258.13 g/mol

Melting point: 275 – 276 °C;

R_f = 0.22 (Dichloromethane/acetone = 5:1)

IR: 3191 cm^{-1} & 3097 cm^{-1}, C=C-H, sp^2; 1693 cm^{-1} C=O; 1610 cm^{-1}, 1470 cm^{-1}, 1435 cm^{-1} aromatic overtone; 1383 R-C=O; 1257 cm^{-1} C-O

^{1}H NMR (DMSO-*d*6) δ = 11.14 (s, 1H, NH), 7.97 - 7.88 (dd, 4H, Ar-H), 5.19 - 5.15 (dd, 1H, *J* = 12.8 Hz & *J* = 5.3 Hz, 3'-H), 2.95-2.86 (ddd, *J* = 17.1 Hz, *J* = 13.6 Hz and *J* = 5.1 Hz, 1H, 5'-H_A), 2.64-2.50 (m, 2H, 4'-H_A, 5'-H_B), 2.11-2.05 (m, 1H, 4'-H_B) ppm;
^{13}C NMR (DMSO-*d*6) δ = 173.2 (C-1' or C-2'or C-2), 170.3 (C-1'or C-2'or C-2), 167.6 (C-1'or C-2'or C-2), 135.3 (Ar-CH), 131.7 (Ar-CH), 123.9 (Ar-CH), 49.4 (C-3'), 31.4 (C-5'), 22.4 (C-4') ppm

The spectral data were in accordance with those reported in literature (Luzzio *et al.*, 2003; Varala *et al.*, 2005).

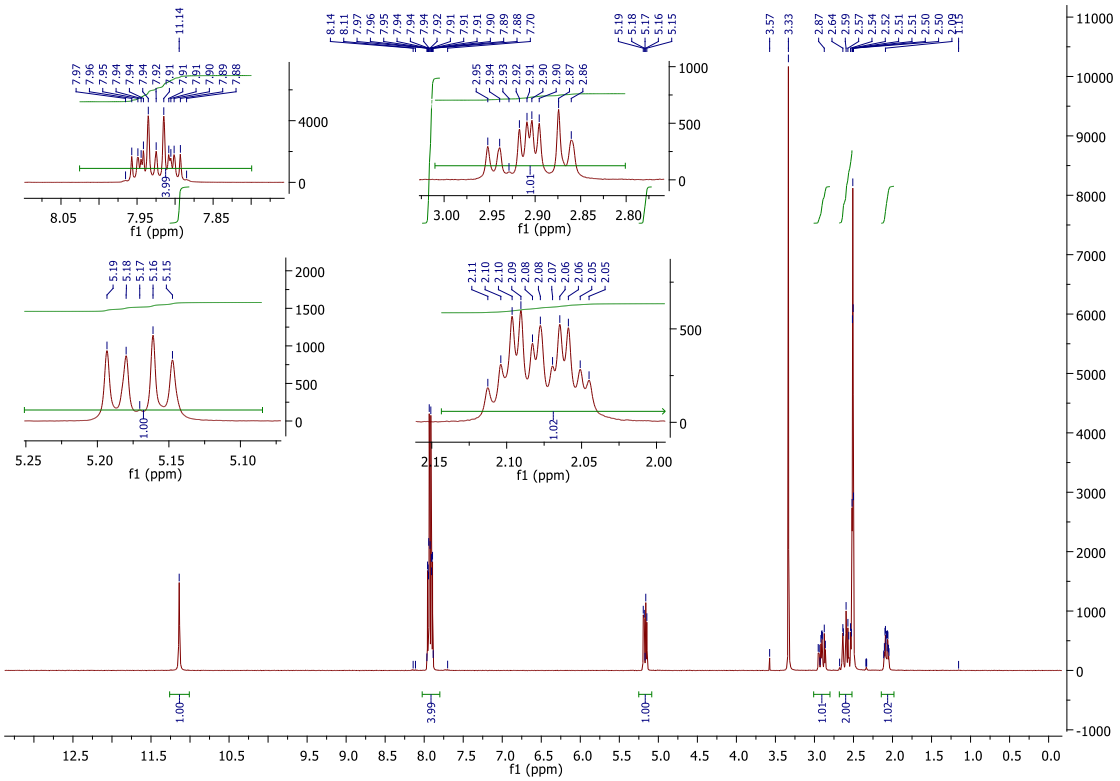

Figure 21: ^{1}H NMR for 2-(2,6-dioxopiperidin-3-yl)isoindole-1,3-dione, thalidomide (Compound **1**)

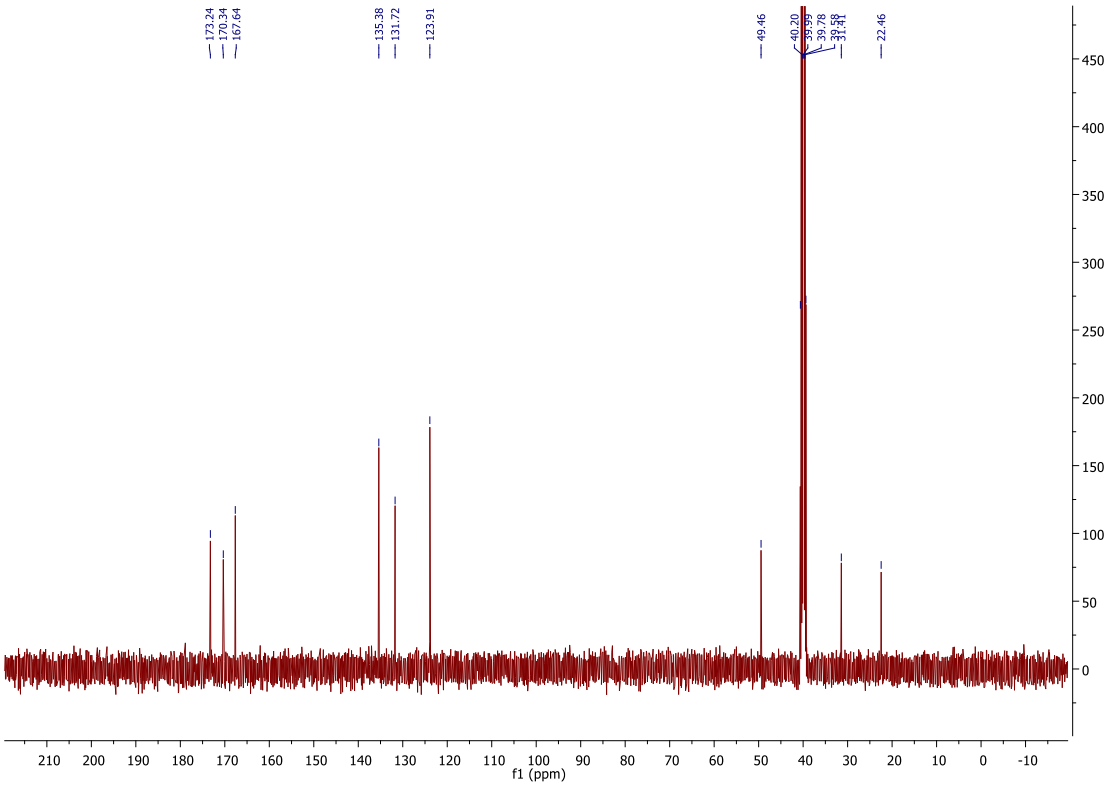

Figure 22: ^{13}C NMR for 2-(2,6-dioxopiperidin-3-yl)isoindole-1,3-dione, thalidomide (Compound **1**)

The salient characterization data of thalidomide is described and discussed in detail in order to aid subsequent analyses for other thalidomide analogues.

The ^{1}H NMR spectrum of thalidomide (Figure 21) shows a characteristic singlet in the far downfield region at δ = 11.14 ppm which can be assigned to the acidic glutarimide NH proton. The centrosymmetric multiplet at δ = 7.97 – 7.88 ppm, resulting from the four aromatic protons, clearly shows an AA'BB' pattern which is typical of ortho disubstituted benzenes. The *N*-methine proton (3'-H) resonates as a doublet of doublets at δ = 5.19 - 5.15 ppm with *J* = 12.8 Hz and *J* = 5.3 Hz, due to the axial-axial and axial-equatorial couplings with the diastereotopic 4'-H protons. The larger coupling constant arises from axial-axial coupling with one of the 4'-H protons, whereas the smaller coupling constant is due to the axial-equatorial coupling of the second 4'-H proton. The upfield region shows a distinct doublet of doublets (dd) at δ = 2.95 – 2.86 ppm with *J* = 17.1 Hz, *J* = 13.6 Hz and *J* = 5.1 Hz. The two larger coupling constants arise from germinal coupling and aa-coupling with one of the adjacent 4'-H protons, respectively. The smaller coupling constant is due to ae-coupling with the second 4'-H proton. The smaller coupling constant is due to ae-coupling with the second 4'-H proton. The complex multiplet at δ = 2.64 – 2.50 ppm stems from two overlapping signals from one of each of the diastereotopic 4'-H and 5'-H protons (4'-H_A and 5'-H_B). Likewise, the multiplet resonating at δ = 2.11 – 2.05 ppm was assigned to 4'-H_B.

The ^{13}C NMR spectrum (Figure 22) of thalidomide shows three peaks in the far downfield region (δ = 173.2, 170.3 and 167.6 ppm) typical of a carbonyl group arising from both a phthalic ring and a glutarimide ring. Thalidomide is a centrosymmetric structure of a phthalic ring, with two carbonyl groups on C-1 and C-2 sharing chemical environment. There are also two carbonyl groups on the glutarimide ring. These peaks at δ = 173.2, 170.3 and 167.6 ppm were assigned to those carbons of the carbonyl group. Another further downfield region at δ = 135.3 ppm, 131.7 ppm, and 123.9 ppm contains three unique carbon chemical environments for carbons on the aromatic ring of the phthalic ring due to a symmetric system. The three peaks were assigned to these three carbon environments. Due to the close proximity of the amide group, the region at δ = 49.4 ppm was assigned to be C-3'. The upfield regions at δ = 31.4 and δ = 22.4 ppm were ascribed to the resonance of C-4' and C-5' nuclei.

Scheme 2: Synthesis of 2-(2,6-dioxopiperidin-3-yl)-phthalimidine (EM-12) (Compound 2)

The synthetic method of Scheme 2 (Figure 23) was based on predominantly the structural similarity referenced from the contribution of Luo and co-workers (Luo et al., 2011), and depends on the coupling between a phthaldialdehyde and a glutarimide ring. The potential mechanism of this one-spot reaction involved addition, rearrangement and elimination reactions (Luo et al., 2011).

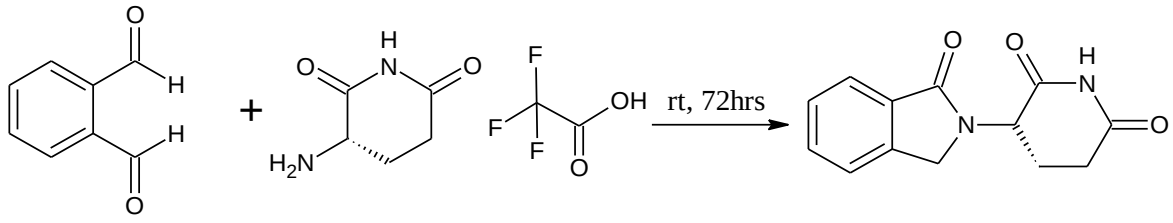

Compound **7** Compound **2**

Figure 23: (a) N_2 condition, room temperature, 71 hrs

Preparation of 2-(2, 6-dioxopiperidin-3-yl)-phthalimidine (EM-12) (Compound 2)

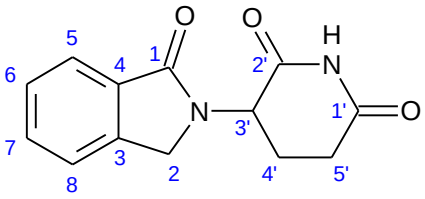

The crude product, 2-(2-oxo-6-thioxo-3-piperidinyl)-1*H*-isoindole-1,3(2*H*)-dione (compound **7**) (950 mg, 3.92 mmol) was dissolved in tetrahydrofuran (THF) (327 mL). Phthaldialdehyde (526 mg, 3.92 mmol) was then added into the reaction solution. The reaction mixture was stirred constantly for 71 hours. All the solvent was completely concentrated, and the crude product was purified with silica gel chromatography to obtain the final purifed product (compound **2**). The solvent system used for purification was actonitrile : dichloromethane (6 : 4) to give purified compound 2 as the brown solid (450 mg, 1.83 mmol, yield: 47%).

Molecular formula: $C_{13}H_{12}N_2O_3$; Molecular weight: 244.25 g/mol;

Melting point: 237 – 238 °C;

R_f = 0.22 dichloromethane/acetone = 5:1;

IR: 3191 cm^{-1} & 3097 cm^{-1}, C=C-H, sp^2; 1693 cm^{-1} C=O; 1610 cm^{-1}, 1470 cm^{-1}, 1435 cm^{-1} aromatic overtone; 1383 R-C=O;

^{1}H NMR (CD_3OD) δ = 7.77-7.75 (d, *J* = 7.5 Hz, 1H, Ar-H), 7.66 – 7.61 (t, *J* = 9.5 Hz & 7.5, 1H, Ar-H), 7.59 – 7.57 (d, *J* = 7.5 Hz, 1H, Ar-H), δ = 7.77-7.75 (d, *J* = 7.9 & 7.5, 1H, Ar-H), 5.16 - 5.11 (dd, *J* = 13.5 Hz & *J* = 5.1 Hz, 1H, 3'-H), 4.50 – 4.32 (dd, *J* = 26.4 Hz & *J* =17.2 Hz, 2H, 2-H), 2.98-2.89 (ddd, *J* = 17.4 Hz, *J* = 15.7 Hz & *J* = 5.4 Hz, 1H, 5'-H), 2.63-2.59 (m, 1H, 5'-H), 2.47-2.37 (m, 1H, 4'-H), 2.07-1.99 (m, 2H, 4'-H) ppm;

^{13}C NMR (CD_3OD) δ = 173.3 (C-1 or C-1' or C-2'), 171.5 (C-1 or C-1' or C-2'), 168.5 (C-1 or C-1' or C-2'), 142.5 (Ar-CH), 132.2 (Ar-CH), 132.1 (Ar-CH), 128.4 (Ar-CH), 124.0 (Ar-CH), 123.4 (Ar-CH), 52.0 (C-2 or C-3'), 47.6 (C-2 or C-3'), 31.6 (C-4'or C-5'), 22.9 (C-4' or C-5') ppm.

The spectral data were in accordance with those reported in literature (Luzzio *et al.*, 2003).

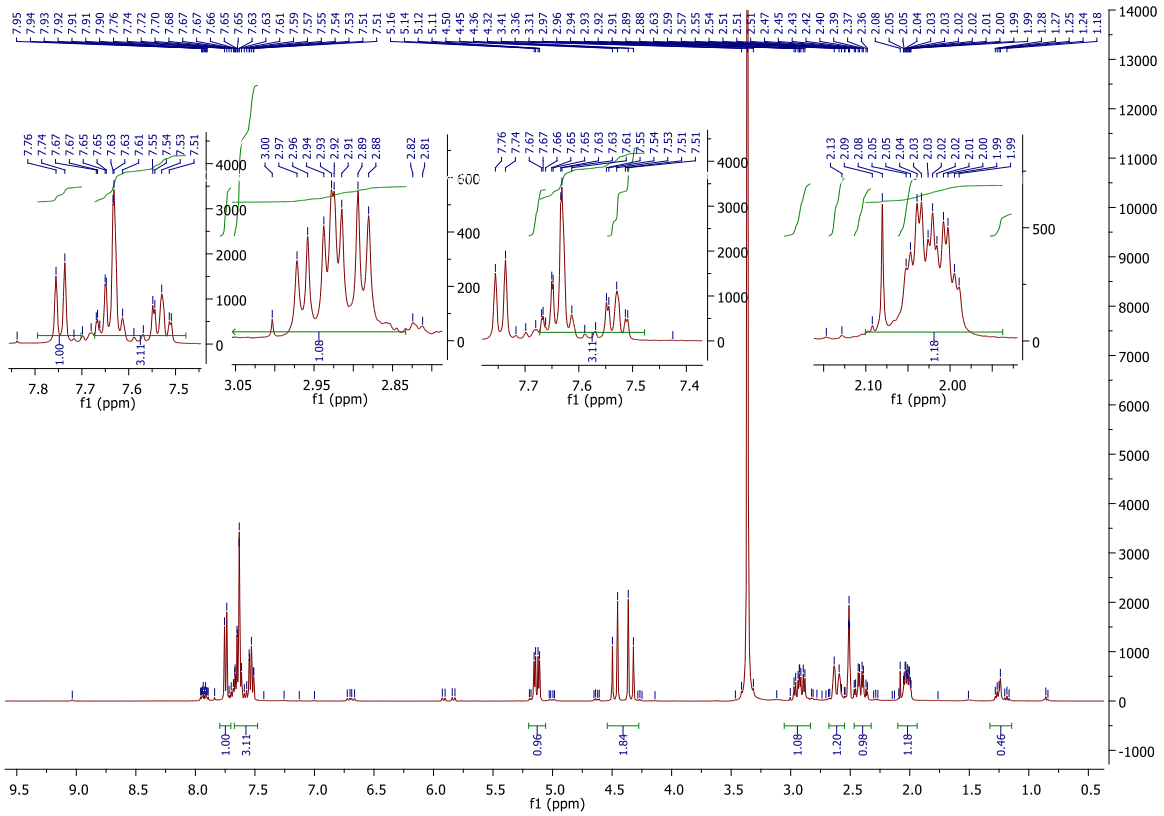

Figure 24: ^{1}H NMR for 2-(2,6-dioxopiperidin-3-yl)-phthalimidine (EM-12) (Compound **2**)

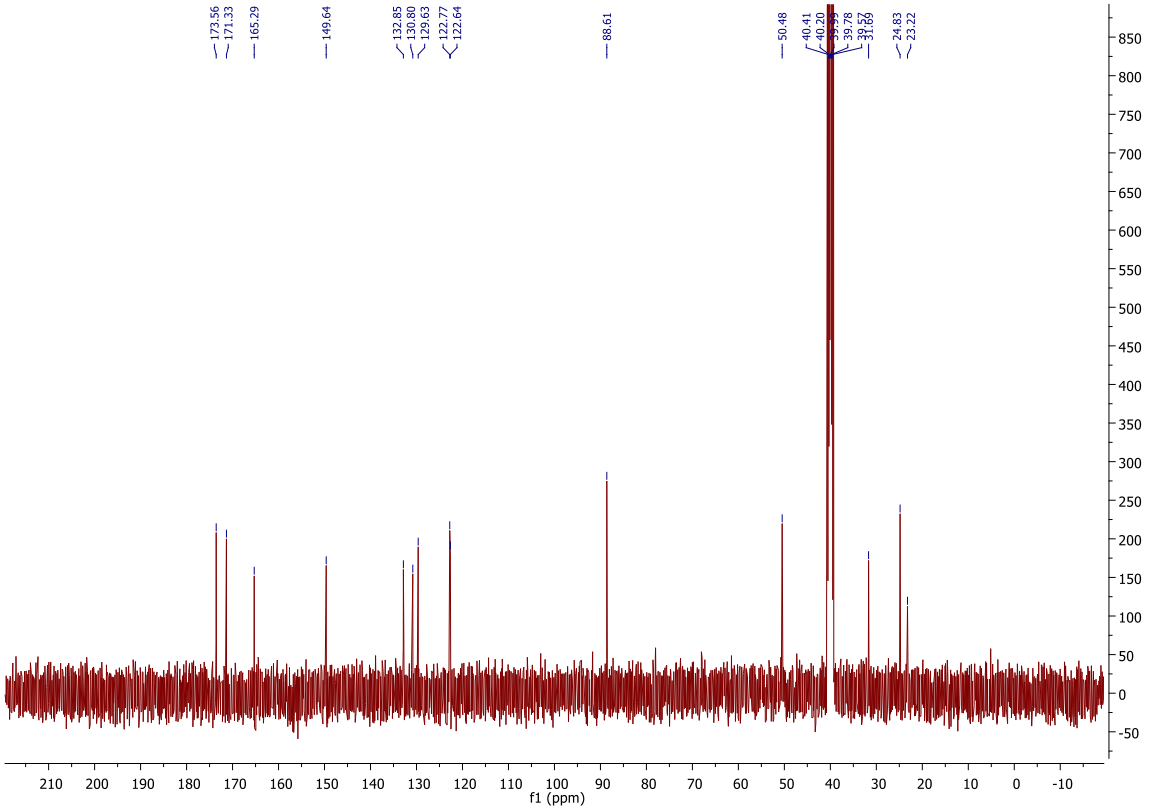

Figure 25: ^{13}C NMR 2-(2,6-dioxopiperidin-3-yl)-phthalimidine (EM-12) (Compound **2**)

The ^{1}H NMR spectrum (Figure 24) of the compound **2** shows the aromatic system of a phthalic ring in the far downfield region around δ = 7.80 to δ =7.50 ppm. The benzene ring of the phthalic ring does not exhibit a centrosysmmetic structure. There are four protons shown on the benzene ring with ortho, meta and para effects occurring between the protons. A characteristic a doublet of doublet in the downfield region at δ = 7.77 – 7.75 ppm with *J* = 7.5 Hz and δ = 7.59 – 7.57 ppm with *J* = 7.5 Hz can be assigned to either the 5-H or 8-H protons due to the effects of coupling-coupling from ortho or meta positions. Both 6-H and 7-H protons resonate as a doublet of triplet at δ = 7.66 – 7.61 ppm with *J* = 9.5 Hz and 7.5 Hz, and δ = 7.55 – 7.51 ppm with *J* = 7.9 Hz and 7.5 Hz. The observed effects are caused by meta and ortho coupling effects from the two sides. The *N*-methine proton (3-H) resonates as a doublet of doublet at δ = 5.16 – 5.11 ppm with *J* = 13.5 Hz and *J* = 5.1 Hz, and can be assigned to 3'-H due to the axial-axial and axial-equatorial couplings with the diastereotopic 4'-H protons as well as proximity to the amide proton. The region at δ = 4.50 – 4.32 ppm showed a doublet of doublet (AB system) with *J* = 26.4 Hz and 17.2 Hz can be assigned as the 2-H. The region at δ = 2.97 – 2.88 ppm showed a doublet of doublet of doublet with *J* = 17.4 Hz, *J* = 15.7 Hz and *J* = 5.4 Hz which can be assigned as the 5'-H. The two larger coupling constants arise from germinal coupling and axial-axial coupling with one of the adjacent 4'-H protons. The smaller coupling constant is due to axial-equatorial coupling with the second 4'-H proton. As expected, the germinal 5'-H proton was assigned to the adjacent a doublet of doublet of doublet at δ = 2.63 – 2.59 ppm, caused by germinal coupling, equatorial-axial coupling and equatorial-equatorial coupling, however, this coupling effect was not shown very clearly in the spectrum results. Both vicinal 4'-H protons resonate as a complex multiplets at δ = 2.47 – 2.37 ppm and δ = 2.05 – 1.99 ppm.

The ^{13}C NMR spectrum (Figure 25) shows three peaks in the far downfield region δ = 173.3, 171.5 and 168.5 ppm typical of a carbonyl group arising from the C-1, C-1' & C-2' nuclei. EM-12 does not react well the thalidomide with centrosymmetic structure, and the EM-12 structure has a six-carbon environment on the benzene ring of the phthalimide ring. The six peaks at δ = 142.5 ppm, 132.2 ppm, 132.1 ppm, 128.4 ppm, 124.0 ppm, and 123.4 ppm were assigned to the aromatic benzene ring. Due to presence of an adjacent amide position, the two peaks at δ = 52.0 ppm and 47.6 ppm were ascribed to resonance of the C-2 and C-3'

nuclei. The aliphatic region of the spectrum displays peaks at 31.6 and 22.9 ppm which were ambiguously ascribed to C-4' and C-5'.

Scheme 3: Synthesis of 3-[(1*R*)-1-hydroxy-1-methyl-3-oxo-1,3-dihydro-2*H*-isoindol-2-yl]piperidine-2,6-dione (Compound 3) & 3-[(1*S*)-1-hydroxy-1-methyl-3-oxo-1,3-dihydro-2*H*-isoindol-2-yl]piperidine-2,6-dione (Compound 4)

The reaction scheme 3 (Figure 26) of this synthesis contains two steps. Step 1 is to activate the carbonyl group of 2-acetylbenzoic acid with thionyl chloride, by changing the hydroxy group to a chloride group as a good leaving group in compound **8**. Compound **8** is a highly reactive compound and immediately proceeded in Step 2 of the synthesis. In Step 2, the primary amine of the glutarimide ring found in compound **7** can attack the carbonyl group with chloride. This carbon is more electro-positive, so that it is more reactive compared to a carbonyl group of a ketone. A second amide structure was generated as a result, and the lone pair of electrons on the nitrogen could attack the carbonyl group of the ketone to finalize the formation of a closed-ring structure.

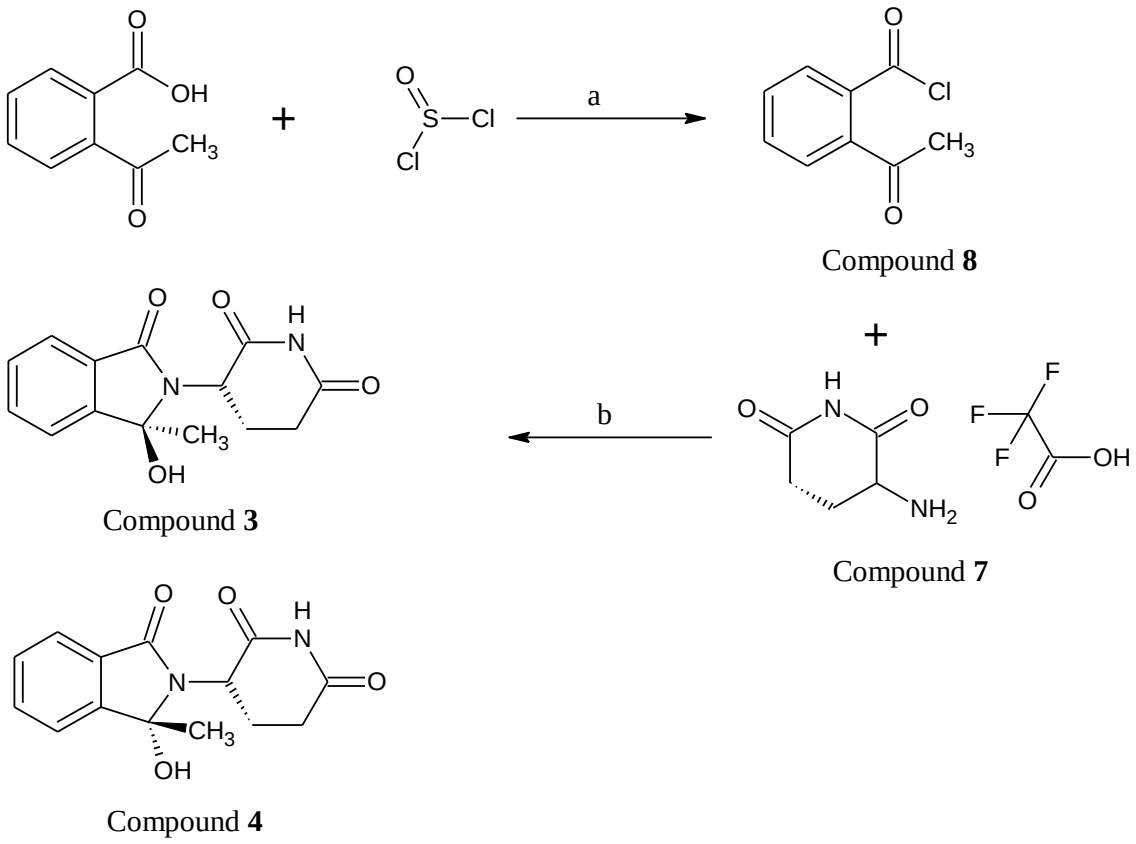

Figure 26: Reagents and conditions: (a) room temperature, 10 hours; (b) triethylamine

Preparation of 2-acetylbenzoic chloride (Compound 8)

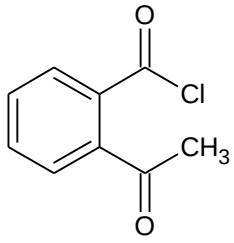

The synthesis method for step 1 was carried out according to published methodologies (Han, 2009; Jin-Guo, 2008). 2-Acetylbenzoic acid (1.64 g, 10 mmol) was mixed with thionyl chloride (3 mL) for 10 hours at room temperature. While still at room temperature, *n*-hexane was added to the reaction solution, and excess thionyl chloride was removed under reduced pressure. Without further purification, the product was used in Step 2.

Preparation of 3-[(1*R*)-1-hydroxy-1-methyl-3-oxo-1,3-dihydro-2*H*-isoindol-2-yl]piperidine-2,6-dione (Compound 3) & 3-[(1*S*)-1-hydroxy-1-methyl-3-oxo-1,3-dihydro-2*H*-isoindol-2-yl]piperidine-2,6-dione (Compound 4)

Following its preparation, compound **7** (350 mg, 1.45 mmol) was dissolved in dimethylformamide (10 mL). 2-Acetylbenzoic chloride (compound 8) (264 mg, 1.45 mmol) prepared from the step above, was dissolved in dimethylformamide (5 mL), and was carefully mixed with compound **7**. Triethylamine (1.02 mL, 7.25 mmol) was then added to the reaction. This reaction was contantly stirred for 18 hours at room temperature. After the reaction was completed, an appropriate amount of distilled water was added into the mixture to stop the reaction. The entire solution was extracted with equal volumes of ethyl acetate, repeated three times. All organic phases were combined and extracted with saturated sodium chloride, and dried with anhydrous magnesium sulfate. After drying, all solvent was completely concentrated under vacumm in reduced pressure, to obtain the crude product. Silica gel chromatography with a solvent system of ethyl acetate : hexane = 2:1 was applied to remove impurities from the final product to give purified compound 3 as white solid (61.4 mg, 0.224 mmol, yield: 10%); to give purified compound 4 (92.1 mg, 0.336 mmol, yield: 15%).

Results for 3-[(1*R*)-1-hydroxy-1-methyl-3-oxo-1,3-dihydro-2*H*-isoindol-2-yl]piperidine-2,6-dione (Compound 3)

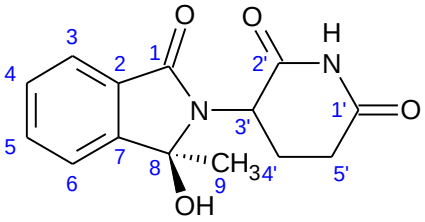

Molecular formula: $C_{14}H_{14}N_2O_4$; Molecular weight: 274.27 g/mol

Melting point: 242 – 243 °C; $[\alpha]_D^{20}$ = -16.79 (DMSO)

R_f = 0.3 Ethyl acetate : Hexane = 2:1

LRMS (Result showed in Appendix II) Found: M^+: 273.2000; HRMS (Result showed in Appendix II) Found (EI): $(M + Na)^+$, 297.0846, $C_{14}H_{14}N_2NaO_4$ requires 297.2598;

IR: 3244 cm^{-1} -OH; 1682 cm^{-1} C=O; 1609 cm^{-1}, 1571 cm^{-1}, 1494 cm^{-1}, 1468 cm^{-1}, 1429.49cm^{-1} aromatic overtone; 1358 R-C=O; 1254 cm^{-1} C-O

^{1}H NMR (DMSO) δ = 7.68-7.50 (ddd, *J* = 7.1Hz & *J* = 1.9 Hz, 3H, Ar-H), 7.55 - 7.50 (td, *J* = 7.1 Hz & *J* = 1.9 Hz, 1H, Ar-H), 6.42 (s, 1H, -NH), 4.63-4.59 (dd, *J* = 13.1 Hz & *J* = 4.9 Hz, 1H, 3'-H), 2.93-2.84 (ddd, *J* = 17.9 Hz, *J* = 15.1 Hz & *J* = 4.8, 1H, 5'-H_A), 2.64-2.54 (m, 1H, 4'-H_A, 5'-H_B), 2.00-1.94 (m, 1H, 4-H_B), 1.61(d, 3H, 9-H) ppm;

^{13}C NMR (DMSO) δ = 173.5 (C-1 or C-1' or C-2'), 171.3 (C-1 or C-1' or C-2'), 166.2 (C-1 or C-1' or C-2'), 149.6 (Ar-CH), 132.8 (Ar-CH), 130.8 (Ar-CH), 129.6 (Ar-CH), 122.7 (Ar-CH), 122.6 (Ar-CH), 88.6 (C-8), 50.4 (C-3'), 31.5 (C-5'), 24.8 (C-9), 23.2 (C-4') ppm.

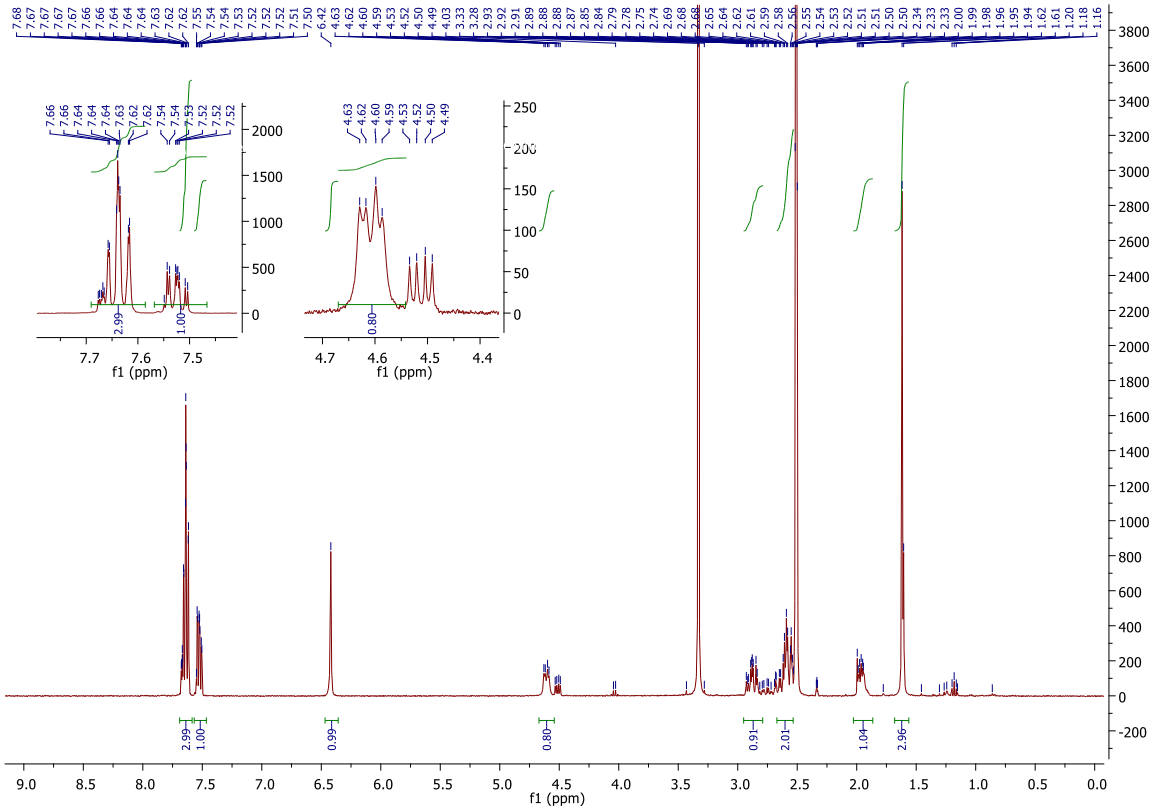

Figure 27: ^{1}H NMR for 3-[(1R)-1-hydroxy-1-methyl-3-oxo-1,3-dihydro-2H-isoindol-2-yl]piperidine-2,6-dione (Compound **3**).

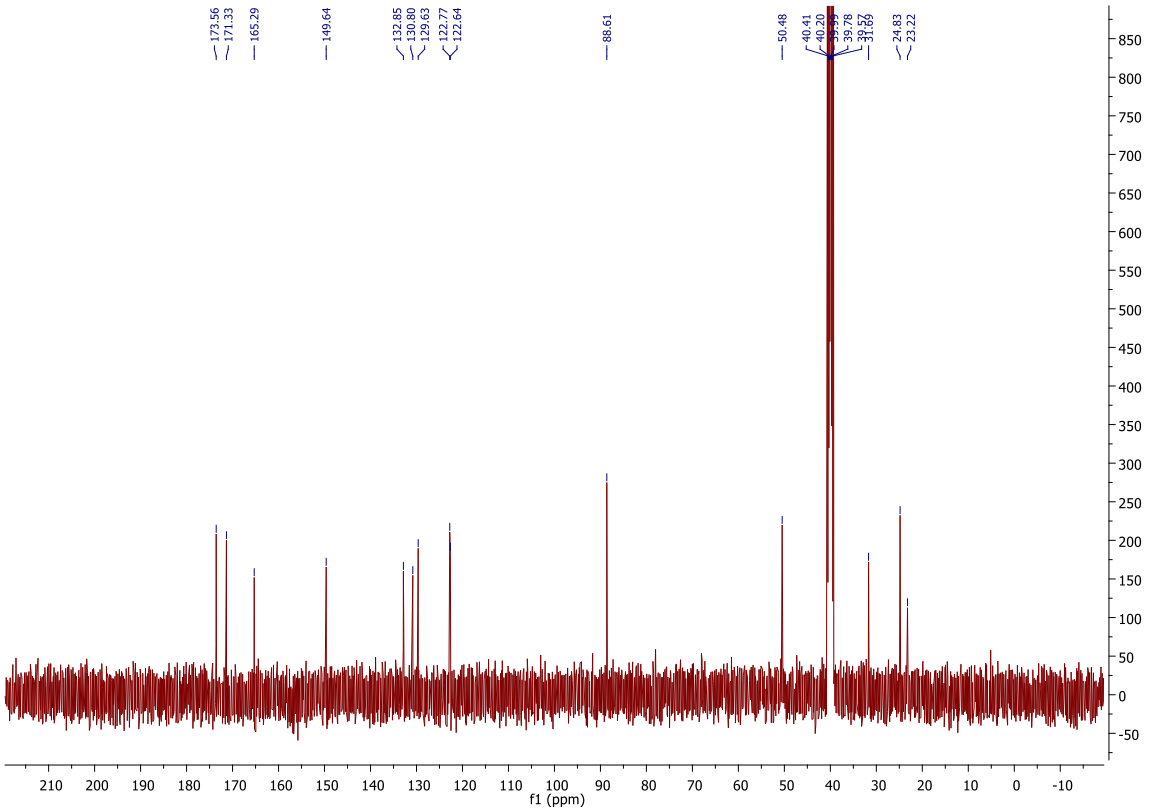

Figure 28: ^{13}C NMR for 3-[(1R)-1-hydroxy-1-methyl-3-oxo-1,3-dihydro-2H-isoindol-2-yl]piperidine-2,6-dione (Compound **3**).

The ^{1}H NMR spectrum (Figure 27) of the compound shows the aromatic system of the phthalic ring in the far downfield region around δ = 7.68 to δ = 7.50 ppm. For the benzene ring of the phthalic ring, there is no centrosysmmetic structure. There are four protons on the benzene ring which demonstrate ortho, meta and para effects between each other. The region at δ = 7.68 – 7.62 ppm showed a doublet of doublet of doublet with *J* = 8.7 Hz, 7.2 Hz and 1.51 Hz for 4-H and 5-H proton from both sides. Both 3-H and 6-H protons resonate as a doublet of triplet at δ = 7.52 – 7.50 ppm, with *J* = 8.2 Hz and 7.9 Hz and δ = 7.49 – 7.39 ppm with *J* = 8.6 Hz and 8.2 Hz, caused by meta and ortho coupling effects from both sides. The region at δ = 6.42 ppm resonates as a broad singlet, which was designated as an NH group in the NMR amide region. The *N*-methine proton (3-H) resonates as a doublet of doublet at δ = 4.63 – 4.59 ppm with *J* = 13.1 Hz and *J* = 4.9 Hz. The proton can be assigned as 3'-H due to the axial-axial and axial-equatorial couplings with the diastereotopic 4'-H protons as well as

proximity to the amide proton. The region at δ = 2.93 – 2.84 ppm shows a doublet of doublet of doublet, and was assigned to 5'-H with *J* = 17.9 Hz, *J* = 15.1 Hz and *J* = 4.8 due to germinal coupling, axial-axial coupling and axial-equatorial coupling with one of the 4'-H proton. The two large coupling values was caused by axial-axial coupling, and the small coupling constant caused by axial-equatorial coupling. The region at δ = 2.97 – 2.88 ppm showed a multiplet which can be assigned as 5'-H. Both vicinal 4'-H proton resonate as more complex multiplets at δ = 2.64 – 2.54 ppm and δ = 2.00 – 1.94 ppm, and showed a multiplet which was ambiguously assigned as C-4' and C-5' nuclei respectively. A more intense peak at δ = 1.62 ppm resonated as a singlet, which was assigned as 9-H.

The ^{13}C NMR spectrum (Figure 28) shows three peaks in the far downfield region (δ = 173.5, 171.3 and 165.2 ppm), typical of a carbonyl group arising from the C-1, C-1' & C-2' nuclei. The six peaks at δ = 149.6 ppm, 132.8 ppm, 130.8 ppm, 129.6 ppm, 122.7 ppm, and 122.6 ppm were assigned for the six carbons of the aromatic benzene ring. Due to the presence of an amide in an adjacent position, the regional peak at δ = 88.61 ppm was ascribed to resonance of C-8 and the regional peak at δ = 50.4 ppm was ascribed to resonance of the C-3' nuclei. The aliphatic region of the spectrum displays peaks at 31.6, 24.8 and 23.2 ppm which were ambiguously ascribed to C-4', C-5' and C-9.

Results for 3-[(1*S*)-1-hydroxy-1-methyl-3-oxo-1,3-dihydro-2*H*-isoindol-2-yl]piperidine-2,6-dione (Compound 4)

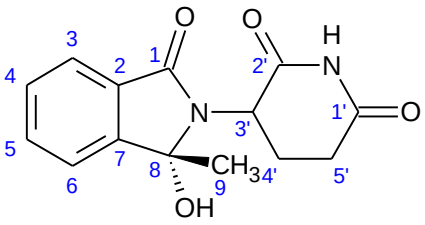

Molecular formula: $C_{14}H_{14}N_2O_4$; Molecular weight: 274.27 g/mol

Melting point: 237 – 238 °C; $[\alpha]_D^{20}$ = -22.40 (DMSO);

R_f = 0.3 Ethyl acetate : Hexane = 2:1

LRMS (Result showed in Appendix II) Found: M^+: 273.2000; HRMS (Result showed in Appendix II) Found (EI): $(M + Na)^+$, 297.0846, $C_{14}H_{14}N_2NaO_4$ requires 297.2598;

IR: 3396 cm^{-1} -OH; 1669 cm^{-1} C=O; 1468 cm^{-1}, 1414 cm^{-1} aromatic overtone; 1317, R-C=O; 1254 cm^{-1} C-O

^1H NMR (DMSO) δ = 7.66-7.62 (m, 2H, Ar-H), 7.54 - 7.50 (m, 2H, Ar-H), 6.42 (s, 1H, -NH), 4.63-4.59 (dd, 1H, 3'-H), 2.89-2.84 (m, 1H, 5'-H_A), 2.65-2.53 (m, 1H, 4'-H_A, 5'-H_B), 2.00-1.94 (m, 1H, 4'-H_B), 1.62-1.60 (d, 3H, 9-H) ppm;

^{13}C NMR (DMSO) δ = 173.3 (C-1 or C-1' or C-2'), 171.5 (C-1 or C-1' or C-2'), 163.5 (C-1 or C-1' or C-2'), 142.5 (Ar-CH), 132.2 (Ar-CH), 132.1 (Ar-CH), 128.4 (Ar-CH), 124.0 (Ar-CH), 123.4 (Ar-CH), 88.6 (C-8), 52.0 (C-3'), 47.8 (C-5'), 31.5 (C-9), 22.9 (C-4') ppm.

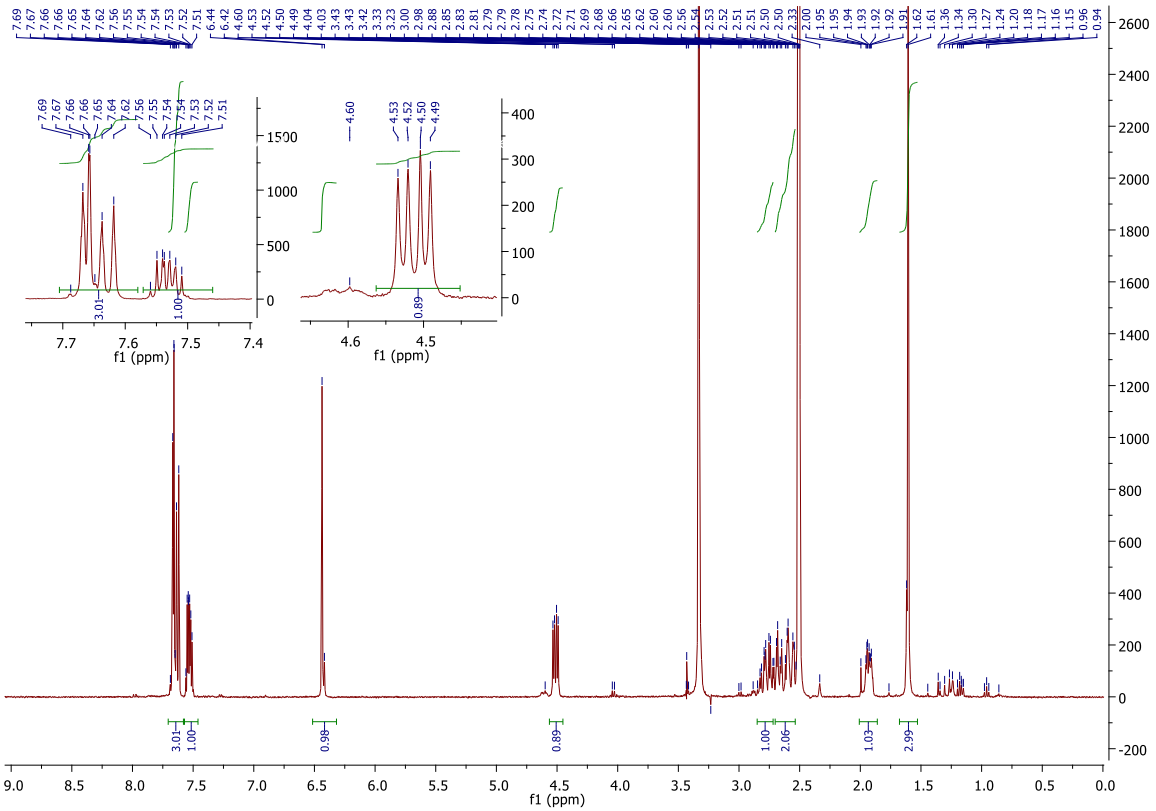

Figure 29: ^1H NMR for 3-[(1S)-1-hydroxy-1-methyl-3-oxo-1,3-dihydro-2H-isoindol-2-yl]piperidine-2,6-dione (Compound **4**).

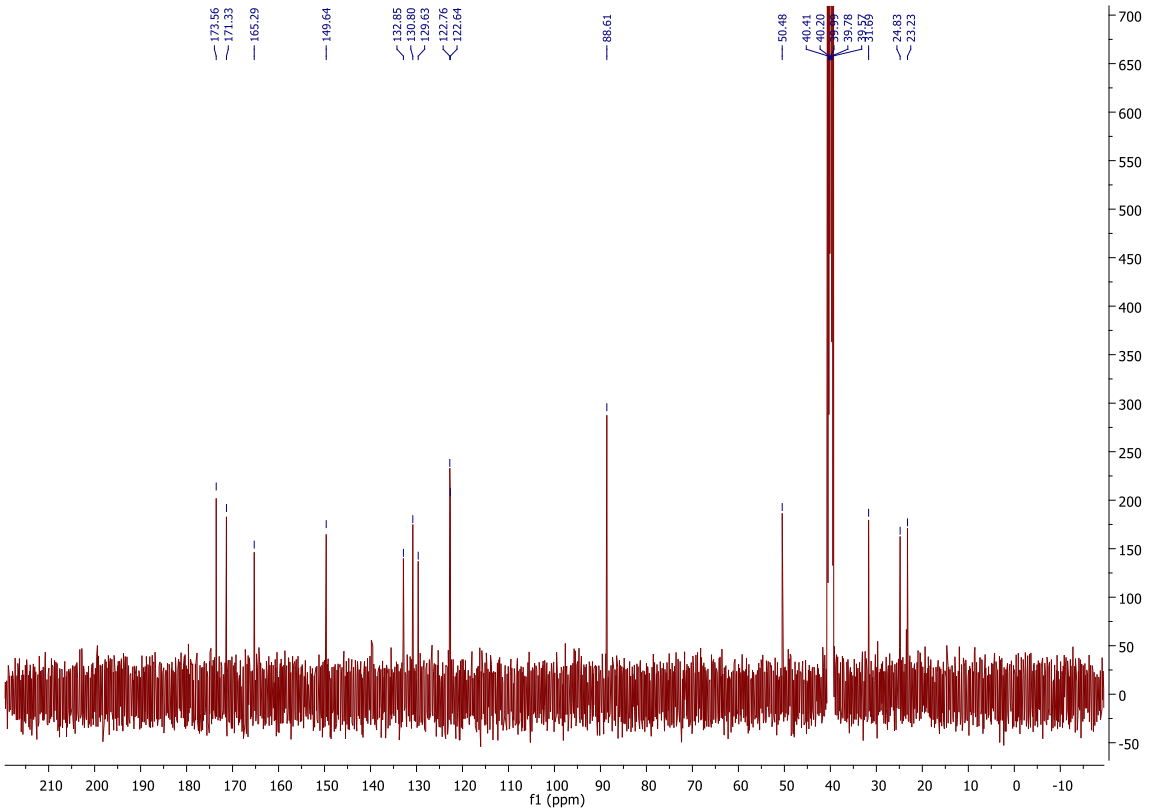

Figure 30: ^{13}C NMR for 3-[(1S)-1-hydroxy-1-methyl-3-oxo-1,3-dihydro-2H-isoindol-2-yl]piperidine-2,6-dione (Compound **4**).

The ^{1}H NMR spectrum (Figure 29) of the compound 4 shows about the aromatic system of the phthalic ring in the far downfield region around δ = 7.69 to δ =7.51 ppm. For the benzene ring of the phthalic ring, there is no a centrosysmmetic structure. There are four protons indicated on the benzene ring with ortho, meta and para effects occurring between each other. As expected, the region at δ = 7.69 – 7.62 ppm shows a doublet of doublet of doublet due to the effects of coupling-coupling from ortho and meta position for 4-H and 5-H protons. However, the peak in that region was not clearly shown in the spectrum. The region at δ = 7.56 – 7.51 ppm shows a multiplet from the effects of coupling-coupling due to ortho and meta positions for 3-H and 6-H. The region at δ = 6.44 ppm resonates a broad singlet, which was assigned as NH in the NMR amide region. The *N*-methine proton (3-H) resonates as a doublet of doublet at δ = 4.53 – 4.49 ppm with *J* = 11.64 Hz and *J* = 5.60 Hz which can be assigned as 3'-H due to the axial-axial and axial-equatorial couplings with the diastereotopic 4'-H protons and proximity of the amide proton. The region at δ = 2.93 – 2.84 ppm shows a

doublet of doublet of doublet was assigned as 5'-H, with J = 17.87 Hz, J = 15.10 Hz and J = 4.82 Hz due to germinal coupling, axial-axial coupling and axial-equatorial coupling with one of the 4'-H proton. The two large coupling values were caused by axial-axial coupling, and small coupling constant caused by axial-equatorial coupling. The region at δ = 2.78 – 2.68 ppm showed a multiplet which can be assigned as 5'-H. Both vicinal 4'-H protons resonate as more complex multiplet at δ = 2.65 – 2.56 ppm and δ = 1.95 – 1.91 ppm showed a multiplet was ambiguously assigned as 4'-H and 5'-H respectively. A more intense peak at δ = 1.62 ppm resonates as a singlet, which was assigned as 9-H.

The ^{13}C NMR spectrum (Figure 30) shows three peaks in the far downfield region (δ = 173.6, 171.3 and 165.3 ppm), typical of a carbonyl group arising from the C-1, C-1' & C-2' nuclei. The six peaks at δ = 149.6 ppm, 132.9 ppm, 130.8 ppm, 129.6 ppm, 122.8 ppm, and 122.6 ppm were assigned for the six carbons of the aromatic benzene ring. Due to the presence of an amide group in an adjacent position, the regional peak at δ = 88.6 ppm was ascribed to resonance of C-8 and the regional peak at 50.5 ppm was ascribed to resonance of the C-3' nuclei. The aliphatic region of the spectrum displays a peak at 31.7, 24.8 and 23.2 ppm which were ambiguously ascribed to C-4', C-5' and C-9.

Scheme 4: Synthesis of 2-(1-chloromethyl-2,6-dioxopiperidin-3-yl)phthalimidine (Compound 5)

The synthesis method of Scheme 4 (Figure 31) was predominantly based on the structural similarities referenced from (Luo et al., 2011). A hydromethyl group was added onto the glutarimide ring to obtain compound **9** by refluxing with formaldehyde solution. The hydroxyl group was then replaced by a chloride by mixing the solution with thionyl chloride to obtain compound **10**. The protecting group for the amine of compound **10** was removed under acidic conditions by adding trifluoroacetic acid, yielding Compound **11**. The amine structure was available for further reaction, and in the following step, phthaldialdehyde was coupled with compound **11** to produce compound **5**.

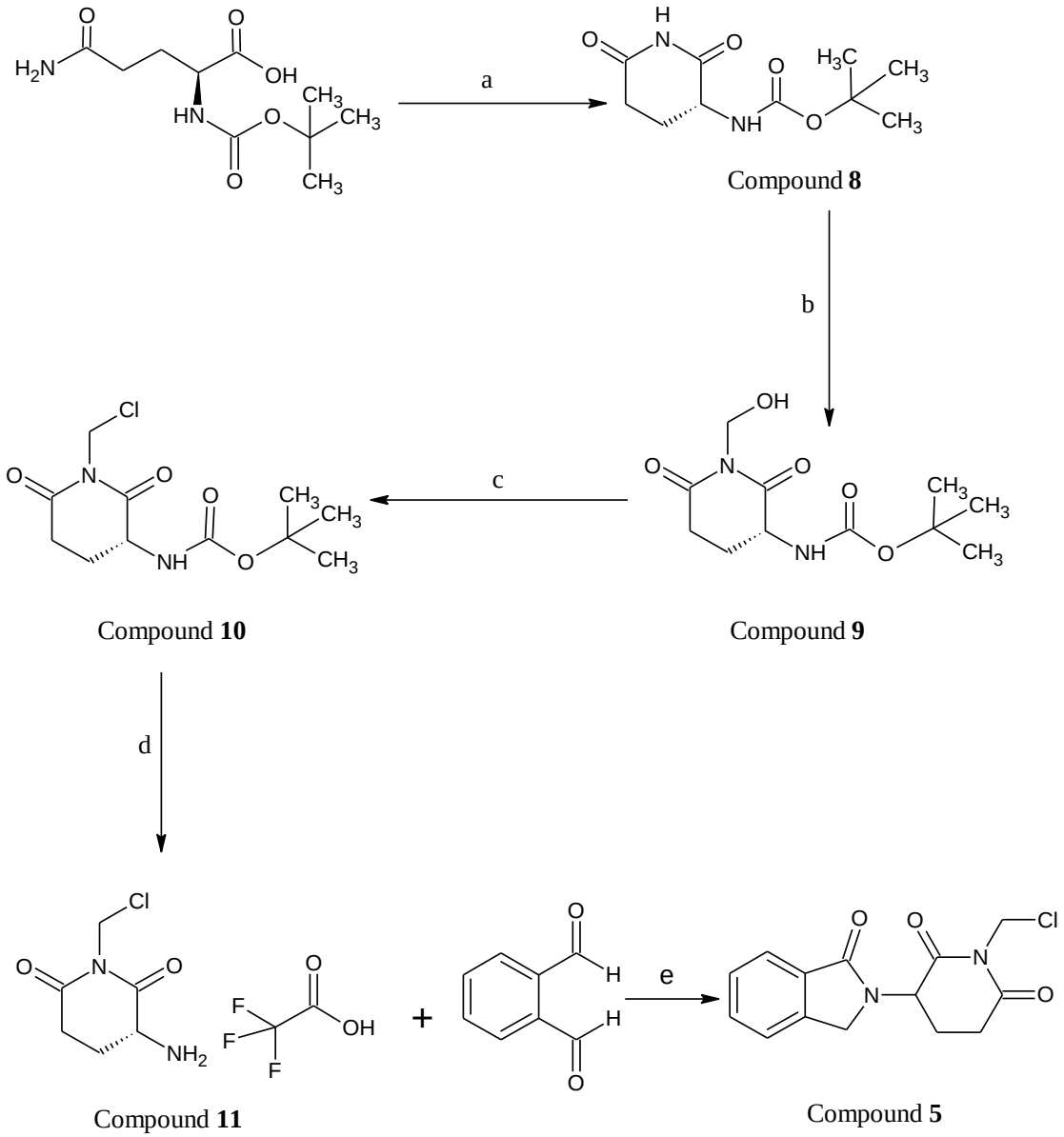

Figure 31: Reagents and conditions: (a) 1, 1'-carbonyldiimidazole (CDI) & tetrahydrofuran (THF); (b) formaldehyde (37% solution in water), N_2, reflux; (c) thionyl chloride, dimethylformamide; (d) trifluoroacetic acid, dichloromethane, N_2, room temperature, 22.5 hours; (e) phthaldialdehyde, tetrahydrofuran, N_2, room temperature, 71 hours; (f) 2-acetylbenzoic chloride, triethylamine, 18 hours

Preparation of 1-hydroxymethyl-3-(*tert*-butoxycarbonylamino)-2,6-dioxopiperidine (Compound 9)

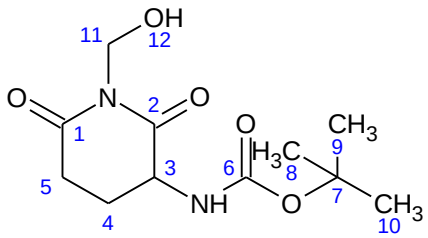

3-(*tert*-Butoxycarbonylamino)-2,6-dioxopiperidine (Compound **8**) (1g, 4.38 mmol) was added into formaldehyde (37% solution in water, 5.24 mL), and mixture was refluxed under an atmosphere of nitrogen with constant stirring. Once 3-(*tert*-butoxycarbonylamino)-2,6-dioxopiperidine was gradually dissolved in the reaction solution, the homogenate continued to stir for another half hour. After cooling, the condensor was completely removed from thereaction setup allowing a gradual overnight, precipitation of the product to come out of the solution. The precipitate was recrystallized with acetone to isolate the final product to give compound 9 as the white crystal (300 mg, 1.162 mmol, yield: 30%).

Molecular formula: $C_{11}H_{18}N_2O_5$; Molecular weight: 258.27 g/mol

Melting point: 216 – 217 °C;

IR: 3421 cm^{-1} -OH stretch; 2980 cm^{-1}, 2923 cm^{-1}, C=C-H sp^2 stretch; 1673 cm^{-1}, C=O stretch.

^{1}H NMR (DMSO-*d6*) δ = 7.31 – 7.29 (d, *J* = 7.23, 1H, -NH-), 6.04 (t, *J* = 10.37 Hz, 1H, -OH), 5.05-4.92 (m, *J* = 9.92 Hz & 9.37 Hz, 2H, 11-H), 4.42-4.35 (m, *J* = 10.96 Hz & *J* = 8.97 Hz, 1H, 3-H), 2.89-2.59 (m, 2H, 5-H), 1.99-1.83 (m, 2H, 4-H), 1.41 (s, 9H, 8-H, 9-H & 10-H) ppm;

^{13}C NMR (DMSO) δ = 172.1 (C-1 or C-2 or C-6), 171.9 (C-1 or C-2 or C-6), 155.8 (C-1 or C-2 or C-6), 78.5 (C-3), 62.7 (C-11), 51.3 (C-5), 31.6 (C-4), 28.5 (C-8, C-9 & C-10) and 23.6 (C-3) ppm.

The spectral data were in accordance with those reported by (Luo et al., 2011).

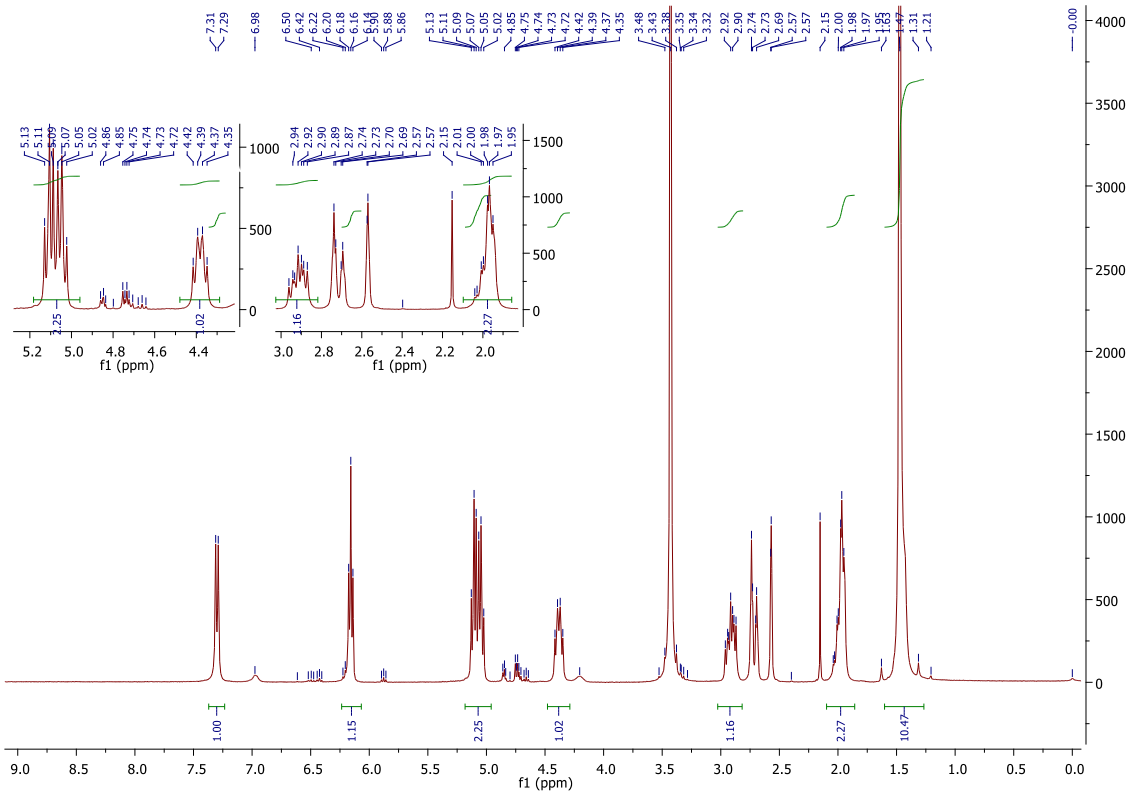

Figure 32: ^{1}H NMR for 1-hydroxymethyl-3-(tert-butoxycarbonylamino)-2,6-dioxopiperidine (Compound **9**).

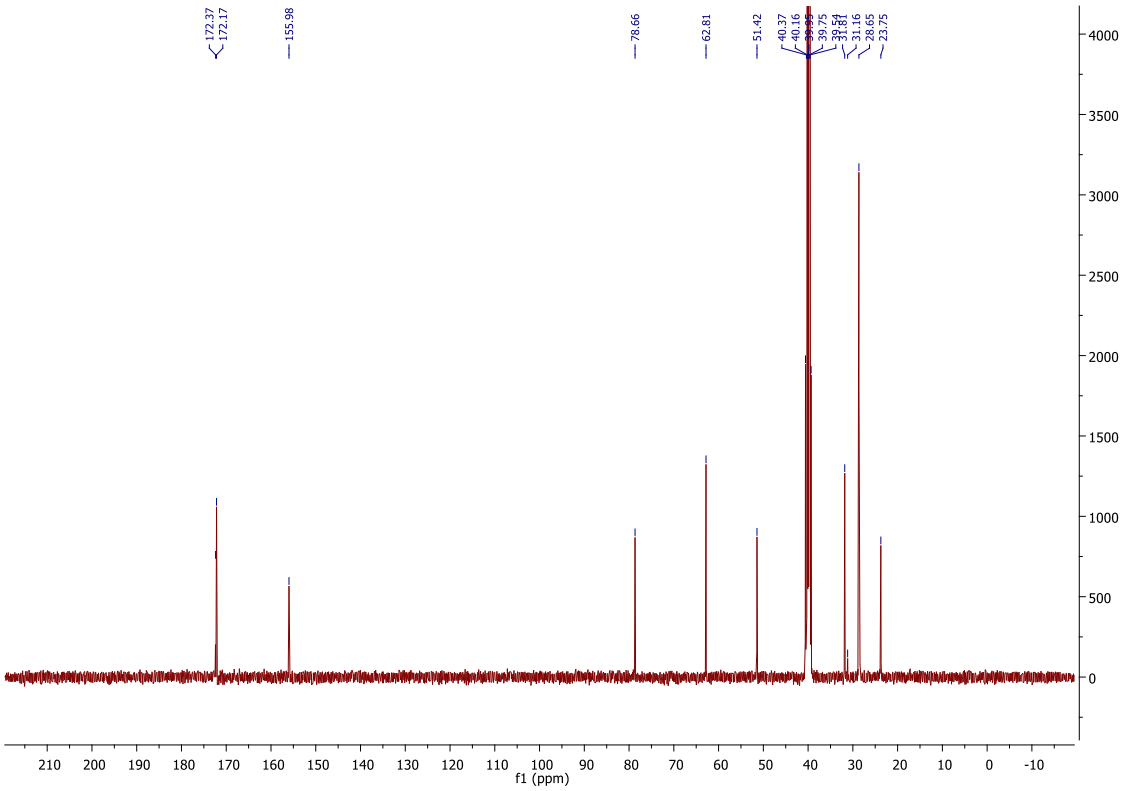

Figure 33: ^{13}C NMR for 1-Hydroxymethyl-3-(tert-butoxycarbonylamino)-2,6-dioxopiperidine (Compound **9**).

The ^{1}H NMR spectrum (Figure 32) of the compound **9** shows a characteristic doublet in the far downfield region at δ = 7.31 – 7.29 ppm. The doublet was assigned to the proton of the acidic glutarimide NH group 3-H, with *J* = 7.2 Hz due to the presence of a proton on the C-3 nuclei. Due to the presence of two neighboring protons, the region at δ = 6.22 – 6.14 ppm shows a typical triplet, and was assigned to the hydroxide group connected to C-11 with *J* = 10.4 Hz. The region at δ = 5.13 – 5.02 ppm showed up a typical triplet of doublet, and this was assigned to two protons on 11-H, with *J* = 9.9 Hz and *J* = 9.4 Hz. The *N*-methine proton (3-H) resonates as a doublet of doublets at δ = 4.42 – 4.35 ppm with *J* = 10.9 Hz and *J* = 8.9 Hz due to the axial-axial and axial-equatorial couplings with the diastereotopic 4-H protons and proximity of the amide. The complex multiplet at δ = 2.96 – 2.87 ppm and δ = 2.04 - 1.95 ppm were ambiguously assigned as 4-H and 5-H. Due to the proximity of a carbonyl group, there was a chemical shift for 5-H, with a singlet in the region at δ = 1.47 ppm. The singlet was assigned to 8-H, 9-H and 10-H, as all three possess the same chemical environment.

The ^{13}C NMR spectrum (Figure 33) shows three peaks in the far downfield region (δ = 172.38, 172.17, 155.98 ppm) typical of a carbonyl group arising from the C-1, C-2 & C-6 nuclei. The peak at δ = 78.63 ppm was ascribed to resonance of the C-3 nuclei due to the presence of a carbonyl group and an amide. The hydroxide group resulted in a chemical shift of C-11 with the region at δ = 62.81 ppm being assigned to resonance of C-11. The more intense peak at δ = 28.65 ppm was assigned to C-8, C-9, and C-10 nuclei. A less intense peak at δ = 23.75 ppm was assigned to C-7.

Preparation of 1-chloromethyl-3-(*tert*-butoxycarbonylamine)-2,6-dioxopiperidine (Compound 10)

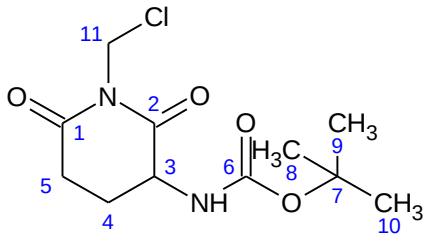

Compound **9** (250 mg, 0.968 mmol) was completely dissolved in dimethylformamide (5 mL) and placed in an ice bath until the mixture cooled to 0 °C. Thionyl chloride (0.192 mL, 2.643 mmol) was added dropwise to the solution. The solution was mixed continuously for 1 hour in ice bath conditions. The mixture (3 g) was then poured onto ice. The precipitate was isolated and was washed with ice water at pH 7. The crude product was re-crystallized with acetone to gather the final product to give compound 10 as the white crysal (237.5 mg, 0.858 mmol, yield: 96%).

Molecular formula: $C_{11}H_{17}N_2O_4$; Molecular weight: 276.72 g/mol

Melting point: 134 – 134.5 °C;

IR: 3305 cm^{-1} -NH stretch; 2971 cm^{-1}, 2915 cm^{-1} -C-H stretch; 1696 cm^{-1}, 1673 cm^{-1} –N-C=O amide stretch;

^{1}H NMR (DMSO-*d*6) δ = 7.35 – 7.33 (d, *J* = 7.6 Hz, 1H, -NH-), 5.48 (s, 2H, 11-H), 4.47 - 4.42 (dd, *J* = 12.1 Hz & *J* = 6.3 Hz, 1H, 3-H), 2.94 - 2.89 (m, 2H, 5-H), 1.99-1.92 (m, 2H, 4-H), 1.48 (s, 9H, 8-H, 9-H & 10-H) ppm;

^{13}C NMR (DMSO-*d*6) δ = 171.5 (C-1), 171.1 (C-2), 155.8 (C-6), 78.7 (C-3), 51.3 (C-11), 48.5 (C-5), 31.4 (C-4), 28.5 (C-7) and 23.3 (C-8, C-9 & C-10) ppm.

The spectral data were in accordance with those reported in the literature from (Luo et al., 2011).

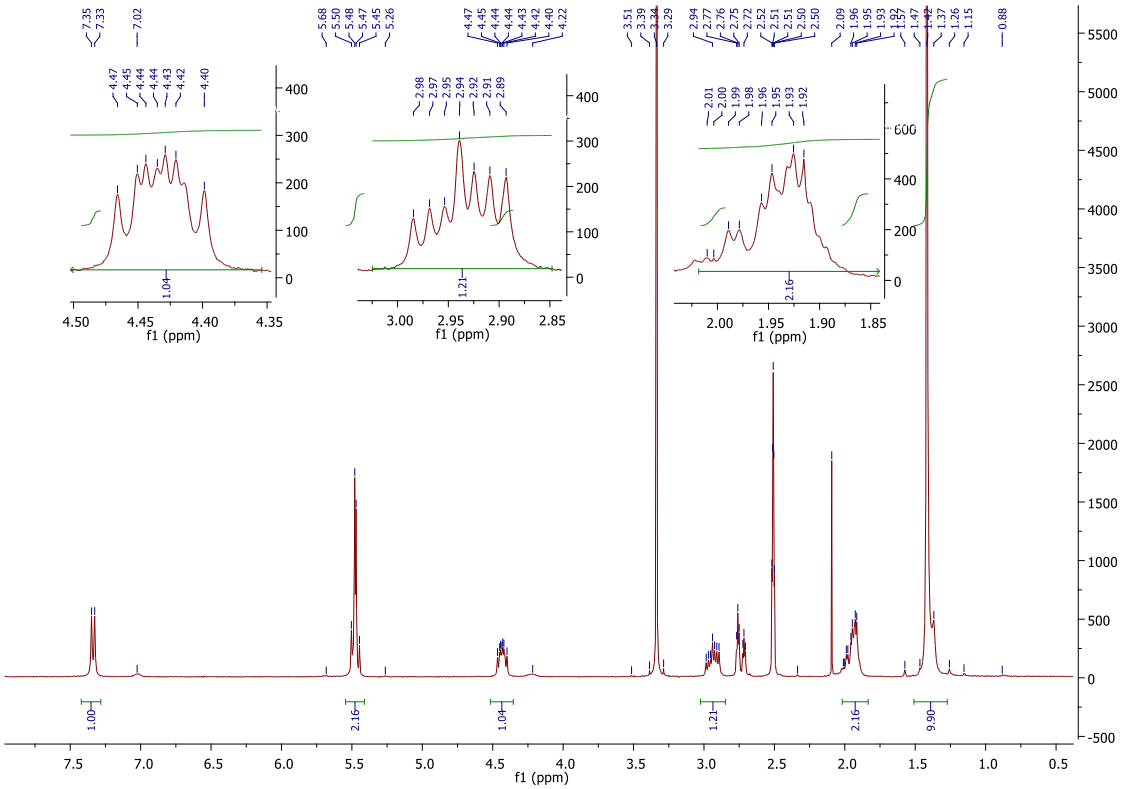

Figure 34: ^{1}H NMR for 1-Chloromethyl-3-(tert-butoxycarbonylamine)-2, 6-dioxopiperidine (Compound **10**).

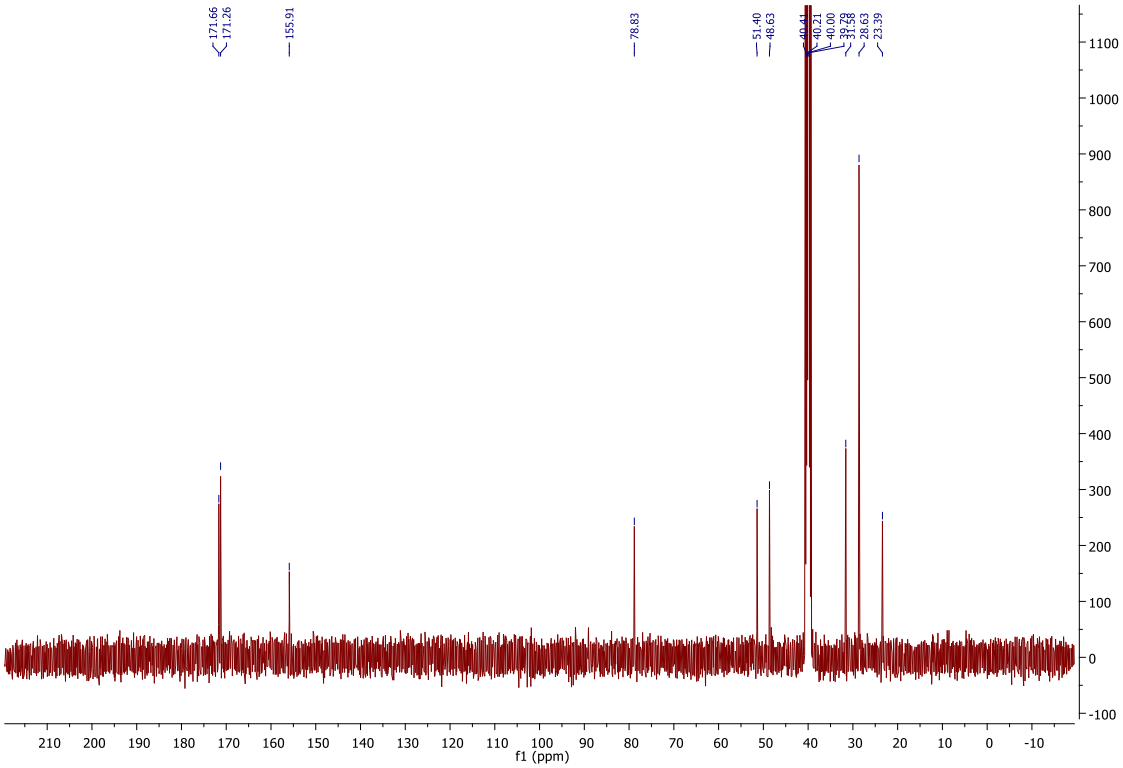

Figure 35: ^{13}C NMR for 1-chloromethyl-3-(tert-butoxycarbonylamine)-2,6-dioxopiperidine (Compound **10**).

The ^{1}H NMR spectrum (Figure 34) of the compound **10** shows a characteristic doublet in the far downfield region at δ = 7.35 – 7.33 ppm, which was assigned to the acidic glutarimide NH proton. The doublet is due to the presence of a proton on 3-H with *J* = 7.6 Hz. The region at δ = 5.5 ppm shows a singlet which can be assigned to 11-H. The *N*-methine proton (3-H) resonates as a doublet of doublets at δ = 4.47 – 4.42 ppm with *J* = 12.1 Hz and *J* = 6.3 Hz due to the axial-axial and axial-equatorial couplings with the diastereotopic 4-H protons and proximity to the amide proton. The complex multiplet at δ = 2.98 – 2.89 ppm and δ = 2.09 - 1.92 ppm were ambiguously assigned as 4-H and 5-H. There is a chemical shift for 5-H due to its proximity to the carbonyl group. A singlet in the region at δ = 1.42 ppm was assigned to 8-H, 9-H and 10-H due to the three protons with identical chemical environment.

The ^{13}C NMR spectrum (Figure 35) of thalidomide shows three peaks in the far downfield region (δ = 171.66, 171.26 and 155.91 ppm), typical of a carbonyl group arising from the C-1, C-2 & C-6 nuclei. The peak at δ = 78.83 ppm was ascribed to resonance of the C-3 nuclei due to the presence of a carbonyl group and an amide. The hydroxide changed the chemical shift observed for C-11, whose resonance was ascribed to the peak in the region of δ = 51.40 ppm. The more intense peak at δ = 28.63 ppm was assigned to C-8. C-9, and C-10, and the less intense peak at δ = 23.39 ppm was assigned to C-7.

Preparation of 3-amino-1-chloromethyl-2,6-dioxopiperidine trifluoroacetate (Compound 11)

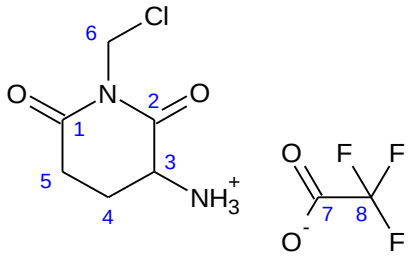

Compound **10** (0.36 g, 1.3 mmol) was completely dissolved in dichloromethane (25 mL), and trifluoroacetic acid (28.4 mL) was added dropwise to the reaction mixture at room temperature. The reaction mixture was stirred continuourly at room temperature under an

atmosphere of nitrogen for 22.5 hours. Following this step, all solvent was completely removed from the reaction mixture and precipitated with ether. The isolated solid was dried overnight to yield the final product to give compound **11** as a light purple solid (342 mg, 1.177 mmol, yield: 95%).

Molecular formula: $C_8H_{10}F_3ClN_2O_4$; Molecular weight: 290.62 g/mol;

^{1}H NMR (DMSO-*d*6) δ = 8.61 (s, 1H, -NH-), 5.57 – 5.49 (AB system, *J* = 9.2Hz, 2H, 6-H), 4.43-4.41 (d, 1 H, 3-H), 2.97-2.82 (m, 2H, 5-H), 2.10-1.99 (m, 2H, 4-H) ppm.

^{13}C NMR (DMSO-*d*6) δ = 170.3 (C-1), 169.3 (C-2), 50.0 (C=6), 48.2 (C=3), 30.7 (C=5) and 21.3 (C=4) ppm.

The spectral data were in accordance with those reported in the literature from (Luo et al., 2011).

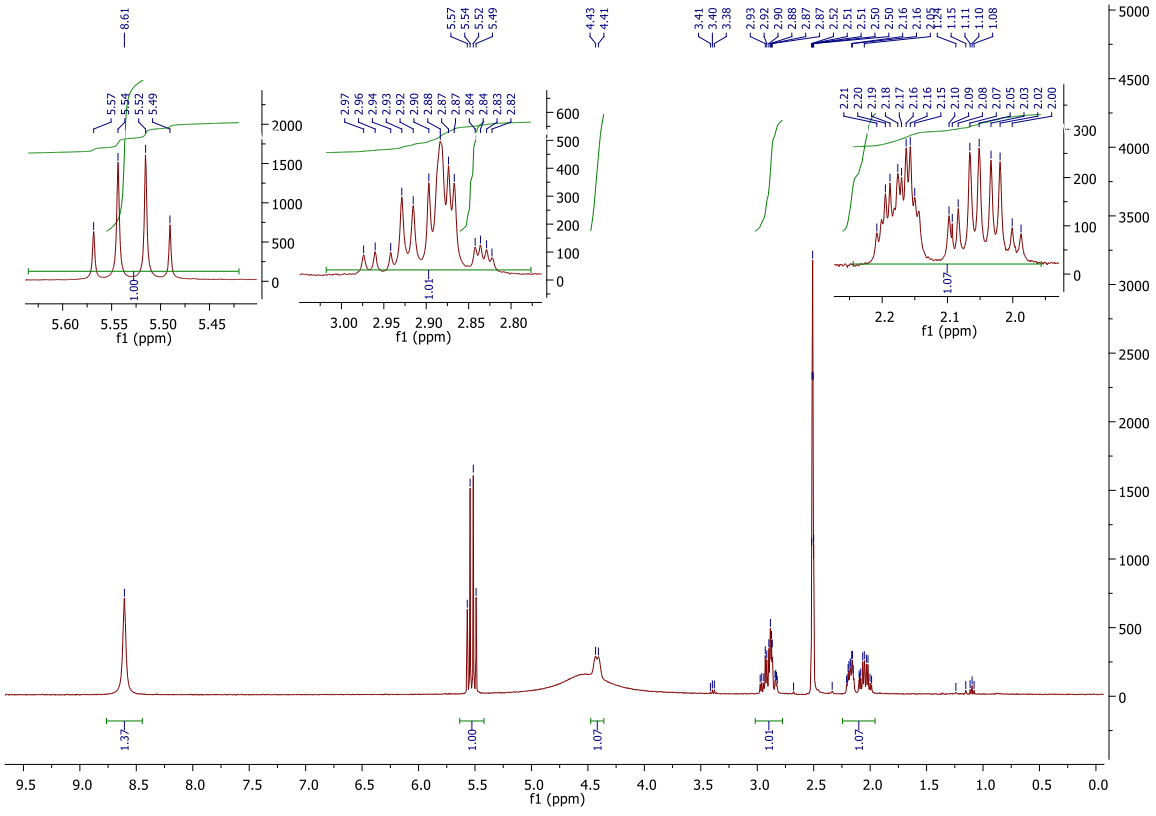

Figure 36: ^{1}H NMR for 3-amino-1-chloromethyl-2,6-dioxopiperidine trifluoroacetate (Compound **11**).

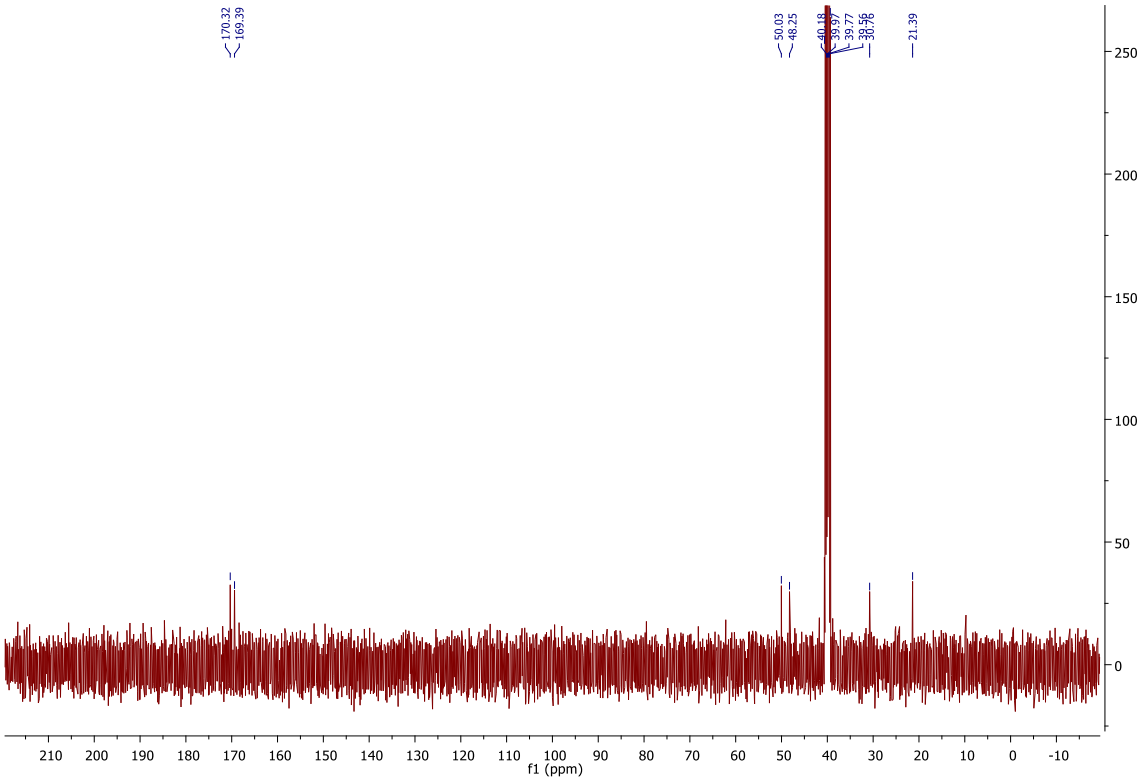

Figure 37: ^{13}C NMR for 3-amino-1-chloromethyl-2,6-dioxopiperidine trifluoroacetate (Compound **11**).

The ^{1}H NMR spectrum (Figure 36) of compound **11** shows a characteristic broad singlet in the far downfield region at δ = 8.61 ppm which was assigned to the three acidic glutarimide NH protons. The region at δ = 5.57 ppm - 5.49 ppm showed an AB system for two protons assigned as 6-H, and further classified as 6-Ha and 6-Hb with *J* = 9.2 Hz. The *N*-methine proton (3-H) resonates at δ = 4.43 – 4.41 ppm, and is shown as a multiplet assigned to 3-H. The region at δ = 2.97 – 2.82 ppm and δ = 2.21 – 1.99 ppm showed a multiplet, which were ambiguously assigned as 4-H and 5-H.

The ^{13}C NMR spectrum (Figure 37) of thalidomide shows two peaks in the far downfield region (δ = 170.3 and 169.3 ppm), typical of a carbonyl group arising from the C-1 & C-2 nuclei. The hydroxide group affected the resonances ascribed C-11, shifting the peak to the region of δ = 50.0 ppm. The peak at δ = 48.2 ppm was ascribed to a resonance of C-3 nuclei due to the presence of carbonyl group and an amide. The region at δ = 30.7 ppm and δ = 21.3 ppm were ambiguously assigned as C-4 and C-5 respectively.

Preparation of 2-(1-chloromethyl-2,6-dioxopiperidin-3-yl)phthalimidine (Compound 5)

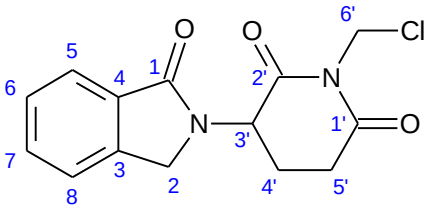

Compound **11** (0.55 g, 1.892 mmol) was dissolved by adding tetrahydrofuran (157 mL) to the solid starting material. Phthaldialdehyde (0.254 g, 1.893 mmol) was added to the reaction solution, and the mixture was stirred for 71 hours under an atmosphere of nitrogen at room temperature. Thereafter, the solvent was completely removed, and the crude product was purified with chromatography on silica gel using an acetonitrile:dichloromethane = 1 : 4 solvent mixture to obtain the product to give compound 5 as a brown solid (322 mg, 1.09 mmol, yield: 40%).

Molecular formula: $C_{14}H_{13}ClN_2O_3$; Molecular weight: 292.72 g/mol

Melting point: 180.5 – 181.5 °C;

R_f = 0.25 acetonitrile : dichloromethane = 1:4

^{1}H NMR (DMSO-*d*6) δ = 7.78 – 7.76 (d, *J* = 8.1 Hz, 1H, Ar-H), 7.52 – 7.50 (t, *J* = 8.2 Hz & 6.9 Hz, Ar-H), 7.49 – 7.39 (t, *J* = 8.6 Hz & 8.2 Hz, Ar-H), 5.47 – 5.38 (AB system, *J* = 9.2 Hz, 2H, 6'-H), 5.22 – 5.18 (dd, *J* = 13.4 Hz & *J* = 5.0 Hz, 1H, 3'-H), 4.27 – 4.41 (AB system, *J* = 17.2 Hz, 2H, 2-H), 2.97-2.88 (m, 2H, 5'-H), 2.23-2.11 (m, 1H, 4'-H), 2.09-2.03 (m, 1H, 4'-H) ppm;

^{13}C NMR (DMSO-*d*6) δ = 169.9 (C-1 or C-1' or C-2'), 167.8 (C-1 or C-1' or C-2'), 167.1 (C-1 or C-1' or C-2'), 139.7 (Ar-CH), 130.5 (Ar-CH), 129.3 (Ar-CH), 126.5 (Ar-CH), 122.1 (Ar-CH), 121.3 (Ar-CH), 50.7 (C-2 or C-3' or C-6'), 45.6 (C-2 or C-3' or C-6'), 45.5 (C-2 or C-3' or C-6'), 30.0 (C-4' or C-5') and 20.3 (C-4' or C-5') ppm.

The spectral data were in accordance with those reported in the literature from (Luo et al., 2011).

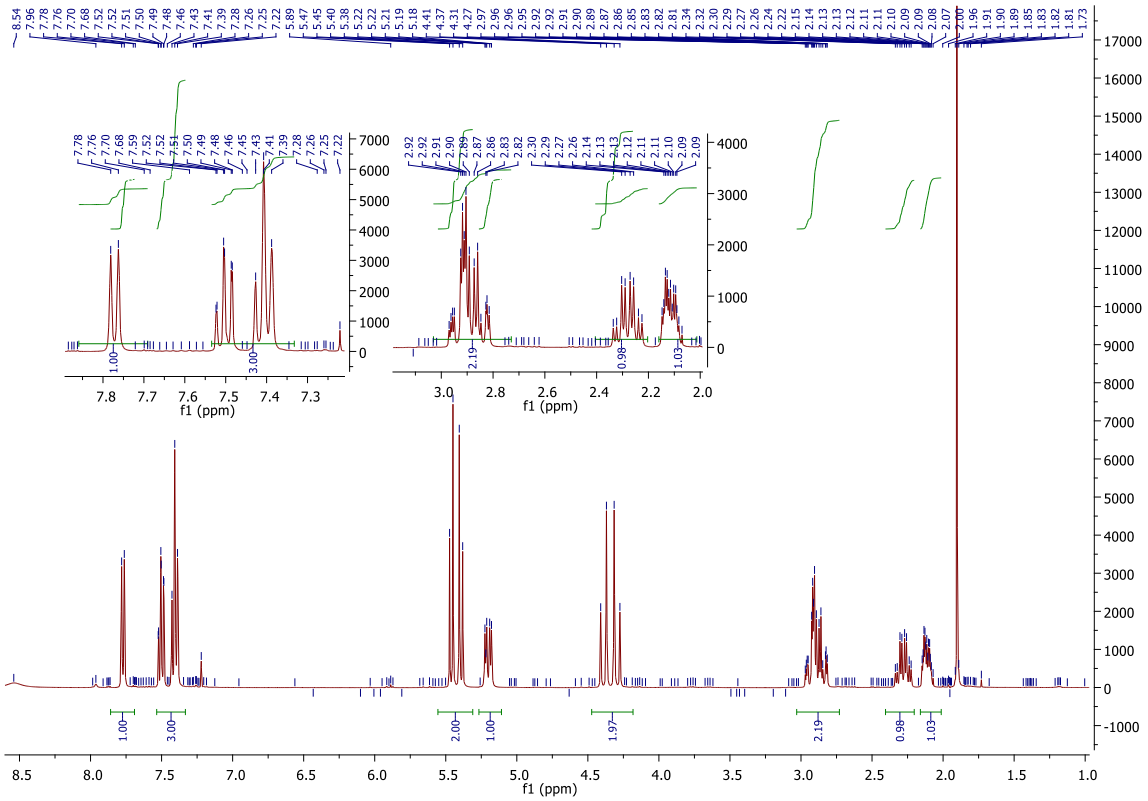

Figure 38: ^{1}H NMR for 2-(1-chloromethyl-2,6-dioxopiperidin-3-yl)phthalimidine (Compound **5**).

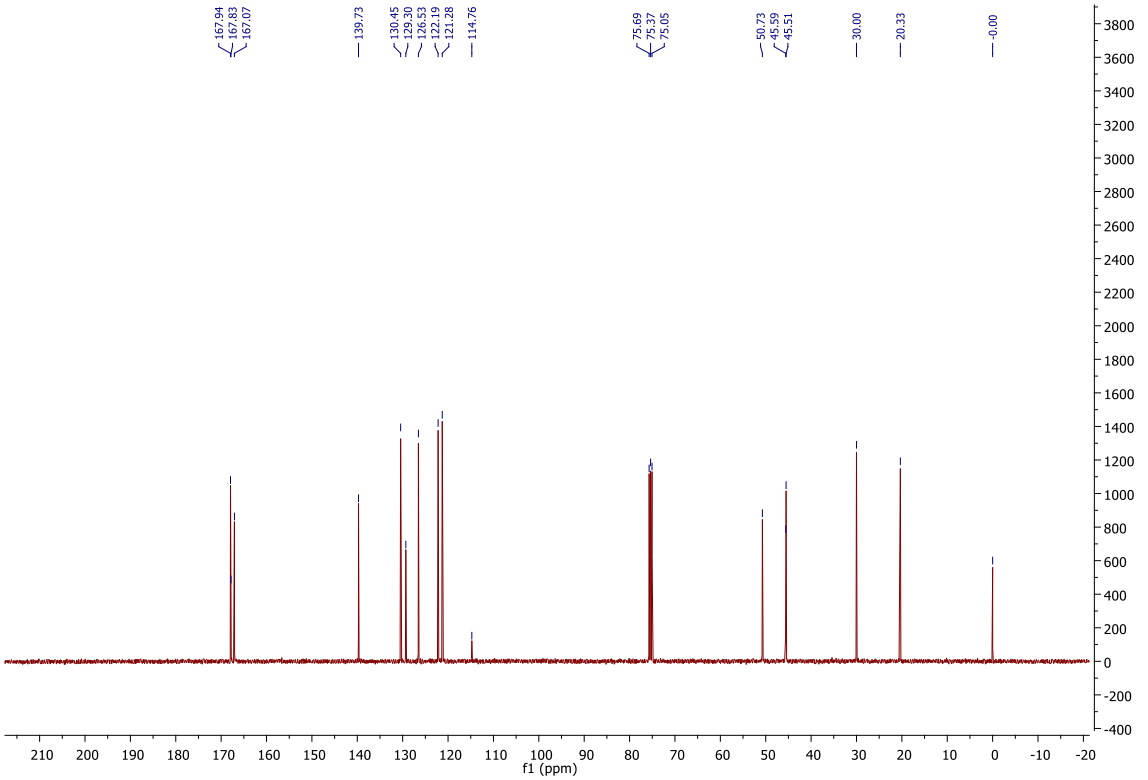

Figure 39: ^{13}C NMR for 2-(1-chloromethyl-2,6-dioxopiperidin-3-yl)phthalimidine (Compound **5**)

The ^{1}H NMR spectrum (Figure 38) of the compound **5** shows the aromatic system of the phthalic ring in the far downfield region, around δ = 7.78 ppm to δ =7.76 ppm. For the benzene ring of the phthalic ring, there is no a centrosysmmetic structure. There are four protons shown on the benzene ring, which exhibit ortho, meta and para effects on each other. As expected, a characteristic a doublet of doublet in the downfield region was detected, and was assigned to either 5-H or 8-H. The doublet of doublet is caused by the coupling-coupling effects of ortho or meta position protons. Unfortunately, this effect was not clearly shown in the region. The region at δ = 7.78 – 7.76 ppm, with *J* = 8.01 Hz showed a doublet with *J* = 7.57 Hz. Both 6-H and 7-H protons resonate as a doublet of triplet at δ = 7.52 – 7.50 ppm, with *J* = 8.2 Hz and 6. 9 Hz and δ = 7.49 – 7.39 ppm, with *J* = 8.6 Hz and 8.2 Hz. Again, the observed effects are caused by meta and ortho coupling effects from both sides. The region at δ = 5.47 – 5.38 ppm showed an AB system for two protons assigned at 6'H_A and 6'-H_B with *J* = 9.2 Hz. The *N*-methine proton (3-H) resonates as a doublet of doublet at δ = 5.22 – 5.18 ppm, with *J* = 13.36 Hz and *J* = 5.00 Hz. The proton can be assigned 3'-H due to the axial-axial and axial-equatorial couplings with the diastereotopic 4'-H protons and proximity to the amide proton. The region at δ = 4.41 – 4.24 ppm showed an AB system for two protons assigned as 2-H_A and 2-H_B with *J* = 17.2 Hz. As discussed above, it is expected that a characteristic a doublet of doublet of doublet can be assigned to 5'-H with germinal coupling, axial-axial coupling and axial-equatorial coupling with one of the 4'-H protons. However, the region at δ = 2.97 – 2.88 ppm showed a multiplet which can be assigned as 5'-H. Both vicinal 4'-H protons resonate as more complex multiplets at δ = 2.23 – 2.11 ppm and δ = 2.09 – 2.03 ppm

The ^{13}C NMR spectrum (Figure 39) shows three peaks in the far downfield region (δ = 167.9, 167.8 and 167.0 ppm), typical of a carbonyl group arising from the C-1, C-1' & C-2' nuclei. The six peaks at δ = 139.7 ppm, 130.4 ppm, 129.3 ppm, 126.5 ppm, 122.1 ppm, and 121.2 ppm were assigned to the aromatic benzene ring. Due to the presence of an adjacent amide position, the three peaks at δ = 50.7 ppm, 45.5 ppm and 45.5 ppm were ascribed to resonance of C-2, C-3' and C-6' nuclei. The aliphatic region of the spectrum displays peaks at 30.0 and 20.3 ppm, which were ambiguously ascribed to C-4' and C-5'.

Therefore, based on all spectrum results including LRMS, HRMS, IR, ^{1}H NMR and ^{13}C NMR, all compounds thalidomide (compound 1), 2-(2,6-dioxopiperidin-3-yl)-phthalimidine (EM-12) (compound 2), and two isomers 3-[(1*R*)-1-hydroxy-1-methyl-3-oxo-1,3-dihydro-2*H*-isoindol-2-yl]piperidine-2,6-dione (compound 3) & 3-[(1*S*)-1-hydroxy-1-methyl-3-oxo-1,3-dihydro-2*H*-isoindol-2-yl]piperidine-2,6-dione (compound 4), and 2-(1-chloromethyl-2, 6-dioxopiperidin-3-yl)phthalimidine (compound 5) have been successfully synthesized. Next, all these compounds are subjected to *in vitro* analysis for comparison of their biological activities in the next Chapter.

Chapter III: In vitro Anti-cancer study of synthesised analogues

3.1 Introduction of Breast Cancer

Breast cancer is the most common cancer in women worldwide with about 1.67 million new cases each year. Breast cancer is a malignant tumour that starts in the breast tissue. The majority of breast cancer begins in the milk duct (ductal cancers). A small number starts in the milk sacs or lobules (lobular cancers). Within these two groups there are different subtypes of breast cancer. Commonly, breast cancer can spread to the lymph glands and to other parts of the body, most commonly to the lung, bones, and livers.

Figure 40: Statistical report about case of breast cancer reported in 2016 from NZ Ministry of Health.

Based on statistical report from Ministry of Health 2016 (Figure 40), the incidence of breast cancer in New Zealand is the geographically second high in rate per 100, 000 population compared with other countries of worldwide (Siegel *et al.*, 2016). In New Zealand, breast cancer is the third most common cancer, and approximately 2, 500 women are diagnosed each year (Torre *et al.*, 2015). The incidence of breast cancer in New Zealand is highly correlated to age. In fact, breast cancer can occur at all ages but is most common in women between the ages of 50 to 70 years, and there was about 70% of women who are diagnosed with breast cancer and around 80% of women who died from it are 50 years or older (Torre *et al.*, 2015). Based on all data above, it is very necessary to determine an effective method for treatment of breast cancer. Thalidomide and its structural analogues as a potential treatment will be tested in *in vitro* for breast cancer. In this section, the significance of anti-angiogenic therapy will be discussed in treatment of breast cancer.

3.1.1 Morphology of Breast Cancer

Breast carcinomas mostly present as discrete lumps, usually within the upper quadrant of the breast and histological examination is required to ensure correct diagnosis (Chaudary *et al.*, 1988). A high majority of breast carcinomas are adenocarcinomas that arise from either glandular or ductal epithelium. The clinical manifestations of invasive breast cancer occur in a progressive manner. A normal duct may progress through several different proliferative conditions that will not necessarily result in a malignant disease; these conditions include fibrocystic changes, adenosis, epithelial hyperplasia and cysts. Breast carcinomas do not develop rapidly from the normal breast; there is a morphological change in the cells in the ducts or lobules, which eventually leads to a malignant disease. The following lists the morphological states in order of lesion severity; (1) Hyperplasia, (2) Atypical hyperplasia, (3) Ductal Carcinoma in situ (DCIS) and (4) Invasive Carcinoma (Ellis, 2010). However, it is important to note that breast cancer progression does not necessarily follow each step in this order of severity, unlike the adenoma-carcinoma sequence in colorectal cancer (Armaghany *et al.*, 2012).

3.1.2 Breast Cancer (Sub-Type)

Breast cancer is not defined as one disease as there are many sub-classifications. This makes the treatment of the disease difficult, as sub-types can present with different risk factors, clinical symptoms, pathological features and response to therapy (Dai et al., 2015). Recent microarray technology has allowed sub-classification of invasive breast cancer based on the molecular profile of the disease. Invasive breast cancer now can be categorized as either (1) luminal A (2) luminal B (3) oestrogen and progesterone negative and human epidermal receptor positive (ER-/PR-/HER+) (4) basal like and (5) normal Breast-like (Onitilo *et al.*, 2009).

Luminal tumours are the most commonly observed sub-type of invasive breast cancer and are further divided into two separate groups; luminal A and luminal B. Both are ER/PR hormone receptor positive however, luminal A breast tumours usually have a lower Ki67 count (proliferative index), have a better prognosis as they are usually classified as low/moderate grade tumours compared to luminal B tumours. Luminal B tumours are usually of a higher grade and are lymph node positive (Inic et al., 2014). The third sub-type of invasive breast cancer account for 10-15% of invasive breast cancer cases and are classified as HER2 tumours that are ER/PR hormone receptor negative but HER2 positive, and are usually lymph node positive and have a poorer prognosis compared to luminal breast cancer, with patients more prone to recurrence and metastasis (Anders *et al.*, 2009). Basal like breast tumours also referred to as triple negative breast cancer lack expression of ER, PR and HER2 but are classified as basal like because they express genes that are commonly expressed by basal epithelial cells, such as cytokeratin 5/6 (Badowska-Kozakiewicz *et al.*, 2016). Basal like breast tumours account for 15-20% of invasive cases and characteristically present with an aggressive phenotype and is commonly observed in younger patients. Triple-negative breast cancer is one of the most difficult disease states to treat (Crown *et al.*, 2012). The best treatment strategy for basal like carcinomas is targeted systemic chemotherapy. The fifth sub-group is the normal breast-like tumours; these are the least common type of invasive breast cancer observed, accounting for approximately 6-10% of cases and are small in size and have a good prognosis, the above sub-classification can also be applied to human breast cancer cell lines that are frequently used for research purposes (Makki, 2015; Malhotra *et al.*, 2010). The grouping of different breast cancer cell lines based on the molecular profile is potentially

an excellent tool in research to allow identification of therapy for specific breast cancer sub-types that could potentially translate to the clinic.

However, the onset of abnormal cell and cancer development is the initial step of the process. It is well understood that once a tumour has established within its primary location, the tumour cells must be able to create a microenvironment in which growth and progress is possible. In order to survive and metastasize, tumours promote the formation of a blood supply (van Zijl *et al.*, 2011). Initially tumours obtain oxygen and nutrients via simple diffusion from neighboring cells; however, for tumours to grow beyond $2mm^3$ there is a requirement to stimulate the formation of a new micro-vascular network by a process known as angiogenesis (Folkman 1971; Hillen *et al.*, 2007).

3.2 Tumour Microenvironment and Angiogenesis

3.2.1 Tumour Microenvironment

The tumour microenvironment is a heterogeneous compartment consisting of different cell types and stromal components, all with capacities to affect tumour progression in both negative and positive ways. In addition to the cancer cells themselves, the tumour tissue is composed of resident cells such as fibroblasts and endothelial cells, and of infiltrating immune cells such as macrophages and lymphocytes. A large amount of cell-secreted bio-active products including components of the extracellular matrix (ECM), cytokines, chemokines, growth factors and proteolytic enzyme regulate the complex cross-talk between tumour cells and other cells. Cell-cell and cell-microenvironment interactions are suggested to modify different steps of tumour progression including proliferation, differentiation and invasiveness. Matrix metalloproteinases (MMPs) are largely involved in the cross-talk of interactive components stromal and cell-bound molecules with abilities to affect both pro- and anti-tumourigenic activities. The impact of the tissue microenvironment on tumour growth has been recognized for more than a 100 years, since Paget hypothesize the “seed and soil” theory in 1889 (Langley *et al.*, 2011; Paget, 1889). The microenvironment has shown to influence tumour-induced angiogenesis, which may be illustrated by studies where breast tumours of the same origin but implanted into different tissue showed diverse angiogenic responses.

3.2.2 Angiogenesis

The development of new conceptual approaches to inhibit tumour growth represents a major challenge to cancer therapy. Conventional chemotherapy and radiotherapy regimes act killing tumour cells directly, relying on subtle differences in proliferation rates, DNA repair capabilities or other features, resulting from the malignant transformation for a greater degree of tumour cell killing over that of normal tissues. An innovative approach to cancer therapy by targeting the tumour vasculature was proposed by Folkman 1971, and has attracted much attention and research (Cristofanilli *et al.*, 2002; Liu *et al.*, 2006). Since solid tumours depend heavily on a functioning vasculature to deliver nutrients necessary for growth, it was proposed by Folkman that strategies that target the tumour vasculature could effectively starve tumour cells to death.

Tumour vascular-targeting strategies to date fall into main categories: inhibition of the development of new vessels (anti-angiogenesis); and the disruption of the existing vasculature (anti-vascular therapy). Angiogenesis is involved when an avascular aggregate of tumour cells establishes a blood supply derived from the host stroma. The acquisition of new vascular elements by an established tumour is also dependent on this angiogenesis (Benjamin *et al.*, 1999; Helfrich *et al.*, 2011). Anti-angiogenic therapy interferes with the development of new vessels and /or the expansion of a neovascular network and is most likely to be effective when administrated as an adjuvant treatment to prevent establishment of small solid tumour or metastases. By contrast, anti-vascular therapy provides rapid destruction of the existing NE vasculature, infracting the tumour. If a capillary or a sector of the capillary bed fails, many thousands of dependent tumour cells will die of nutrient deprivation. Thus, anti-vascular therapy is more likely to be effective on large tumours, where the vasculature is already compromised.

Below, the process of tumour angiogenesis will be described, and this will be followed by a general review of anti-angiogenic agents and anti-vascular agents.

3.2.3 Tumour Vascular-Targeting Therapy

Tumour vascular-targeting therapy is split into two parts including anti-angiogenic and anti-vascular, angiogenesis is involved when an avascular aggregate of tumour cells establish a blood supply derived from the host stroma. The acquisition of new vascular elements by an

established tumour is also dependent on this angiogenesis (Baillie *et al.,* 1995; Denekamp, 1992). Anti-angiogenic therapy interferes with development of new vessels and the expansion of a neovascular network and is most likely to be effective when administrated as adjuvant treatment to prevent establishment of small solid tumour or metastases. By contrast, anti-vascular therapy provides rapid destruction of the existing neovasculature, infracting the tumour (Bicknell *et al.*, 1992; Folkman *et al.*, 1992). If a capillary or a sector of the capillary bed fails, many thousands of dependent tumour cells will die of nutrient deprivation. Thus, anti-vascular therapy is more likely to be effective on large tumours, where the vasculature is already compromised.

The tumour vascular-targeting therapies act on the endothelial cells of the tumour vasculature rather than the tumour cells themselves, and have several advantages over conventional cancer therapies that target tumour cells directly. Firstly, the vascular endothelial cells are directly assessable through the blood to circulating therapeutic agents, thus avoiding the problem of drug delivery to target cells that is encountered with therapy using conventional, cytotoxic anti-cancer agents. Secondly, unlike the tumour cell population, endothelial cells are genetically stable and are unlikely to develop drug resistance. Thirdly, vascular targeting-therapies have a difference spectrum of toxicity to those exhibited by conventional direct cytotoxic agents. This applies particularly to anti-angiogenic therapies, which specifically target proliferating endothelial cells. Under physiologic conditions endothelial cell proliferation is limited to wound healing and reproduction and anti-angiogenic therapies generally tend to have little toxicity on normal tissues. Fourthly, vascular-targeting therapies are most applicable to solid tumours since rely heavily on a functioning blood supply for growth, and these tumours tend to be the most difficult to treat using conventional cancer chemotherapeutic agents.

3.2.4 Angiogenesis in Physiology and in Disease

The term angiogenesis is generally applied to the process of new blood-vessel growth. It plays an essential role in embryonic development, but once the vascular network occurs, the endothelial cells lining the blood vessels remain quiescent and angiogenesis is only induced locally and transiently during a number of physiological processes. Physiological

angiogenesis occurs in reproduction, development, and wound repair (Johnson *et al.*, 2014). It is usually focal, such as in blood coagulation in a wound, and self-limited in time, taking days (ovulation), weeks (wound repair), or months (placentation) (Folkman, 2007). However, angiogenesis also play an essential role in many pathological conditions such as cancer (Nishida *et al.*, 2006). By contrast to the physiological growth of new blood vessels, pathological angiogenesis can persist for years, and is necessary for tumours and their metastases to grow beyond the size of a few millimeters. In such conditions, angiogenesis can give rise to bleeding, vascular leakage, and tissue destruction; consequences that can ultimately be responsible directly or indirectly, for the symptoms, incapacitation or death associated with a broad range of angiogenesis dependent disease. The dependent disease includes cancer, autoimmune disease, age-related macular degeneration, atherosclerosis, and chronic inflammation, where an increase in blood supply may compensate for hypoxia and insufficient delivery of nutrients to the tissue.

Angiogenesis is tightly regulated process that is orchestrated by a range of angiogenic factors and inhibitors (Figure 41 & Figure 42). Thus, angiogenesis in physiological as well as in pathological states is regulated by the net balance of positive and negative effectors of endothelial cell proliferation and migration in the tissue (Judah, 2003). The initial stage is once an angiogenic stimulus has been received, the de-attachment of pericytes from endothelial cells to induce destabilization of the host vasculature which is thought to be mediated by the actions of angiopoietin 2 (Ang-2) (Aguilera *et al.*, 2014; Conway *et al.*, 2001). Then, proteases such as matrix metalloproteinases (MMPs) are secreted, and this results to loosen the interaction between cell and cell basement membrane caused by degradation the adhesion molecules and surrounding matrix. Once basement membrane completely breakdown, the extracellular matrix (ECM) not only allows endothelial cells migration but also causes the release of many pro-angiogenic factors that are sequestered with the extracellular matrix, thereby increasing the number of circulation pro angiogenic factors such as vascular endothelial growth factor (VEGF). In fact, VEGF can increase the permeability of existing blood vessels, acts as an endothelial cell survival factor, and is a potent endothelial cell mitogen. Adhesion molecules including the integrin also play an important role in angiogenesis as they allow ECs to interact with ECM components aiding formation of the sprouting capillary.

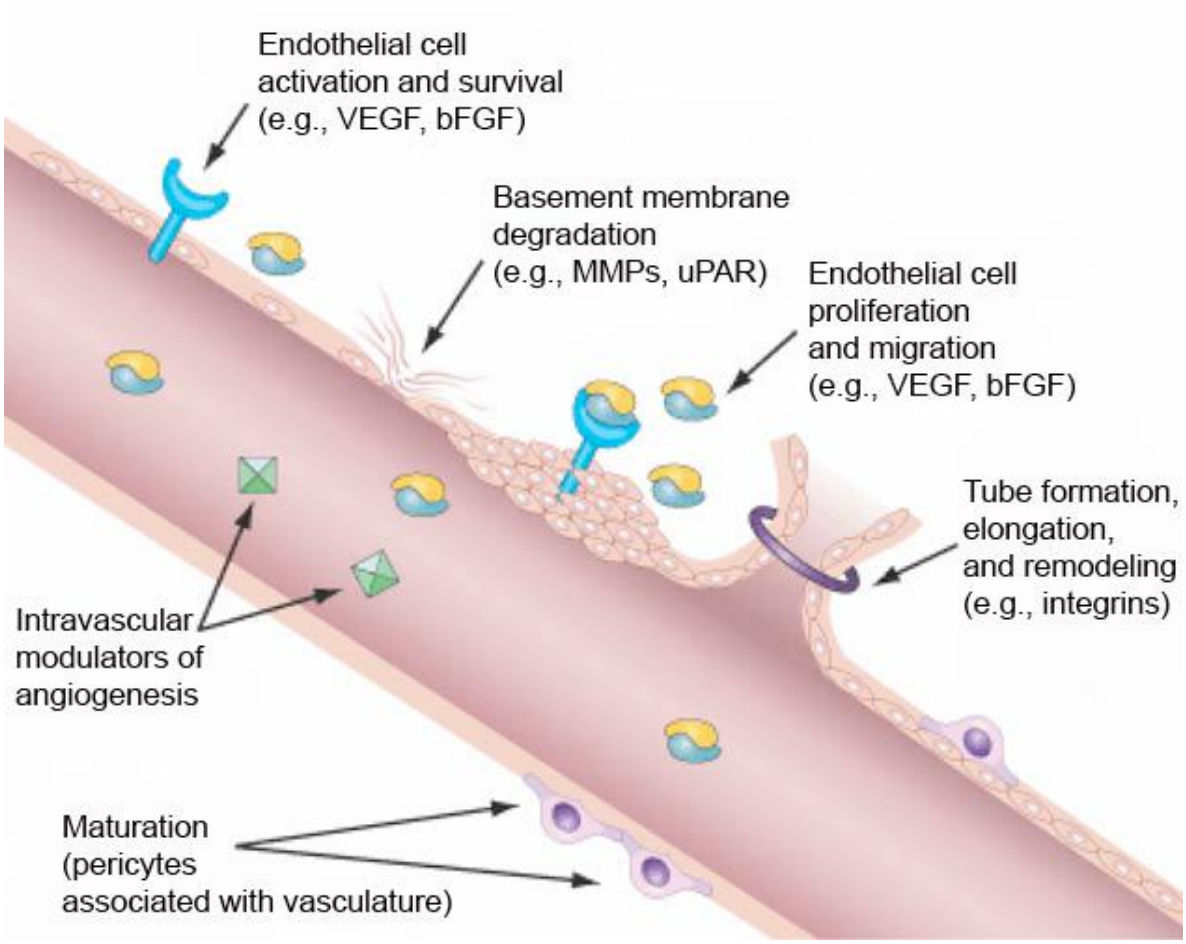

Figure 41: The angiogenic process. Angiogenesis is a complex system featuring numerous inducing and inhibitory proteins**,** which contribute to development of new blood vessels from pre-existing ones (Marlind, 2008)

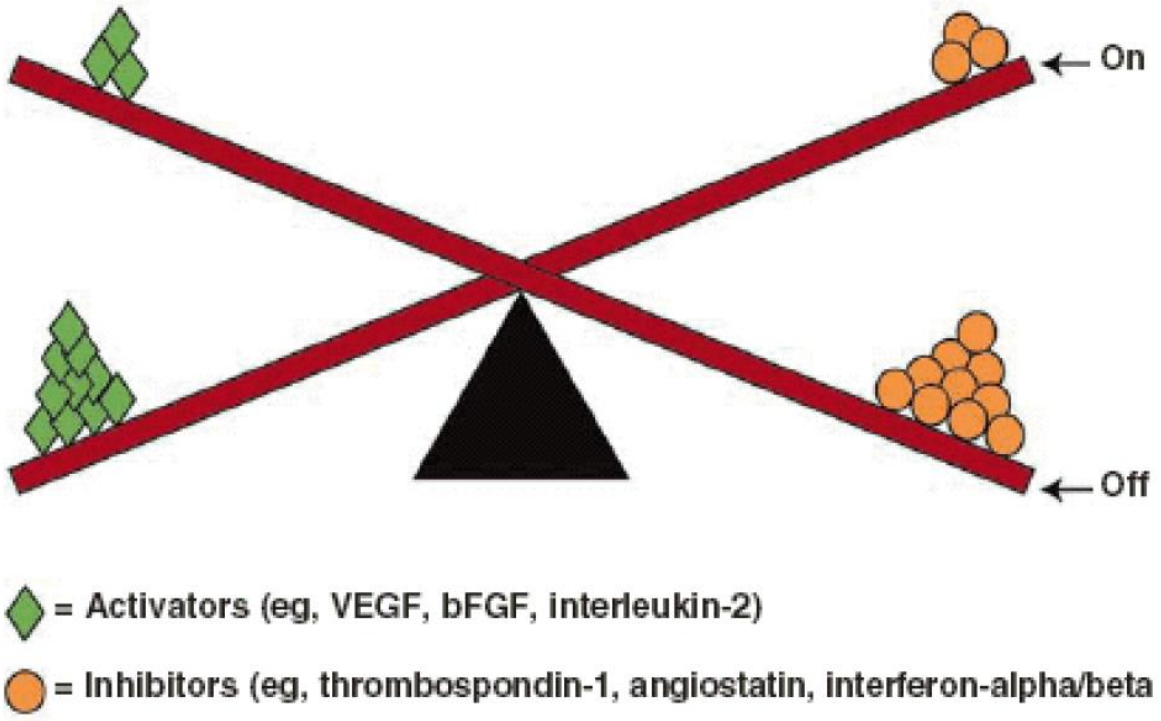

Figure 42: Angiogenic Switch – In healthy tissue, angiogenesis is tightly controlled via a careful balance between positive and negative (proangiogenic and antiangiogenic) factors. In tumours, proangiogenic factors are upregulated, while antiangiogenic factors are downregulated, leading to an imbalance in favor of angiogenesis-the so-called "angiogenic switch". Vascular endothelial growth factor (VEGF) is a principal trigger for the angiogenic switch, and therefore, a good target for therapeutic blockade. bFGF = basic fibroblast growth factor (Olszewski *et al.*, 2005).

3.2.4.1 Tumour Angiogenesis

All cells and tissues are dependent on a regular supply of oxygen and nutrients, so that development of a solid tumour highly depends on its ability to induce vessel growth into the mass of dividing tumour cells. Angiogenesis is a fundamental process by which new blood vessels are formed. The neovasculation process in tumours is so called "tumour angiogenesis" or "angiogenesis switch" (Bergers *et al.*, 2003). Classically, the transition of vascularization results from the angiogenesis switch driven by hypoxia. Tumours can produce several angiogenic activators to attract and activate endothelial cells, which is a critical step to mediate angiogenesis. Activation of endothelial cells initiates the cell proliferation, which in turn induces sprouting from existing vessels, migration, and adhesion of endothelial cells to

a lumen. Ultimately, the invasive vascular sprouts reach the tumour where they differentiate to form new capillaries. The additional nutrients and oxygen provided by the new vasculature, together with the paracrine stimulation of tumour cells by numerous growth factors and proteins produced by the new capillary endothelium allow rapid growth tumour, and continues secretion of angiogenic factors to promote further new vessel development (Ziyad *et al.*, 2011). Tumour angiogenesis also provides a conduit for metastatic tumour cells, which leave the primary site and migrate to local or distant locations where the metastatic cells must again undergo angiogenesis to grow to a clinically detectable size (Gupta *et al.*, 2006; Klein, 2009).

Another process of neovascularization is that tumours make existing host vessels to grow, which has been described. Studies was conducted using a glioma animal model that showed inoculated tumour cells parasitized pre-existing brain vessels to form an initially well-vascularized tumour mass and to initiate blood-dependent tumour growth. The co-opted host vasculature did not immediately undergo angiogenesis but instead regressed, leading to a secondary avascular tumour and massive tumour cell death (Coelho et al., 2017). Ultimately, however, the remaining tumour was rescued by the induction of angiogenesis at the tumour periphery (Benazzi et al., 2014).

The occurrence of angiogenesis highly depends on a net balance of positive angiogenic factors over negative angiogenic inhibitor (Li *et al.*, 2006). Even though the mechanism eliciting the angiogenic switch are not entirely understood to date, it is believed that besides tumour-suppressor mutation and oncogene activation, hypoxia plays a pivotal role (Solaini *et al.*, 2011; Tarrado-Castellarnau *et al.*, 2016). When tumours grow beyond the limit of oxygen diffusion, hypoxia triggers vessel growth by signaling through hypoxia inducible transcription factors (HIFs). These factors induce the production of proangiogenic compounds such as VEGF, placental growth factor (PGF), acidic and basic fibroblast growth factor (aFGF and bFGF), and these factors contribute to directly proliferate or migrate, or to form tubes (Folkman *et al.*, 1992; Ucuzian *et al.*, 2010; Zhong *et al.*, 1996). Some other indirect-acting factors such as transforming growth factor-β (TGF-β), plated-derived endothelial cell growth factor contribute to act indirectly by mobilizing host cells to release endothelial cell growth factors (Chang *et al.*, 2002; Spector *et al.*, 2001).

For angiogenic proteins, bFGF and VEGF are the most commonly reported in human tumours, which play an important role in tumour angiogenesis. bFGF is mitogenic for vascular endothelial cells, and it also a powerful stimulator of endothelial cell mobility (Song *et al.*, 2012). bFGF has been found as one of the most important cytokine in human tumours, and can be the high level in serum and urine of patients with solid tumours (Neufeld *et al.*, 1994). The mechanism of action proposed that VEGF promotes angiogenesis by binding to two high affinity receptors, VEGF-1/flt-1 and VEGFR-2/flk-1 (Cébe-Suarez *et al.*, 2006; Shibuya, 2003), that are mainly expressed on endothelial cells, then endothelial cells after stimulation is proliferated, and expression of proteases was induced from endothelial (Nystedt *et al.*, 1996; Wang *et al.*, 2003), angiogenesis can be finally induced in corneal. VEGF is almost undetectable or present at low levels in healthy individuals, but it is highly up-regulated in patients with a variety of tumour types (Fuhrmann-Benzakein, 2000). Level of VEGF has been highly correlated with high intra-tumoural microvessel density (Obermair et al., 1997) and poor prognosis caused by elevated levels of VEGF receptor found in a variety of human tumours (Obermair et al., 1997).

3.2.5 Anti-angiogenic Therapy

3.2.5.1 Principle of Anti-angiogenic Therapy

The principle of anti-angiogenic therapy is based on the hypothesis that tumour growth is dependent on angiogenesis, and inhibiting angiogenesis might block tumour growth by cutting off the nutrient supply for tumour tissue. Based on this principle, several mechanisms of action can be proposed that first, by inhibition of endothelial cells proliferation and migration, the formation of new blood vessels is blocked. This results in oxygen, growth factors, substrate supply decrease and metabolites increase due to the limited material exchange with the circulation system. Consequently, the tumour grows slower because of a lack of blood supply; secondly, usually in the tumour tissue, blood vessels are extremely disorganized. After anti-angiogenic treatment, these vessels may become normalized, and regain their function, which benefits the drug delivery of CDs. Thereby increase to efficiency of CDs is enhanced; thirdly, anti-angiogenic drugs will also target circulating endothelial progenitor cells, which contribute to angiogenesis. Thus, anti-angiogenic therapy inhibits

tumour growth by directly targeting blood vessels, blocking progenitor cells and assisting the delivery of CDs. Based on these proposed mechanisms of action, several angiogenic inhibitors have been developed and applied in the clinical cancer treatment.

3.2.5.2 Angiogenic Inhibitor

The use of angiogenesis inhibitor for treatment of cancer was first conceptualized over 30 years ago, when Dr. Folkman introduced his idea that angiogenesis is required for continued solid tumour growth. A number of endogenous and synthetic anti-angiogenic agents have been investigated. Some specifically target molecules that are involved in angiogenesis, while some directly inhibit endothelial cell function. Inhibitors of angiogenesis categorize into two classes including 1: endogenous anti-angiogenic inhibitors that occur naturally and are used by the host to counter the angiogenic stimuli produced by tumours; 2: agents that inhibit the activity of angiogenic agents. In the following section, some of these inhibitors will be generally discussed. Especially, thalidomide and its structural analogues will be illustrated as angiogenic inhibitors in the following section.

3.2.5.2.1 Endogenous Inhibitor Cytokines

Anti-angiogenic cytokines are naturally-produced inhibitors of angiogenesis, some examples for anti-angiogenic cytokines include PF-4, IP-10 and IL-12.

PF-4

The anti-angiogenic potential of PF-4 was first noted when it gave rise to avascular zones on CAM (Staton *et al.*, 2005). Subsequently, recombinant human PF-4 (rHuPF-4) was shown to inhibit growth factor-dependent proliferation of endothelial cells, but not the proliferation of tumour cells *in vitro* (Staton *et al.*, 2005). The inhibition of endothelial cell cycle progression was associated with impairment of the down regulation of the cell cycle inhibitor $p21^{Cip/WAF1}$, and consequently, inhibition of cyclin E-cyclin dependent kinase (cdk) 2 activity and retinoblastoma protein (pRb) phosphorylation (Reshetnikova *et al.*, 2000). A PF-4-derived synthetic peptide blocked bFGF- or VEGF-induced endothelial cell tube formation by inhibiting bFGF and VEGF binding to endothelial cells through their receptors, so anti-tumour activity of PF-4 is associated with its inhibition of tumour angiogenesis (Daly *et al.*, 2003).

IP-10

IP-10, a member of the α chemokine family, has been shown to be a potent inhibitor of angiogenesis. IP-10 inhibited bFGF-induce neovascularization in vivo using the rat corral assay for angiogenesis by nearly 80%. It was also shown to inhibit neovascularization in bFGF-impregnated matrigel plugs implanted in athymic node mice. The mechanism for the anti-angiogenic action o fIP-10 is not known, but nanogram concentrations of IP-10 inhibited endothelial cell migration *in vitro*, and differentiation into tube-like structures without inhibiting endothelial cell proliferation. At substantially higher microgram concentrations, IP-10 inhibited endothelial cell growth. Since these concentrations are higher than those required for in vivo inhibition of angiogenesis, the data that IP-10 does not suppress neovascularization through inhibition of endothelial cell proliferation. Thus, IP-10 has been proposed for clinical development an anti-angiogenic therapy.

IL-12

IL-12 is a heterodimeric cytokine with anti-tumour and anti-angiogenic activity. Daily intra-peritoneal (ip) injections of IL-12 for 5 consecutive days inhibited bFGF-induced angiogenesis in the corneal assay, which occurred in the absence of an inhibitory effect of IL-12 on endothelial cell proliferation in vitro. Neutralizing antibodies to IFN-γ abolished the anti-angiogenic action of IL-12, indicating that the actual angiogenesis inhibition by IL-12 was due to IFN-γ. Inhibition of neovascularization by IL-12 in the matrigel assay could be neutralized by antibodies to either IFN-γ or IP-10. These findings confirmed that the anti-angiogenic effects of IL-12 were of IL-12 were mediated by IFN-γ, and established the important role of IP-10 which is induced by IFN-γ as a downstream mediator of the anti-angiogenic action of IL-12.

Angiostatin

Angiostation is a 38 kDa fragment of plasmin formed by autoproteolytic cleavage of plasminogen, Angiostatin can be cleaved by different metalloproteinases. Angiostatin binds ATP (Adenosine-5'-triphosphate) synthase on ECs and inhibits endothelial cell proliferation migration and induced apoptosis. Systemic administration of human angiostatin in mice inhibited angiogenesis in the murine corneal assay by 85%.

Endostatin

Endostatin is a 20 kDa garment derived from type XVIII collagen. It has a high affinity for heparin binding. Endostatin is produced by proteolytic cleavage of collagen XVIII. It has a board spectrum of antiangiogenic effect and interacts with FGF-2 and VEGF. Endostatin inhibits angiogenesis by down-regulating many signaling pathways, including TNF-α, NFkB ephrin, and adhesion cascades, which decrease viability and migration of endothelial cells. Endostatin blocks pro-angiogenic gene expression controlled by c-Jun N-terminal kinase through interfering with TNF-α activation. It reduces the growth of cells by inhibiting cyclin D1, and thus induces apoptosis. Endostatin also regulates FGF signaling transduction and further inhibits migration of ECs. Endostatin may prevent the activity of certain metalloproteinases.

Thrombospondin

Thrombospondins (TSP) are secreted endogenous proteins that inhibit angiogenesis. TSP was discovered by Nancy L. Baenziger. This family has five members (TSP1-5). TSP1 is a well studies protein. It is encoded by THBSa, first isolated from platelets that stimulated with thrombin. TSP1 has been found in multiple biological processes, including angiogenesis, activation of TGF-β and immune regulation. TSP1 binds to several receptors. It inhibits proliferation and migration of ECs by activation of apoptosis.

3.2.5.2.2 Synthetic Angiogenesis Inhibitors

Several angiogenesis inhibitors have been developed and synthesized from organic chemistry methods to have novel compound. These compounds as potential angiogenic drugs have been involved in *in vitro* and *in vivo* analysis. In this section, these compounds are discussed especially for thalidomide.

Bevacizumab

There are many anti-angiogenic drugs widely used by patients. Basically, there are two types of anti-angiogenic drugs. The first type are antibodies. In clinic, one of the most widely used antibodies is bevacizumab, a humanized monoclonal antibody against VEGF-A, named

AVASTIN in the market. By targeting VEGF-A, bevacizumab can inhibit the VEGF/VEGFs signaling pathway resulting in suppression of angiogenesis. Bevacizumab was first approved in 2004 by the Food and Drug Administration (FDA) for combination chemotherapy in the treatment of colorectal cancer. Now it has been approved for various cancers such as non-small cell lung cancer, metastatic renal cell, recurrent glioblastoma multiform and diabetic retinopathy. It was approved for metastatic breast cancer in December 2010. However, later clinical trials showed that bevacizumab did not prolong the overall survival or slower disease progression in breast cancer. The lack of significant benefit to patients and a rise in safety concerns led to the withdrawal of bevacizumab in metastatic breast cancer. Bevacizumab also has adverse effects, since it inhibits blood vessels in all tissues due to the systemic administration of this drug. The main side effects are hypertension, bleeding, intestinal perforation and thrombotic microangiopathy.

Sunitinib

Sunitinib, known commercially as Sutent, was approved by the FDA in 2006 for renal cell cancer, imatinib-resistant gastrointestinal stromal tumours and other tumours. Sunitinib is a tyrosine kinase inhibitor. It targets the intracellular domain of several tyrosine kinase, including VEGFRs, PDGFRs, c-Kit, Ret, CSF-1R and Flt-3. By blocking the signaling pathway of VEF and PDGF, tumour blood vessels are reduced significantly according to several pre-clinical and clinical studies. However, multiple inhibitions in sunitinib treatment caused several side effects such as asthenia, fatigue, hair depigmentation, cardiotoxicity, hypothyroidism, hypertension, hematologic and gastrointestinal toxicities, and dermatologic adverse side effects. Sunitinib has been approved for treating renal cell cancer, Imatinib resistant gastrointestinal stromal tumour and pancreatic neuroendocrine tumours.

3.2.5.2.3 Thalidomide Analogues & Immunomodulatory Thalidomide Analogue (IMiDs)

Thalidomide has emerged as a potent treatment for several disease entities. In fact, thalidomide possesses both anti-angiogenic and anti-inflammatory properties, and was approved in 1998 by the FDA in the USA. As discussed above, with not only anti-angiogenic effects, thalidomide has been shown to inhibit TNF-α, so that combined anti-angiogenic and anti-TNF-α properties of thalidomide have brought to inhibition of anti-angiogenesis that may be a promising strategy in the cancer treatment. Due to number of side effects especially

the serious adverse events of teratogenic toxicity, a number of structural analogues of thalidomide have been synthesized by different researchers and tested for their anti-angiogenic or anti-TNF-α properties. Some of thalidomide analogues have been generally discussed about their angiogenic effects.

Immunomodulatory thalidomide analogues (IMiDs) are potent inhibitors of TNF-α demonstrated in LPS-induced PMCs in both *in vitro* and *in vivo* studies. It has been shown that relative to the parent compound thalidomide, IMiDs generated inhibitory effect on TNF-α more potently, as well as inhibiting LPS-induced monocyte IL1-β and IL-12 production, and enhanced the production of interleukin-10 (IL-10). As pro-apoptotic agents, Hideshima with co-workers first reported that thalidomide and IMiDs induce tumour cell apoptosis, evidenced by increased sub-G1 cells or induction of p21 and related G1 growth arrest. It has been determined that IMiDs generate the anti-proliferation effect of chemoresistant multiple myeloma cells by 20% to 35%, and dexamethasone-resistant MM cells by 50%. After in vitro assay, anti-angiogenic activities of IMiDs was found to inhibit the secretion of two angiogenic cytokines, VEGF and FGF from tumour and stromal cells. By application of a human umbilical arterial explants assay, the IMiD analogues generated a 100-fold increased anti-angiogenic potency compared to thalidomide. Also, the IMiD compounds have been shown to inhibit endothelial cell migration and adhesion perhaps due to downregulation of endothelial cell integrin. Therefore, immunomodulatory thalidomide analogue can be novel analogues as anti-cancer agents, agents such as lenalidomide, CC-4047 and ENMD-9095 were illustrated below.

Lenalidomide

Lenalidomide is an immunomodulatory analogue that has demonstrated its higher potency than thalidomide in to HUVEC proliferation and tube formation assay. The inhibitory effect to proliferation was in a dose-dependent manner with increasing concentration of treatment. The anti-angiogenic effects have been demonstrated in prostate cancer by increased microvessel density, which has been shown as a predictor of tumour stage. In the early studies, thalidomide in prostate cancer led to several studies utilizing thalidomide alone or in combination with chemotherapy in androgen-independent prostate cancer. An open-label phase II randomized trial comparing low-dose (200 mg/day) and high dose (up to 1200 mg/day) of thalidomide was completed in 63 patients (50 patients in the low dose arm, and

13 patients in the high-dose arm) and showed 28% reduction in the serum prostate specific antigen of ⩾50%. The low dose-dose arm showed sustainable response of > 150 days in patients with a > 50% decrease in prostate specific antigen. In contrast, patients on the high-dose arm shown no prostate specific antigen reduction but had adverse effects of sedation and fatigue that limited further dose escalation beyond 200 mg/day in 30% of the patients.

Lenalidomide was examined in patients with refractory solid tumours. Forty-five patients were enrolled, 36 of which patients had prostate cancer. The objectives of the study were to determine the maximum tolerated dose (MTD), characterize the side-effects, and characterize pharmacokinetics in patients with solid tumours. Therapy had been well tolerated with mostly grade 1 or 2 side-effects and only 2 patients with grade 4 neutropenia, and lenalidomide exhibited linear pharmacokinetic values.

Pomalidomide

Pomalidomide is co-stimulatory thalidomide analogue that can prime protective, long-lasting, tumour-specific, Th1-types response *in vivo*.

It has reported that pomalidomide treatment was associated with significantly increased serum IL-2 receptor and IL-12 levels, which is consistent with activation of T cells, monocytes and macrophages. The clinical activity for treatment of multiple myeloma has been found in 67% of patients. However, drug related toxicity thrombosis incidence was 12.5%, similar to treatment with thalidomide alone in multiple myeloma.

ENMD-0995 is a small molecule analogue of thalidomide, that is, the S(-) enantiomer 3-amino thalidomide. Thalidomide is a racemic glutamic acid analogue, consisting of S(-) and R(+)-enantiomers that interconvert under physiological conditions. The S(-) form potently inhibits release of TNF-α from peripheral blood mononuclear blood cells. The 3-amino derivative of thalidomide was demonstrated to have improved angiogenesis inhibitor activity that in animal model has shown no evidence of the toxic side effects as reported for the thalidomide molecule. Patent application were filed with claims directed to a method of treating undesired angiogenesis using 3-amino thalidomide. The S(-) enantiomer has been demonstrated pre-clinically to inhibit angiogenesis more potently than thalidomide in a murine corneal micropocket model. The 3-amino thalidomide has been involved in clinical

trial, all six patients had a decrease in M-spike seen with good partial response. In 2002, it was granted Orphan Drug designation from the FDA of treatment of patients with MM.

CPS49 and other Thalidomide Analogues

Previous studies have demonstrated that thalidomide metabolites are responsible for its anti-angiogenic functions. One of the products of cytochrome P450 2C19 isozyme biotransformation of thalidomide, 5'-OH-thalidomide, retains some anti-angiogenic activity. Another class of thalidomide analogue, N-substituted and tetrafluorinated classes of thalidomide analogues has been synthesized. The rat aortic ring assay was used to screen the analogues for their anti-angiogenic activity, and both classes of analogues showed the significant inhibition on microvessel growth in the assay. Also, anti-angiogenic activity was subsequently confirmed by HUVEC proliferation and tube formation experiments. One N-substituted analogue, CPS-11, and two tetrafluorinated analogues, CPS45 and CPS49, consistently exhibited the highest potency and efficacy in all three assays. The initial patent application for these compounds, as well as related analogues, was filed in 2002, and subsequently licensed to Celgene, Inc, based on promising *in vitro* and *ex vivo* finding, the therapeutic potentials of these agents were subsequently evaluated *in vivo*. Severely combined immunodeficient mice bearing subcutaneous human prostate cancer xenografts were treated with these analogues, at the determined maximum tolerated dose for daily dosing. Though CPS49 was the most potent, all analogues significantly inhibited PC3 tumour growth. In addition, both CPS45 and CPS49 significantly reduced PDGF-AA levels in these tumours, while CPS49 also decreased the intratumourally microvessel density.

CPS11 and CPS49 were also evaluated for their anti-MM activity in vitro. Compared to CPS11, CPS49 exhibited a wider activity spectrum and higher potency against MM cell lines. Importantly, pretreatment of bone marrow stromal cells with CPS11 or CPS49 abrogated their ability to induce proliferation of MM cells, confirming their ability to target tumour cells in the bone marrow microenvironment. This effect was more prominent for CPS49, consistent with its down regulation of IL-6, VEGF and IGF secreted by bone marrow stromal cells after binding to MM cells.

In recent years, it has reported that CPS45 and CPS49 could activate nuclear factor of activated T-cells transcriptional pathways while simultaneously repressing NF-κB via a rapid

intracellular amplification of reactive oxygen species (ROS). This ROS highly correlates to increase concentration of calcium in intracellular environment, also this lead to dissipation of the mitochondrial membrane potential and lead to caspase-independent cell death. Not only, but also this cytotoxicity is highly selective for most lymphoid leukemia cell lines, compared to resting PBMCs.

3.3 The Main Aims of in *in vitro* Testing and Significance

A review of the literature suggests structural activity relationship between thalidomide and its analogues, literature also suggests that substitution on either phthalimide ring or imide position on the glutarimide ring can preserve or even increase its biological activity with regards to TNF-α modulation activity. By consideration of this, all synthesized thalidomide analogues were placed *in vitro* studies, and involved in analysis of TNF-α modulation activity by applying human blood samples from nine healthy human volunteers. Thus, the first aim of this study is to determine and compare TNF-α modulation activity with both (inter-comparisons between thalidomide as control and thalidomide analogues) and (intra-comparison between only the thalidomide analogues).

As mentioned, tumour growth is dependent on angiogenesis, and inhibiting angiogenesis contributes to block tumour growth. Also, the anti-angiogenic effects from the parent compound thalidomide could be modified offer a change of the parent molecular structure. For this reason, the second aim was to determine and compare intra-comparisons and inter-comparisons relative to their anti-angiogenic effects *in vitro*.

Additionally, a breast cancer cell line was utilized for studies. In this study, the breast cancer cell line MDA-MB-231 was isolated by pleural effusion from patients with primary adenocarcinomas in the mammary gland. MDA-MB-231 cells are oestrogen and progesterone receptor negative and are tumourigenic *in vivo*. Thus, this type of cells are metastatic breast cancer cells that are used to learn about breast cancer cells with metastatic potential. Therefore, the anti-proliferative effect of the study's synthesized molecules against this type of cancer cell was necessarily determined for thalidomide and its analogues. The cell line also allows for a basic mechanism of action from treatment with thalidomide or its analogues to be determined and compared in this study.

3.4 Materials & Methods

Part I: *In vitro* Analysis for TNF-α Modulation Activity

3.4.1 Materials for Analysis of TNF-α Modulation Activity

Table 1: List of materials for analysis of TNF-α modulation activity

Number	Material Reagents	Catalogue Number	Suppliers
1	Blood buffy coat	12050-Buffy Coat-Lab use	NZ Blood Service
2	TNF-α Human Uncoated ELISA kit	88-7346-76	Affymetrix eBioscience USA
3	Lipopolysaccharides from E Coli O55:B55	L6529	Sigma Aldrich NZ
4	Sterile filtered fetal bovine serum (FBS)	MG-FBS0820	Medi'Ray NZ
5	Cell culture medium (RPMI1640, no phenol red)	11875093	Life Technologies NZ
6	*L*-glutamine (200 mM)	25030081	Life Technologies NZ
7	Penicillin-Streptomycin (10, 000 U/mL)	15140122	Life Technologies NZ
8	Ficoll-Paque Plus	GEHE17-1440-02	Global Science NZ

3.4.2 Methods for Analysis of TNF-α Modulation Activity

3.4.2.1 Preparation of Complete Medium Used

Complete culture medium contained cell culture fresh medium RPMI 1640 supplemented with 10% FBS, 1% of *L*-glutamine and 1% penicillin-streptomycin.

3.4.2.2 Preparation of Washing Buffer for TNF-α ELISA Assay

Wash buffer contains 0.05% Tween-20 in PBS. For example. 500 µL of Tween-20 was diluted with 999.5 mL of PBS to total of 0.05% Tween-20 in 1L.

3.4.2.3 Preparation of Stop Solution for TNF-α ELISA Assay

1 M Phosphoric acid was prepared that 34 mL of 85% phosphoric acid was diluted with distilled water to obtain 500 mL.

3.4.2.4 Preparation of Thalidomide & its analogues

Thalidomide solution preparation (Table 2): Thalidomide dissolves in DMSO to give stock solution 50 mg/mL. Then, DMSO will be used to dilute the stock solution to have the following concentrations including 12.5, 2.5, 0.5, 0.1 and 0.02 mg/mL. Each well in 24-well plate contains 1 mL of cells, then 2 µL of DMSO solution is added into each well to achieve the preferred treatment concentration 100 µg/ml to 0.04 µg/mL. For toxicity reasoning, 2 µL of DMSO control should be applied to compare with no DMSO negative control.

Table 2: Preparation of treatment from thalidomide and its analogues

Thalidomide & its Analogue Preparation	
Treatment concentration	**Preparation Concentration in DMSO**
100 µg/mL	50 mg/mL
25 µg/mL	12.5 mg/mL
5 µg/mL	2.5 mg/mL
1 µg/mL	0.5 mg/mL
0.2 µg/mL	0.1 mg/mL
0.04 µg/mL	0.02 mg/mL

3.4.2.5 Preparation of Lipopolysaccharides (LPS) from Escherichia coli 055:B5

LPS ordered from Sigma-Aldrich is 1 mg, and was completely dissolved in sterile PBS as 1 mg/ml. Lipopolysaccharide stock solution 1mg/ml was stored in -20 degrees for use around 3 months. Completed cell culture medium is to dilute LPS solution (Table 3).

Table 3: Dilution plan for lipopolysaccharide

Lipopolysaccharides from *E. coli* Preparation	
Stimulating concentration	**Preparation Concentration in Sterile PBS**
1000 pg/mL	1000 ng/mL
100 pg/mL	100 ng/mL
10 pg/mL	10 ng/mL
1 pg/mL	1 ng/mL

LPS will stimulate the production of TNF-α from white blood cells. At this stage, preliminary experiment is necessarily used to find out the appropriate concentration of LPS to use. Several concentrations of LPS including 1, 10, 100 & 1000 pg/mL will be used to quantify

the TNF-α production, and this is to determine sensitivity between white blood cells and different concentration of LPS. In this case, the use of complete culture medium is to dilute LPS stock solution to 1000 ng/mL, 100 ng/mL, 10 ng/mL and 1 ng/mL, then 1μL of each of concentration is to add into each well to achieve the preferred concentration including 1000 pg/mL, 100 pg/mL, 10 pg/mL and 1 pg/mL.

3.4.2.6 Procedure of seeding plate

Once receiving buffy coat from NZ Blood Service, concentration of monocyte was necessarily determined before seeding on the plate. Human blood (20 mL) sample were collected into heparinized tubes, and was overlayed on top of 10 ml of Ficoll-Paque Plus in 50 mL faclon polypropylene conical tubes in a sterile condition. The tubes were centrifudged for 30 mins at 300 × g and 4 degree, and the layer of cells was removed and its concentration was determined by method of cell counting (Section 3.5.2.4 Step 2). Based on the concentration of cells, give appropriate dilute white blood cells with complete medium to 1 × 1,000,000 cells/mL, then seed cells 1 mL of cells on 24 wells plate. After seeding cells, add 2 μL of drug treatment (thalidomide, its analogues dissolved in DMSO as stock solution) to each well, then add 1 μL of LPS to each well. Finally, each well contains 1ml of white blood cells with 2 μL of thalidomide or its analogue solution and 1 μL LPS solution with optimums concentration. After 12 hours of incubation, supernatants from each well will be removed for assayed immediately for TNF-α assay.

3.4.2.7 TNF-α ELISA Assay

Before assay started, ELISA plate was coated with 100 μL/well of capture antibody. The plate was sealed and incubated overnight at 2-8 degree condition in fridge. All capture antibody in each well was completely discarded and washed with 250 μL of ELISA washing buffer for 3 times. Allowing time for soaking about 1 min during each wash step increased the effectiveness of the washes. Absorben paper was applied to blot plate to remove any residual buffer. Then, all wells on the plate will be blocked with 200 μL of ELISA/ELISPOT diluent, and incubated for 1 hour. According to the manufacturer's instructure, ELISA assay standard (100 μL/well) was prepared and placed on the plate. All samples were collected from 24-well plate, and samples (100 μL/well) in triplicate were placed on flat-bottom 96-well plates pre-coated with immobilised monoclonal anti- TNF-α antibody and incubated at room temperature for 8 hour. The wells were then washed for 3-5 times, and biotinylated

polyclonal antibody to TNF-α was added, followed by peroxidase-labelled streptavidin, and incubated at room temperature for 2 hour. The wells were then washed, biotinylated polyclonal antibody to TNF-α was added, followed by peroxidase-labelled streptavidin, and incubated at room temperature for 1 hour. The wells were washed again, and the substrate (tetramethylbenzidine and hydrogen peroxide) was added and after 10 min the reaction was stopped with 1 M phosphoric acid. The absorbance at 450 nm was determined using a microtitre plate reader.

3.4.2.8 Calculation Method of TNF-α Inhibition Rate

This section was to describe about calculation method for inhibition of TNF-α after culturing human monocyte to treatment of thalidomide and its structural analogues. After absorbance OD values obtained, the inhibition rate of TNF-α production was calculated (Mu, 2007). The calculation equation of inhibition rate was shown in the below:

$$Inhibition\ Rate\ (\%) = \frac{OD\ of\ Treatment\ Group}{OD\ of\ Control\ Group} \times 100\%$$

The treatment group: OD absorbance values from cancer cell involving treatment of thaldiomide and its structural analogues. The control group meant OD absorbance values from cancer cell lines without any treatment.

Part II: Anti-aniogenesis Study

3.4.3 Materials for Anti-angiogenesis Assay

3.4.3.1 Cell Line Applied in this Study

Table 4: Cell line applied in this study

Cell line	Catalogue Number	Cell Line Description	Supplier
HUVEC	C0035C	Human Umbilical Vein Endothelial Cells are cells derived from endothelium of veins from the umbilical cord	Life Technologies NZ

The cell lines (Table 4) were stored in liquid nitrogen. After thawing the cell lines, this was maintained in tissue culture flasks containing completed growth culture medium in 37 ºC incubator with 5% carbon dioxide humidified air. HUVEC was maintaind in Medium 200 supplemented with Low Serum Growth Supplement (LSGS) in the absence of antibiotics and antimycotics.

The cell culture protocol and determination of cell doubling time for HUVEC was referred and described in detail in the Section 3.4.6.1 and Section 3.4.6.7. Accroding to the results of cell doubling time in logarithmic growth period for HUVEC is 48 hours (Appendix III Figure 112).

3.4.3.2 Reagents & Equipment of Anti-angigenesis Assay

Table 5: Main reagents & equipment in anti-angiogenic assay

Number	Material Reagents	Catalogue Number	Suppliers
1	Falcon matrigel Basement membrane matrix, 10 mL	FAL354234	In Vitro Technologies, NZ
2	Medium 200	M200500	Life Technologies, NZ
3	Low Serum Growth Supplement (LSGS)	S00310	Life Technologies, NZ
4	Paraformaldehyde	158127	Sigma Aldrich, NZ
5	Inverted Microscopes - ZEISS Primo Vert		Medi'ray NZ
6	Microscopes vision camera/full-color/ ZEISS AxioCam Erc 5s		Medi'ray NZ

3.4.4 Method of Tube Formation Assay

Matrigel was placed in an ice bath and placed in a refrigerator at 4-ºC condition for overnight. 500 µL of matrigel was taken and distributed in Eppendorf, and stored in -20-ºC freezer again for further use.

3.4.4.1 Coating Plates with Matrigel

As other extracellular matrix preparations, matrigel gels quite easily, thus, it is important not to warm it during the thawing process and always to keep it on ice. Also, all pipettes and plates was pre-chilled before starting this experiment. Each well in 24-well plate was coated with 300 µL of matrigel which was allowed to solidify at 37 ºC for 1 hour. It is necessarily to avoid bubble formation.

3.4.4.2 Protocol for Cell Seeding & Tube Counting

The cell concentration of HUVEC was determined, and appropriate dilution was applied to achieve preferred cell concentration through Section 3.5.2.4 cytotoxic assay protocol. The cell concentration was determined at 4×10^4 cells/mL in a final volume of 1 mL in complete

medium containing treatment of thalidomide or its analogue with concentration at 2, 10, 50 and 250 μg/mL (Table 6). Therefore, 500 μL of cells (8×10^4 cells/mL) was prepared, and mixed with 500 μL of completed medium with treatment concentration at 4, 20, 100 and 500 μg/mL. The treatment was prepared through appropriate dilution as shown table below:

Table 6: Preparation of treatment for anti-angiogenic assay

Number	Concentration of Treatment Prepared in DMSO Stock (mg/mL)	Preparation Concentration with Complete Medium (μg/mL)	Treatment Concentration (μg/mL)	Percentage (%) of DMSO
1	50	500	250	1
2	10	100	50	1
3	5	20	10	0.4
4	0.5	4	2	0.8

After completing preparation of cells with medium containing specific concentration of treatment, the cell medium solution was placed onto the matrigel. After 15-18 h of incubation at 37 degrees at 5% carbon dioxide, the culture supernatant was removed. 500 uL of 4% paraformaldehyde PBS solution was applied to fix the cells for 5-10 mins and observe under an inverted microscope. Under an inverted microscope, there were nine viewing fields which were randomly selected in each well. Then, each of viewing pictures was recorded for data collection to calculate the tube formation with its relative area. The data collection from each viewing picture was achieved through imagine software ImageJ including number of tubes and tube area (mm^2). The average number of tubes formation was counted and averaged from all viewing pictures, and another numerical calculation was achieved in average through tube area (mm^2) *vs*. whole area (mm^2).

Part III: Cytotoxic Assay & Cell Cycle Mechanism Study

Cytotoxic Assay

3.4.5 Materials for Cell Culture & Cytotoxic Assay

3.4.5.1 Cell Line Applied in this Study

Table 7: Cell line information

Cell line	Catalogue Number	Cell Line Description	Supplier
MDA-MB-231	HTB-26	Mammary gland/breast; derived from metastatic site: pleural effusion	ATCC

The cell lines (Table 7) were store in liquid nitrogen. After thawing the cell lines, this was maintained in tissue culutre flasks containing completed growth culture medium in 37 ºC incubator with 5% carbon dioxide humidified air. MDA-MB-231 were cultured in Hyclone Leibovitz L-15 Medium with 2.05 mM *L*-glutamine supplemented with 10% fetal bovine serum.

3.4.5.2 Cytotoxic Assay Reagents

Table 8: Main materials in cell culture and cell viability assay

Number	Reagents	Supplier
1	Hyclone Leibovitz L-15 Medium, with 2.05 mM L-glutamine	Life Technologies, NZ
2	Trypan Blue Solution, 0.4%	Life Technologies, NZ
3	TrypLE^{TM} Express Enzyme (1X), no phenol red	Life Technologies, NZ
4	Sterile filtered fetal bovine serum (FBS)	Medica Pacifica, NZ
5	MTT [3-(4, 5-dimethylthiazol-2-yl)-2, 5-diphenyltetrazolium bromide]	Sigma-Aldrich, NZ
6	Dimethyl sulfoxide (DMSO)	Merch-Chemicals
7	Cell culture consumable	Global Science, NZ
8	Phosphate buffered saline, PBS pH 7.2	Prepared by own

3.4.6 Methods for Cell Culture & Cytotoxic Studies

3.4.6.1 Cell Culture Protocol

Thawing cells

The cryovial containing frozen cells was removed from liquid nitrogen storage and immediately placed in ice condition for at least 30 mins. Then, the cryovial with cells was placed in a 37 °C water bath. The cells were quickly and completely thawed within a minute by swirling the vial in the 37 °C water bath. At this stage, the cells were necessarily changed the medium to start to culture into the incubator. Before opening the cell vial, the outside of the vial was wiped with 70% ethanol. The suitable amount of pre-warmed complete growth medium for cell lines was transferred dropwise into the centrifuge tube containing the thawed cells. After centrifuge for 5 mins at speed of 1200 RPM, a clear supernatant and cell pellet were obtained. The supernatant was aseptically decanted without disturbing the cell pellet. Finally, the cells were gently re-suspended in complete growth medium, and then transferred into a 25 cm^2 tissue culture flask and kept in a 37 °C, 5% CO_2, humidified incubator.

Changing Medium

Usually cells culture medium was necessarily changed if cells have been growing properly and its amount did not achieve to more than 80% confluent. The purpose of changing medium is to replenish nutrients and maintain the appropriate pH condition for cell growing. The cell culture medium was discarded from culture flask. PBS without calcium and magnesium (approximately 2 mL per 10 cm^2 culture surface area) was used to wash cells. The wash solution was removed and discarded. Finally, fresh pre-warmed culture medium (approximately 2 mL per 10 cm^2 culture surface area) was added and cells were returned to the 37°C incubator.

Passaging Adherent Cells

Cells were necessarily splited when they achieved 70-80% confluent. The cells were first washed using PBS (without calcium and magnesium), and the wash was removed from the flask. The pre-warmed dissociation reagent TrypLE™ Express Enzyme was added to the side of the flask (approximately 0.5 mL per 10 cm^2). The culture flask was placed in the incubator for approximately 2 minutes (the actual incubation time varies with the cell line used). When

more than 90% of the cells were detached, the equivalent of 2 volumes (twice the volume used for the dissociation reagent) of pre-warmed complete growth medium was added. The cells were transferred to a 15 mL centrifuge tube and centrifuged for 5 to 7 minutes (the centrifuge speed and time vary based on the cell type). The cell pellet was re-suspended in 1 mL pre-warmed complete growth medium and a sample was removed for counting. An appropriate volume of cells was pipetted into a new cell culture flask, and returned to the incubator. Note that most cells must not be split more than 1:10 as the seeding density would be too low for the cells to survive.

Freezing Cells

Freezing medium was prepared and stored at -20°C until use (the appropriate freezing medium depended on the cell line). The freezing medium contains a cryoprotective agent such as DMSO or glycerol. For adherent cells, cells were gently detached from the tissue culture vessel (following the procedure used during the subculture). The cells were then re-suspended in complete medium and the total number of cells was determined by counting. According to the desired viable cell density, the required volume of freezing medium was calculated. After centrifugation and decanting the supernatant, the cell pellet was re-suspended in cold freezing medium at the recommended viable cell density for the specific cell type. Aliquots of the cell suspension were dispensed into cryogenic storage vials. The cryovials containing the cells were placed in an isopropanol chamber and stored at -80°C overnight. The frozen cells were then transferred to liquid nitrogen, and stored in the gas phase above the liquid nitrogen.

3.4.6.2 Preparation of Phosphate Buffered Saline (PBS) pH at 7.2

The phosphate buffered saline (PBS, 10×) was composed of potassium phosphate monobasic (KH_2PH_4, 1, 440 mg/L), sodium chloride (NaCl, 90, 000 mg/L), and sodium phosphate dibasic ($Na_2HPO_4.7H_2O$, 7, 950 mg/L). The phosphate buffered saline (1×) with pH 7.2 was prepared by making 1 in 10 dilution of phosphate buffered saline (10×) in Millipore water. The pH value was adjusted to 7.2 by using 1 M sodium hydroxide (NaOH) or 1 M hydrochloric acid (HCl).

3.4.6.3 Preparation of MTT

5 mM of MTT solution was prepared in the phosphate buffered saline (PBS). Before use, the 5 mM MTT phosphate buffered saline was filtered through a sterile Millex GV 0.22 µm syringe filter to remove any pathogens, undissolved MTT and any spontaneously formed formazan crystals.

3.4.6.4 Cytotoxic Assay Protocols

The MTT assay protocol used in this study was first described by Mosmann (Mosmann, 1983). The general protocol step of MTT assay included cell stock preparation, cell counting, seeding cells on the plate, adding treatment to cells, changing medium and MTT quantification.

Step 1: Cell Stock Preparation

The old culture medium was carefully removed with the aid of a pipette. 5 mL of sterile pre-warmed PBS was used to wash cancer cells. Approximately 2.5 mL of TrypLE^{TM} Express solution was used to treat cells for no more than 15 minutes in cell incubator to detach cells. 5-10 mL of completed growth medium was then added into culture flask to stop trypsinization. Solution was transferred into 15 mL centrifuge tube, and centrifuged (HITACHI) at 125*g* x for 5-7 mins. The supernante was then carefully removed and 1 mL of new completed culture medium was added into tube to re-suspend cells gently but thoroughly. This is the cell stock for further steps.

Step 2: Cell Counting

10 µL of the cell suspension was placed onto a piece of parafilm and mixed thoroughly with 10 µL of Trypan Blue. 10 µL of this mixture was then placed to one side of the hemocytometer and the number of cells was determined under the microscope. After counting at least four squares, average number of cells was generated. The total number of cell in 1 mL culture medium was calculated by using the formula below:

$$\text{Average number of cells per square} \times 2 \times 10^4 = \text{number of cells/mL}$$

Step 3: Seeding Cells

Based on cell concentration, the supplement of complete culture medium was applied to make preferred cell concentration, then 100 µL of cells with specific cell density was seeded on 96-well plates.

Step 4: Adding Treatment

After cell seeding, 100 µL of thalidomide or its structural analogues treatment prepared were added to a 96-well plate to determine the anti-proliferative effects

Step 5: Changing Medium

After incubation for a set of time (24, 48 & 72 hours), the medium containing treatment was carefully removed and replaced with 100 µL of fresh complete culture medium. In this step, it is very necessary to use prepared PBS solution to wash each well if the treatment was known to impact MTT assay results.

Step 6: MTT Quantification

An aliquot of 20 µL of MTT reagent was added into each well. The whole plate was incubated in cell incubator for at least 4 hours at 37°C. When purple precipitate was clearly visible under inverted microscope, 80 µL solution was carefully removed from each well and was replaced by 150 µL of dimethyl sulfoxide to dissolve all purple precipitate. The UV absorbance (OD value) was measured by a plate reader (FLUOstar Omega, Alphatech) at the wavelength of 540 nm with reference wavelength at 680 nm. The average absorbance value (OD value) was determined from triplicate readings, and then these average values subtracted the average value from the blank for final recording.

For cell linearity standard curve, plot absorbance (OD value) graph was plotted on the y-axis versus cell number per mL on the x-axis. The cell number selected should fall within the linear portion of the curve.

For dose dependent anti-proliferative effect curve, the cell viability was plotted on the y-axis against log concentration (thalidomide and its structural analogues concentration: µg/mL) on the x-axis. The cell viability (Growth rate) calculation was described in Section 3.5.2.5.4.

3.4.6.5 Cytotoxic Effects Determination from Thalidomide and its Synthetic Analogues

Before proceeding with MTT cell viability assay, it is necessary to determine the cell seeding density and incubation time for all cell lines used in this study. Thus, cell linearity MTT assay and cell doubling time are important to ensure a perfect linear relationship between MTT formazan assay and cell number. The cell number vs. absorbance standard curve was applied to determine linearity of the MTT assay, the cell number used in the cell viability studies hall within the linear portion of the curve.

3.4.6.6 Linearity of MTT Assay

The highest cell concentration was 800,000 cells/mL in this study. After a series one in two (1:2) dilution of cells bu culture medium, an aliquot of 100 µL cells were seeded in each well in triplicates on a 96-well plate (Table 9). After seeding for 18 hours, step 6 in Section 3.5.2.4 was undertaken to measure absobance at 540 nm. A linear relationship between absorbance value (OD value) and cell number was generated by plotting absorbance on the Y-axis against cell numbers on the X-axis.

Table 9: The dilution plan for cell linearity standard curve

Cancer Cell Line Growth Curve determination on 96-well plate			
Number	**Label Tubes (Cells/mL)**	**Cell Number/ per well (Cells/µL)**	**Cell Culture Concentration**
1	800,000	80,000	100 µL of 8×10^5 cells/mL stock
2	400,000	40,000	100 µL of 4×10^5 cells/mL stock
3	200,000	20,000	100 µL of 2×10^5 cells/mL stock
4	100,000	10,000	100 µL of 1×10^5 cells/mL stock
5	50,000	5,000	100 µL of 5×10^4 cells/mL stock
6	25,000	2,500	100 µL of 2.5×10^4 cells/mL stock
7	12,500	1,250	100 µL of 1.25×10^4 cells/mL stock
8	6,250	625	100 µL of 6.25×10^3 cells/mL stock
9	3,130	313	100 µL of 3.13×10^3 cells/mL stock

3.4.6.7 Determination of Cells Doubling Time

Cells doubling time (or more accuarately, cells doubling time is logarithmic growth period) is the period of time required for cells number to be double. Two method were used to calculate the doubling time of cells in this study. One was obtained directly through the formula beow and the second was calculated from the cell growth curve.

The cell doubling time calculation formula is shown below:

$$Td = T \times \frac{Lg2}{Lg(N/N0)}$$

Td: Doubling time; T: Time interval; N: Final Cell Number, N0: Initial cell number

100 µL of cells was seeded on the six 96-well plates with cell density at 5,000 cells/mL. Incubation time was set at time point for 0, 24, 48, 72, 96 and 120 hours. The MTT assay was applied at the each time point. The relationship was determined between absorbance and time. According to the cell number vs. absorbance standard curve, cell numbers at different time points were calculated by cell growth curve fitting. The results (Figure 113) were attached in the Appendix III. According to the results cells doubling time in logarithmic growth period for MDA-MB-231 is 36 hours.

3.4.7 Method to Cytotoxic Effect Determination from Synthetic Compounds of Thalidomide & Its Analogues

The optimized cell density was 10,000 cells/well. Each well contained 100 µL of cells. An aliquot of 100 µL culture medium containing thalidomide or its analogues at different concentration was added into each well, after cells was completed attached om the 96-well plate for overnight. There were four 96-well plates that were used with a series of ceontration treatment for each time point including Day 0 (0 Hour), Day 1 (24 Hours), Day 2 (48 Hours) and Day 3 (72 Hours) respectivley. This was to determine whether synthetic compounds thalidomide or its analogues that could generate anti-proliferative effect to cells in dose- and time- dependent manners. The UV absorbance (OD) values from MTT assay were used to determine the IC_{50} values. The effective concentration for 50% growth inhibition (IC_{50})

represents the effective concentration of treatment which gives 50% inhibition of maximum achieved.

Thalidomide and its analogues were synthesized in Chemistry Laboratory in AUT and used in *in vitro* studies. The purity of all synthetic compounds was determined by NMR. All synthetic compounds were dissolved in DMSO to a final concentration of 50 mg/mL as stock solution (Table 10). Aliquots of stock solution were separated and kept in -80-degree freezer. Then, DMSO stock solutions were diluted to achieve the treatment concentration as shown the table below.

Table 10: Thalidomide & its Analogues Dilution Plan in DMSO for Treatment in Breast Cancer Cell Line MDA-MB-231

Protocol to Prepare Thalidomide Analogue in DMSO with Completed Medium Dilution					
Number	**Concentration of Thalidomide Analogue in DMSO Stock (mg/mL)**	**Preparation of Thalidomide Analogue Concentration (µg/mL)**	**Volume of Thalidomide Concentration (µL)**	**Volume of Medium Added for Dilution (µL)**	**Final Volume (mL)**
1	**10**	**200**	**20**	**980**	**1**
2	**8**	**160**	**20**	**980**	**1**
3	**5**	**100**	**20**	**980**	**1**
4	**2.5**	**50**	**20**	**980**	**1**
5	**0.5**	**10**	**20**	**980**	**1**
6	**0.1**	**2**	**20**	**980**	**1**
7	**0.02**	**0.4**	**20**	**980**	**1**
8	**0.004**	**0.08**	**20**	**980**	**1**

3.4.7.1 Calculation Method of Cancer Cell Growth Rate

This section was to describe calculation method for inhibition of growth rate after culturing cancer cell lines to treatment of thalidomide and its structureal analogues. After absobance OD values obtained, the growth rate of cancer cell was calculated (Mu, 2007). The calculation equation of growth rate and inhibitory rate was shown in the below:

$$Cell\ Viability\ (Growth\ Rate)\ (\%) = \frac{OD\ of\ Treatment\ Group}{OD\ of\ Control\ Group} \times 100\%$$

$$Inhibition\ Rate\ (\%) = \frac{1 - OD\ of\ Treatment\ Group}{OD\ of\ Control\ Group} \times 100\%$$

The treatment group: OD absorbance values from cancer cell involding treatment of thaldiomide and its structural analogues. The control group meant OD absorbance values from cancer cell lines without any treatment.

Analysis of Cell Cycle Mechanism Study

The cell cycle is an ordered set of events culminating in cell growth and division into two daughter cells. The cell cycle consists of four distinct phases, including G1 phase, S phase, G2 phase and M phase. The cell cycle follow a sequence of G1-S-G2-M. The G1 phase stands for “GAP 1”, and the S phase stands for “Synthesis” in the stage of DNA replication. The G2 phase represents “GAP 2”, and cells are involved in stage of growing. The M phase means “Mitosis”, and in this stage chromosomes completely separate and cytokinesis occurs. The G0 phase in cell cycle is a resting phase and cells stop dividing.

Commonly, cellular DNA content is an important paramater and applied for cell cycle studies. fluorescent molecules are specifically and stoichiometrically used to bind DNA. Base on this, a linear relationship between cullular fluorescence intensity and DNA amount can be measured. The emited fluorescence of the DNA specific dyes is proportional to DNA content present in different phases of the cell cycle. PI as the fluorescent molecule can specifically intercalate to DNA content. PI also can bind to RNA, so that ribonublease (RNAse) is necessarily used to distringuish between RNA and DNA. Therefore, in order to determine the possible mechanism of action, MDA-MB-231 after treatment of thalidomide or its analogues was analysed for cell cycle alterations by staining with propidium iodide (PI).

3.4.8 Materials Applied for Cell Cycle Analysis

Table 11: Major materials in cell cycle analysis

Number	Materials	Supplier
1	Ribonuclease A from bovine pancreas, 1mg/mL stored in -20 ℃	Sigma-Aldrich, NZ
2	Triton TM X-100 for molecular biology	Sigma-Aldrich, NZ
3	Absolute Ethanol	Sigma-Aldrich, NZ
4	Propidium iodide, PI, 1mg/mL, stored in aluminum-foil paper and stored in 0-20 ℃	Sigma-Aldrich, NZ

3.4.9 Protocols for Cell Cycle Analysis

Cell cycle analysis was performed on 6-well plates. Each well contained the same number of cells (1×10^5 cells/mL) in 1mL and treatment with a series of dilution in the prepared concentration in 1mL, so the actual cell density was 50, 000 cells/mL and actual treatment concentration was achieved through the same volume of cells (Table 12).

Table 12: Treatment Preparation in Cell Cycle Analysis

Number	Concentration of Treatment in DMSO Stock (mg/mL)	Prepared Concentration with Completed Medium (μg/mL)	Treatment Concentration (μg/mL)	Percentage (%) of DMSO
1	50	1000	500	1
2	5	200	100	2
3	2.5	20	10	0.4
4	0.5	2	1	0.2

All treatments were prepared in 1.6 mL eppendorf tubes with prepared with completed culture medium. The 6-well plate was designed including control group and treatment groups. The control well was set in the plate of treatment group with 2 mL complete culture medium, and all treatments in 1 mL were added into treatment wells on the 6-well plate. Then, cells with concentration at 1×10^5 cells/mL was prepared after detaching, counting and dilution cells follow cell preparation referred to Section 3.5.2.4. After cell seeding on the plates, gentle mix was necessarily required to evenly make cells distribute on the plate. All of the

plates were kept in the incubator for 72 hours (day 3). Cells was collected and prepared for analysis of cell cycle by following procedure.

3.4.9.1 Cell Harvesting

After cells being cultured for the determined time, cells were collected and stored for analysis by flow cytmetry. All experiment procedure was preformed on the ice condition.

All suspension in each well was collected into 15 mL centrifuge tubes. 1 mL of PBS was added to wash cells and then transferred in tubes. 500 μL TrypLE^{TM} Express Enzyme was used to detach cells and the plate was placed in cell incubator for no more than 5 mins. After detaching, the cell solution was transferred to relevant 15 mL tubes, 1 mL PBS was applied to was wash each well, and collected into tubes. Then, the cells were centrifuged at 1200 RPM at 4 degree for 5 mins. The supernatant from each tube was discard, and cells were washed by PBS in 1 mL again. After centrifuge, most of the supernatant in each tube was discarded, and cells was re-suspended with the rest of PBS. 1 mL ice cold 80% ethanol was slowly added into each tube with mixing by vortex at low speed. The tube was title diagonally so the ethanol was added to the sides and not directly onto the cells, thereby avoiding formation of aggregates. Each tube was sealed with parafilm and kept at -20 ºC for at least overnight and not more than 10-14 days.

3.4.9.2 Cell Cycle Analysis

Step 1: Preparation of Cell Permeabilizing Solution

The permeabilizing solution contains 0.1% Triton × 100 (1μL for each 1 mL) + RNAse A (50 μg/mL from stock solution of 1mg/mL). For example for 20 tubes, 20 μL Triton ×100 + 1000 μL RNAse + 19,980 μL PBS.

Step 2: PI Staining

All tubes was centrifuged first at 125*g* for 5 mins after taking out from -20 degree freezer. The ethanol suspension was genetly r emoved, and 3 mL of ice cold PBS was applied to each tube and wash the cells twice. After discarding supernatant, 1 mL cell permeabilizing solution was applied to each tubes and incubated at 37 degree for 45 mins. After permeabilization, 5

μg/mL of PI (5 μL of 1 mL in each tubes) was added to each tube and kept for 5 mins. Finally everything from tubes was transferred to flow cytomety test tube and run.

3.4.10 Data Analysis

3.4.10.1 Analysis of MTT Assay Results

IC_{50}, the half maximal inhibitory concentration, is commonly used as a measure of drug effectiveness. IC_{50} was an important reference to measure the inhibitory effect of treatment in this study. It was calculated by dose-response inhibition, nonlinear regression (curve fit): Log (inhibitory) vs. Response-Variable slop (four parameters). IC_{50} calculation was performed by statistical software PRISM® software (Graphpad, Version 6.0).

3.4.10.2 Analysis of Cell Cycle Assay Results

Kaluza® flow cytometry analysis software (Version 1.3) bought from Beckman Coulter was the software applied in cell cycle results analysis to measure the cell cycle distribution in this study.

3.4.10.3 Statistical Analysis

All experiments in this study were performed at least three times. Statistical difference in multiple groups was determined by one-way ANOVA (Analysis of Variance) with PRISM® software (Graphpad, Version 6.0). Statistical comparisons were made by Post Hoc (Turkey's test). Analysis between two groups was determined by using unpaired Student's t test data are expressed as means ± S.D (standard deviation). Differences with $P < 0.05$ were considered significant and $P < 0.01$ were considered very significant.

3.5 Results

Part I: Tumour Necrosis Factor Modulation Activity

3.5.1 Results for Tumour Necrosis Modulation Activity

3.5.1.1 Results for LPS Sensitivity on TNF-α

Exposing human white blood cells to increasing concentrations of LPS from Escherichia coli O55:B5 induced a significant concentration-dependent elevation in secreted TNF-α levels in complete culture medium (Figure 43). Four concentrations of LPS between 1 and 1000 ng/mL were applied to determine the LPS sensitivity to production of TNF-α. A linear relationship was evident between the levels of secreted TNF-α protein and concentrations of LPS administrated. However, once the concentration of LPS increased to 1000 ng/mL, the level of TNF-α decreased to about 1.5-fold from an absorbance value of 0.4176 at 100 ng/mL LPS to an absorbance value of 0.2859 at 1000 ng/mL. 100 ng/mL with the highest amount of TNF-α secreted was applied for further experiment.

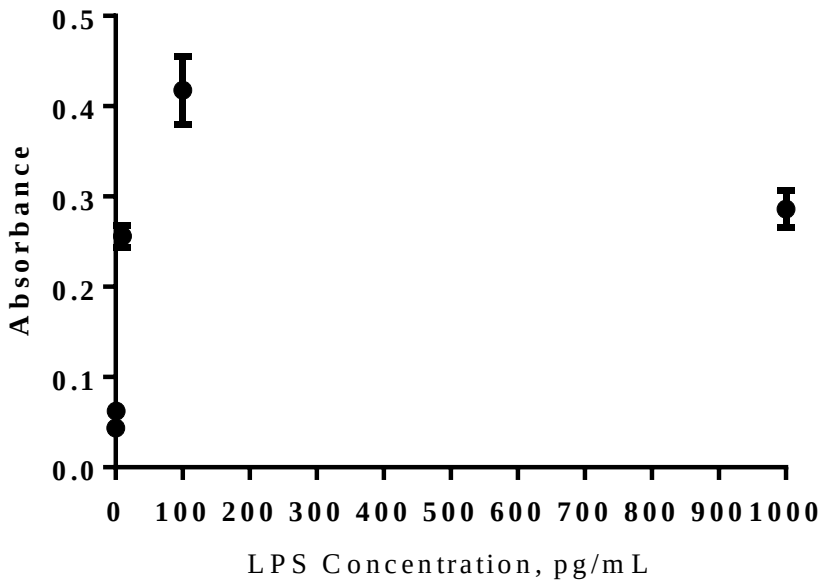

Figure 43: Optimization of level of TNF-α from human white blood cells induced by different concentration of Lipopolysaccharides (including 1 pg/mL, 10 pg/mL, 100 pg/mL and 1000 pg/mL).

3.5.1.2 Results for Effect of DMSO to Secretion of TNF-α

In the methodology indicated, DMSO was utilized to dissolve thalidomide and its analogues as 50 mg/mL, 12.5 mg/mL, 2.5 mg/mL, 0.5 mg/mL, 0.1 mg/mL and 0.02 mg/mL preparations of DMSO stock solutions. The appropriate amount of complete culture medium was applied to dilute the DMSO stock solutions. Finally, the treatment concentration of thalidomide or its analogues were achieved by diluting the stocks to 100 μg/mL, 25 μg/mL, 5 μg/mL, 1 μg/mL, 0.2 μg/mL and 0.04 μg/mL respectively. All cell treatments were characterized by a 500-fold dilution of DMSO: 2 μL of treatment concentrations were diluted in 1 mL of media for each sample well. Therefore, it was necessary to determine whether 0.2% DMSO affected the secretion of TNF-α. The effect of DMSO was analyzed (in triplicate) for each patient in this study. After comparisons of absorbance values at 450 nm and 570 nm, the results showed that there was no significant difference between the presence of DMSO and the absence of DMSO, with the *P*-value > 0.05. This initial set of analyses ruled out any interference from DMSO on the effects of thalidomide or its analogues in the modulation activity of TNF-α. These results were consistent across in all thalidomide analogues analysed.

3.5.1.3 Results for Standard Curve of Human TNF-α ELISA

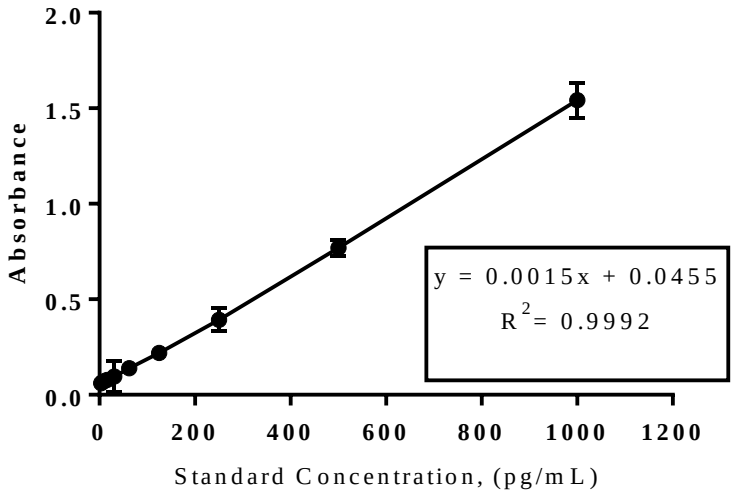

Figure 44: Standard curve of Human TNF-α and absorbance values. Data are presented as means ± S.D, n = 6.

The Log value of standard concentration vs. Log value of absorbance OD value at 580 nm is shown in Figure 44. The linear relationship between Log value of absorbance OD value at 450 nm wavelength and a series of standard concentrations (from 500 pg/mL to 3.906 pg/mL) is good ($R^2 = 0.9973$). This result indicated that the quality of the ELISA assay kits was quite good and they were ready for the subsequent experiments. Additionally, the linear relationship suggested a dose dependent relationship achieved within the concentration range of TNF-α. The concentration range for the following TNF-α modulation activity assay fell within the linear portion of this standard curve.

3.5.1.4 Effects of Thalidomide & its Analogues on LPS-induced TNF-α Production

Significant TNF-α production was obtained when human white blood cells were cultured with 100 pg/mL of LPS, which was determined from prior experiments. Human white blood cells were cultured with LPS plus thalidomide or its analogues at various concentrations for 12 hours, and the supernatants were assayed for effects of LPS-induced TNF-α production. All blood samples were collected from NZ Blood Service from nine healthy volunteers. Thalidomide, 2-(2,6-dioxopiperidin-3-yl)-phthalimidine (EM-12) (compound 2), 3-[(1*R*)-1-hydroxy-1-methyl-3-oxo-1,3-dihydro-2*H*-isoindol-2-yl]piperidine-2,6-dione (compound 3), 3-[(1*S*)-1-hydroxy-1-methyl-3-oxo-1,3-dihydro-2*H*-isoindol-2-yl]piperidine-2,6-dione (compound 4) and 2-(1-Chloromethyl-2,6-dioxopiperidin-3-yl)phthalimidine (compound 5) have been found to decrease LPS-induced TNF-α level in all human blood samples tested. In the following section, TNF-α modulation activity will be described and compared in detail.

Volunteer I

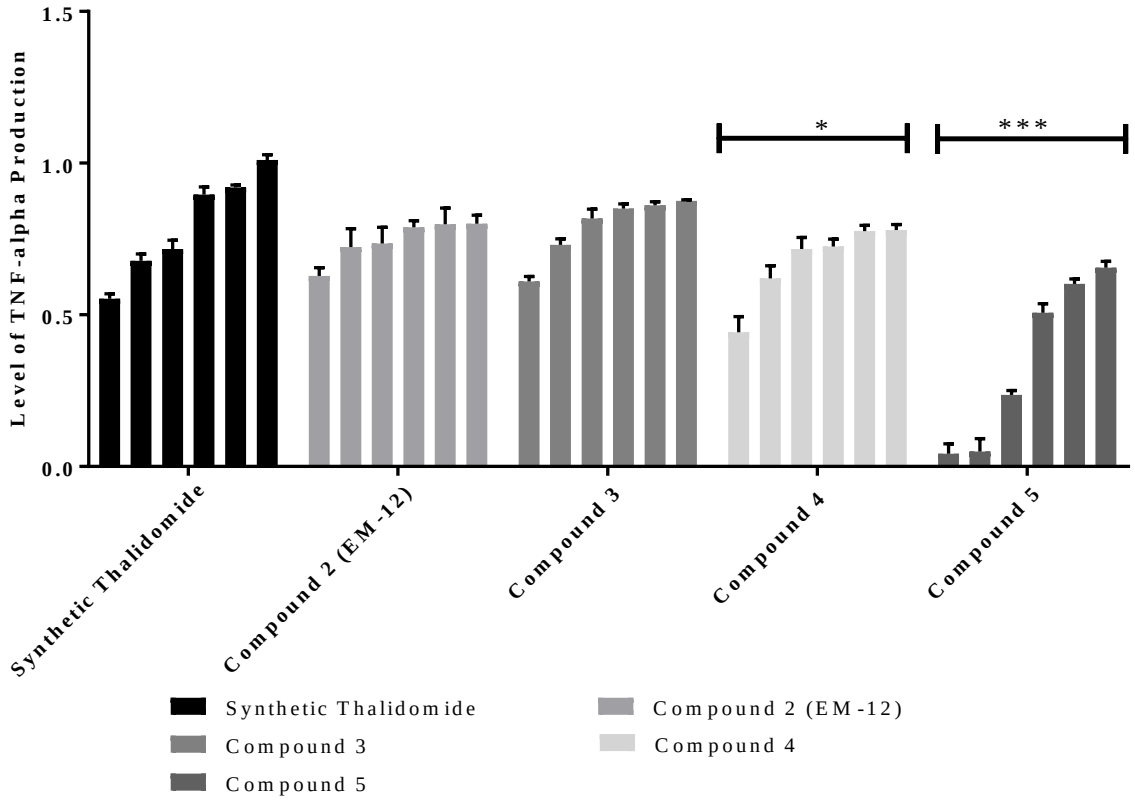

Figure 45: Inhibitory effects of all treatments on LPS-induced TNF-α production for healthy human volunteer I. The treatments included: thalidomide (compound **1**), 2-(2,6-dioxopiperidin-3-yl)-phthalimidine (EM-12) (compound **2**), 3-[(1R)-1-hydroxy-1-methyl-3-oxo-1,3-dihydro-2H-isoindol-2-yl]piperidine-2,6-dione (compound **3**), 3-[(1S)-1-hydroxy-1-methyl-3-oxo-1,3-dihydro-2H-isoindol-2-yl]piperidine-2,6-dione (compound **4**) and 2-(1-chloromethyl-2,6-dioxopiperidin-3-yl)phthalimidine (compound **5**). Human white blood cells from human volunteer I were treated with different concentrations at 0.04 μg/ml, 0.2 μg/ml, 1 μg/ml, 5 μg/ml, 25 μg/ml & 100 μg/ml for 12 hours. Data are means ± Standard Errors (n = 3). Asterisks indicated a value significantly different from the control value, *P < 0.05, **P < 0.01, ***P < 0.001 (Student's t test).

For human blood samples from volunteer I, results for TNF-α modulation activity assays are shown in Figure 45. TNF-α production after treatment with thalidomide and all other analogues was decreased in a dose-dependent manner, with P-value < 0.05. In the case of thalidomide, the gradual decrease of TNF-α production was clearly shown in all treatment concentration ranges from 1.01 ± 0.017 at 0.04 μg/mL to 0.58 ± 0.016 at 100 μg/mL.

However, for thalidomide analogues compound **2**, compound **3** and compound **4**, the level of TNF-α production was changed remarkably with treatment concentrations higher than 5 μg/mL. There was a small change in the level of TNF-α production for treatment concentrations lower than 5 μg/mL. For compound **5**, there was a sharp decrease in TNF-α production as treatment concentrations increased to 5 μg/mL, and nearly all TNF-α production was inhibited when the concentration of compound **5** increased to 25 μg/mL and 100 μg/mL.

When comparing the level of TNF-α production between treatment of thalidomide and other analogues, the level of TNF-α products after treatment with thalidomide was statistically similar to analogues observed with compound **2** and compound **3**, especially in the highest concentration (0.58 ± 0.016 for thalidomide versus 0.61 ± 0.027 for compound **2** versus 0.60 ± 0.017 for compound **3**) with *P*-value > 0.05. However, the level of TNF-α production after treatment with compound **4** and compound **5** were statistically and significantly lower than its level of TNF-α production in other treatments since *P*-value < 0.05.

Volunteer II

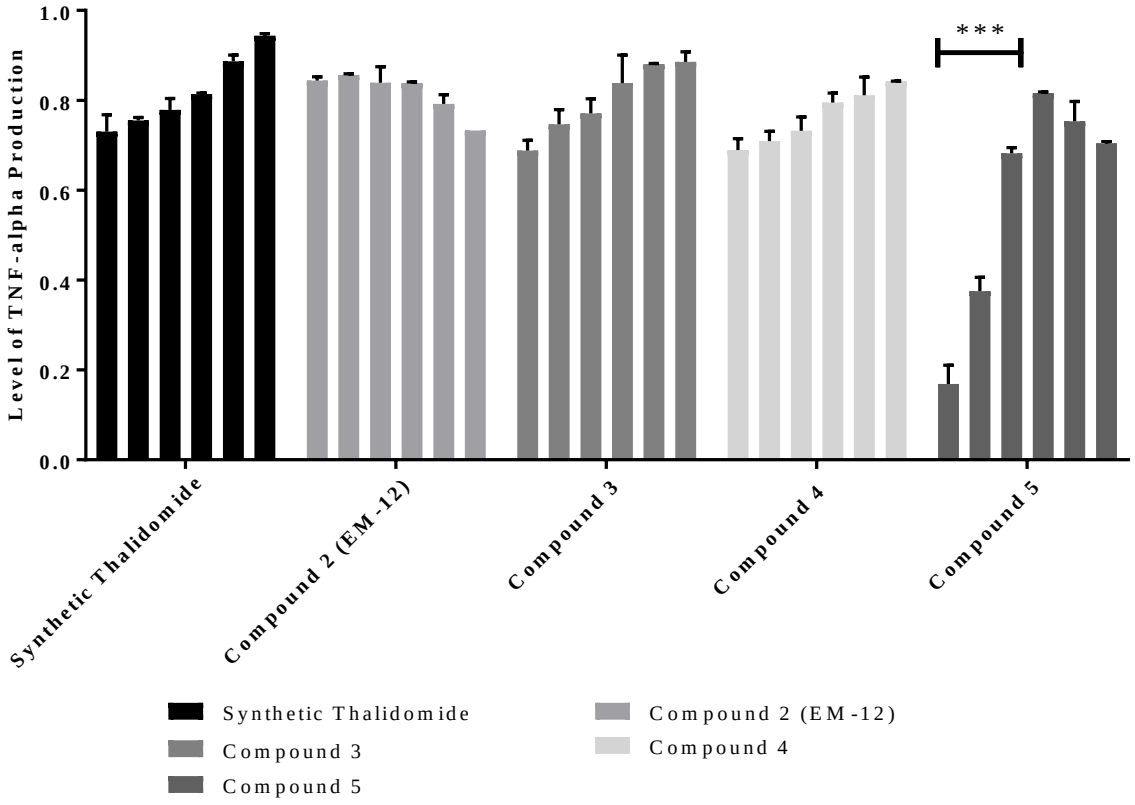

Figure 46: Inhibitory effects of all treatments on LPS-induced TNF-α production for healthy human volunteer II. The treatments included: thalidomide (compound **1**), 2-(2,6-dioxopiperidin-3-yl)-phthalimidine (EM-12) (compound **2**), 3-[(1R)-1-hydroxy-1-methyl-3-oxo-1,3-dihydro-2H-isoindol-2-yl]piperidine-2,6-dione (compound **3**), 3-[(1S)-1-hydroxy-1-methyl-3-oxo-1,3-dihydro-2H-isoindol-2-yl]piperidine-2,6-dione (compound **4**) and 2-(1-chloromethyl-2,6-dioxopiperidin-3-yl)phthalimidine (compound **5**). Human white blood cells from human volunteer II were treated with different concentrations at 0.04 μg/ml, 0.2 μg/ml, 1 μg/ml, 5 μg/ml, 25 μg/ml & 100 μg/ml for 12 hours. Data are means ± Standard Errors (n = 3). Asterisks indicated a value significantly different from the control value, **P* < 0.05, ***P* < 0.01, ****P* < 0.001 (Student's t test).

For human blood sample from volunteer II, results for TNF-α modulation activity assay have been shown Figure 46. TNF-α production after treatment from thalidomide, compound **3** and compound **4** was dramatically decreased with increasing treatment concentration from 0.04 μg/mL to 100 μg/mL, so that there was a negative relationship between dosage of treatment and level of TNF-α production in treatment of thalidomide, compound **3** and compound **4** with *P*-value < 0.05. However, for treatment of compound **2**, the compound **2** promoted the

growth of TNF-α product within its treatment concentration range from 0.04 μg/mL to 100 μg/mL. For compound **5**, the level of TNF-α production was dramatically decreased from treatment concentration 0.82 ± 0.003 at 1 μg/mL to 0.68 ± 0.025 at 100 μg/mL. In comparing the treatments, compound **5** could generate significant inhibition to reduce the level of TNF-α production since *P*-value < 0.05, especially with its treatment concentration increased to 25 μg/mL.

Volunteer III

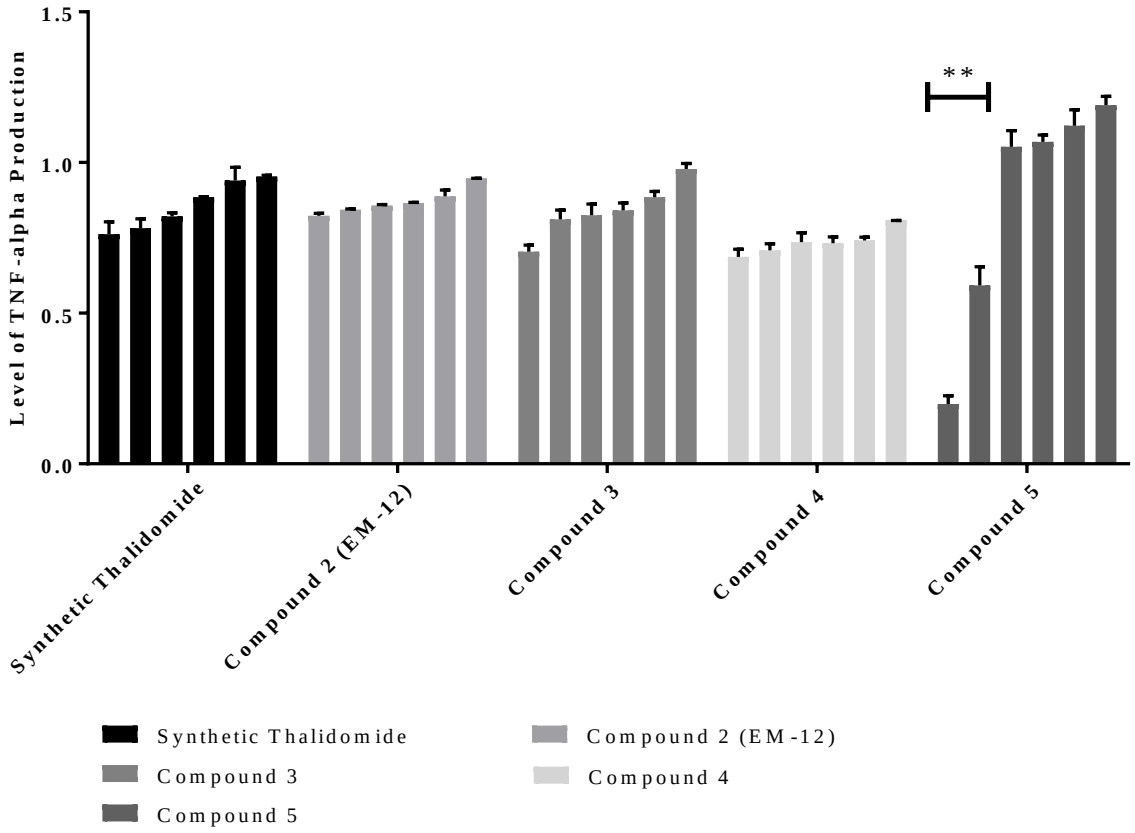

Figure 47: Inhibitory effects of all treatments on LPS-induced TNF-α production for healthy human volunteer III. The treatments included: thalidomide (compound **1**), 2-(2,6-dioxopiperidin-3-yl)-phthalimidine (EM-12) (compound **2**), 3-[(1R)-1-hydroxy-1-methyl-3-oxo-1,3-dihydro-2H-isoindol-2-yl]piperidine-2,6-dione (compound **3**), 3-[(1S)-1-hydroxy-1-methyl-3-oxo-1,3-dihydro-2H-isoindol-2-yl]piperidine-2,6-dione (compound **4**) and 2-(1-chloromethyl-2,6-dioxopiperidin-3-yl)phthalimidine (compound **5**). Human white blood cells from human volunteer III were treated with different concentrations at 0.04 μg/ml, 0.2 μg/ml, 1 μg/ml, 5 μg/ml, 25 μg/ml & 100 μg/ml for 12 hours. Data are means ± Standard

Errors (n = 3). Asterisks indicated a value significantly different from the control value, *P < 0.05, **P < 0.01, ***P < 0.001 (Student's t test).

For human blood sample from volunteer III, results for TNF-α modulation activity assays are shown in Figure 47. TNF-α production after treatment with thalidomide and all other analogues was decreased in a dose-dependent manner since P-value < 0.05. There was a negative relationship between treatment concentration and level of TNF-α product, with P-value < 0.05. For treatment of thalidomide and compound **2**, compound **3** and compound **4**, the level of TNF-α production was gradually decreased although the treatment concentration was increased 2500-fold from 0.04 μg/mL to 100 μg/mL. However, there was a slight drop in the level of TNF-α production from compound **5** in treatment concentrations of 0.04 μg/mL to 5 μg/mL, as well as a steep decrease after compound **5** treatment concentrations of 5 μg/mL to 100 μg/mL.

When comparing the inhibitory effect, the level of TNF-α production was reduced dramatically after treatment of compound **3** and compound **4**, and its effects were statistically higher than inhibitory effects from other treatments including thalidomide and compound **2**, with P-value < 0.05. For compound **5**, the level of TNF-α production was higher than other treatment within the treatment concentration range from 0.04 μg/mL to 5 μg/mL since as the P-value < 0.05. However, after the concentration kept increased from to 25 μg/mL to 100 μg/mL, the level of TNF-α production was significantly reduced to 0.16 ± 0.042 at 100 μg/mL.

Volunteer IV

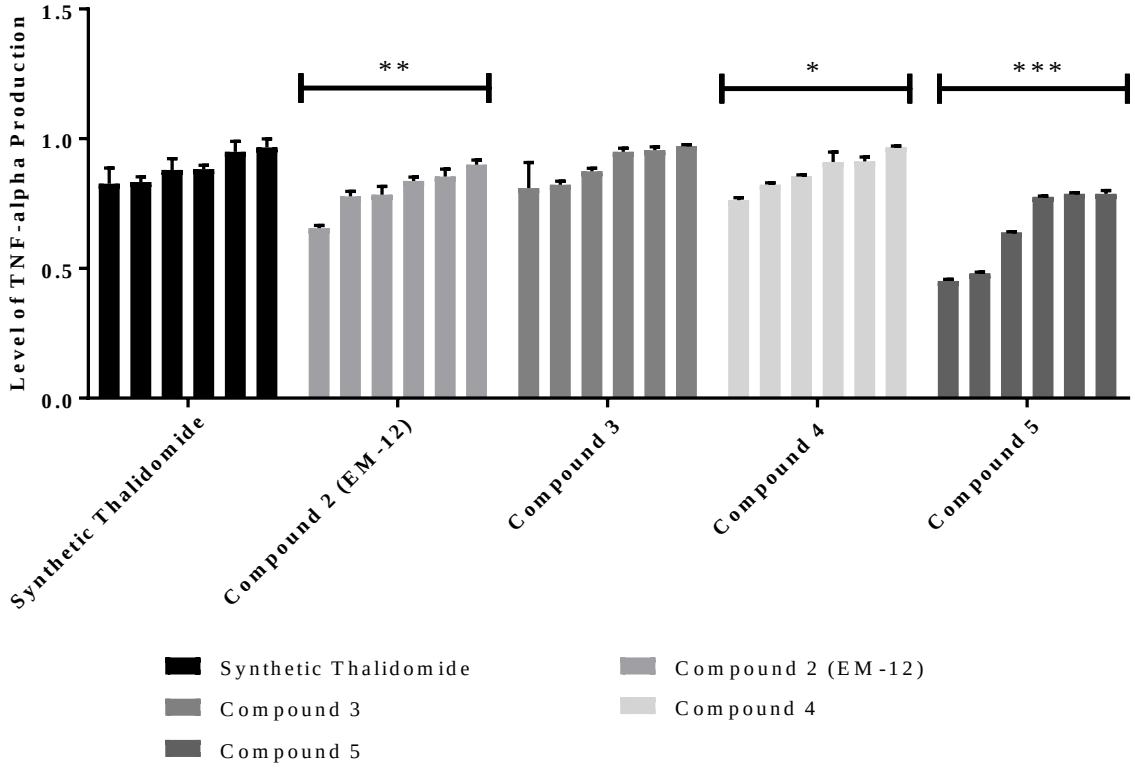

Figure 48: Inhibitory effects of all treatments on LPS-induced TNF-α production for healthy human volunteer IV. The treatments included: thalidomide (compound **1**), 2-(2,6-dioxopiperidin-3-yl)-phthalimidine (EM-12) (compound **2**), 3-[(1R)-1-hydroxy-1-methyl-3-oxo-1,3-dihydro-2H-isoindol-2-yl]piperidine-2,6-dione (compound **3**), 3-[(1S)-1-hydroxy-1-methyl-3-oxo-1,3-dihydro-2H-isoindol-2-yl]piperidine-2,6-dione (compound **4**) and 2-(1-chloromethyl-2,6-dioxopiperidin-3-yl)phthalimidine (compound **5**). Human white blood cells from human volunteer IV were treated with different concentrations at 0.04 μg/ml, 0.2 μg/ml, 1 μg/ml, 5 μg/ml, 25 μg/ml & 100 μg/ml for 12 hours. Data are means ± Standard Errors (n = 3). Asterisks indicated a value significantly different from the control value, *P < 0.05, **P < 0.01, ***P < 0.001 (Student's t test).

For the human blood sample from volunteer IV, results for TNF-α modulation activity assays are shown in Figure 48. TNF-α production after treatment with thalidomide and all other analogues was decreased in a dose-dependent manner since P-value < 0.05. Thus, there was a negative relationship between treatment concentration and level of TNF-α production with P-value < 0.05. For treatment of thalidomide, compound **2**, compound **3** and compound **4**, there was a gradual decrease about the level of TNF-α production in treatment concentrations

range from 0.04 μg/mL to 100 μg/mL. However, there was a significant decrease about the level of TNF-α production within the concentration range from treatment of compound **5**. The level of TNF-α production after treatment of compound **5** at 100 μg/mL was 0.45 ± 0.006, which is the lowest level of TNF-α production when compared with other treatments of thalidomide analogues (*P*-value < 0.05). When compared with thalidomide, compound **2** and compound **4** generated the higher inhibitory effect to reduce the level of TNF-α production with *P*-value < 0.05.

Volunteer V

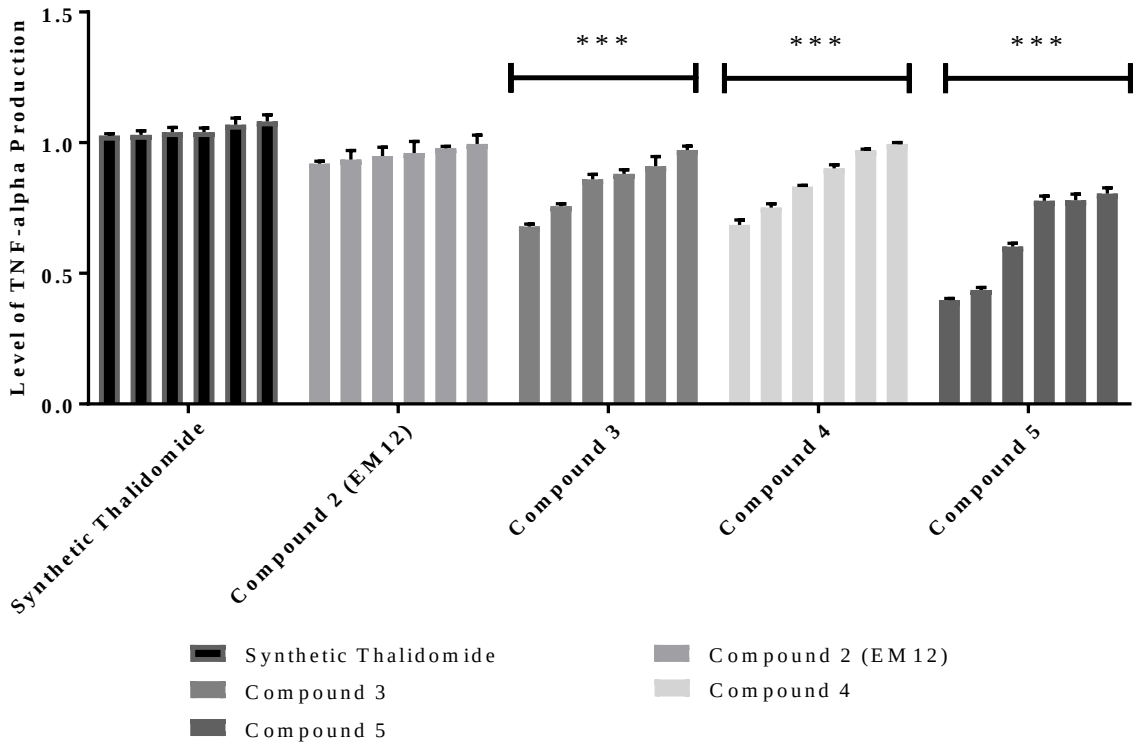

Figure 49: Inhibitory effects of all treatments on LPS-induced TNF-α production for healthy human volunteer V. The treatments included: thalidomide (compound **1**), 2-(2,6-dioxopiperidin-3-yl)-phthalimidine (EM-12) (compound **2**), 3-[(1R)-1-hydroxy-1-methyl-3-oxo-1,3-dihydro-2H-isoindol-2-yl]piperidine-2,6-dione (compound **3**), 3-[(1S)-1-hydroxy-1-methyl-3-oxo-1,3-dihydro-2H-isoindol-2-yl]piperidine-2,6-dione (compound **4**) and 2-(1-chloromethyl-2,6-dioxopiperidin-3-yl)phthalimidine (compound **5**). Human white blood cells from human volunteer V were treated with different concentrations at 0.04 μg/ml, 0.2 μg/ml, 1 μg/ml, 5 μg/ml, 25 μg/ml & 100 μg/ml for 12 hours. Data are means ± Standard

Errors (n = 3). Asterisks indicated a value significantly different from the control value, *P < 0.05, **P < 0.01, ***P < 0.001 (Student's t test).

For the human blood sample from volunteer V, results for TNF-α modulation activity assays are shown in Figure 49. TNF-α production after treatment with thalidomide and all other analogues was decreased in a dose-dependent manner since P-value < 0.05. Thus, there was a negative relationship between treatment concentration and the level of TNF-α production with P-value < 0.05. There was a slight decrease in the level of TNF-α production within the treatment concentrations from 0.04 μg/mL to 100 μg/mL from the treatment of thalidomide and compound **2**.

When compared to thalidomide, the higher inhibitory effect was found after treatment of compound **3**, compound **4** and compound **5** with P-value < 0.05. The significant inhibitory effect to reduce the level of TNF-α production was found from the treatment of compound **5** with P-value < 0.05. Of particular interest, after treatment of compound **5** at a concentration of 100 μg/mL, the level of TNF-α was about 0.39 ± 0.007, which was the lowest value for the TNF-α production after treatment from thalidomide and other structural analogues.

Volunteer VI

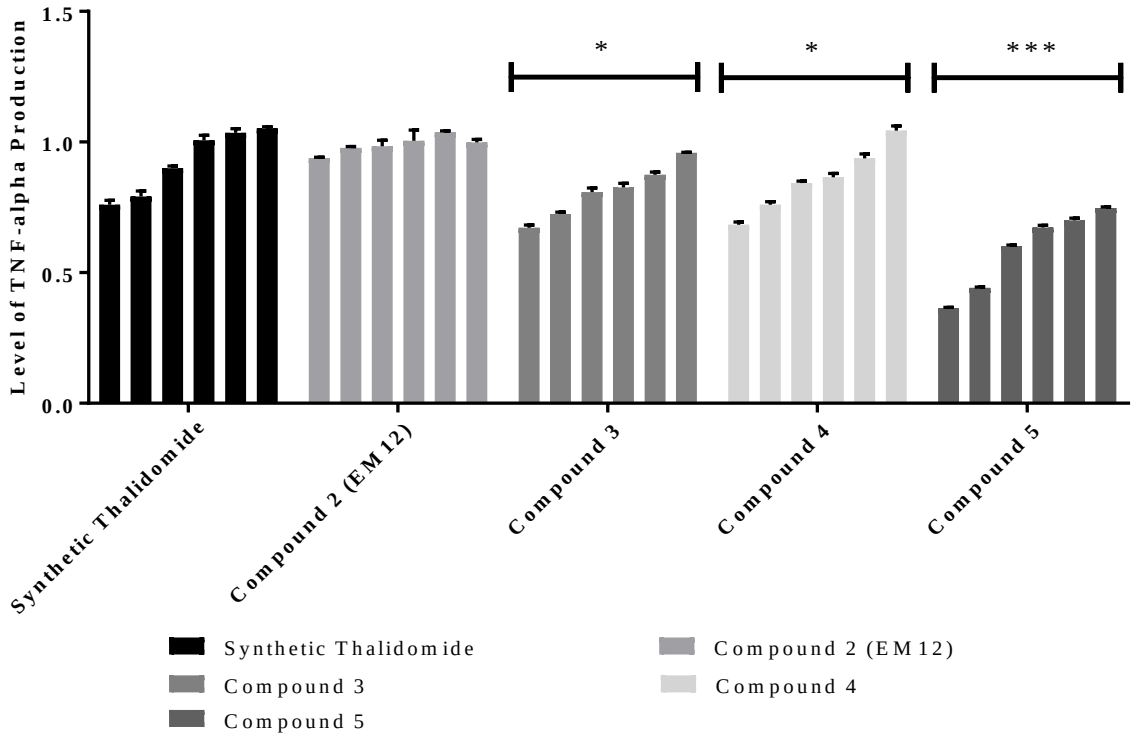

Figure 50: Inhibitory effects of all treatments on LPS-induced TNF-α production for healthy human volunteer VI. The treatments included: thalidomide (compound **1**), 2-(2,6-dioxopiperidin-3-yl)-phthalimidine (EM-12) (compound **2**), 3-[(1R)-1-hydroxy-1-methyl-3-oxo-1,3-dihydro-2H-isoindol-2-yl]piperidine-2,6-dione (compound **3**), 3-[(1S)-1-hydroxy-1-methyl-3-oxo-1,3-dihydro-2H-isoindol-2-yl]piperidine-2,6-dione (compound **4**) and 2-(1-chloromethyl-2,6-dioxopiperidin-3-yl)phthalimidine (compound **5**). Human white blood cells from human volunteer VI were treated with different concentrations at 0.04 μg/ml, 0.2 μg/ml, 1 μg/ml, 5 μg/ml, 25 μg/ml & 100 μg/ml for 12 hours. Data are means ± Standard Errors (n = 3). Asterisks indicated a value significantly different from the control value, *P < 0.05, **P < 0.01, ***P < 0.001 (Student's t test).

For the human blood sample from volunteer VI, results for TNF-α modulation activity assays are shown in Figure 50. TNF-α production after treatment from thalidomide and all other analogues was decreased in a dose-dependent manner since P-value < 0.05. Thus, there was a negative relationship between treatment concentration and the level of TNF-α production with P-value < 0.05. There was a slight decrease in the level of TNF-α production within the treatment concentrations from 0.04 μg/mL to 100 μg/mL from the treatment of compound **2**.

As compared to thalidomide, the higher inhibitory effect was found after treatment of compound **3**, compound **4** and compound **5** with *P*-value < 0.05. The significant inhibitory effect to reduce the level of TNF-α production was found in the treatment of compound **5** (*P*-value < 0.05). Of note, after treatment of compound **5** at a concentration of 100 μg/mL, the level of TNF-α production was about 0.36 ± 0.0041, and it was the lowest value of reduction about level of TNF-α production after treatment from thalidomide and other structural analogues.

Volunteer VII

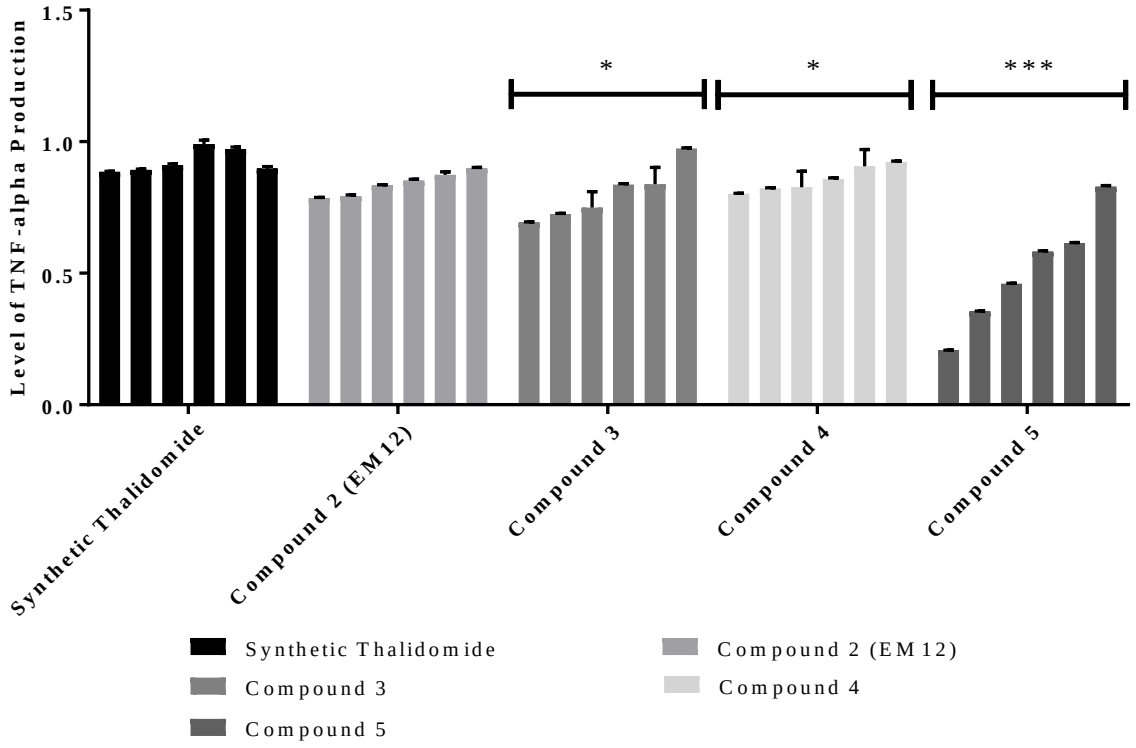

Figure 51: Inhibitory effects of all treatments on LPS-induced TNF-α production for healthy human volunteer VII. The treatments included: thalidomide (compound **1**), 2-(2,6-dioxopiperidin-3-yl)-phthalimidine (EM-12) (compound **2**), 3-[(1R)-1-hydroxy-1-methyl-3-oxo-1,3-dihydro-2H-isoindol-2-yl]piperidine-2,6-dione (compound **3**), 3-[(1S)-1-hydroxy-1-methyl-3-oxo-1,3-dihydro-2H-isoindol-2-yl]piperidine-2,6-dione (compound **4**) and 2-(1-chloromethyl-2,6-dioxopiperidin-3-yl)phthalimidine (compound **5**). Human white blood cells from human volunteer VII were treated with different concentrations at 0.04 μg/ml, 0.2 μg/ml, 1 μg/ml, 5 μg/ml, 25 μg/ml & 100 μg/ml for 12 hours. Data are means ± Standard

Errors (n = 3). Asterisks indicated a value significantly different from the control value, *P < 0.05, **P < 0.01, ***P < 0.001 (Student's t test).

For the human blood sample from volunteer VII, results for TNF-α modulation activity assays are shown in Figure 51. TNF-α production after treatment with thalidomide and all other analogues was decreased in a dose-dependent manner since P-value < 0.05. Thus, there was a negative relationship between treatment concentration and the level of TNF-α production with P-value < 0.05. The level of TNF-α production was slightly increased as a result of treatment the thalidomide at treatment concentrations of 0.04 μg/mL to 1 μg/mL, then its level of TNF-α production was slightly reduced within the treatment concentration range from 1 μg/mL to 100 μg/mL. Similarly, the level of TNF-α production was decreased to gradually from 0.89± 0.0027 at 0.04 μg/mL to 0.78 ± 0.002 at 100 μg/mL with treatment of compound **2**.

For compound **3** and compound **4**, the level of TNF-α production were moderately decreased within the treatment concentration range, but the level of TNF-α production after treatment of compound **3** and compound **4** were also statistically lower than the level from treatment of thalidomide, with P-value < 0.05. However, a negative relationship was clearly shown after treatment with compound **5** when comparing treatment concentration and the level of TNF-α production since P-value < 0.05.

Volunteer VIII

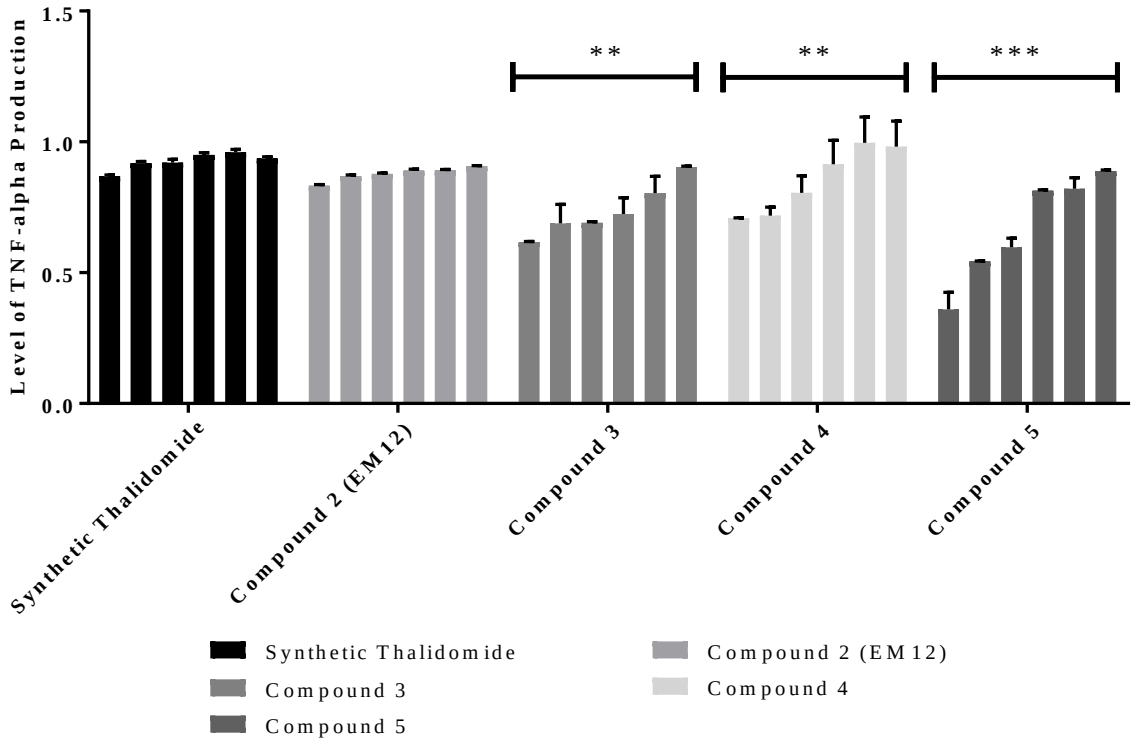

Figure 52: Inhibitory effects of all treatments on LPS-induced TNF-α production for healthy human volunteer VIII. The treatments included: thalidomide (compound **1**), 2-(2,6-dioxopiperidin-3-yl)-phthalimidine (EM-12) (compound **2**), 3-[(1R)-1-hydroxy-1-methyl-3-oxo-1,3-dihydro-2H-isoindol-2-yl]piperidine-2,6-dione (compound **3**), 3-[(1S)-1-hydroxy-1-methyl-3-oxo-1,3-dihydro-2H-isoindol-2-yl]piperidine-2,6-dione (compound **4**) and 2-(1-chloromethyl-2,6-dioxopiperidin-3-yl)phthalimidine (compound **5**). Human white blood cells from human volunteer VIII were treated with different concentrations at 0.04 µg/ml, 0.2 µg/ml, 1 µg/ml, 5 µg/ml, 25 µg/ml & 100 µg/ml for 12 hours. Data are means ± Standard Errors (n = 3). Asterisks indicated a value significantly different from the control value, **P* < 0.05, ***P* < 0.01, ****P* < 0.001 (Student's t test).

For the human blood sample from volunteer VIII, results for TNF-α modulation activity assays are shown in Figure 52. TNF-α production after treatment with thalidomide and all other analogues was decreased in a dose-dependent manner since *P*-value < 0.05. Thus, there was a negative relationship between treatment concentration and the level of TNF-α production with *P*-value < 0.05. The level of TNF-α production slightly dropped within the

treatment concentration range from 0.04 μg/mL to 100 μg/mL after treatment with thalidomide and compound **2**. However, other treatments including compound **3**, compound **4** and compound **5**, could generate an inhibitory effect to significantly reduce the level of TNF-α production within the treatment concentration range.

Comparing the inhibitory effects, compound **3**, compound **4** and compound **5** generated the higher effects in reducing the level of TNF-α production (*P*-value < 0.05) after treatment with thalidomide and compound **2**. For compound **5** especially, its inhibitory effect reduced the level of TNF-α at the treatment concentration of 100 μg/mL to its lowest level.

Volunteer IX

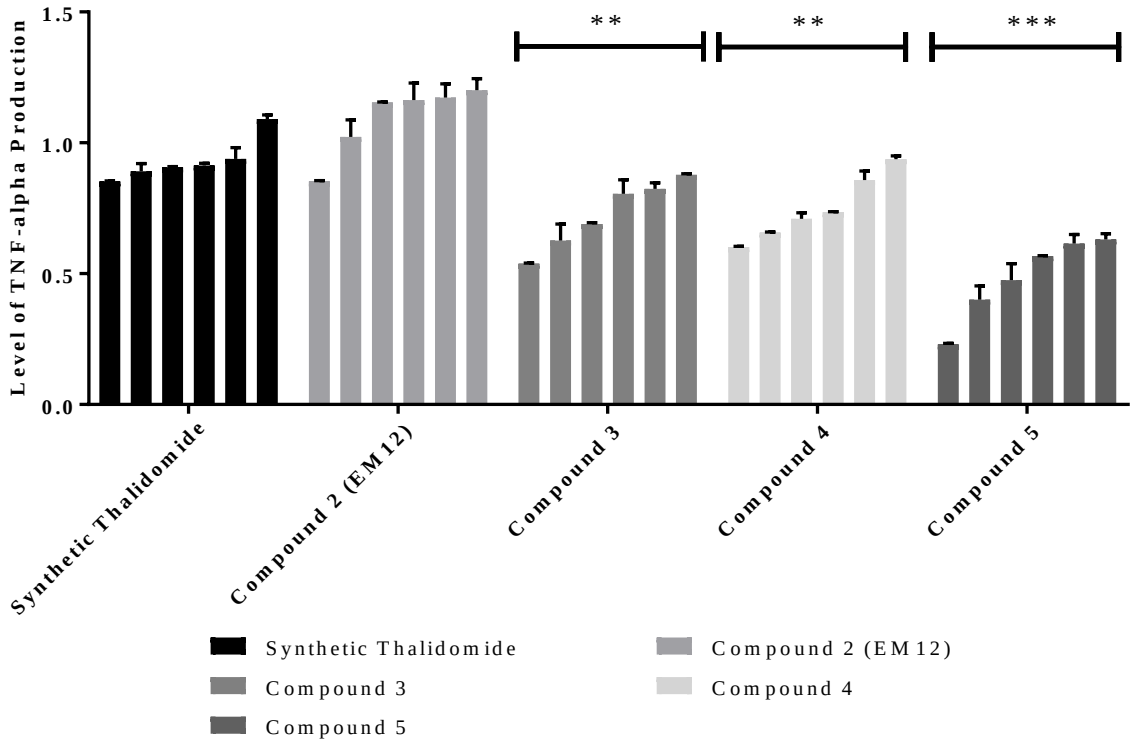

Figure 53: Inhibitory effects of all treatments on LPS-induced TNF-α production for healthy human volunteer IX. The treatments included: thalidomide (compound **1**), 2-(2,6-dioxopiperidin-3-yl)-phthalimidine (EM-12) (compound **2**), 3-[(1R)-1-hydroxy-1-methyl-3-oxo-1,3-dihydro-2H-isoindol-2-yl]piperidine-2,6-dione (compound **3**), 3-[(1S)-1-hydroxy-1-methyl-3-oxo-1,3-dihydro-2H-isoindol-2-yl]piperidine-2,6-dione (compound **4**) and 2-(1-chloromethyl-2,6-dioxopiperidin-3-yl)phthalimidine (compound **5**). Human white blood cells from human volunteer IX were treated with different concentrations at 0.04 μg/ml, 0.2

μg/ml, 1 μg/ml, 5 μg/ml, 25 μg/ml & 100 μg/ml for 12 hours. Data are means ± Standard Errors (n = 3). Asterisks indicated a value significantly different from the control value, *P < 0.05, **P < 0.01, ***P < 0.001 (Student's t test).

For the human blood sample from volunteer IX, results for TNF-α modulation activity assays are shown in Figure 53. TNF-α production after treatment with thalidomide and all other analogues was decreased in a dose-dependent manner since P-value < 0.05. Thus, there was a negative relationship between treatment concentration and the level of TNF-α production with P-value < 0.05. The level of TNF-α production slightly dropped within the treatment concentration range from 0.04 μg/mL to 100 μg/mL after treatment of thalidomide. For compound **2**, its inhibitory effect could reduce the level of TNF-α production to 0.85 ± 0.003 at a treatment concentration of 100 μg/mL, and its value is statistically similar to the inhibitory effect in treatments with thalidomide at 100 μg/mL. For compound **3**, compound **4** and compound **5**, there was a steep drop about the level of TNF-α production within treatment concentrations from 0.04 μg/mL to 100 μg/mL. When comparing the inhibitory effects, the level of TNF-α production after treatment with compound **3**, compound **4** and compound **5** were significantly higher than inhibitory effects from treatment with thalidomide and compound **2**, with P-value < 0.05. In comparing between compound **3** and compound **4**, LPS-induced TNF-α modulation activity was not statistically and significantly different between them. For compound **5** at a concentration of 100 μg/mL, its production level of 0.23 ± 0.032 was the lowest value as compared against other treatments with thalidomide and structural analogues.

Part II: *In vitro* Assay for Anti-angiogenic Effects

3.5.2 Results for Anti-angiogenic effects from treatment of thalidomide and its structural Analogues.

3.5.2.1 Linearity of Cell Line for HUVEC

In a standard (linearity) curve (Figure 54) and calculation of HUVEC cells doubling time (Appendix III Figure 112), the values from these are important to determine quality of cells before setting up experiment based on the HUVEC cells. A good linearity curve reflects a good quality status. Cell numbers used in cell viability studies should fall within the linear portion of the curve. Cell seeding concentration can neither be too high nor too low. Therefore, a good quality of cell growing conditions for cells can be defined for further experimental conditions applied. Figure 54 shows the linearity curve of HUVEC values. It shows a good linear relationship (R^2= 0.9409) between the absorbance measured at 540 nm wavelength and different cell densities (from 800, 000 cells/mL to 3, 125 cells/mL).

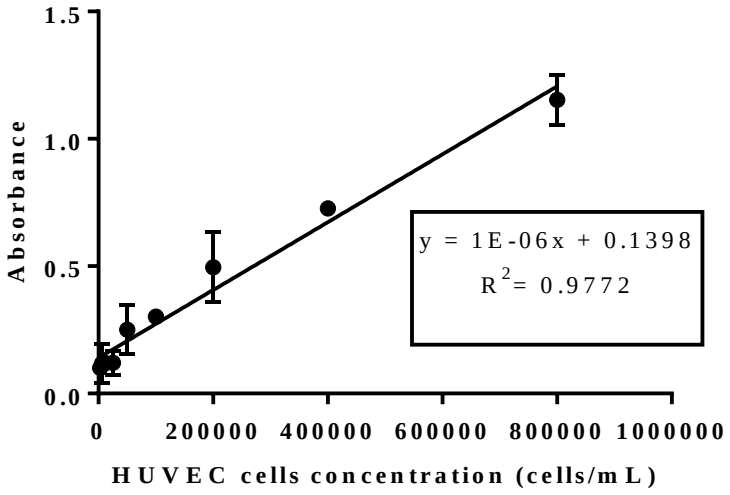

Figure 54: Linearity between HUVEC cell numbers and absorbance values. Data are presented as means ± S.D, n = 6.

3.5.2.2 Inhibitory Effect of Tube Formation in Matrigel

Tube formation by HUVEC on matrigel layers was used as an *in vitro* model for angiogenesis, and the ability of thalidomide or its synthetic analogues to inhibit tube formation was tested. There were nine viewing picture records for non-treatment, non-treatment with vehicle solvent and all thalidomide structural analogues. In the following, there were three views that have been shown in the results section, and all other viewing records are shown in the Appendix IV. The Figure 55 show that tube formations on matrigel layers in the medium-only condition. The average number of tubes in this condition was 20.89 ± 3.41, and the area of tube formation was 0.13 ± 0.03. Due to a solubility problem in the medium, thalidomide or its analogue was dissolved in DMSO initially as a DMSO stock solution. Then, complete cell culture medium was applied to dilute the stock solution to achieve appropriate treatment concentrations. In this case, DMSO was the vehicle solvent. Therefore, the presence of DMSO was tested against whether it affected cell viability or not. Figure 55 shows the tube formations on matrigel layers in medium in the presence of vehicle solvent. The average number of tubes in this condition was 21.87 ± 2.87, and the area of tube formation was 0.131 ±0.024.

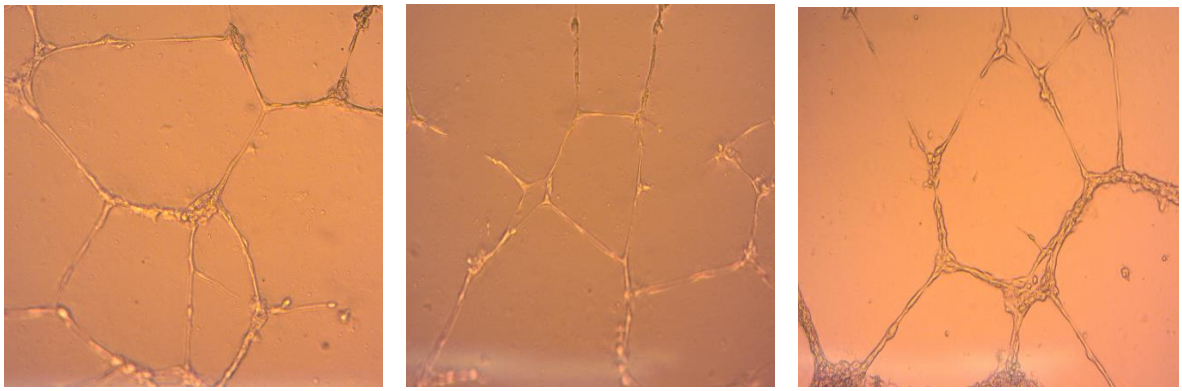

(1) (2) (3)

Figure 55: Tube formation of HUVEC cells in matrigel. Cells were treated with medium only. Nine viewing pictures that have been recorded.

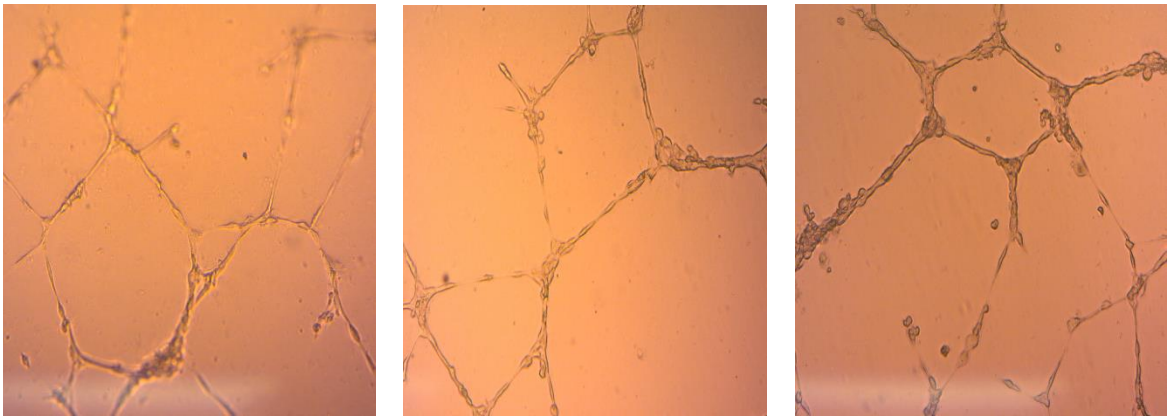

(1) (2) (3)

Figure 56: Tube formation of HUVEC cells in matrigel. Cells were treated with medium with vehicle. Nine viewing pictures that have been recorded.

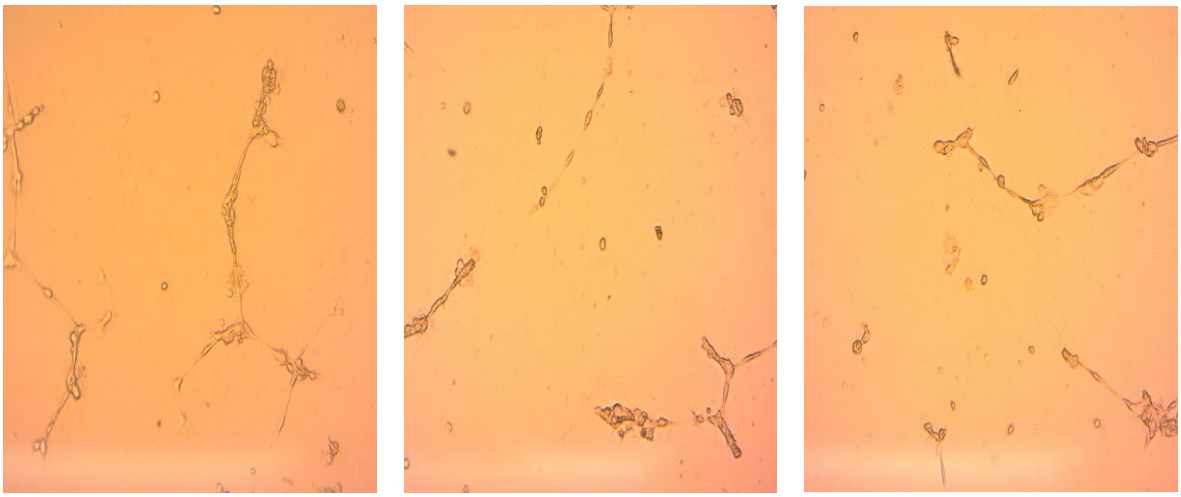

(1) (2) (3)

Figure 57: Tube formation of HUVEC cells in matrigel. Cells were treated with thalidomide (Compound **1**) in the concentration at 250 μg/mL. Nine viewing pictures that have been recorded.

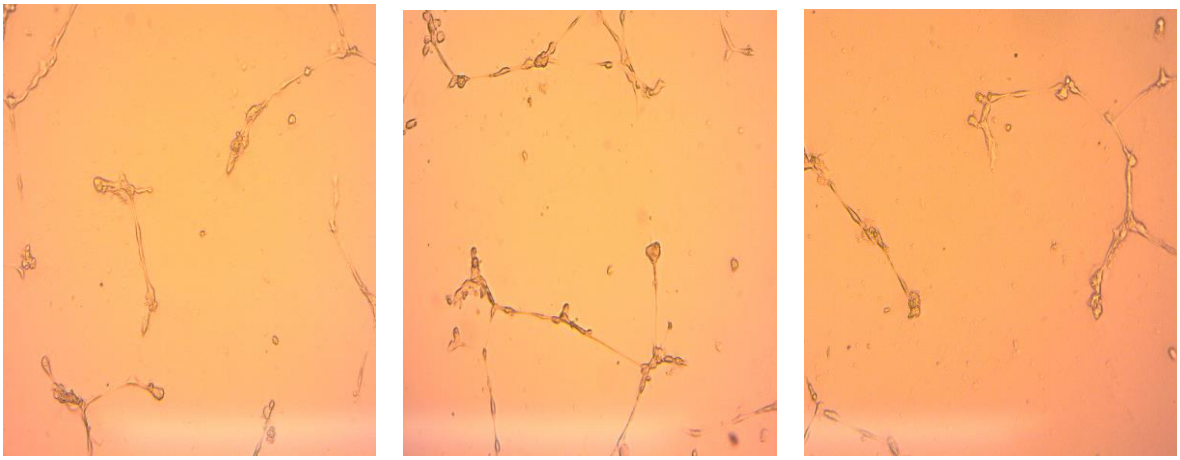

(1) (2) (3)

Figure 58: Tube formation of HUVEC cells in matrigel. Cells were treated with thalidomide (Compound **1**) in the concentration at 50 μg/mL. Nine viewing pictures that have been recorded.

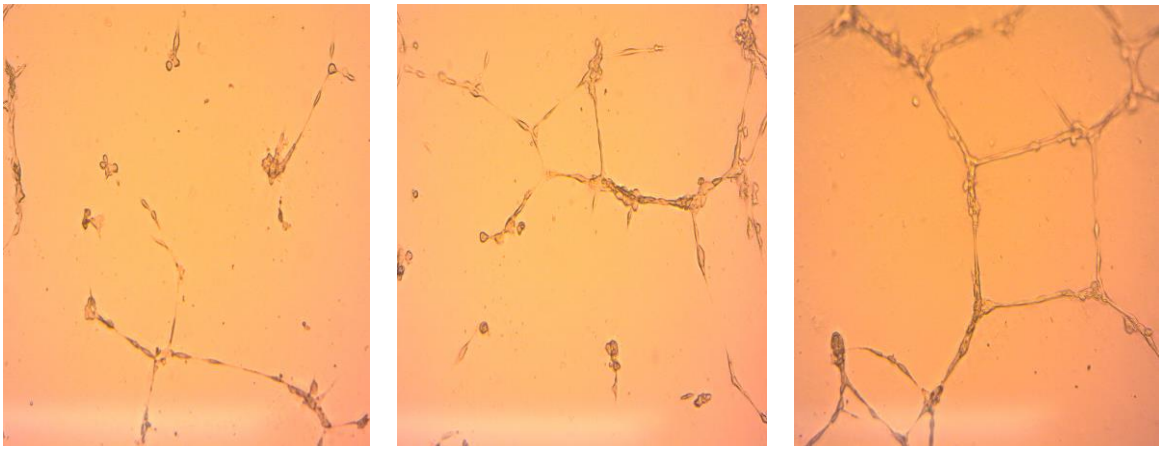

(1) (2) (3)

Figure 59: Tube formation of HUVEC cells in matrigel. Cells were treated with thalidomide (Compound **1**) in the concentration at 10 μg/mL. Nine viewing pictures that have been recorded.

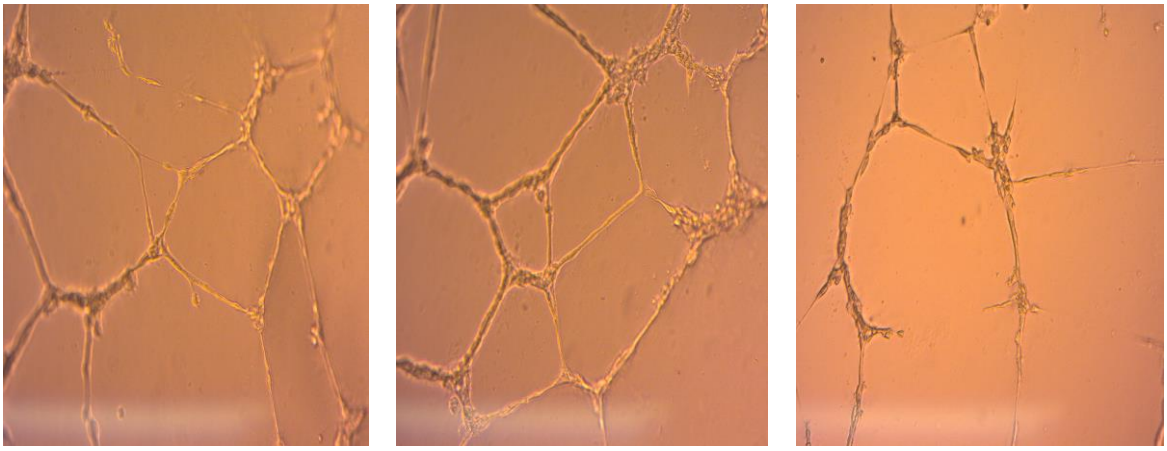

(1) (2) (3)

Figure 60: Tube formation of HUVEC cells in matrigel. Cells were treated with thalidomide (Compound **1**) in the concentration at 2 µg/mL. Nine viewing pictures that have been recorded.

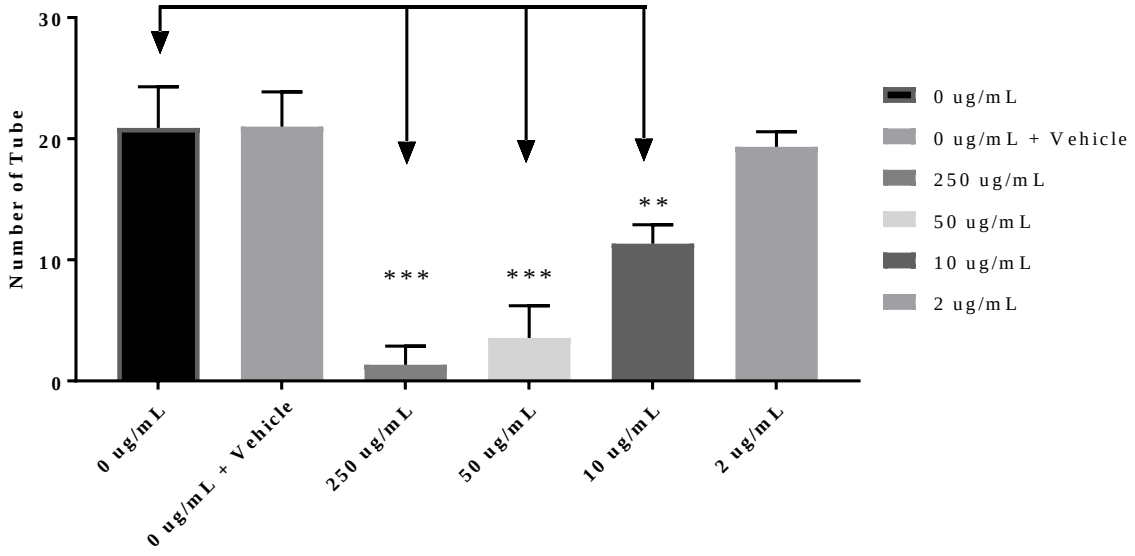

Figure 61: Comparison about number of tube formation of HUVEC cells in matrigel layer between non-treatment, non-treatment with vehicle solvent and treatment of thalidomide (compound **1**) at 250 µg/mL, 50 µg/mL, 10 µg/mL & 2 µg/m, (n=9). Asterisks indicated a value significantly different from the control value, *$P < 0.05$, **$P < 0.01$, ***$P < 0.001$ (Student's t test).

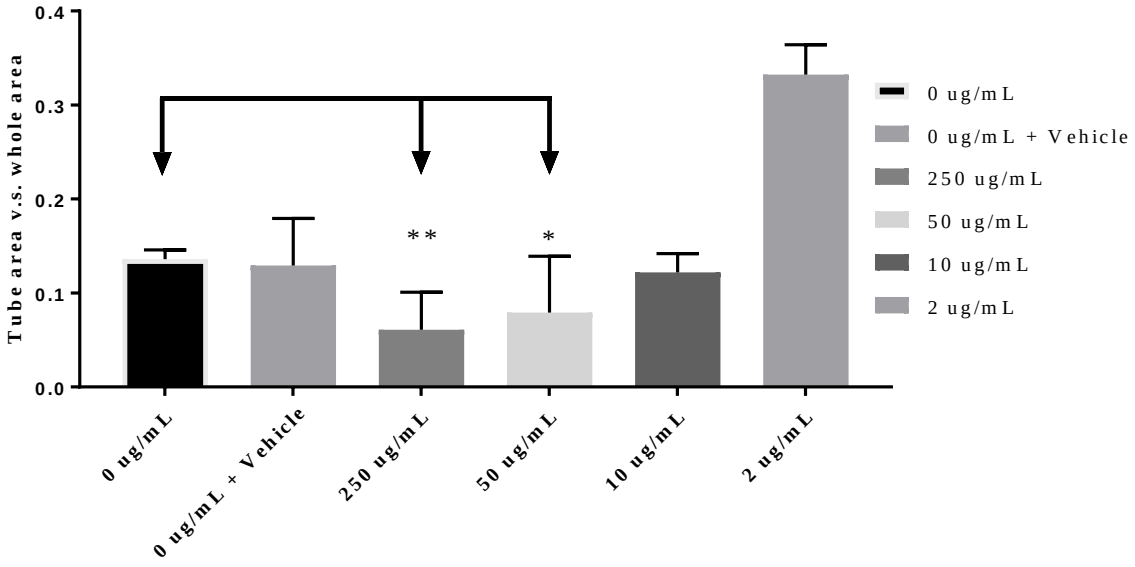

Figure 62: Comparison about area comparison (Tube area mm^2 *vs*. the Whole Area mm^2) of HUVEC cells in matrigel layer between non-treatment, non-treatment with vehicle solvent and treatment of thalidomide (compound **1**) at 250 µg/mL, 50 µg/mL, 10 µg/mL & 2 µg/mL, (n=9). Asterisks indicated a value significantly different from the control value, $*P < 0.05$, $**P < 0.01$, $***P < 0.001$ (Student's t test).

From Figure 57 to Figure 60 observations under an inverted microscope showed the tube formations on matrigel layer in complete culture medium with treatment of thalidomide (Compound **1**) at concentrations of 250 µg/mL, 50 µg/mL, 10 µg/mL and 2 µg/mL respectively. These figures contributed to visually determine change of tube formations after treatment with thalidomide. Both Figure 61 and Figure 62 show comparisons of the tube formations and tube area (Tube area, mm^2 *vs*. the Whole Area, mm^2) between the medium conditions, vehicle solvent and treatments from thalidomide at concentrations from 2 µg/mL to 250 µg/mL. These two figures contributed to comparisons of the capability of tube formations to determine the efficacy of treatment for anti-angiogenic agents in *in vitro* conditions, but also provided visual comparison for the number of tubes and tubes area between tube formation in medium-only and medium with vehicle solvent conditions.

As indicated in Figure 61 and Figure 62, the tube formation in both the numbers of tubes and tube areas seem to have no difference between them. This observation was statistically

approved in that there was no difference between tube formation in medium condition-only and medium with vehicle solvent conditions, since as *P*-value < 0.05.

Figure 57 indicates that few numbers with tubes formed after treatment with thalidomide at a treatment concentration of 250 μg/mL. The number of tubes formed after treatment with thalidomide (Compound **1**) at 250 μg/mL was 1.33 ± 1.12. From Figure 58 it is shown that after treatment with thalidomide (Compound **1**) at 50 μg/mL, more intact tubes formed on matrigel layers with an area number of 3.56 ± 0.88. With decreasing treatment concentrations to 1 μg/mL, a lot of intact tubes were formed. Therefore, there was a negative relationship between treatment concentration and the number of tubes formed, with *P*-value < 0.05. Comparing the percentage of tube area within the treatment concentration range, the percentage of tube area gradually increased even as treatment concentrations decreased 25-fold from 10 μg/mL to 250 μg/mL. There was a large difference in the percentage of tube area after treatment concentrations increased 5-fold from 2 μg/mL to 10 μg/mL. Also, the percentage of tube area from the treatment concentration at 2 μg/mL was significant higher than the value from other treatment concentrations. This result was visually approved from the observation that the tubes seemed to accumulate to a larger size, as shown in figure. In addition, statistical analysis indicated that there was a negative relationship between treatment concentration and the percentage of tube area, with *P*-value < 0.05.

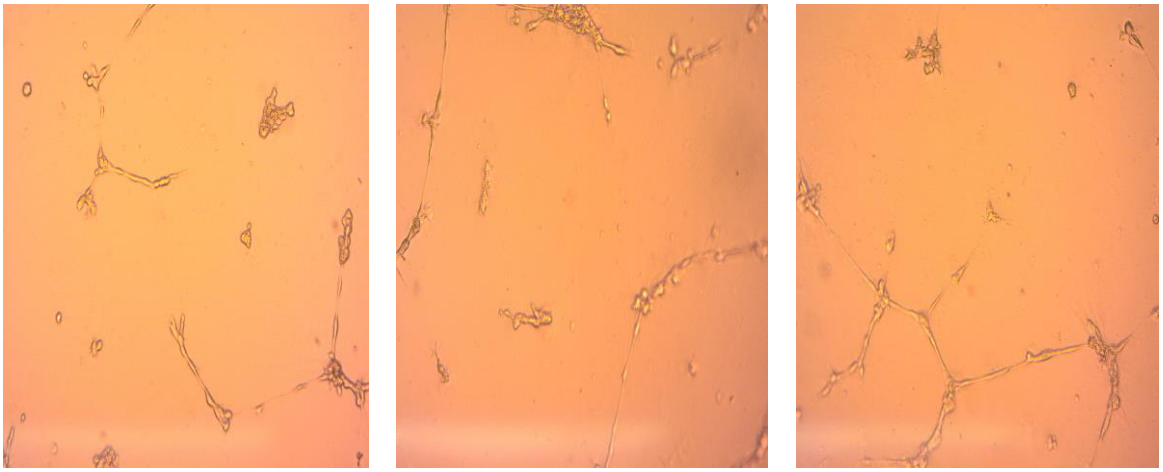

(1) (2) (3)

Figure 63: Tube formation of HUVEC cells in matrigel. Cells were treated with 2-(2,6-dioxopiperidin-3-yl)-phthalimidine (EM-12) (Compound **2**) in the concentration at 250 µg/mL. Nine viewing pictures that have been recorded.

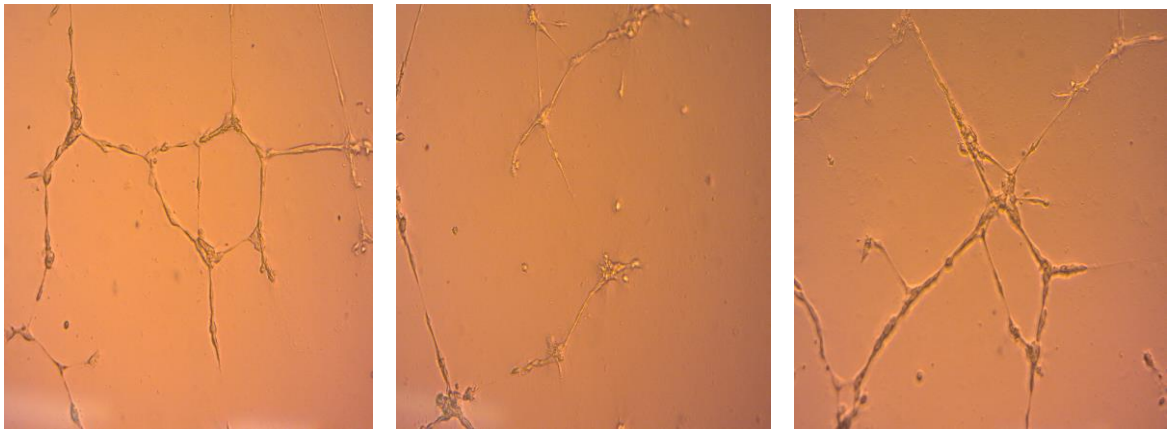

(1) (2) (3)

Figure 64: Tube formation of HUVEC cells in matrigel. Cells were treated with 2-(2,6-dioxopiperidin-3-yl)-phthalimidine (EM-12) (Compound **2**) in the concentration at 50 µg/mL. Nine viewing pictures that have been recorded.

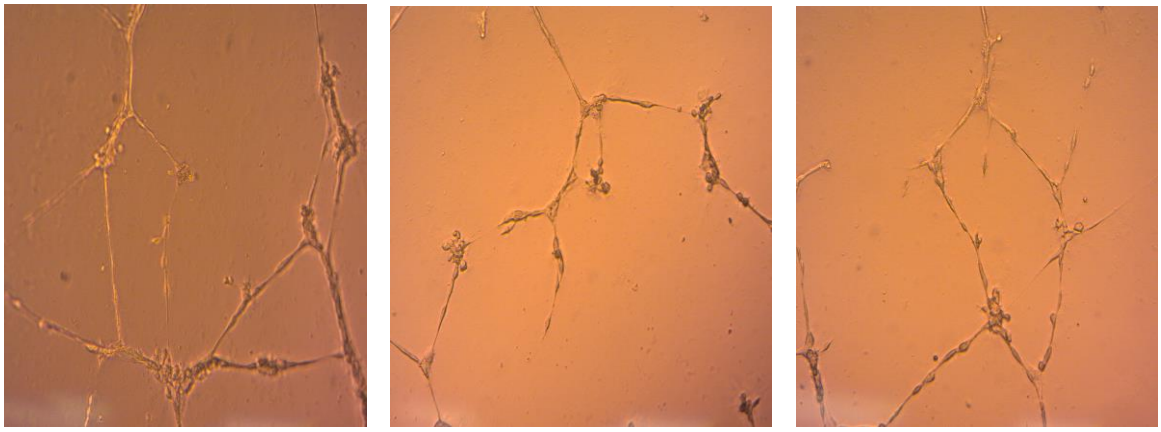

(1) (2) (3)

Figure 65: Tube formation of HUVEC cells in matrigel. Cells were treated with 2-(2,6-dioxopiperidin-3-yl)-phthalimidine (EM-12) (Compound **2**) in the concentration at 10 μg/mL. Nine viewing pictures that have been recorded.

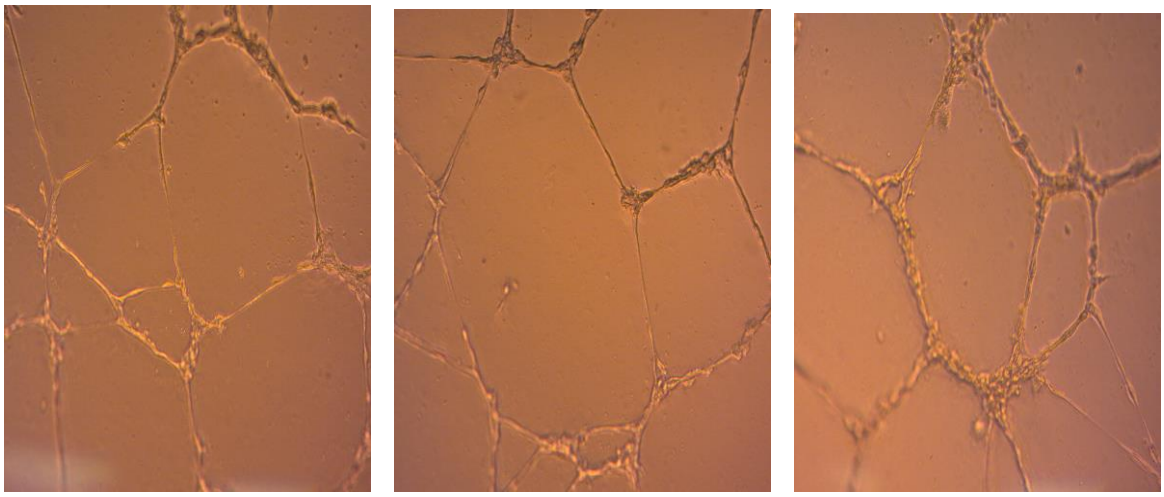

(1) (2) (3)

Figure 66: Tube formation of HUVEC cells in matrigel. Cells were treated with 2-(2,6-dioxopiperidin-3-yl)-phthalimidine (EM-12) (Compound **2**) in the concentration at 2 μg/mL. Nine viewing pictures that have been recorded.

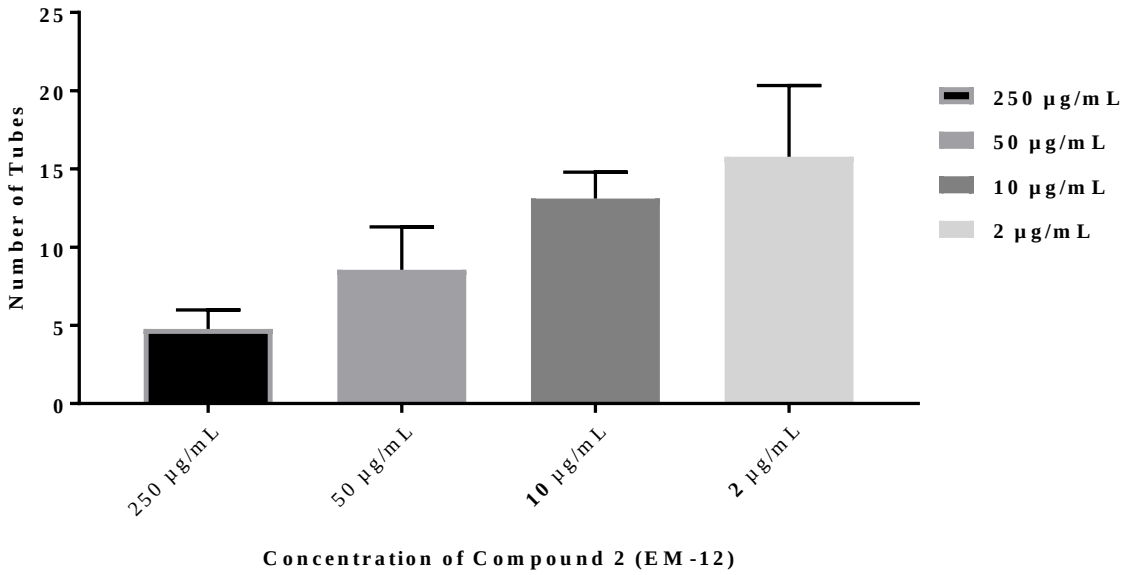

Figure 67: Number of tube formation of HUVEC cells in matrigel layer after inhibitory treatment of 2-(2,6-dioxopiperidin-3-yl)-phthalimidine (EM-12) (Compound **2**) at different concentration, (n=9).

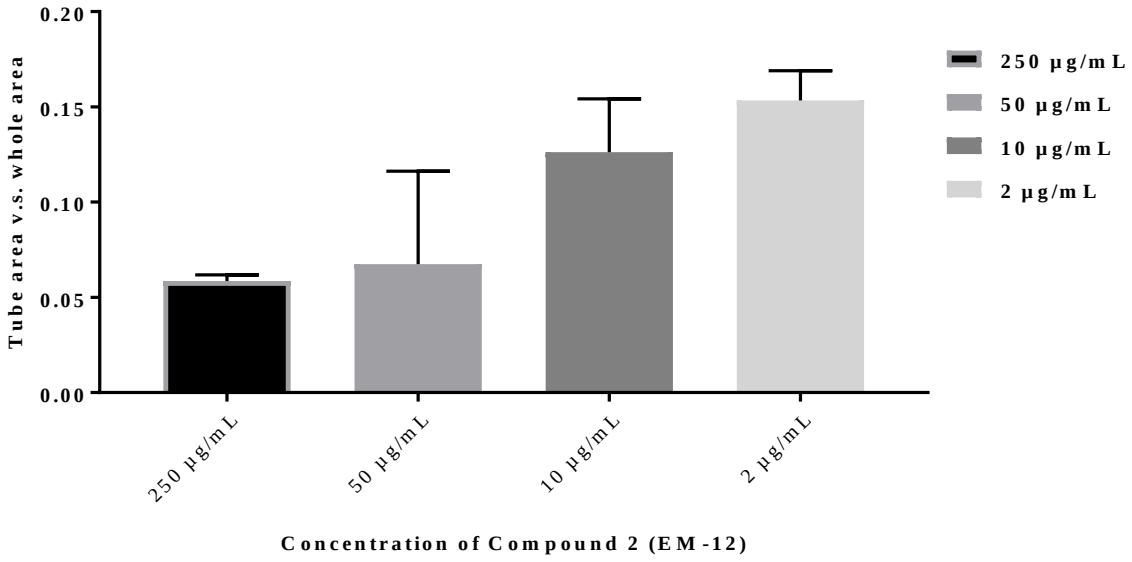

Figure 68: Area comparison (tube area, mm^2 vs. the whole area mm^2) of HUVEC cells in matrigel layer after inhibitory treatment of 2-(2,6-dioxopiperidin-3-yl)-phthalimidine (EM-12) (Compound **2**) at different concentration, (n=9).

From Figure 63 to Figure 66 above observation are shown from under an inverted microscope presenting tube formations on matrigel layers of HUVEC cells after treatment with compound **2** at concentrations of 250 μg/mL, 50 μg/mL, 10 μg/mL and 2 μg/mL respectively. Figure 67 shows the comparison of tubes formed on the matrigel layers of HUVEC cells after different treatments with compound **2** ranging from 2 μg/mL to 250 μg/mL. Figure 68 shows the comparison of the percentage of tube areas (tube area vs. the whole area) after treatment with compound **2** at concentrations ranging from 2 μg/mL to 250 μg/mL. As statistically determined, there was a negative relationship between the number of tubes formed and compound **2** treatment concentrations from 2 μg/mL to 250 μg/mL, with *P*-value < 0.05. This negative relationship was consistently found in comparisons of the percentage of tube areas with increasing treatment concentrations range from 2 μg/mL to 250 μg/mL, with *P*-value < 0.05.

As observed under an inverted microscope, few numbers of tubes were formed after treatment with compound **2** at 250 μg/mL, and more numbers of tubes were formed at the treatment concentration of 50 μg/mL. The average numbers of tubes and averages of percentage of tube areas (tube area vs. the whole area, mm^2) formed after treatment with compound 2 at 250 μg/mL and 50 μg/mL are 4.78 ± 1.20, 5.9% ± 0.0033 and 8.56 ± 2.74, 6.7 % ± 0.049 respectively. Additionally, a small number of tubes formed were found after treatment with compound **2** at a concentration of 10 μg/mL. At treatment concentrations of 2 μg/mL, more tubes were formed after treatment with compound **2**. Also, the larger size of tubes was found in the treatment concentration of 2 μg/mL compared with tubes treated with compound **2** at other concentrations. It seemed that several tubes were accumulated after the treatment with compound **2**. These results were consistent with the observation that there was a large difference in the percentage of tube areas found after the treatment concentration at 2 μg/mL.

(1) (2) (3)

Figure 69: Tube formation of HUVEC cells in matrigel. Cells were treated with 3-[(1R)-1-hydroxy-1-methyl-3-oxo-1,3-dihydro-2H-isoindol-2-yl]piperidine-2,6-dione (Compound **3**) in the concentration at 250 μg/mL. Nine viewing pictures were recorded.

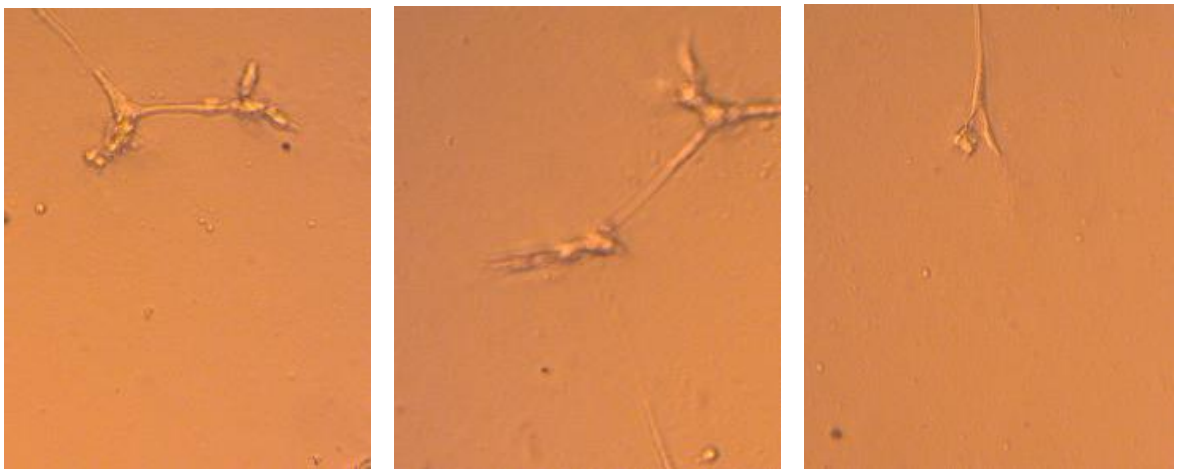

(1) (2) (3)

Figure 70: Tube formation of HUVEC cells in matrigel. Cells were treated with 3-[(1R)-1-hydroxy-1-methyl-3-oxo-1,3-dihydro-2H-isoindol-2-yl]piperidine-2,6-dione (Compound **3**) in the concentration at 50 μg/mL. Nine viewing pictures were recorded.

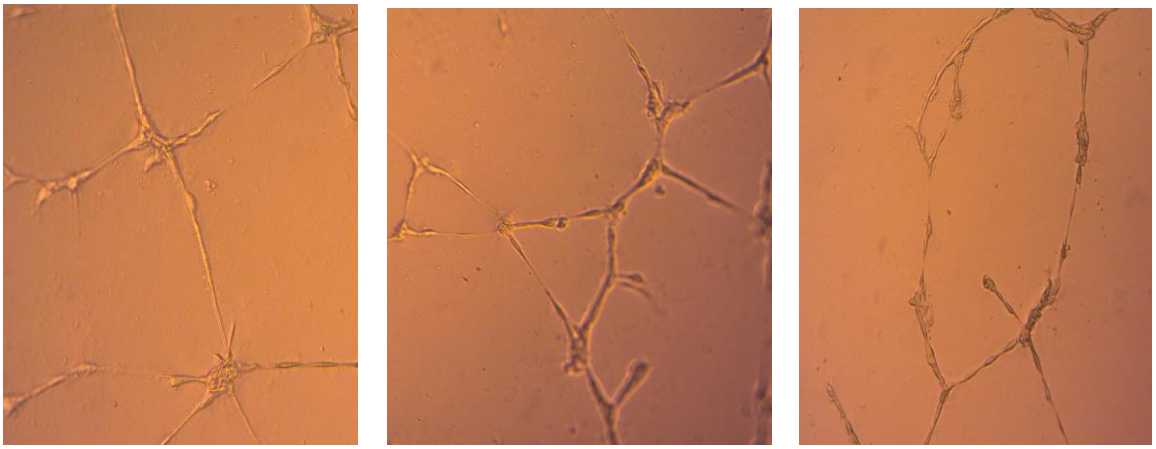

(1) (2) (3)

Figure 71: Tube formation of HUVEC cells in matrigel. Cells were treated with 3-[(1R)-1-hydroxy-1-methyl-3-oxo-1,3-dihydro-2H-isoindol-2-yl]piperidine-2,6-dione (Compound **3**) in the concentration at 10 μg/mL. Nine viewing pictures were recorded.

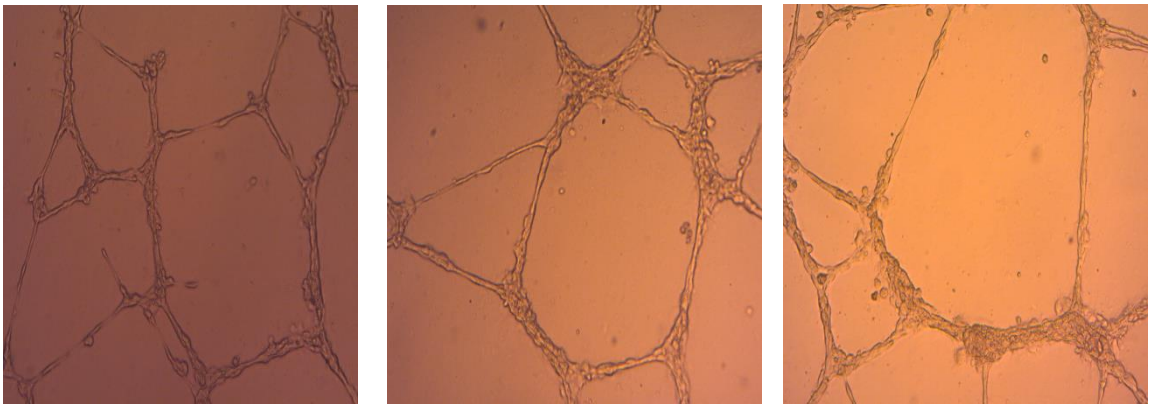

(1) (2) (3)

Figure 72: Tube formation of HUVEC cells in matrigel. Cells were treated with 3-[(1R)-1-hydroxy-1-methyl-3-oxo-1,3-dihydro-2H-isoindol-2-yl]piperidine-2,6-dione (Compound **3**) in the concentration at 2 μg/mL. Nine viewing pictures were recorded.

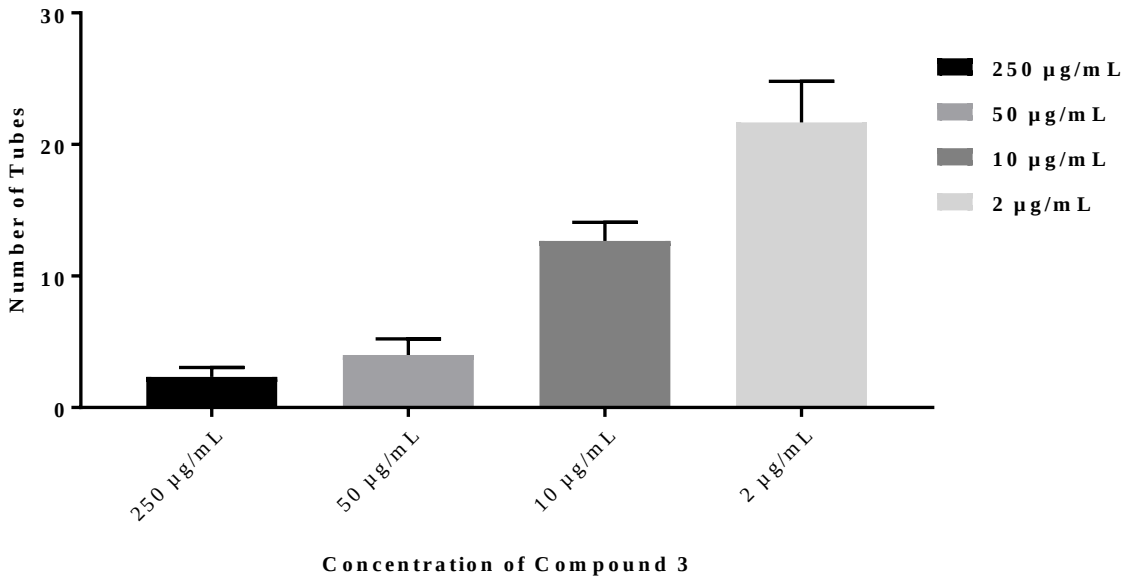

Figure 73: Number of tube formation of HUVEC cells in matrigel layer after inhibitory treatment of 3-[(1R)-1-hydroxy-1-methyl-3-oxo-1,3-dihydro-2H-isoindol-2-yl]piperidine-2,6-dione (Compound **3**) at different concentration, (n=9).

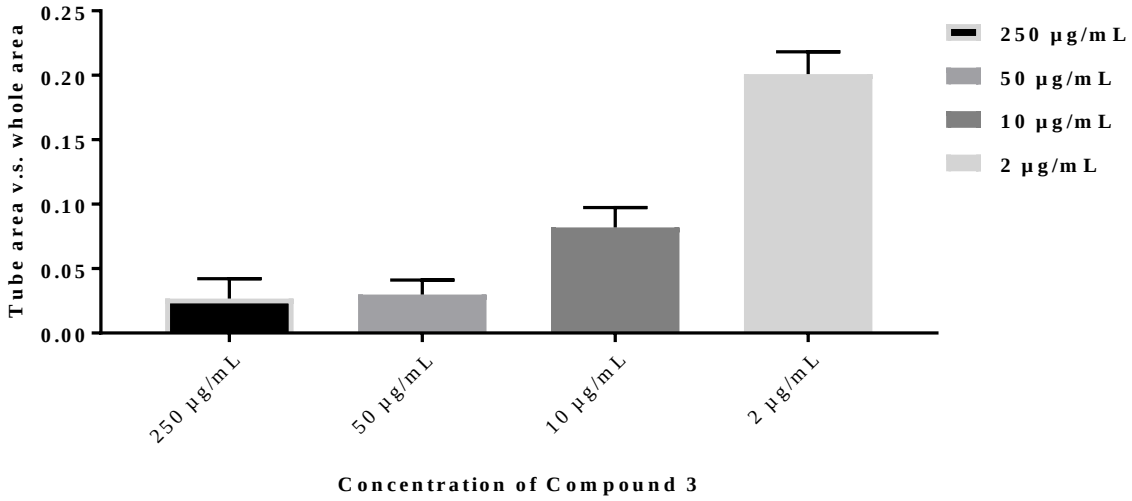

Figure 74: Area comparison (tube area mm^2 *vs*. the whole Area mm^2) of HUVEC cells in matrigel layer after inhibitory treatment of 3-[(1R)-1-hydroxy-1-methyl-3-oxo-1,3-dihydro-2H-isoindol-2-yl]piperidine-2,6-dione (Compound **3**) at different concentration, (n=9).

From Figure 69 to Figure 72, observations under an inverted microscope show tube formations on matrigel layers of HUVEC cells after treatment with compound **3** at concentrations of 250 μg/mL, 50 μg/mL, 10 μg/mL and 2 μg/mL respectively. Figure 73 shows the comparison of tubes formed on the matrigel layer of HUVEC cells after different treatments with compound **3** from 2 μg/mL to 250 μg/mL. Figure 74 shows the comparison of the percentages of tube area (tube area vs. the whole area) after treatment with compound **3** at a concentration range from 2 μg/mL to 250 μg/mL. As statistically determined, there was a negative relationship between the number of tubes formed and compound **3** treatment concentrations from 2 μg/mL to 250 μg/mL with *P*-value < 0.05. The negative relationship was consistently found in comparisons of the percentages of tube area with increasing treatment concentration ranges from 2 μg/mL to 250 μg/mL, with *P*-value < 0.05.

As observed under an inverted microscope, almost no intact tubes formed after treatment with compound **3** at 250 μg/mL. Similarly, there were few intact tubes found in the treatment concentration of 50 μg/mL. The average number of tubes and averages of the percentages of tube area (Tube area vs. the whole area, mm^2) formed after treatment with compound 3 at 250 μg/mL and 50 μg/mL are 1.11 ± 0.78, 0.015 ± 0.00122 and 4.22 ± 1.09, 0.016 ± 0.0022 respectively. A small number of tubes formed after treatment with compound **3** at a concentration of 10 μg/mL. In the treatment concentration of 2 μg/mL, more tubes were formed after treatment with Compound **3**. Also, the larger size of tube was found in the treatment concentration of 2 μg/mL compared with tubes treated with compound **3** at other concentrations. It seemed that several tubes were accumulated after the treatment with compound **3**. These results were consistent with observations that there was a small change in the number of tubes and the percentage of tube area vs the whole area figure from treatment concentration at 50 μg/mL. However, large differences in the number of tubes and percentages of tube area vs the whole area figure was found below treatment concentrations of 10 μg/mL.

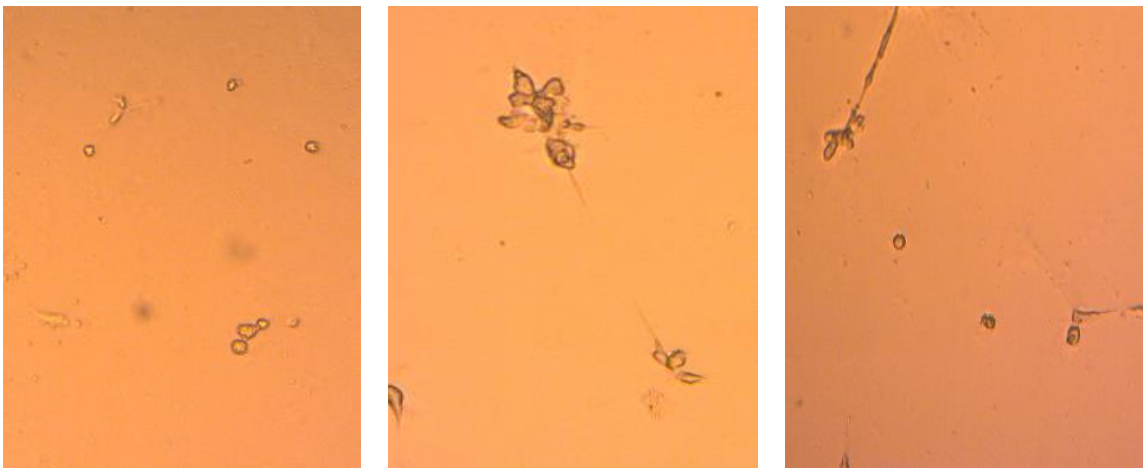

(1) (2) (3)

Figure 75: Tube formation of HUVEC cells in matrigel. Cells were treated with 3-[(1S)-1-hydroxy-1-methyl-3-oxo-1,3-dihydro-2H-isoindol-2-yl]piperidine-2,6-dione (Compound **4**) in the concentration at 250 μg/mL. Nine viewing pictures that have been recorded.

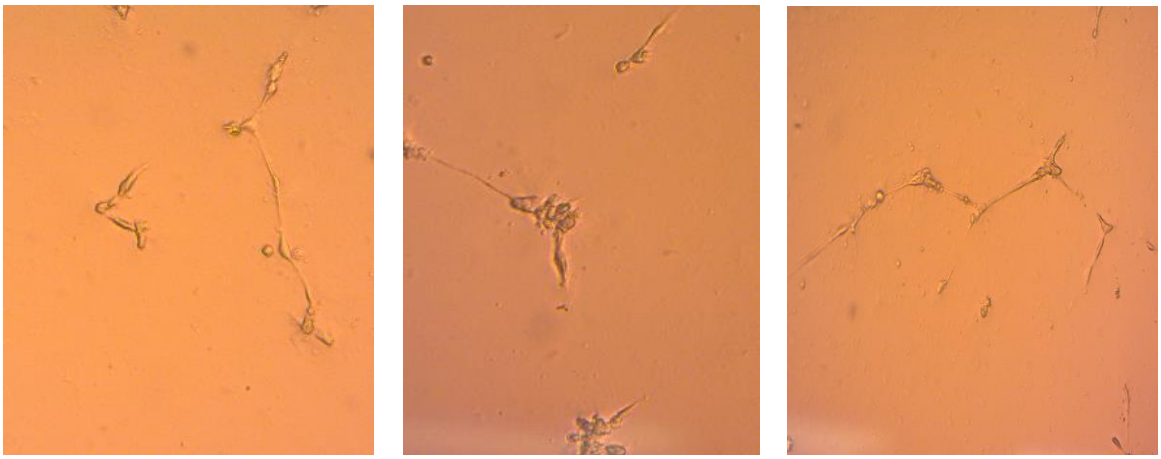

(1) (2) (3)

Figure 76: Tube formation of HUVEC cells in matrigel. Cells were treated with 3-[(1S)-1-hydroxy-1-methyl-3-oxo-1,3-dihydro-2H-isoindol-2-yl]piperidine-2,6-dione (Compound **4**) in the concentration at 50 μg/mL. Nine viewing pictures that have been recorded.

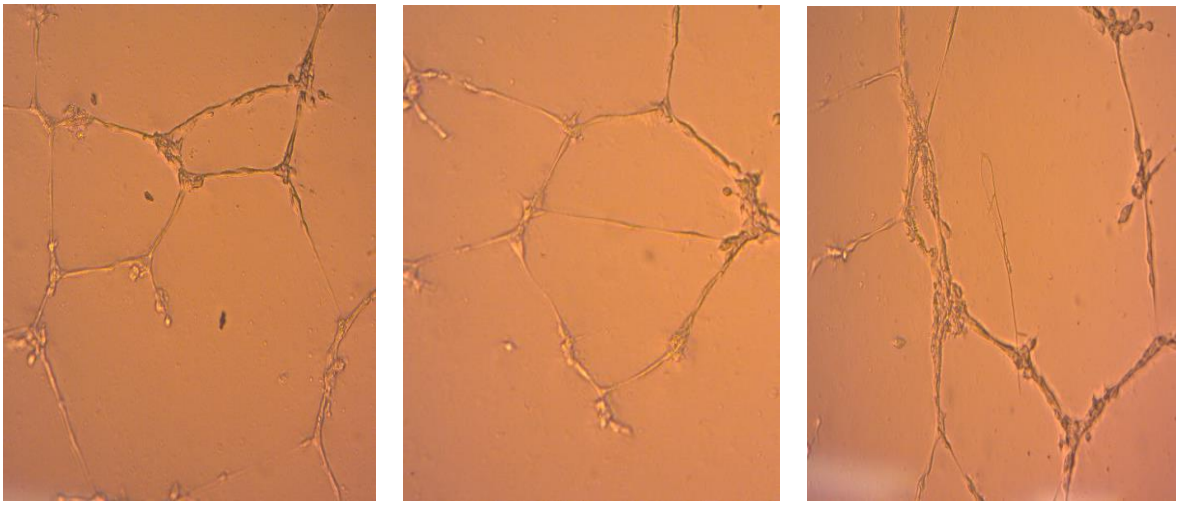

(1) (2) (3)

Figure 77: Tube formation of HUVEC cells in matrigel. Cells were treated with 3-[(1S)-1-hydroxy-1-methyl-3-oxo-1,3-dihydro-2H-isoindol-2-yl]piperidine-2,6-dione (Compound **4**) in the concentration at 10 μg/mL. Nine viewing pictures that have been recorded.

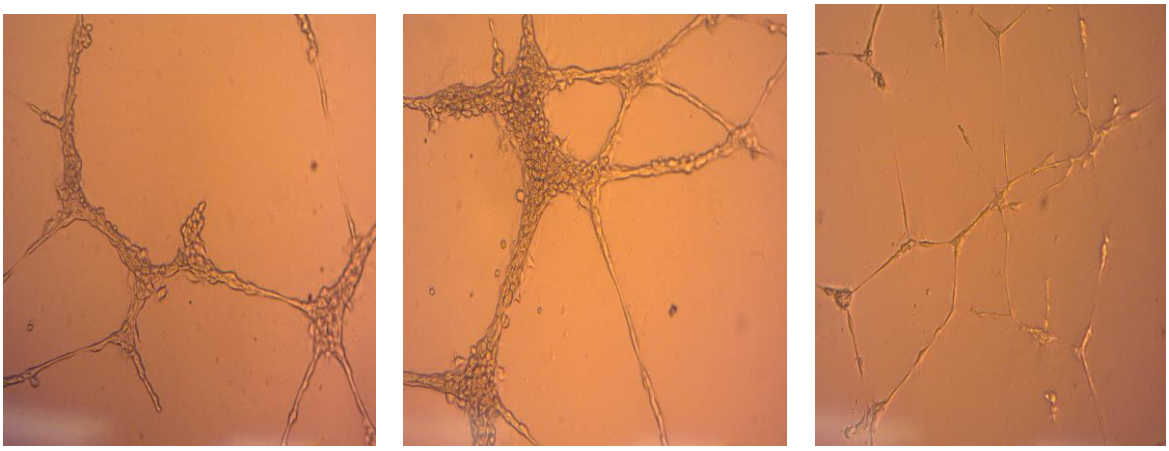

(1) (2) (3)

Figure 78: Tube formation of HUVEC cells in matrigel. Cells were treated with 3-[(1S)-1-hydroxy-1-methyl-3-oxo-1,3-dihydro-2H-isoindol-2-yl]piperidine-2,6-dione (Compound **4**) in the concentration at 2 μg/mL. Nine viewing pictures that have been recorded.

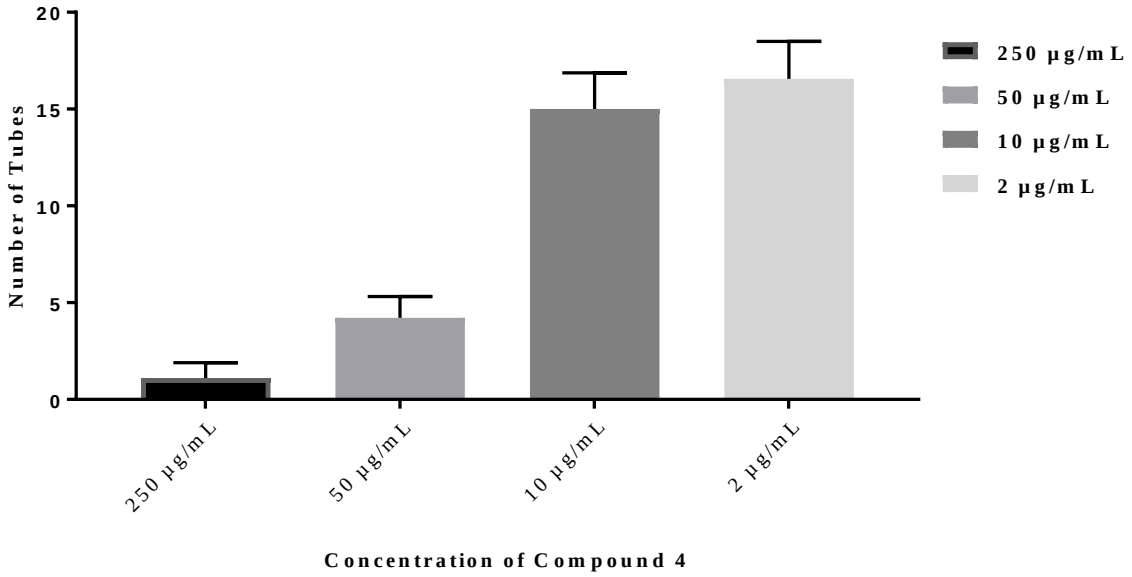

Figure 79: Number of tube formation of HUVEC cells in matrigel layer after inhibitory treatment of 3-[(1S)-1-hydroxy-1-methyl-3-oxo-1,3-dihydro-2H-isoindol-2-yl]piperidine-2,6-dione (Compound **4**) at different concentration, (n=9).

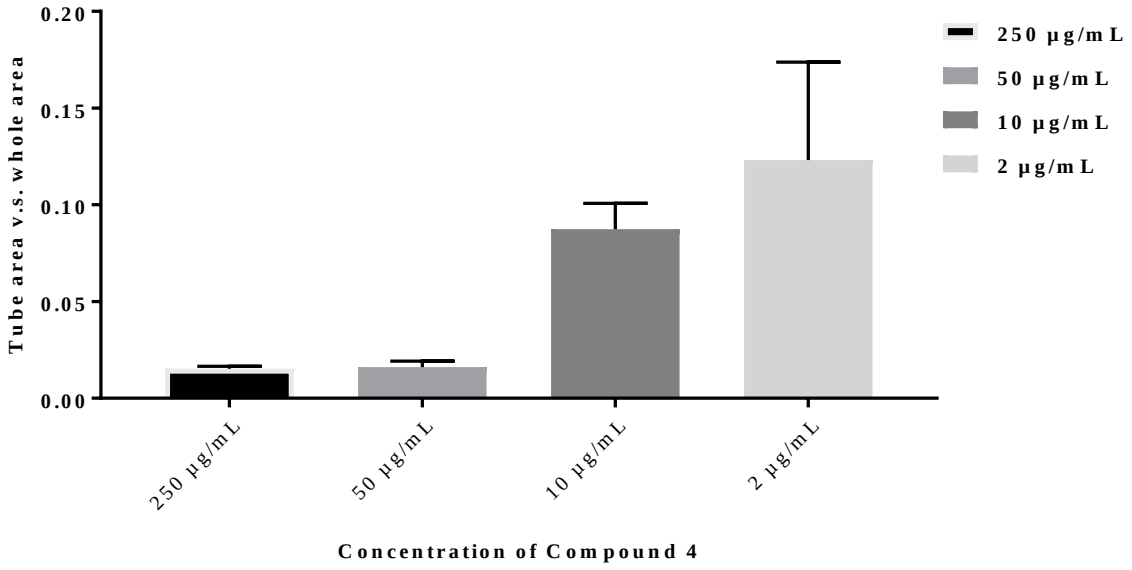

Figure 80: Area comparison (tube area mm^2 *vs*. the whole Area mm^2) of HUVEC cells in matrigel layer after inhibitory treatment of 3-[(1S)-1-hydroxy-1-methyl-3-oxo-1,3-dihydro-2H-isoindol-2-yl]piperidine-2,6-dione (Compound **4**) at different concentration, (n=9).

Figure 75 to Figure 78 (above) are from observations taken under an inverted microscope, showing tube formations on matrigel layers of HUVEC cells after treatment with compound **4** at concentrations of 250 μg/mL, 50 μg/mL, 10 μg/mL and 2 μg/mL respectively. Figure 79 shows the comparison of tubes formed on the matrigel layers of HUVEC cells after different treatments with compound **4** from 2 μg/mL to 250 μg/mL. Figure 80 shows the comparison of percentages of tube areas (tube area vs. the whole area) after treatment with compound **4** at concentrations ranging from 2 μg/mL to 250 μg/mL. As statistically determined, there was a negative relationship between the number of tubes formed and compound **4** treatment concentrations from 2 μg/mL to 250 μg/mL, with *P*-value < 0.05. This negative relationship was consistently found in comparisons of the percentage of tube areas with increasing treatment concentrations ranging from 2 μg/mL to 250 μg/mL (*P*-value < 0.05).

As observed under an inverted microscope, almost no intact tubes formed after treatment with compound **4** at 250 μg/mL. Similarly, there were few intact tubes found in the treatment concentration of 50 μg/mL. The average number of tubes and averages of percentages of tube areas (Tube area, mm^2 *vs*. the whole area, mm^2) formed after treatments with compound 4 at 250 μg/mL and 50 μg/mL are 1.11 ± 0.78, 0.015 ± 0.00122 and 4.22 ± 1.09, 0.016 ± 0.0022 respectively. A small number of tubes were found after treatment with compound **4** at a concentration of 10 μg/mL. In the treatment concentration of 2 μg/mL, more tubes were formed after treatment with compound **4**. Also, the larger size of tubes was found in the treatment concentration of 2 μg/mL compared with tubes treated with compound **4** at other concentrations. It seemed that several tubes accumulated after the treatments with compound **4**. These results were consistent with observation that there was a small change in the number of tubes and percentages of tube areas vs the whole area figure from treatment concentration at 50 μg/mL. However, a large difference in the number of tubes and percentages of tube area *vs*. the whole area figure was found below the treatment concentration of 10 μg/mL.

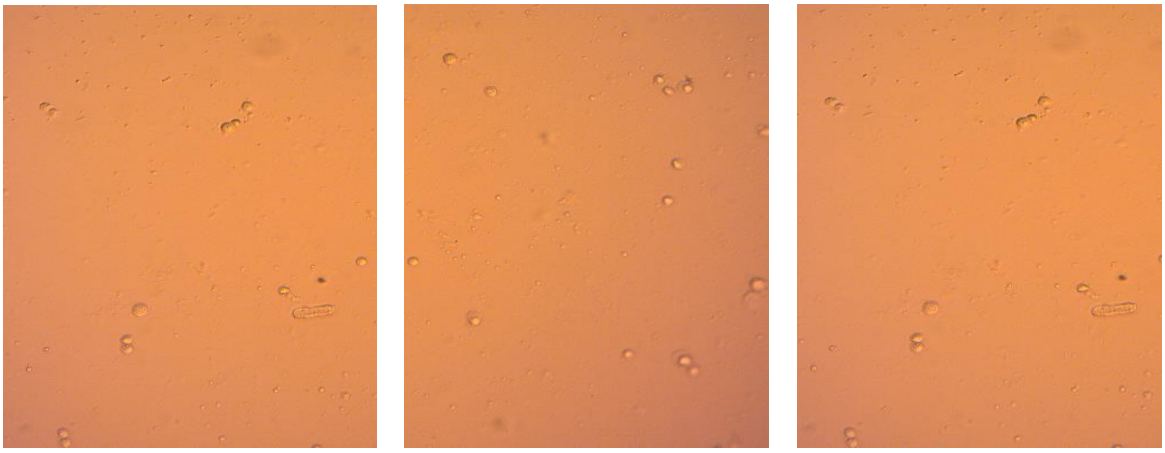

(1) (2) (3)

Figure 81: Tube formation of HUVEC cells in matrigel. Cells were treated with 2-(1-chloromethyl-2,6-dioxopiperidin-3-yl)phthalimidine (Compound **5**) in the concentration at 250 μg/mL. Nine viewing pictures that have been recorded.

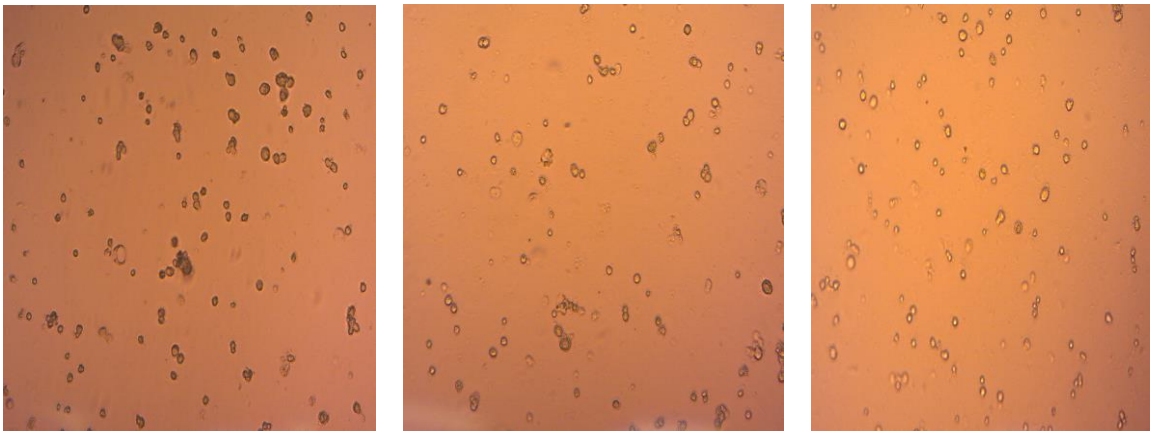

(1) (2) (3)

Figure 82: Tube formation of HUVEC cells in matrigel. Cells were treated with 2-(1-chloromethyl-2,6-dioxopiperidin-3-yl)phthalimidine (Compound **5**) in the concentration at 50 μg/mL. Nine viewing pictures that have been recorded.

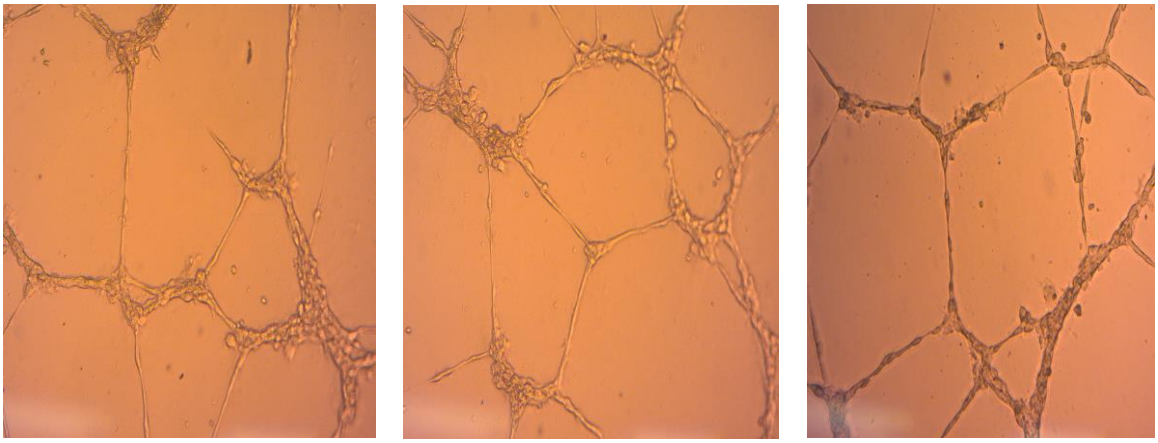

(1) (2) (3)

Figure 83: Tube formation of HUVEC cells in matrigel. Cells were treated with 2-(1-chloromethyl-2,6-dioxopiperidin-3-yl)phthalimidine (Compound **5**) in the concentration at 10 μg/mL. Nine viewing pictures that have been recorded.

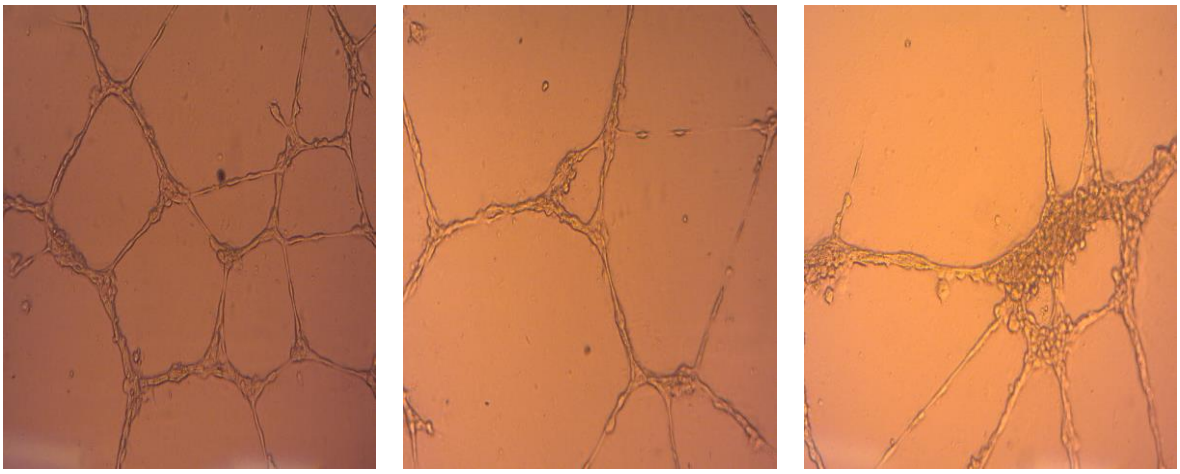

(1) (2) (3)

Figure 84: Tube formation of HUVEC cells in matrigel. Cells were treated with 2-(1-chloromethyl-2,6-dioxopiperidin-3-yl)phthalimidine (Compound **5**) in the concentration at 2 μg/mL. Nine viewing pictures that have been recorded.

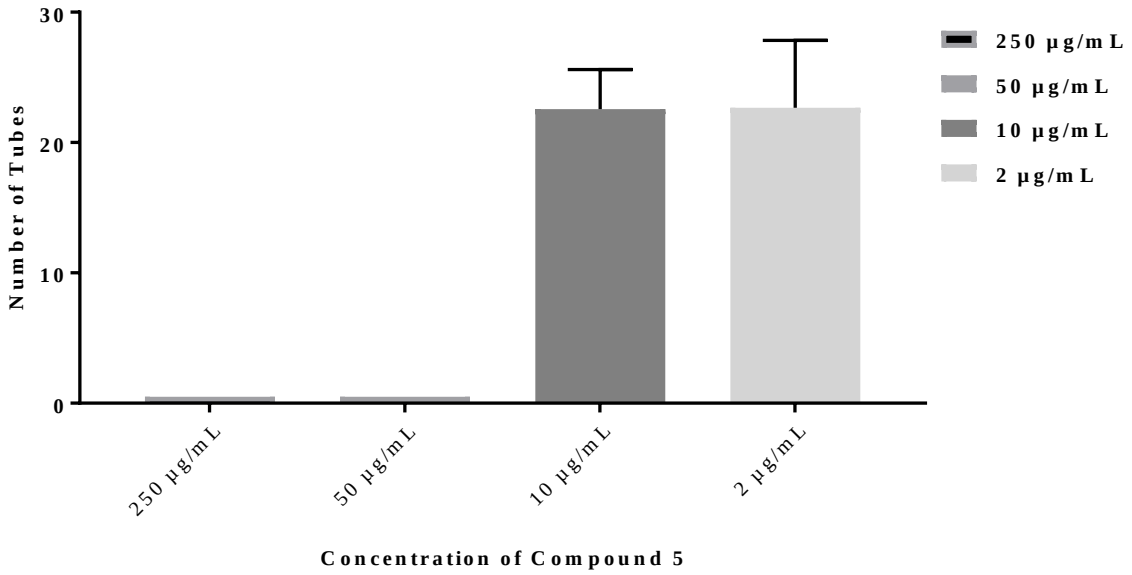

Figure 85: Number of tube formation of HUVEC cells in matrigel layer after inhibitory treatment of 2-(1-chloromethyl-2,6-dioxopiperidin-3-yl)phthalimidine (Compound **5**) at different concentration, (n=9).

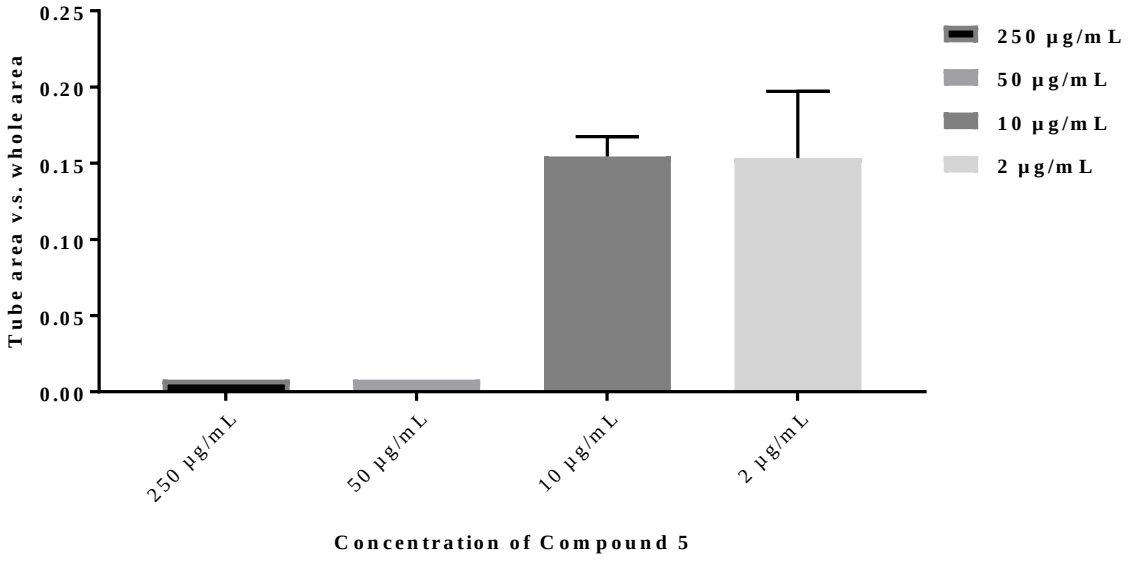

Figure 86: Area comparison (tube area mm^2 *vs*. the whole Area mm^2) of HUVEC cells in matrigel layer after inhibitory treatment of 2-(1-chloromethyl-2,6-dioxopiperidin-3-yl)phthalimidine (Compound **5**) at different concentration, (n=9).

From Figure 81 to Figure 84 (above), observations under an inverted microscope showed tube formations on matrigel layers of HUVEC cells after treatment with compound **4** at concentrations of 250 μg/mL, 50 μg/mL, 10 μg/mL and 2 μg/mL respectively. No tubes formed (Figure 81 and Figure 82) after treatment with compound **5** at concentrations from 50 μg/mL to 250 μg/mL. Additionally, the tube area consistently could not be determined after treatment with compound **5** at the concentrations from 50 μg/mL to 250 μg/mL. However, some tubes formed after treatment with compound **5** at treatment concentrations from 2 μg/mL to 10 μg/mL. Also, Figure 83 and Figure 84 shows that tubes seemed to accumulate to generally a large size. Thus, the significant difference in the number of tubes and percentages of tube areas was found when the treatment concentration increased from 10 μg/mL to 50 μg/mL with *P*-value < 0.05. Due to no tube formation from the treatment concentration at 50 μg/mL, the dose-dependent relationship could not be statistically determined for tube formation and tube area. Instead, the observation is noted that the number of tubes and percentages of tube area (Figure 85 and Figure 86) were not statistically different in treatment concentrations between 2 μg/mL and 50 μg/mL, with *P*-value > 0.05.

3.5.2.3 Comparison of Tube Formation between Thalidomide and Its Analogues

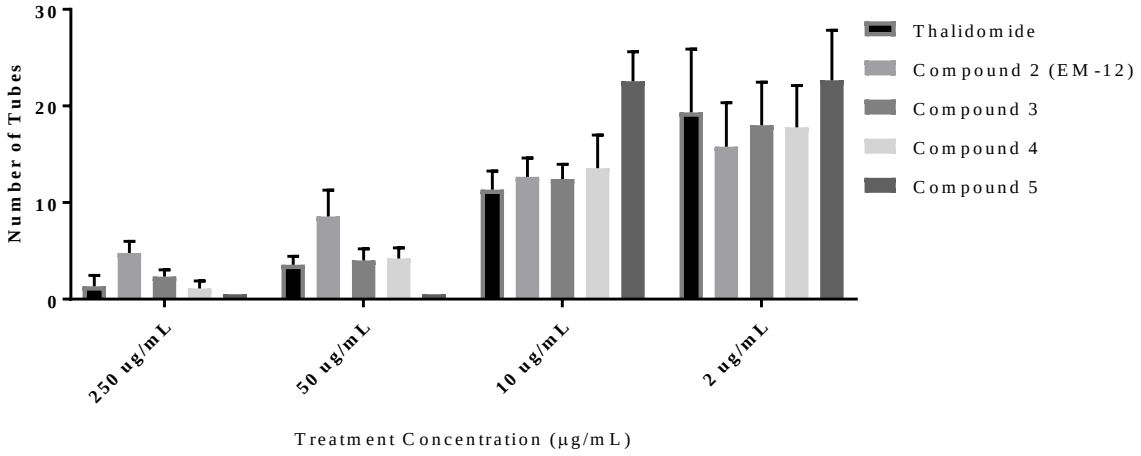

Figure 87: Comparison about number of tube formation of HUVEC cells in matrigel layer after inhibitory treatment of thalidomide & its structural analogues at concentration of 2, 10, 50 and 250 μg/mL. Treatment included: Thalidomide; Compound **2**: 2-(2,6-dioxopiperidin-3-yl)-phthalimidine; Compound **3**: 3-[(1R)-1-hydroxy-1-methyl-3-oxo-1,3-dihydro-2H-isoindol-2-yl]piperidine-2,6-dione; Compound **4**: 3-[(1S)-1-hydroxy-1-methyl-3-oxo-1,3-dihydro-2H-isoindol-2-yl]piperidine-2,6-dione; Compound **5**: 2-(1-chloromethyl-2,6-dioxopiperidin-3-yl)phthalimidine. All the values are means ± standard errors of nine records

of view. Asterisks indicated a value significantly different from the control value, *$P < 0.05$, **$P < 0.01$, ***$P < 0.001$ (Student's t-test).

3.5.2.4 Comparison about Percentage of Tube Area (Tube area vs. the whole area, mm^2) between Thalidomide and Its Structural Analogues

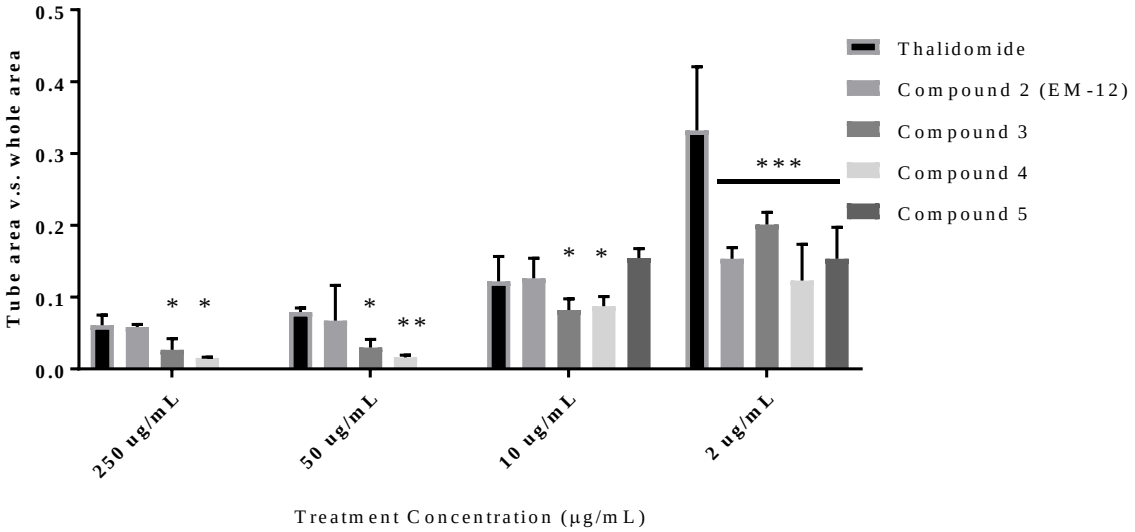

Figure 88: Comparison about percentage of tube area (tube area *vs*. the whole area, mm^2) of HUVEC cells in Matrigel layer after inhibitory treatment of thalidomide & its structural analogues within concentration at 2 µg/mL, 10 µg/mL, 50 µg/mL and 250 µg/mL. Treatment included: thalidomide (Compound **1**); Compound **2**: 2-(2,6-dioxopiperidin-3-yl)-phthalimidine (EM-12); Compound **3**: 3-[(1R)-1-hydroxy-1-methyl-3-oxo-1,3-dihydro-2H-isoindol-2-yl]piperidine-2,6-dione; Compound **4**: 3-[(1S)-1-hydroxy-1-methyl-3-oxo-1,3-dihydro-2H-isoindol-2-yl]piperidine-2,6-dione; Compound **5**: 2-(1-chloromethyl-2,6-dioxopiperidin-3-yl)phthalimidine. All the values are means ± standard errors of nine records of view. Asterisks indicated a value significantly different from the control value, *$P < 0.05$, **$P < 0.01$, ***$P < 0.001$ (Student's t-test).

As described individually, relative to tube inhibitory effects described above, all treatment compounds except compound **5** could generate inhibitory effects to reduce the number of tubes formed and percentages of tube areas in dose-dependent manners, with *P*-value < 0.05. For compound **5**, however, there were no tubes formed after the treatment concentration reached 50 µg/mL. The percentage of tube area was similar between treatment concentrations at 2 µg/mL and 10 µg/mL.

Figure 87 shows the comparison of the numbers of tube formations of HUVEC cells in matrigel layers after inhibitory treatment with thalidomide and its structural analogues within a concentration range of 2 µg/mL to 250 µg/mL. Compared to thalidomide, both treatment concentrations at 50 µg/mL and 250 µg/mL, indicated that the number of tubes after treatment with compound **3** and compound **4** were statistically similar to the numbers of tubes formed with treatments of thalidomide (*P*-value > 0.05). However, the number of tubes formed after treatment with compound **2** was statistically and significantly more than the number of tubes formed from other treatments (*P*-value < 0.05). The number of tubes formed within the treatment concentration of 10 µg/mL was not statistically different between thalidomide and compound **2**, compound **3** and compound **4** (*P*-value > 0.05). There was also a slight difference in the number of tubes formed after treatment of thalidomide, compound **2**, compound **3** and compound **4** at a treatment concentration of 2 µg/mL (*P*-value < 0.05). For compound **5**, the number of tube formations after a treatment concentration of 2 µg/mL was significantly more than tubes formed from other treatments, with *P*-value < 0.05.

In looking at the percentage of tube area (tube area, mm^2 *vs.* whole area, mm^2), Figure 88 shows comparisons of the percentage of tube area between thalidomide and compound **2**, compound **3**, compound **4** and compound **5**. The percentage of tube area after treatment with thalidomide and compound **2** at a concentration of 10 µg/mL, 50 µg/mL and 250 µg/mL were statistically higher than the percentages of tube areas from treatments with compound 3 and compound **4**. The percentage of tube area after treatment with thalidomide at a concentration of 2 µg/mL was dramatically more than the percentages of tube areas from other treatments, with *P*-value < 0.05. Due to no tube formations, the percentage of tube area achieved its lowest value after treatment with compound **5** at concentrations of 50 µg/mL and 250 µg/mL. Moreover, of there was no statistical change in the percentage tube area after treatment with compound **5** at 2 µg/mL, with *P*-value > 0.05.

Part III Cytotoxic Assay

3.5.3 Cytotoxic Assay for Breast Cancer Cell MDA-MB-231

3.5.3.1 Linearity of Cell Line for MDA-MB-231

Comparing cell numbers against UV absorbance in a standard (linearity) curve (Figure 89) was important in setting up a starting point in the MTT assay portion of the study. A good linearity curve reflects a good quality status. Cell numbers used in cell viability studies should fall within the linear portion of the curve. Cell seeding concentrations can neither be too high nor too low. Therefore, a good quality of cell growing conditions for cells can be defined for further experimental conditions applied. Figure 89 shows the linearity curve of MDA-MB-231. It shows a good linear relationship (R^2= 0.9409) between the absorbance measured at 540 nm wavelength and different cell densities (from 800, 000 cells/mL to 3, 125 cells/mL).

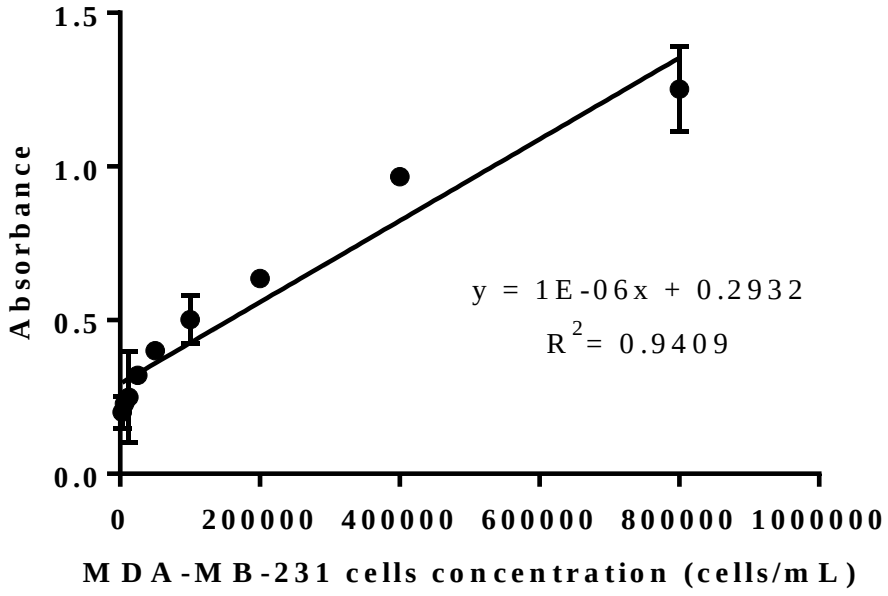

Figure 89: Linearity between MDA-MB-231 cell numbers and absorbance values. Data are presented as means ± S.D, n = 6.

3.5.3.2 Effects of Pure Dimethyl Sulfoxide (DMSO) on Cancer Cell Growth

As discussed, the cell culture medium could not directly applied as a liquid solvent to dissolve thalidomide or its analogues in order to prepare the treatment concentrations. It was necessary that DMSO was used to dissolve thalidomide or its analogues, and estabolish DMSO stock solutions first. Then, complete cell culture medium was used to dilute the DMSO stock solution to obtain appropriate treatment concentrations which were applied as treatments to cancer cells. The percentage of DMSO in each treatment group was calculated to be 2% in the prepared concentrations.

After adding treatments to the cells, 1% DMSO was the final amount of solvent in each well. Therefore, cell viability comparisons were required for conditions between culture medium without DMSO and with 1% DMSO. As MTT results shown after 24, 48 and 72 hours treatment, the cell viability in the presence of 1% DMSO was nearly the same as the cell viability in cell culture medium without DMSO (p-value > 0.05).

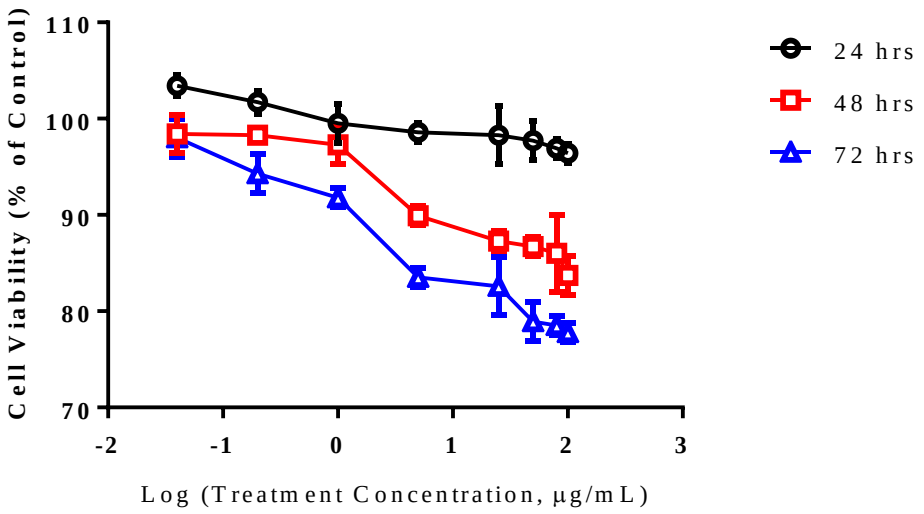

Figure 90: Inhibitory effects of the thalidomide (Compound **1**) on the cell proliferation in human breast cancer cell MDA-MB-231 with 0.04, 0.2, 1, 5, 25, 50, 80 & 100µg/mL for 24 hours, 48 hours & 72 hours. Data are means ± standard errors (n=6).

3.5.3.3 Anti-proliferative Effects from Single Treatment of Thalidomide

The effect of thalidomide on cell viability in MDA-MB-231 was investigated by MTT assays within the treatment concentration range from 0.04 μg/mL to 100 μg/mL. As shown in Figure 90 shown, cell viability gradually decreased with significantly increasing concentrations of treatment. After 24-hours treatment with thalidomide, cell viability was increased from an initial concentration of 0.04 μg/mL to 1 μg/mL. Even with a treatment concentration increase of 100-fold to 100 μg/mL, the cell viability was decreased no more than 10%. After 48-hours treatment with thalidomide, the cell viability had decreased slightly as treatment concentrations from 0.04 μg/mL to 1 μg/mL. There was a sharp decrease in cell viability to (around 85%) at the treatment concentration of 100 μg/mL. At 72 hours of treatment, the cell viability was decreased to about 80% at the highest concentration of 100 μg/mL.

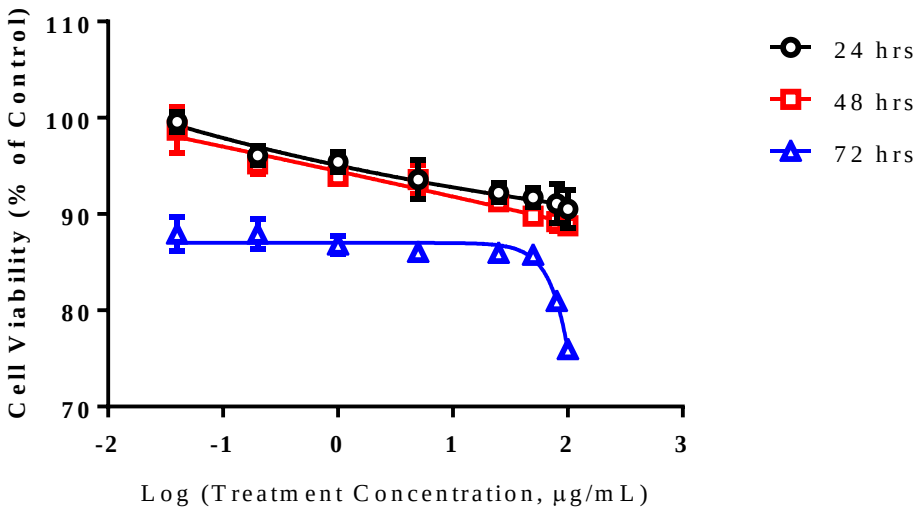

Figure 91: Inhibitory effects of 2-(2,6-dioxopiperidin-3-yl)-phthalimidine (EM-12) (Compound **2**) on the cell proliferation in human breast cancer cell MDA-MB-231 with 0.04, 0.2, 1, 5, 25, 50, 80 & 100μg/mL for 24 hours, 48 hours & 72 hours. Data are means ± standard errors (n=6).

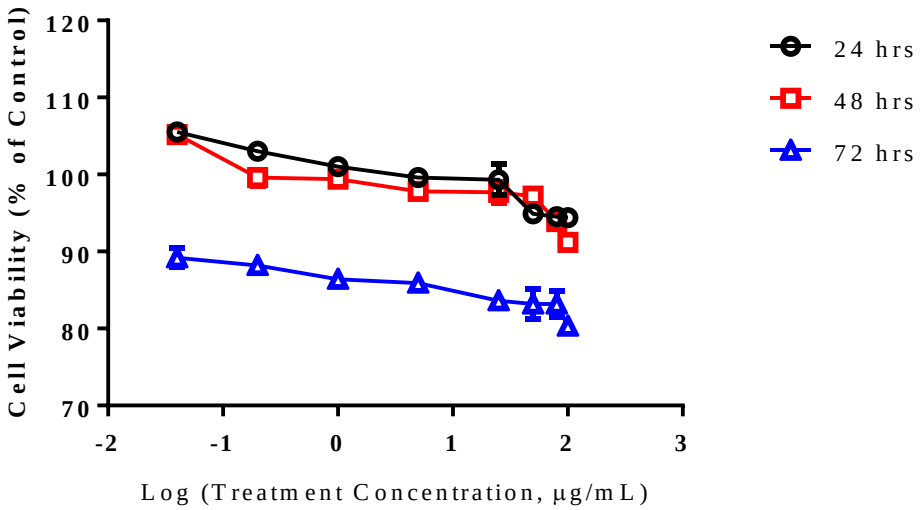

Figure 92: Inhibitory effects of 3-[(1R)-1-hydroxy-1-methyl-3-oxo-1,3-dihydro-2H-isoindol-2-yl]piperidine-2,6-dione (Compound **3**) on the cell proliferation in human breast cancer cell MDA-MB-231 with 0.04, 0.2, 1, 5, 25, 50, 80 & 100µg/mL for 24 hours, 48 hours & 72 hours. Data are means ± standard errors (n=6).

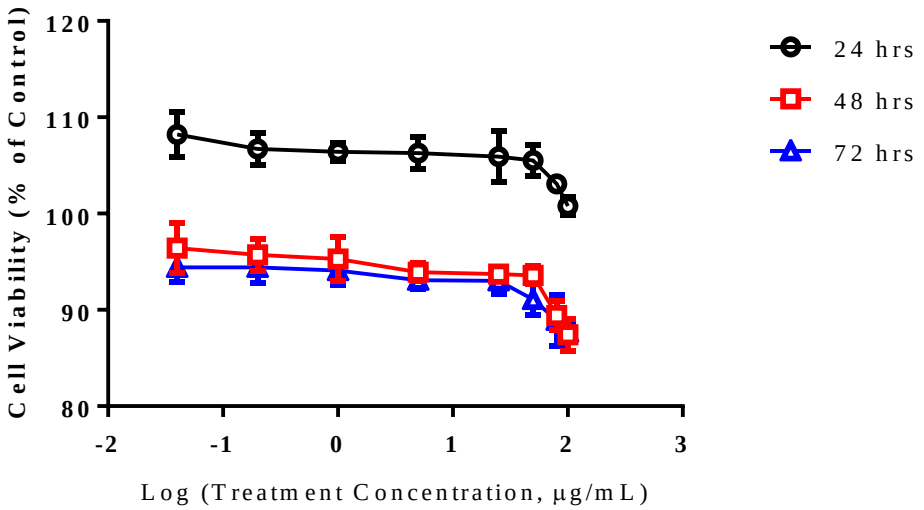

Figure 93: Inhibitory effects of 3-[(1S)-1-hydroxy-1-methyl-3-oxo-1,3-dihydro-2H-isoindol-2-yl]piperidine-2,6-dione (Compound **4**) on the cell proliferation in human breast cancer cell MDA-MB-231 with 0.04, 0.2, 1, 5, 25, 50, 80 & 100µg/mL for 24 hours, 48 hours & 72 hours. Data are means ± standard errors (n=6).

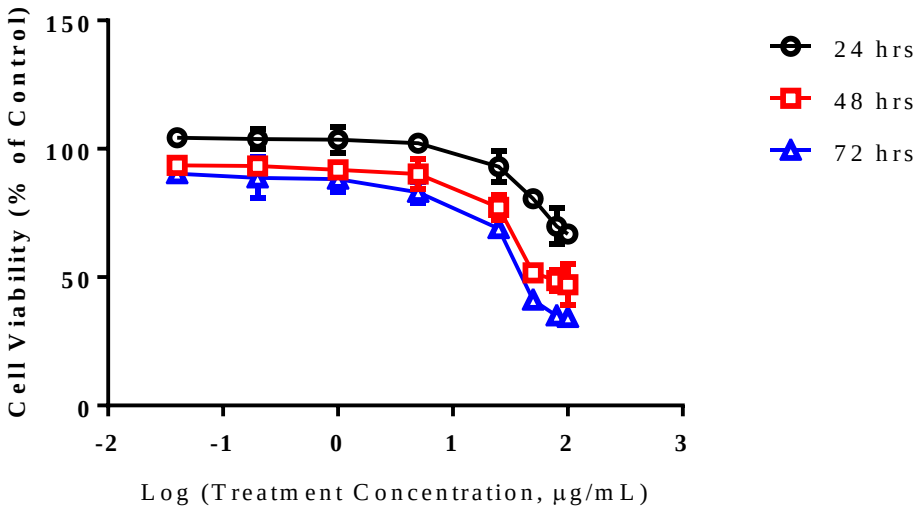

Figure 94: Inhibitory effects of 2-(1-chloromethyl-2,6-dioxopiperidin-3-yl)phthalimidine (Compound **5**) on the cell proliferation in human breast cancer cell MDA-MB-231 with 0.04, 0.2, 1, 5, 25, 50, 80 & 100 µg/mL for 24 hours, 48 hours & 72 hours. Data are means ± standard errors (n=6).

3.5.3.4 Anti-proliferative Effects from Single Treatment of Thalidomide Analogues

The effects of all synthetic compounds on cell viability in MDA-MB-231 cells were investigated by MTT assays within the treatment concentration range of 0.04 µg/mL to 100 µg/mL. Overall, the anti-proliferative effects were statistically significant from all synthetic compounds in dose and time-dependent manners since *p*-value < 0.05. However, the anti-proliferative effects from all synthetic compounds were quite low, except for compound **5**. As the results indicated, for cell treatments after time points of 48 hours and 72 hours, IC_{50} values were only achieved with compound **5** in treatments.

For treatments with thalidomide (Figure 90), after 24 hours, cell growth increased for concentrations below 1 µg/mL. Even with the treatment concentration increased 100-fold, cell viability was not significantly decreased. After treatment time of 48 hours, there was a decrease in cell viability in treatment concentrations higher than 1 µg/mL. In the treatment concentration of 100 µg/mL, cell viability was reduced about 15%. After treatment for 72 hours, cell viability was reduced about 20% by the treatment concentration at 100 µg/mL. For treatments with compound **2** (Figure 91) and compound **3** (Figure 92), cell viability

number were quite similar. After 24-hour and 48-hour treatments, cell viabilities gradually decreased, with only 10% of cell viability reduced after the highest concentration of 100 μg/mL. After 72-hours treatment, cell viability dropped more remarkably than shorter timepoints. Cell viability dropped to approximately 80%. For treatments with compound **4** (Figure 93), at the 24-hours timepoint, all concentrations promoted cell viability. Even at the highest concentration treatment at 100 μg/mL there was only a small decrease in cell viability. However, cell viability after 48-hours and 72-hours was decreased by treatments. Around 95% cell viability was achieved after 72-hours treatment at 100 μg/mL. In addition, observations under an inverted microscope showed that in all three days of the treatments (culturing for 24, 48 and 72 hours), there were no remarkable morphological changes.

An exception to the morphological changes is noted in treatments with compound **5** (Figure 94). Once treatment was placed in the samples, the morphology of cells immediately changed to small rounded-shape. (The changes in cell morphology will be described and discussed in detail in following sections.) After treatment for 48 hours and 72 hours, the cell attachment rate was reduced with the increase of treatment concentrations. After treatment at 72 hours, the cell viability was reduced to around 30% at a treatment concentration of 100 μg/mL.

Therefore, based on all the results above, typical concentrations of treatments were selected for assays of the cell cycle in order to analyze changes in DNA contents during different treatments.

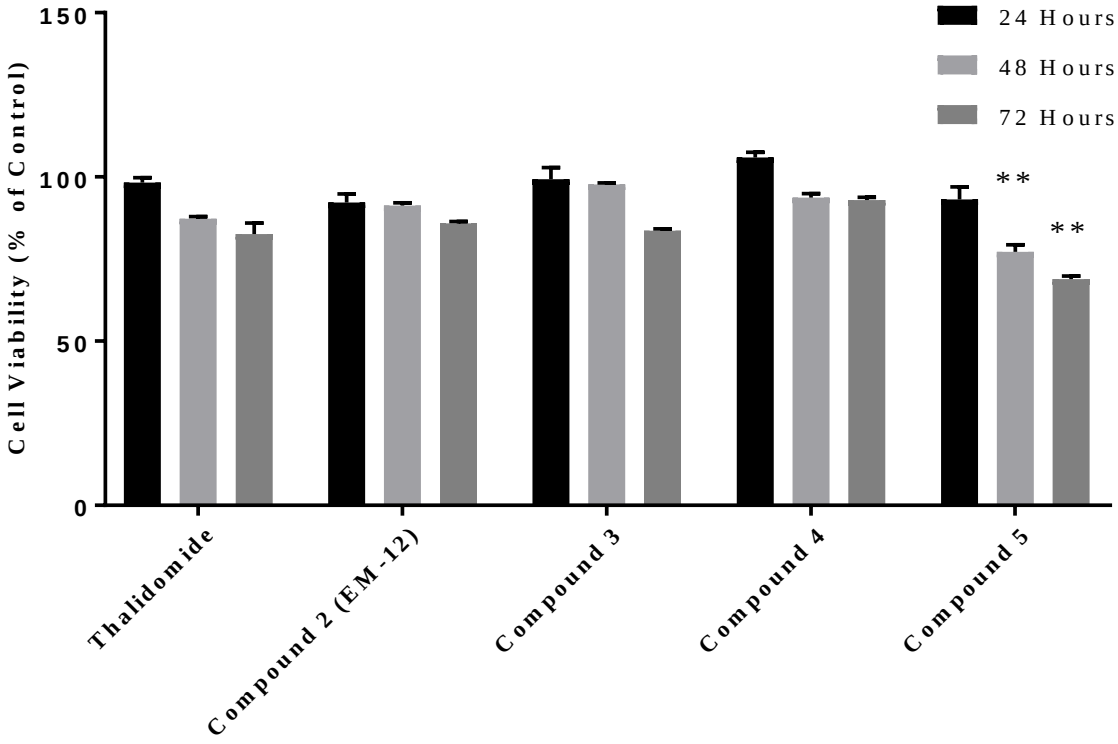

Figure 95: Comparison of MDA-MB-231 Breast cancer cell viability after treatment from thalidomide (Control) and thalidomide structural analogues for 24 hours, 48 hours and 72 hours within the treatment concentration at 25 μg/mL. Compound **2**: 2-(2,6-dioxopiperidin-3-yl)-phthalimidine (EM-12); Compound **3**: 3-[(1R)-1-hydroxy-1-methyl-3-oxo-1,3-dihydro-2H-isoindol-2-yl]piperidine-2,6-dione; Compound **4**: 3-[(1S)-1-hydroxy-1-methyl-3-oxo-1,3-dihydro-2H-isoindol-2-yl]piperidine-2,6-dione; Compound **5**: 2-(1-chloromethyl-2,6-dioxopiperidin-3-yl)phthalimidine. All the values are means ± standard errors of six treatment replicates. Asterisks indicated a value significantly different from the control value, $*P < 0.05$, $**P < 0.01$, $***P < 0.001$ (Student's t-test).

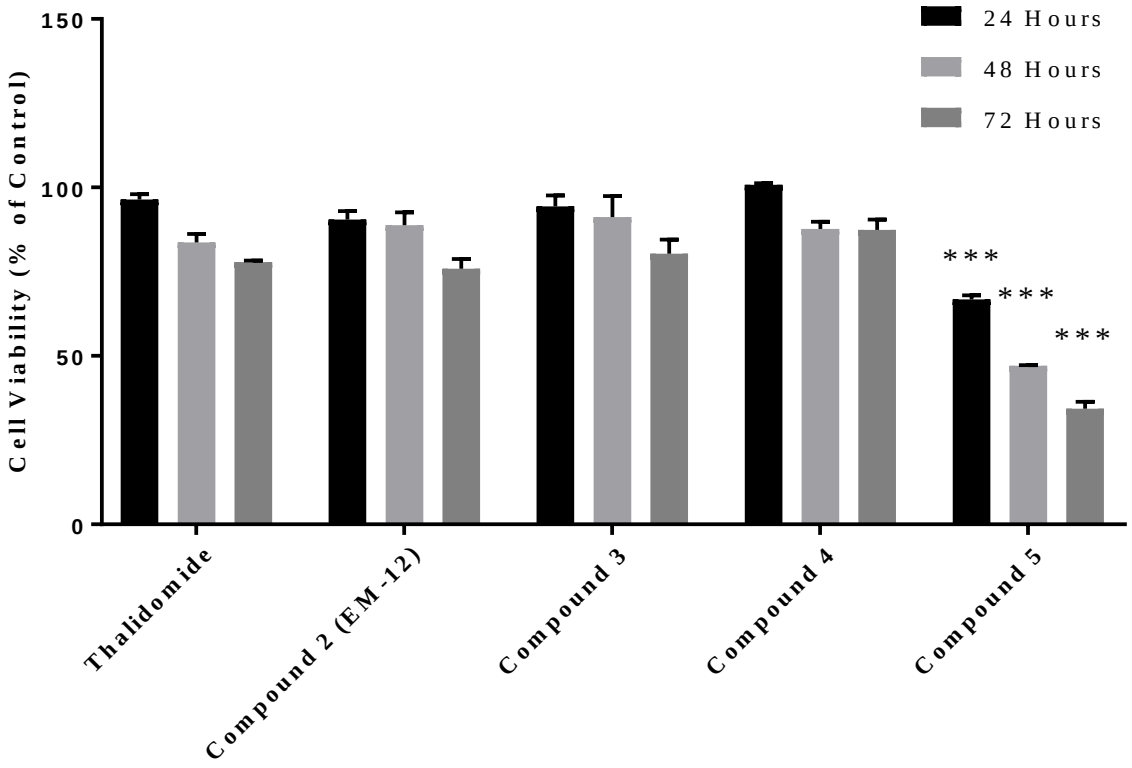

Figure 96: Comparison of MDA-MB-231 Breast cancer cell viability after treatment from thalidomide (Control) and thalidomide structural analogues for 24 hours, 48 hours and 72 hours within the treatment concentration at 100 μg/mL. Compound **2**: 2-(2,6-dioxopiperidin-3-yl)-phthalimidine (EM-12); Compound **3**: 3-[(1R)-1-hydroxy-1-methyl-3-oxo-1,3-dihydro-2H-isoindol-2-yl]piperidine-2,6-dione; Compound **4**: 3-[(1S)-1-hydroxy-1-methyl-3-oxo-1,3-dihydro-2H-isoindol-2-yl]piperidine-2,6-dione; Compound **5**: 2-(1-chloromethyl-2, 6-dioxopiperidin-3-yl)phthalimidine. All the values are means ± standard errors of six treatment replicates. Asterisks indicated a value significantly different from the control value, $*P < 0.05$, $**P < 0.01$, $***P < 0.001$ (Student's t-test).

3.5.3.5 Comparison (Intra-comparison & Inter-comparison) of MDA-MB-231 Breast Cancer Cell Viability after Treatment

Figure 95 shows the comparison of MDA-MB-231 breast cancer cell viability in treatments with thalidomide and its analogues for 24 hours, 48 hours and 72 hours at treatment concentrations of 25 μg/mL and 100 μg/mL. At the treatment concentration of 25 μg/mL, there was no significant difference between thalidomide and its analogue in both intra-comparison and inter-comparison with *P*-value = 1.19 > 0.05. After treatment for 48 hours, the cell viability showed no significant difference between treatment with thalidomide and

compound **2**, compound **3** and compound **4**. The cell viability after treatment with compound 5 at 48 hours was remarkably less than cell viability treated by other compounds with *P*-value < 0.05. In addition, a large difference was found in cell viability between those treated by compound **5** and the cells treated by thalidomide and other structural analogues, with *P*-value < 0.05.

At the treatment concentration of 100 μg/mL (Figure 96), there was no significant difference in cell viability between thalidomide and its structural analogues, including compound 2, compound **3** and compound **4**, in all three-day treatments, with *P*-value > 0.05. However, there was a significant difference found in treatments with compound **5** for all three days (*P* value < 0.05). Cell viability at 48 hours and 72 hours was dramatically reduced to around 40% at 48 hours and 30 % at 72 hours with *P*-value < 0.01.

3.5.4 Cell Cycle Analysis Results

The effects of thalidomide and its analogues on cell cycle progression of human breast cancer cell line MDA-MB-231 was studied. This assay was only conducted after a treatment time of 72 hours. Flow cytometry was used to analyze the DNA content in each phase of the cell cycle. Each experiment was performed in triplicate.

By theory of flow cytometry, light scattering occurs when a particle deflects laser light. The extent to which this occurs depends on the physical properties of the particles, namely their size and internal complexity. There are a number of factors that affect the inside of the cell. Cell shape and surface topography also contribute to the total light scatter. Forward-scatter light (FSC) is proportional to cell-surface area or size. FSC is a measurement of mostly diffracted light and is detected just off the axis of the incident laser beam in the forward direction by a photodiode. FSC provides a sutiable method of detecting particles greater than a specific size, and is independent of their florescence. For this reason, the technique is often used in immunophenotyping to trigger signal processing. Side-scattered light (SSC) is prortional to cell granularity or internal complexity. SSC is a measurement of mostly refracted and reflected light that occurs at any artefact within the cell where there is a changein refractive index. Correlated measurements of FSC and SSC can allow for

differentiation of cell types in a heteogeneous cell population. In this study, the results of FSC *vs.* SSC were applied to differentiate MDA-MB-231 cell types and distinguish change of MDA-MB-231 cell size and morphology. In addition, flow cytometry is predominantly used to measure fluorescence intensity produced by fluorescent-labeled antibodies detecting targetted proteins, or ligands that bind to specific cell-assoicated molecules, such as propidium iodide binding to DNA. Based on amount of DNA in cell cycle, flow cytometry contributes to quatitatively determine change of DNA contents in cell cycle after treatment. The staining procedure involves taking a single-cell suspension from cell culture or tissue samples. The cells are then incubated in tubes or microtiter plates with fluorochrome-labeled antibodies and analyzed on the flow cytometer. All values were the negative control to compare the change of cell morphology and percentage of DNA content in different phases of the cell cycle 72-hours after being.

Figure 97 shows human breast cancer cell line MDA-MB-231 seeded on the plate for 72 hours without any treatment. Figure 97-A1 shows the morphology of cells obtained under an inverted microscopes 72 hours after cell seeding on plates. Figure 97-A2 shows the DNA content distribution in the cell cycle 72 hours after cell seeding and analysis by flow cytometry. The results of FSC *vs.* SSC are shown in the Figure 137 in Appendix V to describe and distinguish changes of MDA-MB-231 cell size and internal morphological structure. All values were the negative control to compare the change of cell morphology and percentage of DNA content in different phases of the cell cycle 72 hours after treatment.

3.5.4.1 Cell Cycle Distribution Results of Non-treatment group After Incubation for 72 hours

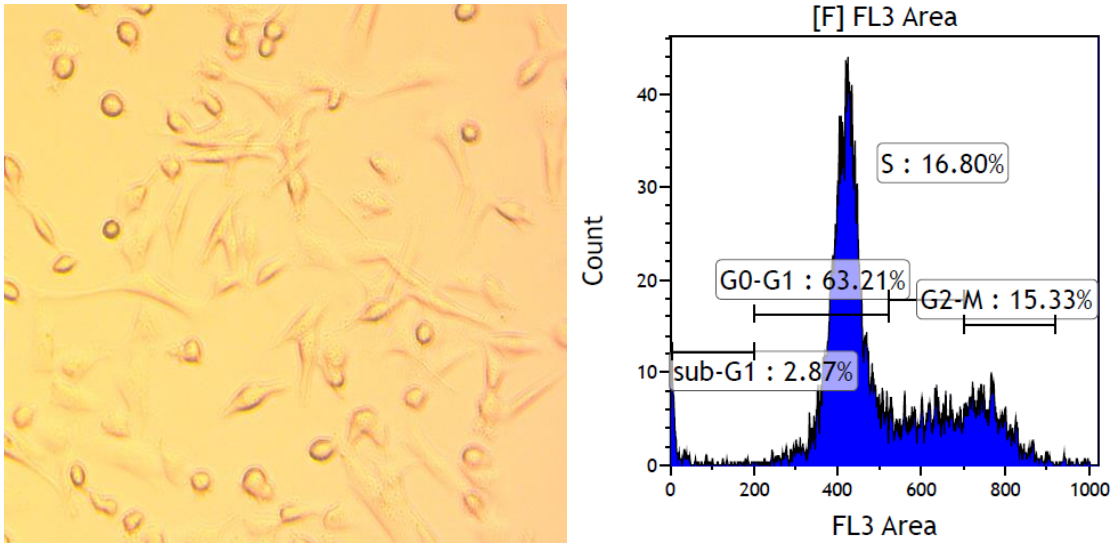

A1 **A2**

Figure 97: MDA-MB-231 Cell cycle distribution without treatment at 72 hours; A1: Description of cell cycle distribution obeserved under inverted microscope; A2: Description of cell cycle distribution in histogram

3.5.4.2 Cell Cycle Distribution Results of After Treatment with Thalidomide for 72 hours

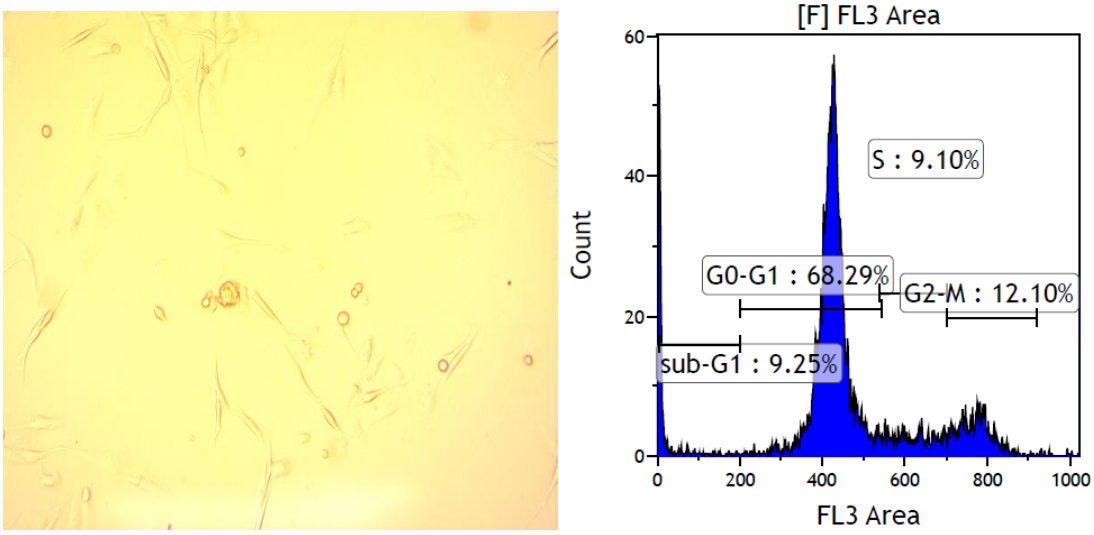

A1 **A2**

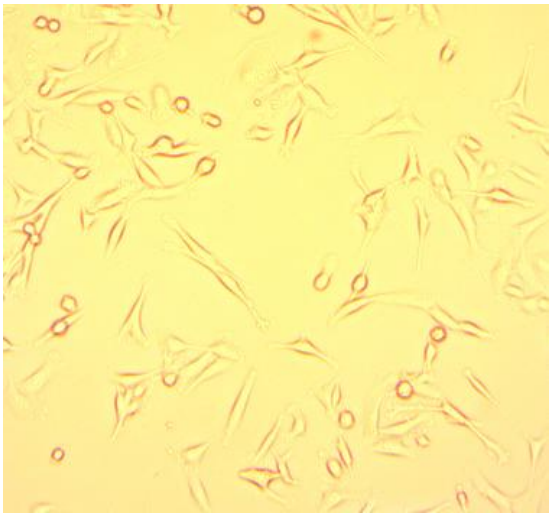

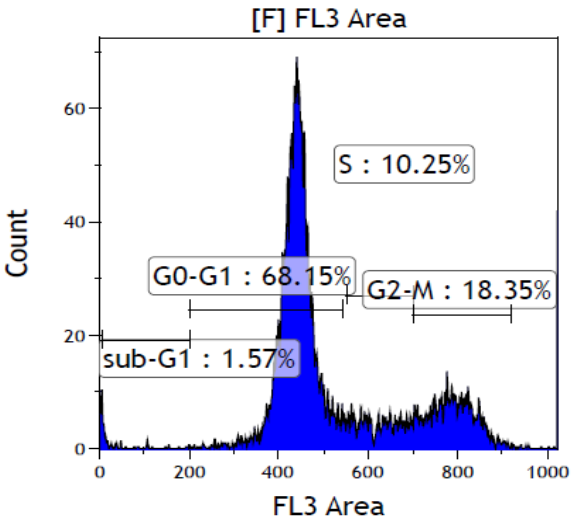
[F] FL3 Area
S : 10.25%
G0-G1 : 68.15%
G2-M : 18.35%
sub-G1 : 1.57%
Count
FL3 Area

B1 **B2**

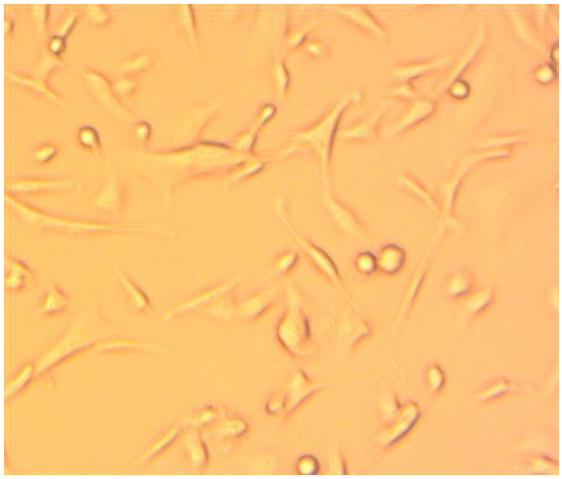

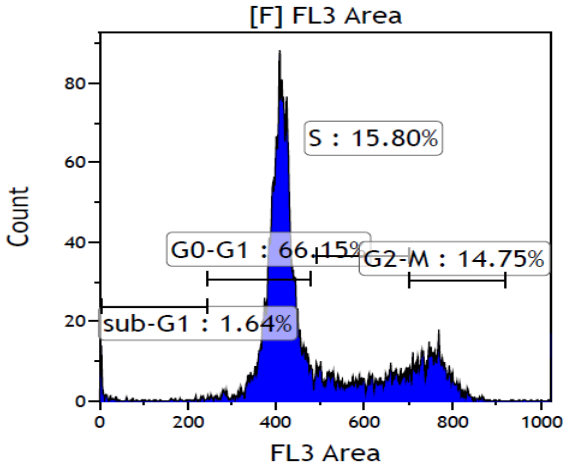
[F] FL3 Area
S : 15.80%
G0-G1 : 66.15%
G2-M : 14.75%
sub-G1 : 1.64%
Count
FL3 Area

C1 **C2**

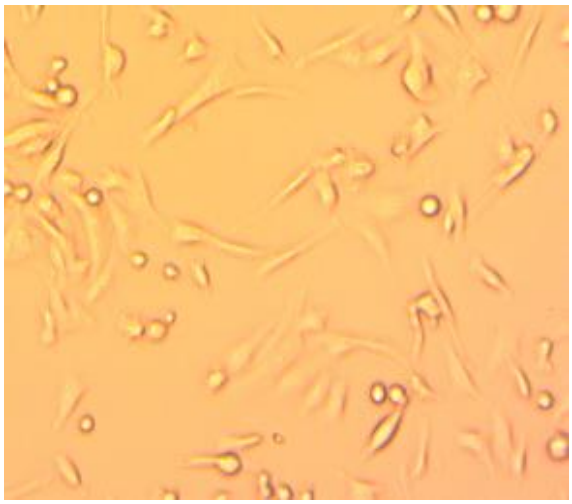

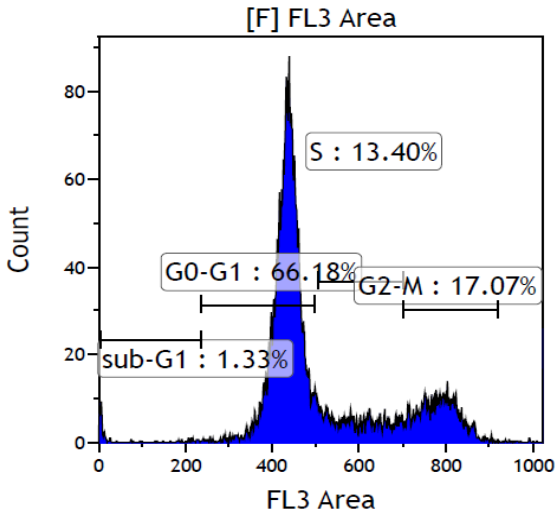
[F] FL3 Area
S : 13.40%
G0-G1 : 66.18%
G2-M : 17.07%
sub-G1 : 1.33%
Count
FL3 Area

D1 **D2**

Figure 98: MDA-MB-231 cell cycle distribution with treatment of thalidomide (Compound **1**) at 72 hours; A1, B1, C1 & D1: Description of cell cycle distribution obeserved under inverted microscope; A2, B2, C2 & D2: Description of cell cycle distribution in histogram. The treatment concentration of thalidomide (Compound 1) includes: 500 μg/mL (A1 & A2); 100 μg/mL (B1 & B2); 10 μg/mL (C1 & C2) & 1 μg/mL (D1 & D2).

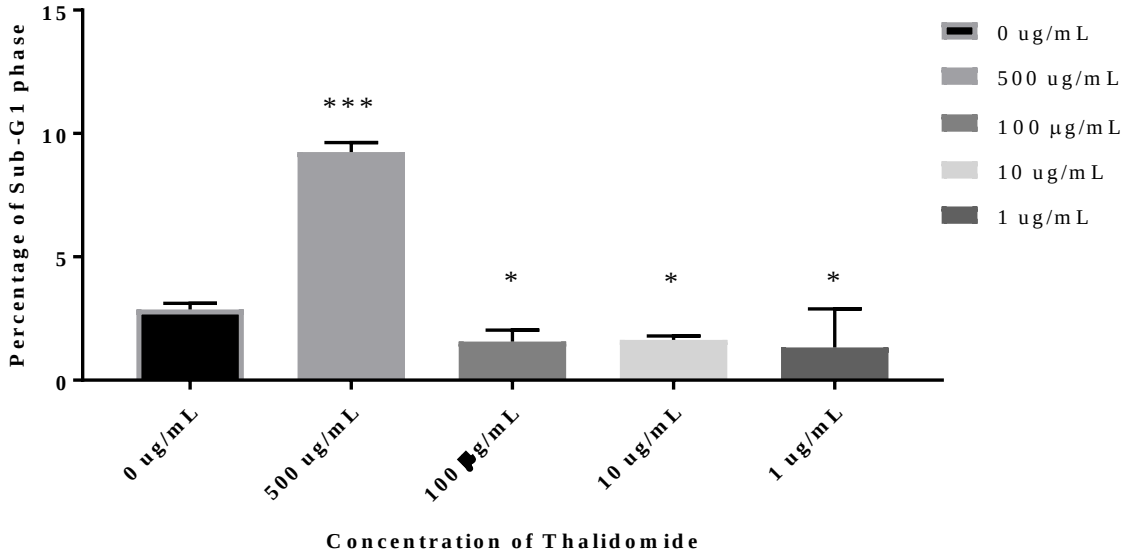

Figure 99: Comparison about change of sub-G1 phase in percentage between non-treatment and treatment with thalidomide with a series of concentraton for 72 hours. Asterisks indicated a value significantly different from the control value, $*P < 0.05$, $**P < 0.01$, $***P < 0.001$ (Student's t-test).

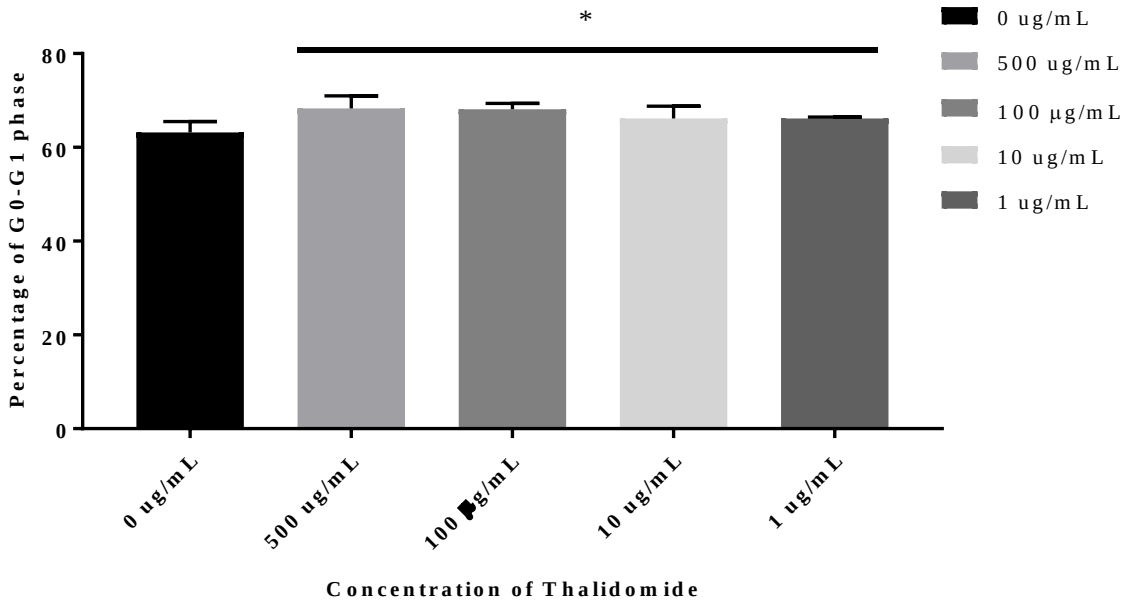

Figure 100: Comparison about change of G0-G1 phase in percentage between non-treatment and treatment with thalidomide with a series of concentraton for 72 hours. Asterisks indicated a value significantly different from the control value, **P* < 0.05, ***P* < 0.01, ****P* < 0.001 (Student's t-test).

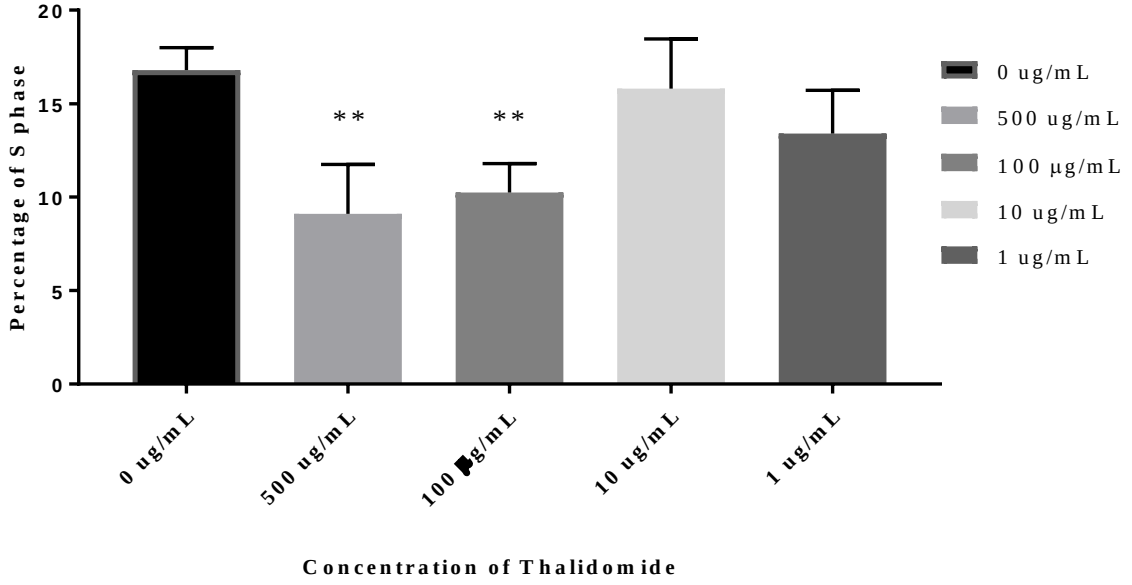

Figure 101: Comparison about change of S phase in percentage between non-treatment and treatment with thalidomide with a series of concentraton for 72 hours. Asterisks indicated a value significantly different from the control value, **P* < 0.05, ***P* < 0.01, ****P* < 0.001 (Student's t-test).

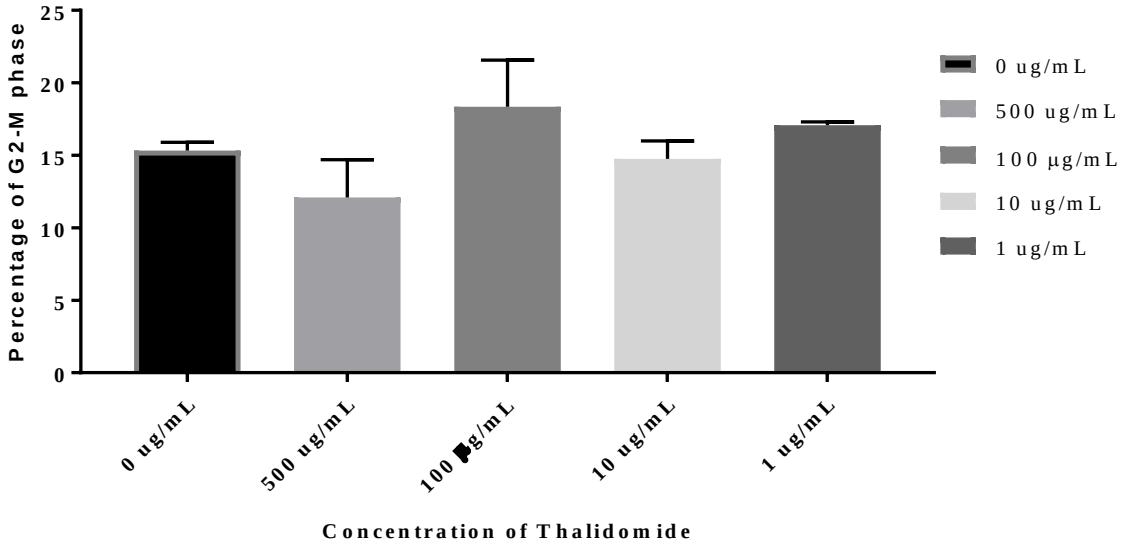

Figure 102: Comparison about change of G2-M phase in percentage between non-treatment and treatment with thalidomide with a series of concentraton for 72 hours.

Figure 98-A1 to 98-D1 show cell density and cell morphology after 72-hours treatment with thalidomide at concentrations of 500 µg/mL (Figure 98-A1), 100 µg/mL (Figure 98-B1), 10 µg/mL (Figure 98-C1) and 1 µg/mL (Figure 98-D1). As observed under an inverted microscope, the size of cells and the morphology of cells were not significantly changed. This result was consistent with the results of FCS *vs*. SSC analysis by flow cytometry as shown in Figure 139 Appendix V. In addition, there was a remarkable drop in cell density with increasing concentrations of treatments. The cell density in the treatment concentration of 500 µg/mL was significantly lower that cell densities in other concentration treatments.

In addition, Figure 98-A2 to 98-D2 show that the percentages of cell distribution of different phases were changed after treatment with thalidomide in a series of treament concentrations at 72 hours. In order to describe the changes of percentages in all phases of the cell cycle, Figure 99 to Figure 102 showed comparisons of change due to the presence of treatments at different concentrations of thalidomide. Compared to untreated cells, the percentage of sub-G1 (Figure 99) population gradually increased from treatment concentrations of 1 µg/mL to 100 µg/mL. There was a significant increase of sub-G1 phase in the treatment concentration

of thalidomide at 500 µg/mL (from 1.89% at 100 µg/mL to 9.06% at 500 µg/mL) after 72-hours treatment. For G0-G1 phase (Figure 100) identification, the changes were quite large compared to changes in sub-G1 phase. From all treatment concentrations ranging from 1 µg/mL to 500 µg/mL, all percentages of G0-G1 phase were significantly higher than values from non-treatment groups with *P*-value < 0.01. Of note, for treatment concentrations higher than 100 µg/mL, the percentage of G0-G1 phase was largely higher than values in treatment concentrations lower than 10 µg/mL. For S phase analysis (Figure 101), the percentage after treatment for 72 hours at concentrations of 100 µg/mL and 500 µg/mL were statistically and significantly lower than the percentage of S phase in the non-treatment group. For G2-M phase (Figure 102), a significant decrease was only found in the highest treatment concentration of 500 µg/mL for 72 hours.

3.5.4.3 Cell Cycle Distribution Results of After Treatment with Thalidomide Analogues for 72 hours

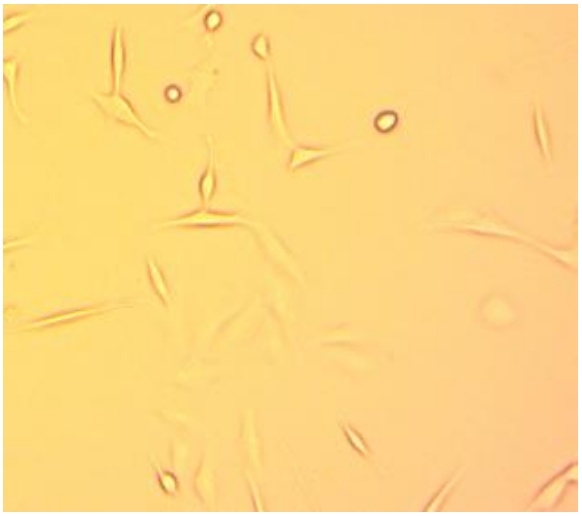

A1

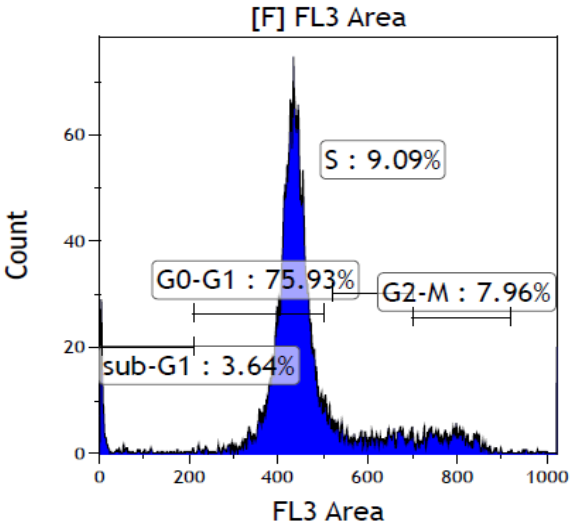

A2

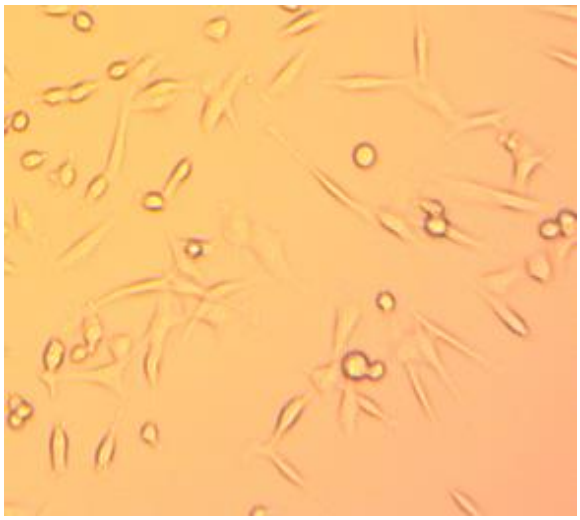

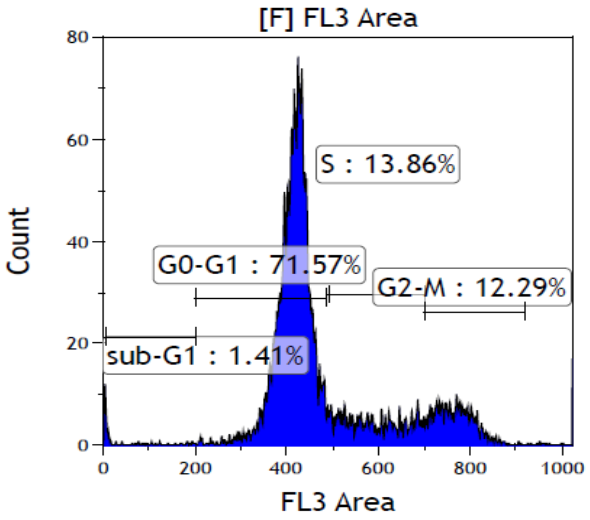
[F] FL3 Area
Count
S : 13.86%
G0-G1 : 71.57%
G2-M : 12.29%
sub-G1 : 1.41%
FL3 Area

B1 **B2**

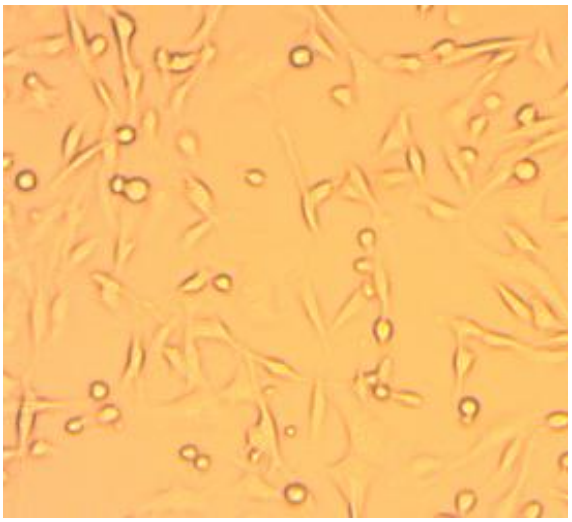

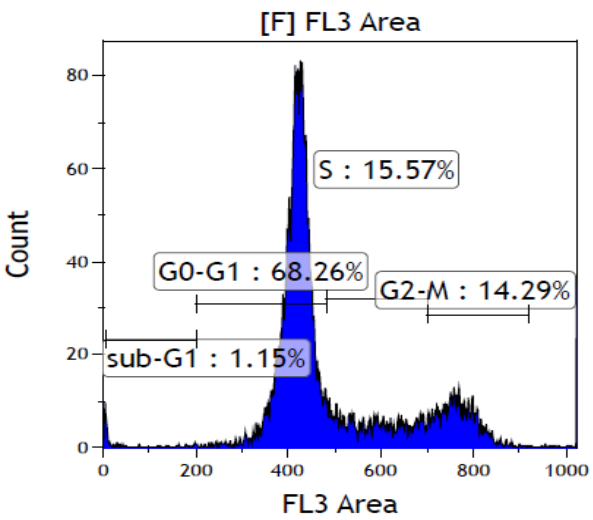
[F] FL3 Area
Count
S : 15.57%
G0-G1 : 68.26%
G2-M : 14.29%
sub-G1 : 1.15%
FL3 Area

C1 **C2**

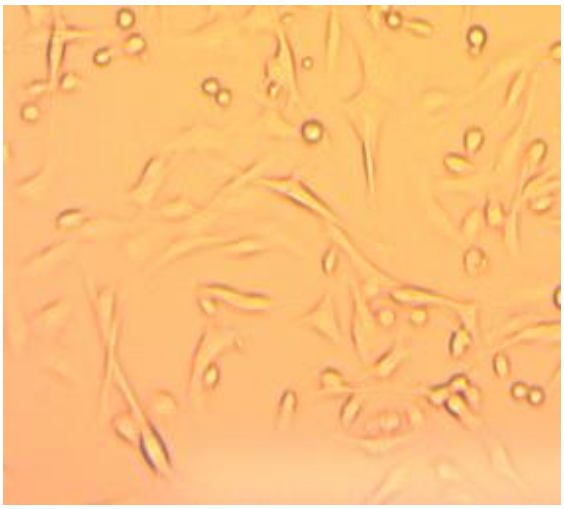

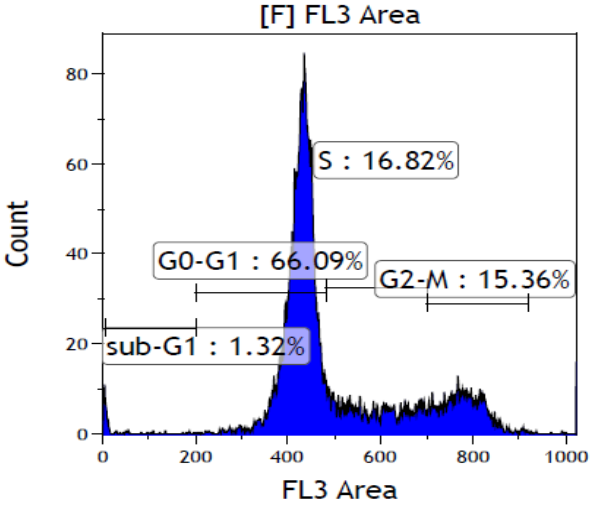
[F] FL3 Area
Count
S : 16.82%
G0-G1 : 66.09%
G2-M : 15.36%
sub-G1 : 1.32%
FL3 Area

D1 **D2**

Figure 103: MDA-MB-231 cell cycle distribution with treatment of 2-(2,6-dioxopiperidin-3-yl)-phthalimidine (Compound **2**) at 72 hours; A1, B1, C1 & D1: Description of cell cycle distribution observed under an inverted microscope; A2, B2, C2 & D2: Description of cell cycle distribution in histogram. The treatment concentration of 2-(2,6-dioxopiperidin-3-yl)-phthalimidine (Compound **2**) includes: 500 μg/mL (A1 & A2); 100 μg/mL (B1 & B2); 10 μg/mL (C1 & C2) & 1 μg/mL (D1 & D2).

Figure 103-A1 to 103-D1 show cell density and cell morphology after 72-hours treatment with compound **2** at concentrations of 500 μg/mL (Figure 103-A1), 100 μg/mL (Figure 103-B1), 10 μg/mL (Figure 103-C1) and 1 μg/mL (Figure 103-D1). As observed under an inverted microscope, the size of cell and the morphology of cells were not significantly changed. These results were consistent with the results of FCS *vs.* SSC analysed by flow cytometry as shown in Figure 140 Appendix V. In addition, there was a remarkable drop of cell density with increasing concentration of treatment. The cell density in treatment concentration of 500 μg/mL was significantly lower that cell density in other concentration treatments. This cell density was consistent with results of cell cycle distribution after treatment with compound **2** for 72 hours.

Figure 103-A2 to 103-D2 show that the percentages of cell distribution of different phases were changed after treatment with compound **2** in a series of treament concentrations at 72 hours. The percentage of sub-G1 after a treatment concentration of 500 μg/mL for 72 hours was 3.64. This value was the highest value after treatment with compound **2** in the highest treatment concentration for 72 hours, suggesting a large number of cells were inhibited due to the presence of compound **2**. For G0-G1 phase analysis, there was an increasing relationship between percentage of cell distribution and treatment concentrations. Conversely, for both S phase and G2-M phase, there was a trend of decreasing distribution percentages with increasing treatment concentrations of compound **2** (from 9.09% for S phase and 7.96% for G2-M phase to 16.82% for S phase and 15.36% for G2-M phase).

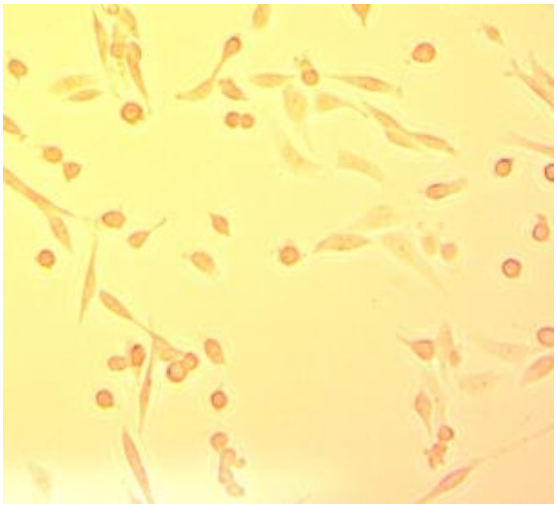

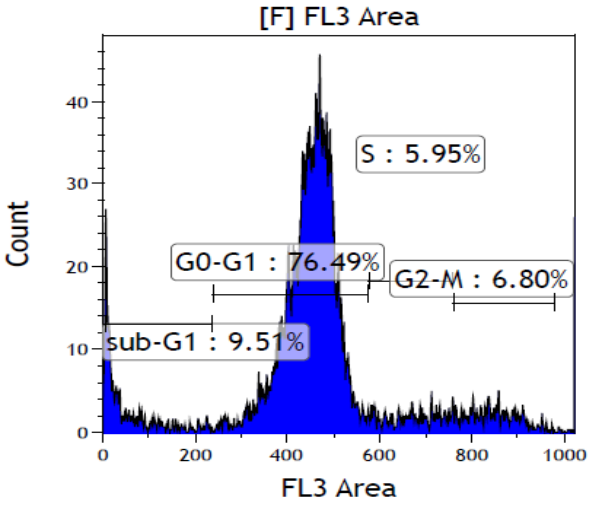
[F] FL3 Area
Count
S : 5.95%
G0-G1 : 76.49%
G2-M : 6.80%
sub-G1 : 9.51%
FL3 Area

A1 **A2**

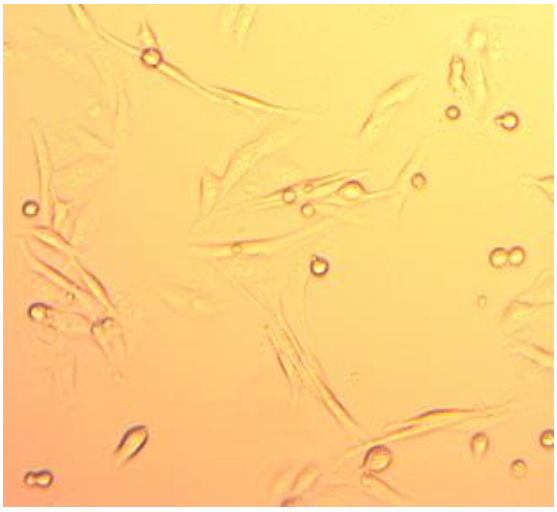

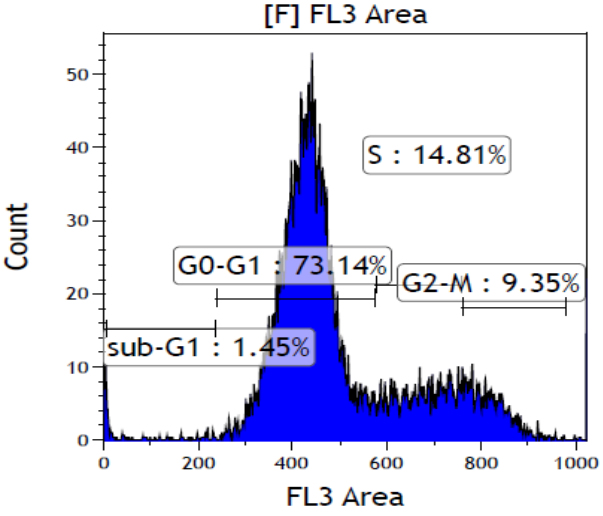
[F] FL3 Area
Count
S : 14.81%
G0-G1 : 73.14%
G2-M : 9.35%
sub-G1 : 1.45%
FL3 Area

B1 **B2**

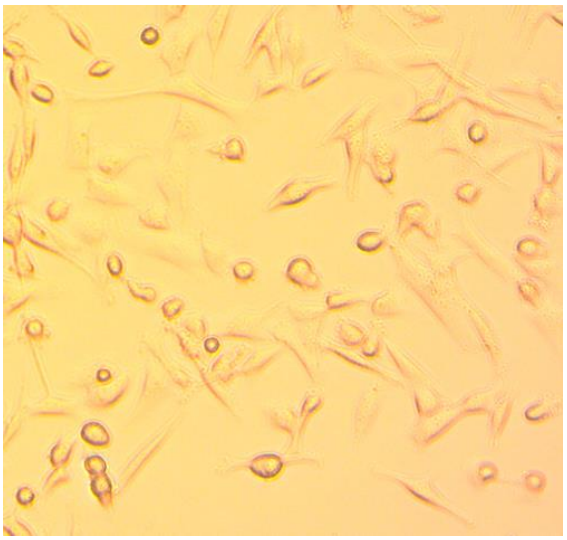

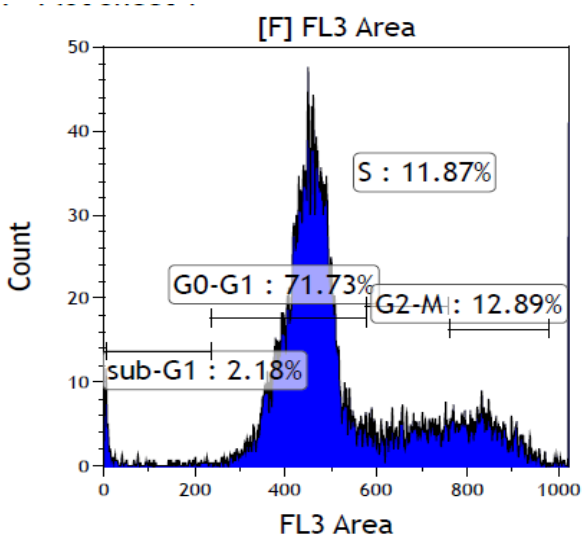
[F] FL3 Area
Count
S : 11.87%
G0-G1 : 71.73%
G2-M : 12.89%
sub-G1 : 2.18%
FL3 Area

C1 **C2**

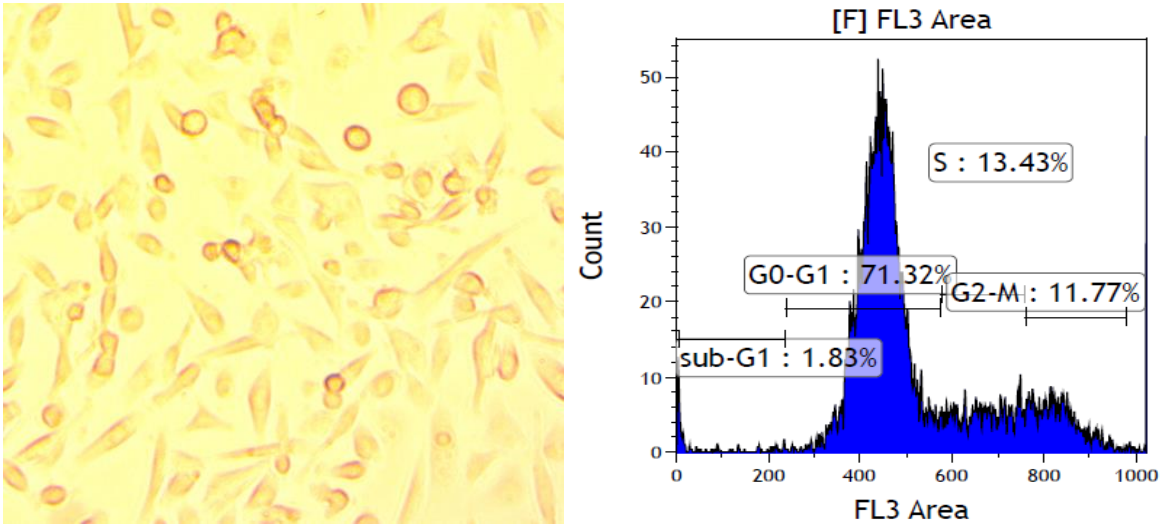

D1 **D2**

Figure 104: MDA-MB-231 cell cycle distribution with treatment of 3-[(1R)-1-hydroxy-1-methyl-3-oxo-1,3-dihydro-2H-isoindol-2-yl]piperidine-2,6-dione (Compound **3**) at 72 hours; A1, B1, C1 & D1: Description of cell cycle distribution obeserved under inverted microscope; A2, B2, C2 & D2: Description of cell cycle distribution in histogram. The treatment concentration of 3-[(1R)-1-hydroxy-1-methyl-3-oxo-1,3-dihydro-2H-isoindol-2-yl]piperidine-2,6-dione (Compound **3**) includes: 500 µg/mL (A1 & A2); 100 µg/mL (B1 & B2); 10 µg/mL (C1 & C2) & 1 µg/mL (D1 & D2).

Figure 104-A1 to 104-D1 show cell density and cell morphology after 72-hours treatment with Compound **3** at concentrations of 500 µg/mL (Figure 104-A1), 100 µg/mL (Figure 104-B1), 10 µg/mL (Figure 104-C1) and 1 µg/mL (Figure 104-D1). As observed under an inverted microscope, the size of cells and the morphology of cells were not significantly changed. This result was consistent with the results of FCS *vs.* SSC analysis by flow cytometry as shown in Figure 141 Appendix V. In addition, there was a remarkable drop in cell density with increasing concentrations of treatments. The cell density in treatment concentrations of 500 µg/mL were significantly lower that cell densities in other concentration treatments.

Figure 104-A2 to 104-D2 show that the percentages of cell distribution of different phases were changed after treatment with compound **3** in a series of treatment concentrations at 72 hours. After treatment with compound **3** for 72 hours, it was found that the distribution of the cell cycle was changed by incubation with different concentrations. The percentage of sub-G1 gradually decreased with decreasing concentration of treatment. The percentage of sub-

G1 after 72-hours treatment at 500 µg/mL was 9.51%, and its values significantly higher than sub-G1 in other concentration treatment 1.45% for 100 µg/mL, 2.18% for 10 µg/mL and 1.83% for 1 µg/mL. Consistently, the percentage of G0-G1 phase was gradually decreased based on the dramatic drop of treatment concentrations from 500 µg/mL to 1 µg/mL.

However, for both the S-phase and the G2-M phase, there was a dramatical increase coresponding with a decreasing of treatment concentrations. For S phase, the percentage of S phase after 72-hours treatment was 5.95% at a concentration of 500 µg/mL, This value was remarkably lower than the percentage of S phase cells after treatment at the concentrations of 100 µg/mL, 10 µg/mL and 1 µg/mL. Similarly, in G2-M phase, the percentage after treatments were 12.89% for 10 µg/mL, which was significantly higher than the percentage with increasing concentration (6.80% for 500 µg/mL).

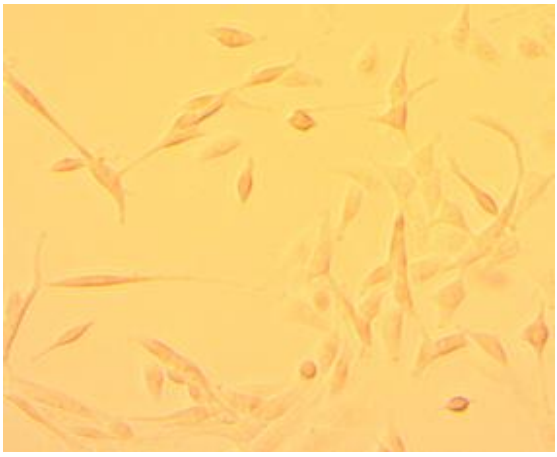

A1

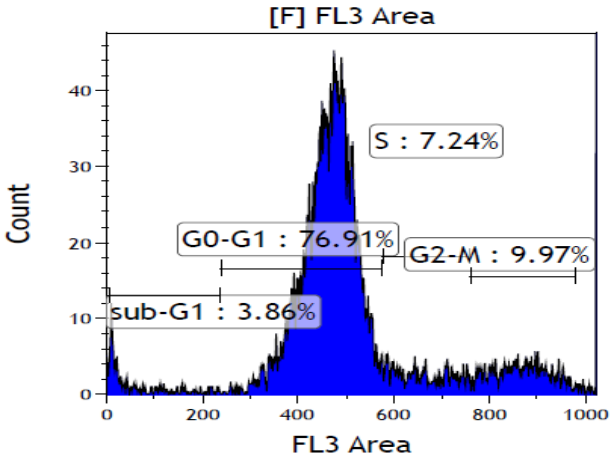

A2

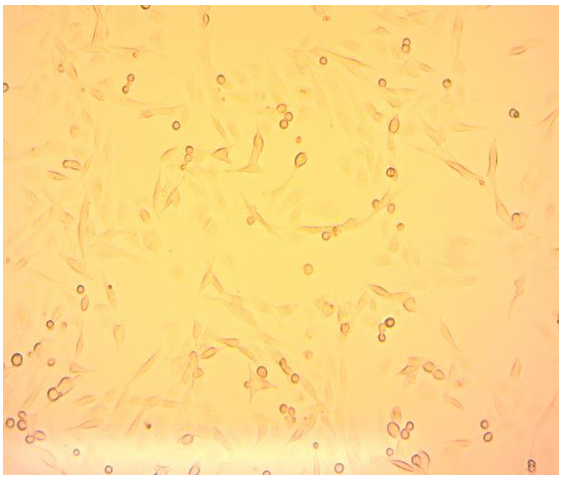

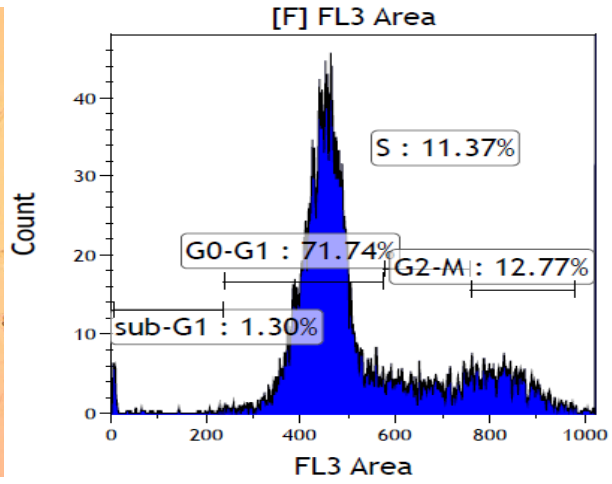

B1 **B2**

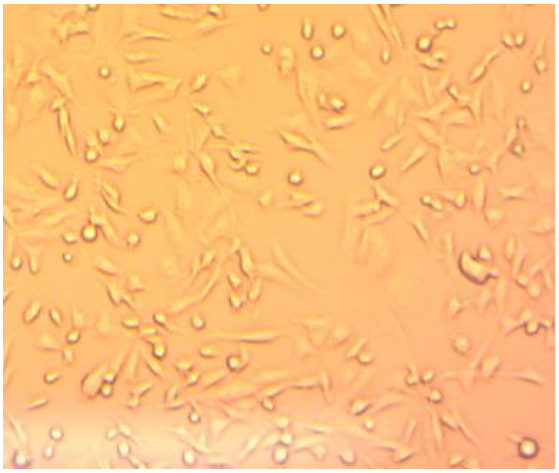

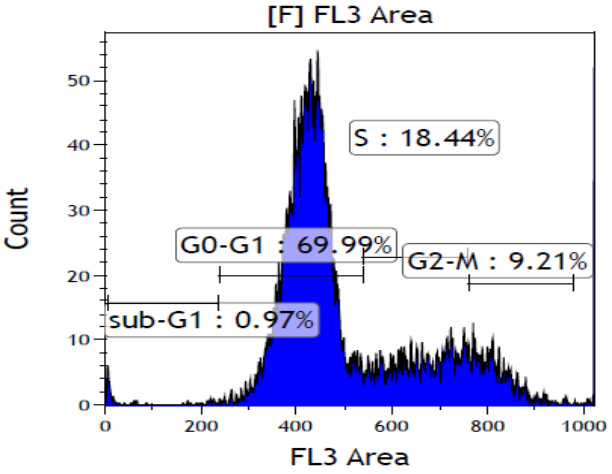

C1 **C2**

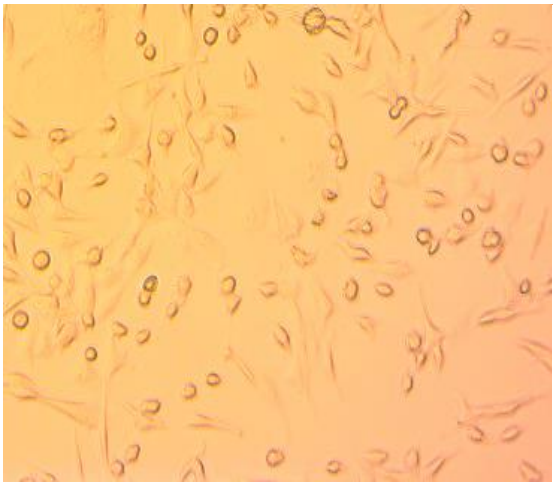

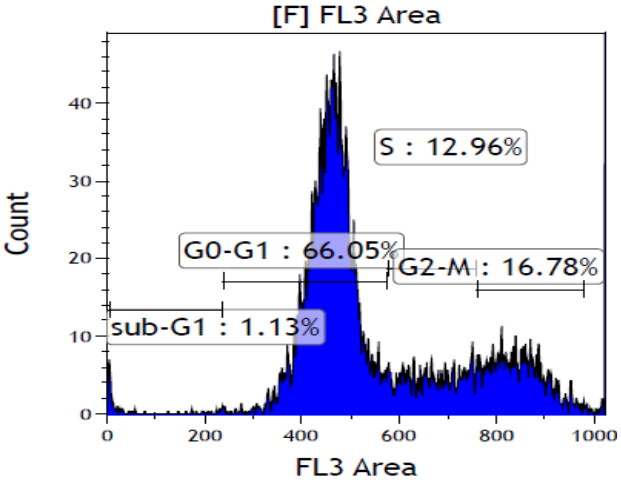

D1 **D2**

Figure 105: MDA-MB-231 cell cycle distribution with treatment of 3-[(1S)-1-hydroxy-1-methyl-3-oxo-1,3-dihydro-2H-isoindol-2-yl]piperidine-2,6-dione (Compound **4**) at 72 hours; A1, B1, C1 & D1: Description of cell cycle distribution obeserved under inverted microscope; A2, B2, C2 & D2: Description of cell cycle distribution in histogram. The treatment concentration of 3-[(1S)-1-hydroxy-1-methyl-3-oxo-1,3-dihydro-2H-isoindol-2-yl]piperidine-2,6-dione (Compound **4**) includes: 500 μg/mL (A1 & A2); 100 μg/mL (B1 & B2); 10 μg/mL (C1 & C2) & 1 μg/mL (D1 & D2).

Figure 105-A1 to 105-D1 show cell density and cell morphology after 72-hours treatment with compound **4** at concentrations of 500 μg/mL (Figure 105-A1), 100 μg/mL (Figure 105-B1), 10 μg/mL (Figure 105-C1) and 1 μg/mL (Figure 105-D1). As observed under an inverted microscope, the size of cell and the morphology of cells were not significantly changed. This results was consistent with the results of FCS *vs.* SSC analysis by flow cytometry as shown in Figure 142 Appendix V. In addition, there was a remarkable drop in cell density with increasing concentrations of treatments. The cell density in treatment concentrations of 500 μg/mL was significantly lower that cell densities in other concentration treatments.

Figure 105-A2 to 105-D2 show that the percentages of cell distribution of different phases were changed after treatment with compound **4** in a series of treament concentrations at 72 hours. After treatment of compound **4** for 72 hours, it was found that the distribution of the cell cycle was changed by incubation with different concentrations of treatments for 72 hours. The percentage of sub-G1 gradually decreased with decreasing concentrations of treatments. The percentage of sub-G1 after 72-hours treatment at 500 μg/mL was 3.86%, and its values were significantly higher than sub-G1 in other concentration treatments: 1.30% for 100 μg/mL, 0.97% for 10 μg/mL and 1.13% for 1 μg/mL. Consistently, the percentage of G0-G1 was gradually decreased based on the decreasing trend of concentration. For concentrations of 500 μg/mL, the percentage of G0-G1 was 76.91%, and it was significantly higher than percentage of G0-G1 phase after treatment in concentrations of 100 μg/mL (71.74%), 10 μg/mL (69.99%) and 1 μg/mL (66.05%).

However, for both the S-phase and the G2-M phase, there was a dramatical increase corresponsing with the decrease in treatment concentrations. For S phase, the precentage of S phase after 72-hours treatment was 7.24% at the concentration at 500 μg/mL, and its value was remarkably lower than the percentage of S phase after treated cells in the concentrations

of 100 μg/mL, 10 μg/mL and 1 μg/mL. For G2-M phase, there was no clear relationship between changes of percentage and the treatment concentrations after 72 hours treatment.

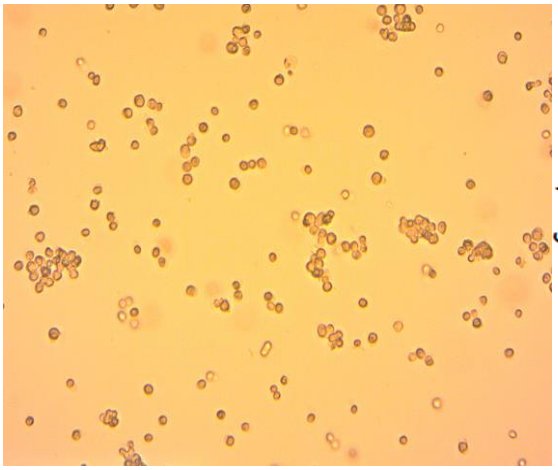

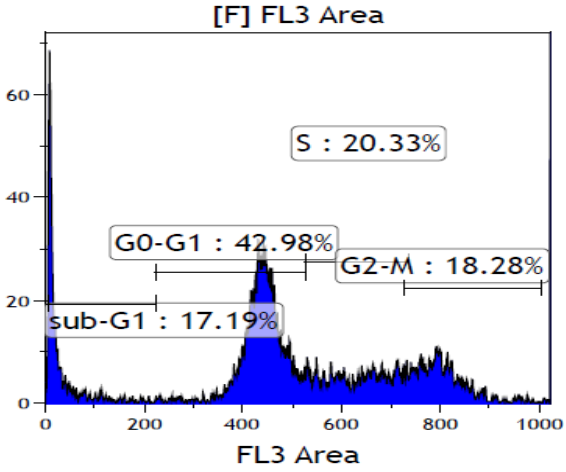

A1 **A2**

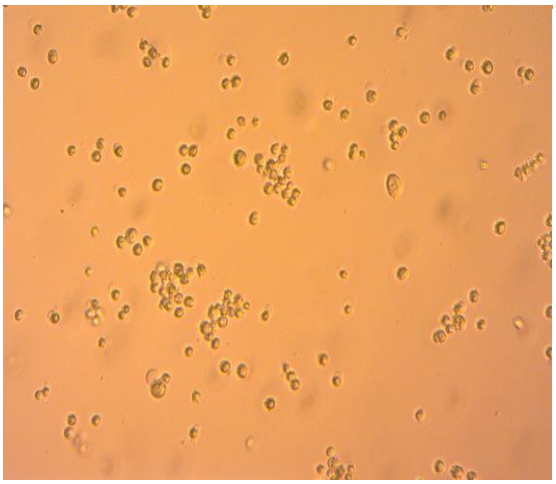

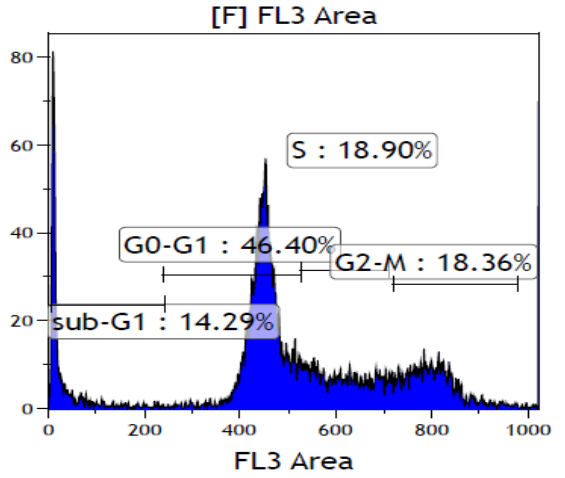

B1 **B2**

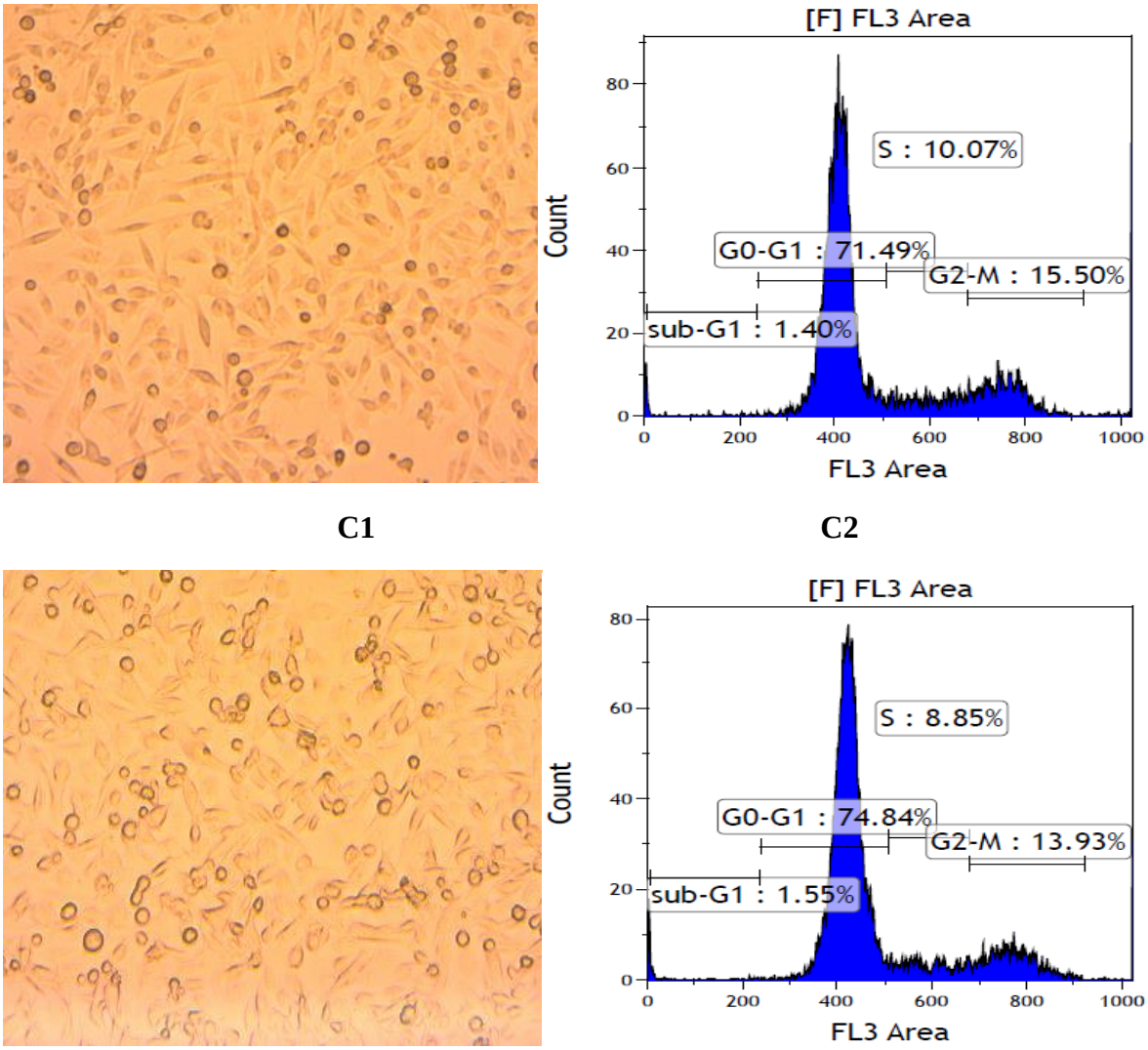

Figure 106: MDA-MB-231 cell cycle distribution with treatment of 2-(1-chloromethyl-2,6-dioxopiperidin-3-yl)phthalimidine (Compound **5**) at 72 hours; A1, B1, C1 & D1: Description of cell cycle distribution obeserved under inverted microscope; A2, B2, C2 & D2: Description of cell cycle distribution in histogram. The treatment concentration of 2-(1-chloromethyl-2,6-dioxopiperidin-3-yl)phthalimidine (Compound **5**) includes: 500 µg/mL (A1 & A2); 100 µg/mL (B1 & B2); 10 µg/mL (C1 & C2) & 1 µg/mL (D1 & D2).

Figure 106-A1 to 106-D1 show cell density and cell morphology after 72-hours treatment with compound **5** at concentrations of 500 µg/mL (Figure 106-A1), 100 µg/mL (Figure 106-B1), 10 µg/mL (Figure 106-C1) and 1 µg/mL (Figure 106-D1). As observed under an inverted microscope, there was a clear, noteable change in cell morphology after treatment cells with concentrations of 100 µg/mL and 500 µg/mL. As observed, the cells were changed to small,

rounded shapes, and furthermore, cell density at these concentrations were much lower than cell densities in treatment concentrations of 10 μg/mL and 1 μg/mL. This result was consistent with the results of FCS *vs*. SSC analysis by flow cytometry as shown in Figure 143 Appendix V, in that the position of the cell population changed to the left side, which indicated that the size of cells decreased.

Figure 106-A2 to 106-D2 show that the percentages of cell distributions of different phases were changed after treatments with compound **3** in a series of treatment concentrations at 72 hours. After treatment with compound **5** for 72 hours, it was found that the distribution of the cell cycle was dramatically changed by incubation with different concentrations. The percentage of sub-G1 gradually decreased with decreasing concentrations of treatments. The percentage of sub-G1 after 72-hours treatment at 500 μg/mL and 100 μg/mL was 17.19% and 14.291% respectively, and these values were significantly higher than sub-G1 at other concentration treatments: 1.40% for 10 μg/mL and 1.55% for 1 μg/mL. Consistently, treatments generated the same trend of change relative to percentages in both S phase and G2-M phase as observed in Sub-G1 phase. At concentrations of 500 μg/mL and 100 μg/mL, the treatments generated an increased percentage of S-phase (20.33% for 500 μg/mL and 18.90% for 100 μg/mL), and G2-M phase (18.28% for 500 μg/mL and 18.36% for 100 μg/mL). These values are higher than percentages of S-phase (10.07% for 10 μg/mL and 8.85% for 1 μg/mL), and G2-M phase (15.50% for 10 μg/mL and 13.93% for 1 μg/mL).

However, for the G0-G1 phase, there was a remarkable decrease observed for treatment concentrations of 500 μg/mL (42.98%) and 100 μg/mL (46.40%), while there was an increase in the percentage of G0-G1phase (71.49% for 10 μg/mL and 74.84% for 100 μg/mL).

3.5.4.4 Comparison of MDA-MB-231 Cell Cycle Ditribution After Treatment of Thalidomide & Its Analogues

Table 13: Cell cycle distribution of MDA-MB-231cells after treatment with thalidomide. Cell cycle distribution of MDA-MB-231cells after treatment with thalidomide or it analogues for 72 hours; Data shows the percentage of each phase (%), and are expressed as mean ± S.D. (n=3).

Treatment	Concentration (µg/mL)	Sub-G1	G0-G1	S	G2-M
Negative Control	**0**	2.87± 0.47	63.21 ± 0.80	16.80 ± 0.62	15.33 ± 0.51
Thalidomide (Compound 1)	**500**	9.25 ± 0.39	68.29 ± 0.11	9.10 ± 0.87	12.10 ± 0.21
	100	1.57 ± 0.48	66.53 ± 0.30	10.25 ± 1.07	18.35 ± 0.12
	10	1.64 ± 0.66	66.15 ± 0.82	15.80 ± 0.13	14.75 ± 0.22
	1	1.33± 0.55	66.18 ± 0.26	13.40 ± 0.56	17.07 ± 0.31
2-(2,6-dioxopiperidin-3-yl)-phthalimidine, EM-12 (Compound 2)	**500**	3.58 ± 0.11	75.93 ± 0.12	9.09 ± 0.26	7.96 ± 0.68
	100	1.41 ± 0.21	71.57 ± 0.47	13.86 ± 0.53	12.29 ± 0.19
	10	1.25 ± 0.30	68.26± 0.44	15.57 ± 1.08	14.29 ± 0.20
	1	1.22 ± 0.21	66.09 ± 0.34	16.82 ± 0.36	15.36 ± 0.16
3-[(1*R*)-1-hydroxy-1-methyl-3-oxo-1,3-dihydro-2*H*-isoindol-2-yl]piperidine-2,6-dione (Compound 3)	**500**	9.51 ± 0.76	76.49 ± 0.33	5.95 ± 0.94	6.80 ± 0.61
	100	1.45 ± 0.14	73.14 ± 0.19	14.81 ± 0.21	9.35 ± 0.86
	10	2.18 ± 0.57	71.73 ± 0.35	11.87 ± 0.16	12.89 ± 0.26
	1	1.83 ± 0.26	71.32 ± 0.14	13.43 ± 0.45	11.77 ± 0.12
3-[(1*S*)-1-hydroxy-1-methyl-3-oxo-1,3-dihydro-2*H*-isoindol-2-yl]piperidine-2,6-dione (Compound 4)	**500**	3.86 ± 0.53	76.91 ± 0.33	7.24 ± 0.81	9.97 ± 0.23
	100	1.30 ± 0.14	71.74 ± 0.47	11.37 ± 0.33	12.77 ± 0.26
	10	0.97 ± 0.45	69.99 ± 0.43	18.44 ± 0.12	9.21 ± 0.23
	1	1.13 ± 0.12	66.05 ± 0.23	12.96 ± 0.55	16.78 ± 0.24

2-(1-Chloromethyl-2, 6-dioxopiperidin-3-yl)phthalimidine (Compound 5)	**500**	17.19 ± 1.08	42.98 ± 0.19	20.33 ± 0.23	18.28 ± 0.12
	100	14.29 ± 0.85	46.40 ± 0.92	18.90 ± 0.24	18.36 ± 0.27
	10	1.40 ± 0.57	71.49 ± 0.19	10.07 ± 0.12	15.50 ± 0.23
	1	1.55 ± 0.20	74.84 ± 0.53	8.85 ± 0.19	13.93 ± 0.33

Table 13 summarizes the MDA-MB-231 cell cycle distribution (Sub-G1, G0-G1 phase, S phase and G2-M phase) percentage values after treatment with thalidomide and its thalidomide structural analogues for 72 hours. Due to different treatments given in a series of concentrations, cell cycle distributions were changed. From Figure 101 to Figure 104 shown, all phases in MDA-MB-231 cell cycles were compared between thalidomide and its analogues.

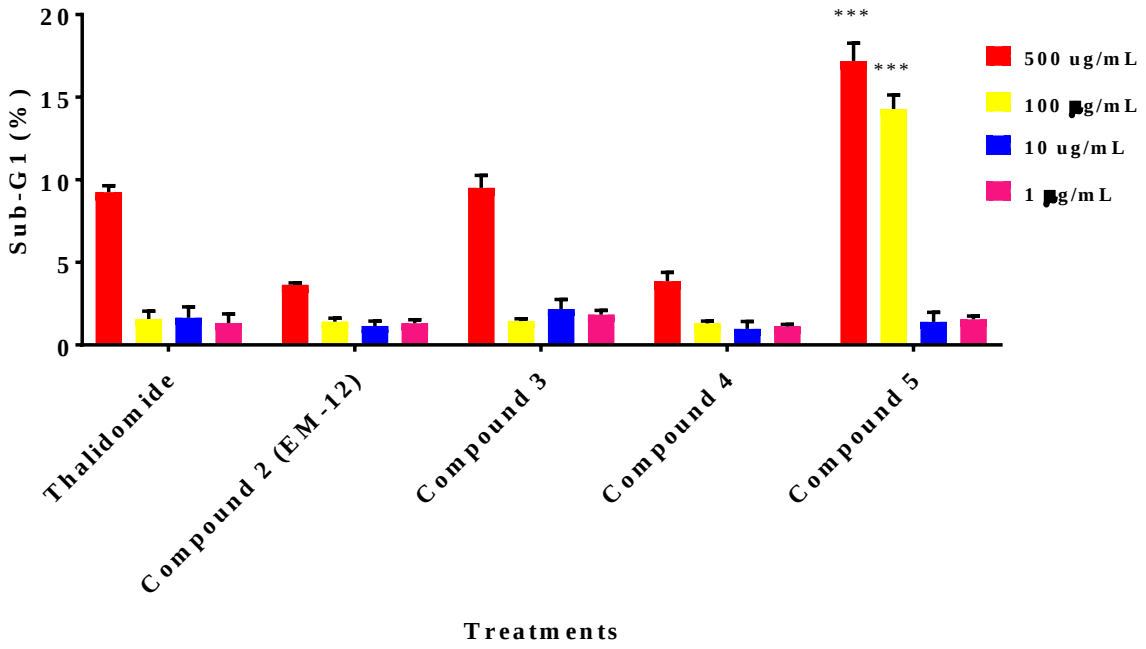

Figure 107: Effects of different treatments induced cell cycle arrest in MDA-MB-231. Data are presented as means ± S.D., n=3. It shows percentages of MDA-MB-231 in sub-G1 after treatment for 72 hours; Treatments included: Compound **1**: thalidomide; Compound **2**: 2-(2,6-dioxopiperidin-3-yl)-phthalimidine (EM-12); Compound **3**: 3-[(1R)-1-hydroxy-1-methyl-3-oxo-1,3-dihydro-2H-isoindol-2-yl]piperidine-2,6-dione; Compound **4**: 3-[(1S)-1-hydroxy-1-methyl-3-oxo-1,3-dihydro-2H-isoindol-2-yl]piperidine-2,6-dione & Compound **5**: 2-(1-chloromethyl-2,6-dioxopiperidin-3-yl)phthalimidine. Asterisks indicated a value

significantly different from the control value, *$P < 0.05$, **$P < 0.01$, ***$P < 0.001$ (Student's t-test).

Figure 107 shows that the percentage of sub-G1 was changed after 72 hour treatments with thalidomide and its structural analogues at treatment concentrations ranging from 1 μg/mL to 500 μg/mL. Overall, the percentage of sub-G1 (all 72 hour treatments) showed a dose dependent relationship, with *P*-value < 0.05. The highest concentration of treatment at 500 μg/mL is especially noteable, with its percentage of sub-G1 significantly higher than its values after treatments at other concentrations. Another observation from the results was that the significant increase in sub-G1 phase of the MDA-MB-231 cells was found in treatment concentrations higher than 100 μg/mL. Thalidomide, compound **2**, compound **3** and compound **4**, were especially interesting, with large increase of sub-G1 populations for the breast cancer cells only found at the highest treatment concentration of 500 μg/mL. There was also a gradual increase in the percentage of sub-G1 from treatment concentrations ranging from 1 μg/mL to 100 μg/mL. However, for compound 5, the remarkable increase in percentages of sub-G1 was found in the treatment concentrations of both 100 μg/mL and 500 μg/mL.

Comparion of thalidomide with all treatments, showed that the highest sub-G1 value was found in treatments with compound 5 at concentrations of 100 μg/mL and 500 μg/mL. The percentages of sub-G1 after treatments with compound **2** and compound **4** at concentrations of 500 μg/mL was significantly lower than its relative value from other compounds.

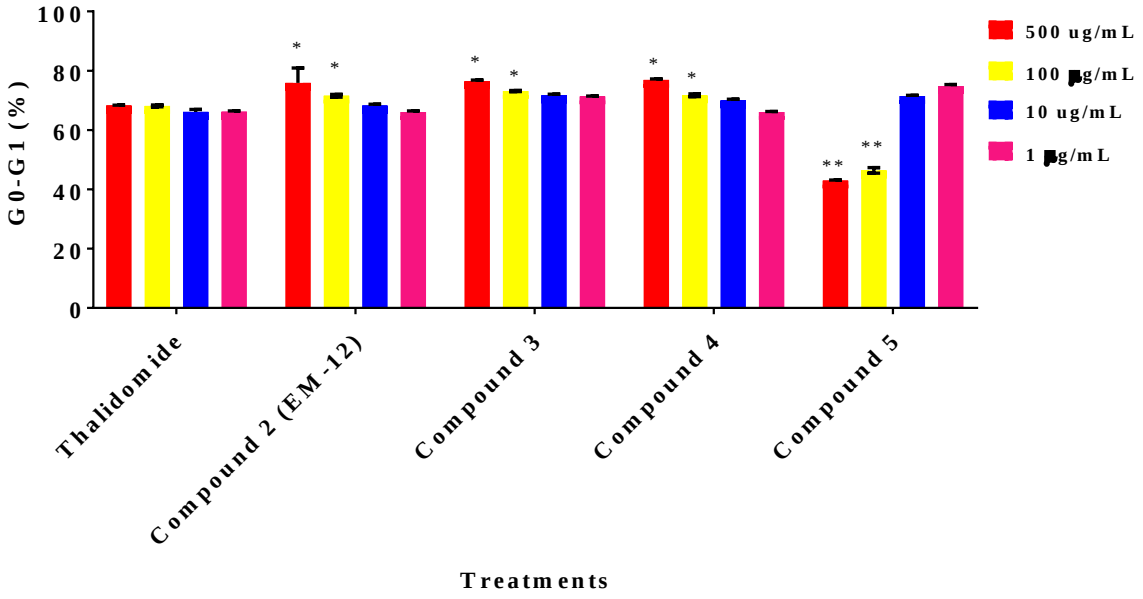

Figure 108: Effects of different treatments induced cell cycle arrest in MDA-MB-231.Data are presented as means ± S.D., n=3. It shows percentages of MDA-MB-231 in G0-G1 phase after treatment for 72 hours; Treatments included: Compound **1**: thalidomide; Compound **2**: 2-(2,6-dioxopiperidin-3-yl)-phthalimidine (EM-12); Compound **3**: 3-[(1R)-1-hydroxy-1-methyl-3-oxo-1,3-dihydro-2H-isoindol-2-yl]piperidine-2,6-dione; Compound **4**: 3-[(1S)-1-hydroxy-1-methyl-3-oxo-1,3-dihydro-2H-isoindol-2-yl]piperidine-2,6-dione & Compound **5**: 2-(1-chloromethyl-2,6-dioxopiperidin-3-yl)phthalimidine. Asterisks indicated a value significantly different from the control value, *$P < 0.05$, **$P < 0.01$, ***$P < 0.001$ (Student's t-test).

The Figure 108 shows that the percentage of G0-G1 phase was changed after treatment with thalidomide and its structural analogures for 72 hours at concentrations ranging from 1 μg/mL to 500 μg/mL. Overall, the change in percentage of G0-G1 was shown to be a dose-dependent effect in all treatments applied to MDA-MB-231 cells, with *P*-values < 0.05. For treatments with thalidomide, compound **2**, compound **3** and compound **4**, these treatments generated an increase of cell distribution at the G0-G1 phase with increasing treatment concentrations. However, the change was not significant, despite the fact that treatment concentrations increased dramatically. Conversely, for compound **5**, this type of treatment generated a decrease in cell distribution at the G0-G1 phase with an increase in treatment concentrations.

Comparison of treatments with thalidomide and all other treatments, indicate that the percentages of G0-G1 phase after treatment with compound **2**, compound **3** and compound **4** (at 100 µg/mL and 500 µg/mL concentrations) were statistically higher than their values after treatment with thalidomide with the remaining treatment concentrations (*P*-value < 0.05). Another large difference was found relative to compound **5** in that the percentage of G0-G1 phase at concentrations of 100 µg/mL and 500 µg/mL were significantly lower than their values at other treatment concentrations.

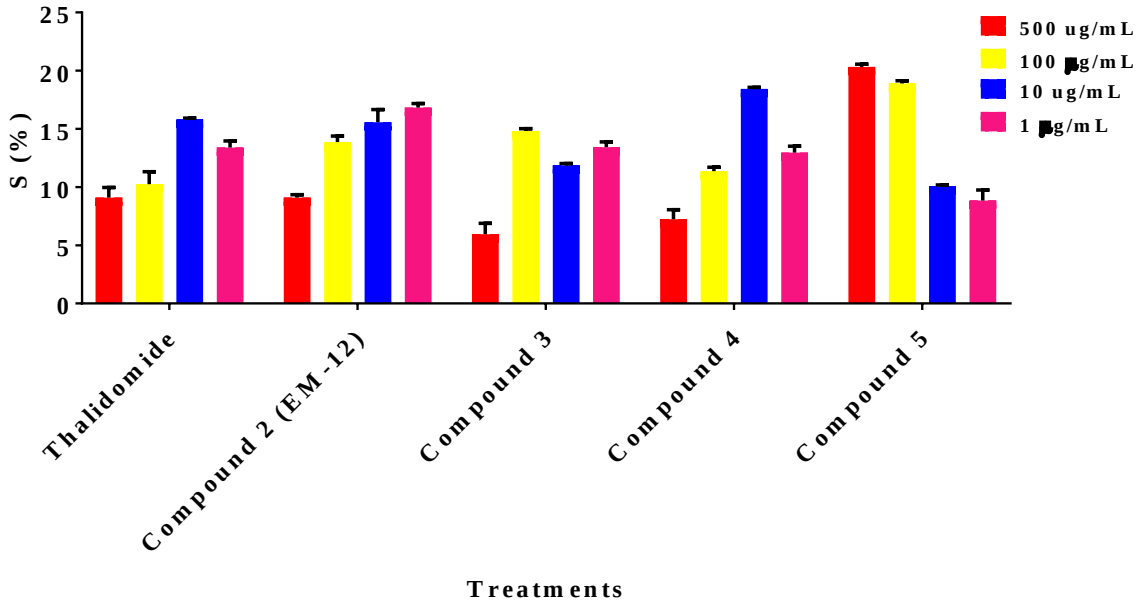

Figure 109: Effects of different treatments induced cell cycle arrest in MDA-MB-231.Data are presented as means ± S.D., n=3. It shows percentages of MDA-MB-231 in S phase after treatment for 72 hours; Treatments included: Compound **1**: thalidomide; Compound **2**: 2-(2,6-dioxopiperidin-3-yl)-phthalimidine (EM-12); Compound **3**: 3-[(1R)-1-hydroxy-1-methyl-3-oxo-1,3-dihydro-2H-isoindol-2-yl]piperidine-2,6-dione; Compound **4**: 3-[(1S)-1-hydroxy-1-methyl-3-oxo-1,3-dihydro-2H-isoindol-2-yl]piperidine-2,6-dione & Compound **5**: 2-(1-chloromethyl-2,6-dioxopiperidin-3-yl)phthalimidine.

Figure 109 shows that the percentage of S phase was changed after treatment with thalidomide and its structural analogues for 72 hours, with treatment concentrations ranging from 1 µg/mL to 500 µg/mL. Overall, the treatments including synthetic thaliomide, compound **2**, compound **3** and compound **4** resulted in a decrease in cell distribution of S

phase with increasing treatment concentration. Regarding compound **2**, a clear relationship was shown where a gradual increase of percentage of S phase is associated with a decreasing trend of treatment concentrations, with *P*-value < 0.05. However, for compound **5**, its treatment generated an opposite effect: treatment with increasing concentrations led to a decrease in the cell distribution at S phase with *P*-value < 0.05.

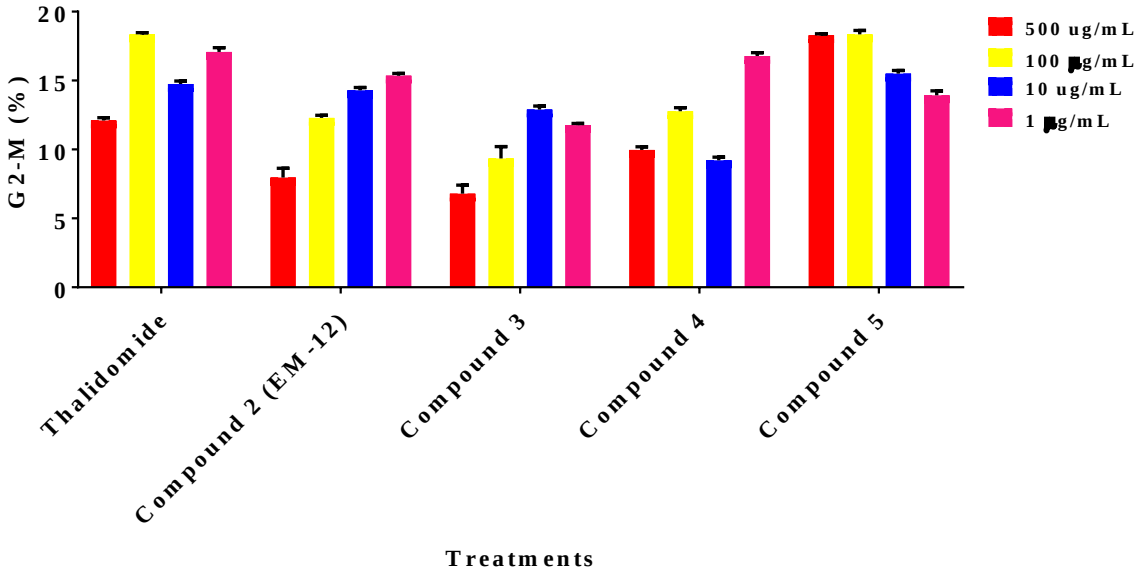

Figure 110: Effects of different treatments induced cell cycle arrest in MDA-MB-231. Data are presented as means ± S.D., n=3. It shows percentages of MDA-MB-231 in G2-M phase after treatment for 72 hours; Treatments included: Compound **1**: thalidomide; Compound **2**: 2-(2,6-dioxopiperidin-3-yl)-phthalimidine (EM-12); Compound **3**: 3-[(1R)-1-hydroxy-1-methyl-3-oxo-1,3-dihydro-2H-isoindol-2-yl]piperidine-2,6-dione; Compound **4**: 3-[(1S)-1-hydroxy-1-methyl-3-oxo-1,3-dihydro-2H-isoindol-2-yl]piperidine-2,6-dione & Compound **5**: 2-(1-chloromethyl-2,6-dioxopiperidin-3-yl)phthalimidine.

Figure 110 shows that the percenage of G2-M phase was changed after treatment with thalidomide and its structural analogues for 72 hours at concentrations ranging from 1 μg/mL to 500 μg/mL. The outcome of MDA-MB-231 cell distribution analysis of G2-M phase was similar to S phase after treatment from thalidomide and all structural analogues. There was a relationship between change relative to the percentage of G2-M phase and treatment concentration. The treatments including thalidomide, compound **2**, compound **3** and compound **4** generated a decrease in cell distribution in percentage of G2-M phase with an

increased treatment concentration. In particular for compound **2**, there is a clear relationship in the observed decrease of G2-M phase with an increase in treatment concentrations, with a *P*-value < 0.05. Whereas with compound 5, there is an increase in the changes of cell distribution in G2-M phase, with a decreasing trend in the percentage of G2-M phase for MDA-MB-231 cells. Another significant difference was found regarding the percentages of cell distribution in G2-M phase after treatment with compound **2**, compound **3** and compound **4**: all values were significantly lower than the relative percentage value from treatment with thalidomide and compound 5, with *P*-value < 0.05.

3.6 Discussion

Part I: Modulation of TNF-α Activity

3.6.1 Modulation of TNF-α Activity

3.6.1.1 Optimization of Level of TNF-α induced by Lipopolysaccharides

Human monocytes are triggered to produce large quantities of proinflammatory cytokines such as TNF-α in response to endotoxin (LPS). It is necessary to define the optimal concentration of LPS in order to induce the maximal level of TNF-α. As results have shown the highest level of TNF-α was induced from LPS at 100 pg/mL. Using 100 pg/mL as the optimal concentration, LPS was applied to induce TNF-α to be available for assay by anti-TNF-α antibodies.

3.6.1.2 Cell Seeding Density and Effect of Vehicle Solvent Pure DMSO

According to the standard curve for TNF-α detection by ELISA method and corresponding OD value at 580 nm, all OD values applied in TNF-α modulation activity studies fell within the linearity of this standard curve, Therefore, all values applied and analyzed in the study achieved a linear relationship between the level of TNF-α production and the treatment concentrations. This also suggested that the cell seeding density of human white blood cell was quite suitable for this study.

Due to solubility of thalidomide or its structural analogues in completed cell culture medium, pure DMSO was used as a vehicle solvent in order to dissolve compounds as initial DMSO stock solutions. As a result, all treatments to inhibit production of TNF-α contained 1% DMSO. After examination of both, there was no statistical difference in the solvent's effect on TNF-α production, suggesting that pure DMSO as a vehicle solvent in this study did not generate any effects relative to the TNF-α modulation activity assays.

3.6.1.3 Effects of Thalidomide on LPS-induced TNF-α Production.

As discussed, based on the mechanism of action for thalidomide, down-regulation of NF-κB, an essential transcription factor for TNF-α and other cytokines under thalidomide treatment leads to reduction in the TNF-α expression. Thalidomide treatment also leads to destruction

of TNF-α mRNA thus, reducing the total expression of TNF-α protein. Thalidomide also targets reactive oxygen species (ROS) and α(1)-acid glycoprotein (AGP) to regulate TNF-α (Syamantak *et al.*, 2012). Commonly, TNF-α modulation activity contributes to feedback efficacy of thalidomide.

In the present study, thalidomide reduced LPS-induced TNF-α in dose-dependent manners in all nine healthy human volunteers. Especially for volunteer 1, volunteer 2 and volunteer 6, the inhibitory effect to reduce LPS-induced TNF-α was clearly shown in a dose-dependent manner. However, for volunteer 3, volunteer 4, volunteer 5, volunteer 7, volunteer 8 and volunteer 9, the inhibitory effect for thalidomide to reduced LPS-induced TNF-α production was not significant, since the treatment concentration increased from 0.04 μg/mL to 100 μg/mL (about 2,500-fold), while only approximately 20% of inhibition effect was determined. Whereas, the inhibition effect throughout the treatment of thalidomide was found within the range of treatment concentration. Therefore, this assay was still effectively validated, although the treatment from thalidomide was not sensitive to these human blood samples.

3.6.1.4 Comparison of Modulation of TNF-α Activity by Thalidomide and Its Structural Analogues

Immunomodulatory drugs are a group of compounds that are analogues of thalidomide, a glutamic acid derivative with anti-angiogenic properties and potent anti-inflammatory effects owing to its anti-TNF-α activity. TNF-α modulation activity contributes to comparing the clinical efficacy of thalidomide analogues.

Concerning thalidomide, most of the volunteers, including volunteer 1, volunteer 3, volunteer 5, volunteer 7, volunteer 8 and volunteer 9, indicated a modulation activity for TNF-α from treatments with compound **3**, compound **4** and compound **5**. These three compounds generated a higher efficacy of the inhibitory effects to decrease levels of the TNF-α product. This suggests that thalidomide analogues such as compound **3**, compound **4** and compound **5** could generate potentially higher clinical efficacy in patients. However, the modulation activity for compound **2** was not higher than thalidomide in reducing the level of TNF-α, with P-value < 0.05. This was found in volunteer 1, volunteer 2, volunteer 3 and volunteer 6. This finding possibly suggests that thalidomide potentially generates higher clinical efficacy

when compared with compound **2**. As discussed, regarding the inhibitory effect of TNF-α production in most of the volunteers, thalidomide in the present study was not sensitive to reduce levels of TNF-α production, with significant increasing concentrations of thalidomide from 0.04 μg/mL to 100 μg/mL. This was also found in treatments with compound **3**, compound **4** and compound **5**. However, only 2 volunteers, including volunteer 3 and volunteer 4, were not sensitive to treatments with thalidomide analogues. For other volunteers (volunteer 1, volunteer 2, volunteer 5, volunteer 6, volunteer 7, volunteer 8 and volunteer 9), the TNF-α production was remarkably decreased within the treatment concentrations which increased from 0.04 μg/mL to 100 μg/mL. For both compound **3** and compound **4**, the capability to reduce levels of TNF-α production was statistically similar to each other, suggesting that the potential clinical efficacy of these two compounds were not statistically different. As compared with thalidomide and other analogues, compound **5** generated the highest inhibitory effect to reduce LPS-induced levels of TNF-α production in all volunteers, especially after treatment with concentrations higher than 25 μg/mL.

3.6.1.5 Overall Comparison about Structural Relationship of Modulation Activity of TNF-α for Thalidomide & Its Analogues

For determation of structural relationships, the chemical structure of thalidomide is similar to compound **2**, compound **3** and compound **4**. The only difference about the structure within these compounds is on the C-2 carbon (Figure 1). For compound **2**, there is no carbonyl group at the C-2 position. However, as discussed above, compound **2**'s biological activity of inhibiting the production of TNF-α was quite low compared to treatment with thalidomide, suggesting that the carbonyl group present in the structure potentially contributes to an increase in its relative biological activity. The structures of compound **3** and compound **4** are diastereomers with similar biological activities in reducing the levels of TNF-α produced. The similar activities indicates that the chemical diastereomers do not statistically generate any effects for inhibiting TNF-α production. In terms of biological activity (relative to inhibiting TNF-α production), both compound **3** and compound **4** are potentially the same molecule. In addition, there are two substitutions, including a methyl group and a hydroxyl group instread of the carbonyl group at the C-2 position of thalidomide. These two substitutions in compound **3** and compound **4** contribute to increase modulation of acitivty

to TNF-α production. Based on results from this modulation of activity of TNF-α production, the subsitution on the phthalimide ring not only preserves the biological activity of the original structure, but also increases its original TNF-α modulation activity.

Compound **5** has the highest capibility of reducing LPS-induced TNF-α production in the present study, and could potentially generate the highest clinical efficacy when compared with thalidomide and other analogues. As compared about the molecular structure of compound **5** with thalidomide and other thalidomide analogues, the main difference is the substitution in presence of imide position of glutarimide ring (Figure 1). Thus, the first possible reason to explain about the highest capibility for modulation of TNF-α activity is that *N*-substitution on the glutarimide ring contributes to an increase in efficacy of the compound's biological activity. As results (From Figure 45 to Figure 53) about modulation TNF-α production activity, *N*-substitution on glutarimide ring could potentially generate higher change of biological effects as compared to its change from substitution on glutarimide ring of thalidomide analogues. Another possibility is that chloromethyl group in structure of compound **5** in connecting to imide position (Figure 1) of glutarimide ring acts as an alkylating agent, and contributes to cytotoxic effects to cancer cells. The alkylating agents are compounds that react with electron-rich atoms in biologic molecules such as amino acids or proteins to form covalent bonds (Lepoittevin, 2006). Commonly, alkylating agents form highly reactive compounds that are able to transfer alhyl groups to DNA, and resulting in miscoding of DNA strands, excessive cross-linking of DNA, and inhibition of strand separation at mitosis or DNA strands breakage and lead to cell death (Damia *et al.*, 1998). In this case, compound **5** is a reactive structure, and is easily interact with biological molecules to generate cytotoxic effects. Combination of both possibilities maybe give the reasoning that compound **5** could generate the highest effects to reduce TNF-α production: As a type of immunomodulatory drug, compound **5** contribute to inhibit TNF-α production, also as a type of cytoxic agent, compound **5** generated the cytotoxic effect to reduce number of cells in dose dependent manners. Thus, as discussed compound **5** potentially possess bi-functional effects.

Part II: Anti-angiogenic Effect Study

3.6.2 Anti-angiogenic Effect Study

Angiogenesis is characterized by a number of well-described cellular events, including endothelial cell migration, invasion and differentiation into capillaries. *In vitro* endothelial tube formation assays are used as a model for studying endothelial differentiation and modulation of endothelial tube formation by anti-angiogenic agents.

3.6.2.1 Cell Seeding Density & Effect of the Vehicle

According to the cell linearity curve, the cell seeding density on 24-well plates was 4×10^4 cells/mL in a final volume of 1 mL. The linearity indicated that the seeding density was reasonable, owning to this point falling within the linear portion of the curve.

Due to the insolubility of thalidomide and its structural analogues in complete HUVEC cell culture medium, pure DMSO was used as a vehicle solution and applied to dissolve those compounds as initial DMSO stock solutions of 50 mg/mL. Appropriate amounts of DMSO were applied to dilute this stock solution further. Finally, each treatment contained 0.5% DMSO. As results have shown, there was no statistical difference in the tube formations when comparing those assayed in medium and those in medium with vehicle solvent. This suggests that pure DMSO as the vehicle solvent in this study did not generate any effects to tube formation. Therefore, the different numbers of tubes formed and the percentages of tube sizes were only caused by treatments with thalidomide and its structural analogues.

3.6.2.2 Effects of Thalidomide on Tube Formation

Thalidomide is a type of immunomodulatory drug with anti-angiogenic effects. Its mechanism of anti-angiogenic effect has been demonstrated to be secondary to the inhibition of secretion of two angiogenic cytokines, VEGF and FGF from both tumour and stromal cells (Marriott *et al.*, 1999). Human HUVEC cells as a type of endothelial cells, allowed the visualization of multicellular tube-like structures which resemble microvascular networks when grown on matrigel.

Matrigel tube formation assays have been applied in a lot of studies to compare the capability of tube formation based on treatments with thalidomide and its analogues. Rafiee with co-

workers in 2010 assessed and finally demonstrated the *in vitro* effect of thalidomide on human intestinal microvascular endothelial cell (HIMEC) activation by TNF-α/LPS with a thalidomide treatment concentration range from 0.1 μg/mL to 10 μg/mL (Rafiee *et al.*, 2010). Another study reported that a thalidomide concentration of 0.1 μM (0.0258 μg/mL) to 10 μM (2.58 μg/mL) decreased the number of formed capillary tubes (Komorowski et al., 2006). However, Ng with co-workers in 2003, reported that thalidomide at the concentrations of 12.5 μM (3.225 μg/mL) to 200 μM (51.6 μg/mL) failed to block angiogenesis in vitro (Ng et al., 2003). Similar results was also observed by El-Aarag in 2014 (El-Aarag et al., 2014). In the present study, the concentration range was enlarged from 2 μg/mL to 250 μg/mL. For the number of tubes formed, the inhibition was demonstrated to occur in a dose-dependent manner. However, for the percentage of tube area, the results regarding a failure to block angiogenesis were also present in the result. As Figure 62 shows, the percentage of tube area was largely increased after treatment with thalidomide at a concentration of 2 μg/mL compared to the percentage of tube area in cultures without treatment, suggesting thalidomide treatment at a concentration of 2 μg/mL possibly increased the interaction between capillary tubes enough to result in the formation of an aggregate. In addition, the percentage of tube area was not significantly reduced by thalidomide treatment from concentrations of 10 μg/mL to 250 μg/mL. This result was consistent with previous studies that tube blockage was less sensitive to treatment with thalidomide at concentrations ranging from 12.5 μM (3.225 μg/mL) to 200 μM (51.6 μg/mL).

3.6.2.3 Comparison about Tube Formation by Thalidomide and Its Structural Analogues

Thalidomide analogues are also a type of immunomodulatory drugs, and possess anti-angiogenic activity with the same mechanism as thalidomide. In the current study, all thalidomide analogues belong to the class of immunomodulatory drugs, and were expected to undergo the same mechanism of activation to generate an inhibitory effect and thereby reduce tube formation. As results have shown, with the exception compound **5**, all thalidomide analogues could generate the inhibitory effects to reduce numbers of tubes and percentages of tube areas in a dose dependent manner. As discussed, thalidomide at concentrations of 12.5 μM (3.225 μg/mL) to 200 μM (51.6 μg/mL) failed to block

angiogenesis *in vitro* (El-Aarag et al., 2014). Within this concentration range, the capability of cells to participate in tube formation could be compared between thalidomide and its structural analogues.

For comparison of the numbers of tubes (Figure 87), the anti-angiogenic effect of thalidomide was statistically similar to the effects observed from treatments with compound **3** and compound **4** at treatment concentrations of 10 μg/mL, 50 μg/mL and 250 μg/mL. However, the anti-angiogenic effect of compound **2** was significantly lower than the same effects from thalidomide, compound **3** and compound **4** at treatment concentrations of 50 μg/mL and 250 μg/mL. For comparisons of the percentages of tube area (Figure 86), the size of tube formations after treatment of thalidomide was statistically and significantly higher than the size of tubes from treatments with compound **3** and compound **4**, within concentration range of 2 μg/mL to 250 μg/mL, suggesting compound **3** and compound **4** reduced the interaction between capillary tubes in order to prevent them from aggregating to form a larger size of capillary tube. Thus, compared to thalidomide within concentrations ranging from 12.5 μM (3.225 μg/mL) to 200 μM (51.6 μg/mL), compound **3** and compound **4** could generate higher efficacy of treatments to reduce angiogenic effects. In fact, three key stages of metastasis include transformation, migration, and invasion (Liu *et al.*, 2009). Thus, compound **3** and compound **4** potentially contributed to reduce the more invasive risk of metastasis for solid tumours.

For compound **5**, the inhibitory effect seen relative to the number of tubes and percentages of tube area was not shown to occur in a dose-dependent manner (P-value > 0.05) within treatment concentrations of 2 μg/mL, 10 μg/mL, 50 μg/mL and 250 μg/mL respectively. There was a dramatic change in the number of tubes and percentages of tubes between treatment concentrations of 10 μg/mL and 50 μg/mL, suggesting that the inhibitory effect occurring in a dose-dependent manner could be shown within this range. This result was further validated from observations that cell morphology was changed to small and rounded shapes at a treatment concentration of 50 μg/mL (Figure 82) and 250 μg/mL (Figure 81), although tube formation was found in the treatment concentration of 10 μg/mL. The possible explanation can be made that structure of compound **5** containing chloromethyl substitution on imide position of glutarimide ring (Figure 1) as alkylating agents generated the cytotoxic effect to reduce number of cells, and this cytotoxic effects related to reduce tube formation.

Especially in treatment concentration of 250 μg/mL, a large number of cell was killed by strongly cytotoxic effects from compound **5**. Once concentration decreased to 50 μg/mL, cytotoxic effect from compound **5** was not strong enough to kill cells, and only reduce cell aggregate to generate the tubes. In addition, the most important characteristic of the compound 5 treatment is that the number of tube formation in treatment concentration of 2 μg/mL and 10 μg/mL was remarkably more than tube formation from treatment of thalidomide, even higher than from non-treatment (Figure 87). This result suggested that HUVEC cells was promoted from treatment of compound 5 in concentration of 2 μg/mL and 10 μg/mL. Therefore, the cytotoxic effects from treatment of compound **5** in concentrations less than 10 μg/mL did not potentially affect the capillary tube formation, however if the concentration of treatment kept increasing, a potential cytotoxic effect could generate the effect necessary to change HUVEC cell morphology, and thereby directly induce cell apoptosis.

The capability of anti-tube formation from compound **3** and compound **4** as demonstrated in the present study, was higher than thalidomide and other structural analogues. Also, due to presence of chloromethyl group on the imide of the glutarimide ring in the structure of thalidomide analogue, the mechanism of action has been changed to cytotoxicity.

Part III Anti-Proliferative Studies for Breast Cancer

3.6.3 Anti-proliferative Studies for Breast Cancer

The breast cancer cell line, MDA-MB-231, is associated with metastatic breast cancer cells, and can be used to learn metastatic potential in *in vitro* studies (Ma et al., 2016). Angiogenesis is a crucial regulator of tumour growth and metastasis. Inhibition of angiogenesis has been perceived as being a promising strategy in the treatment of cancer. Thalidomide as an angiogenic inhibitor is placed in clinical treatments to anti-cancer activities. Based on the structure of the parent compound thalidomide, many analogues have been developed in order to minimize drug-related teratogenic toxicity and improve the efficacy of treatments. The initial focus and primary selection of thalidomide analogues in previous studies were based on the degree of their inhibition of TNF-α production in activated human peripheral blood mononuclear cells (PBMC) (Corral et al., 1996). As anti-tumour agents, moreover, the emphasis in the development of thalidomide analogues also focused directly on the tumour anti-proliferative activity compared with thalidomide. It is necessary to determine the changes in anti-proliferative effects relative to MDA-MB-231 from the treatments with thalidomide and its analogues.

3.6.3.1 Cytotoxicity

The MTT assay is a representative method of cytotoxicity assays, which is often used to assess cytotoxicity of substances by exposure to cells. This method is widely used in *in vitro* cell cytotoxicity studies in routine laboratories, with the advantages of reproducibility, ease of performance, economy and safety. Thus, the MTT assay was utilized in this study to assess the cytotoxicity of thalidomide and its analogues to MDA-MB-231 cells.

3.6.3.1.1 Cell Seeding Density & Effect of Vehicle Solvent Pure DMSO

According to the cell linearity curve, the cell seeding density used in this study was 100,000 cells/mL. The linearity indicated the seeding density was reasonable, owing to this point falling within the linear portion of the curve.

Due to the insolubility of thalidomide and its structural analogues in completed cell culture medium, pure DMSO was applied to dissolve the compounds as initial DMSO stock solutions

at a concentration of 10 mg/mL, Appropriate amounts of DMSO were applied to dilute the DMSO stock solutions into series including 10 mg/mL, 8 mg/mL, 5 mg/mL, 2.5 mg/mL, 0.5 mg/mL, 0.1 mg/mL, 0.02 mg/mL and 0.04 mg/mL. 20 µL of DMSO stock solution was then diluted 50-fold by using complete cell culture medium, so that DMSO concentrations were diluted to 2%. After 100 µL of treatment volume was added into 100 µL of cells, the final DMSO concentration was 1%. Compared with the control group (no DMSO), cell viability was not affected by pure DMSO, suggesting pure DMSO in treatment concentrations with 1% DMSO has no positive or negative effects on cancer cell growth. Therefore, all treatments of breast cancer cell line MDA-MB-231 were from thalidomide or its structural analogues at concentrations including 100 µg/mL, 80 µg/mL, 50 µg/mL, 25 µg/mL, 5 µg/mL, 1 µg/mL, 0.2 µg/mL and 0.04 µg/mL respectively.

3.6.3.1.2 Anti-proliferative Effect from Thalidomide

Based on the discussion above, the main mechanism of action for thalidomide contains two important pathways (anti-angiogenesis and immune modulation activity), both of which represent elements of the leading hypotheses regarding thalidomide's anti-tumour activity. In fact, these two effects may be closely related through the effects of thalidomide on cytokine secretion (Corral et al., 1999; Ogawara et al., 2005; Quach et al., 2008). For anti-angiogenic activity, thalidomide generates inhibitory effects to angiogenesis through suppression of vessel proliferation. It suppresses TNF-α and IFN-γ secretion, both of which deregulate endothelial cell integrin expression, a process crucial for a new vessel formation (Brown *et al.*, 2001; Corral *et al.*, 1999). In addition, thalidomide has a broad range of inhibitory and stimulatory effects on the immune system. Thalidomide triggers proliferation of stimulated T cells and natural killer (NK) cells, accompanied by an increase in interferon-γ and IL-2 secretion. The lysis of multiple myeloma cells is mediated by NK cells rather than T-cells (Gao et al., 2014). It seems probable that all the aforementioned mechanisms are relevant to the efficacy of thalidomide in treatments of multiple myeloma (Minuk *et al.*, 2010).

Additionally, but also thalidomide or its metabolites may have anti-tumour effects. In cell culture, thalidomide suppresses the proliferation of human myeloma cells. Thalidomide

modestly triggers the actual proliferation of multiple myeloma cells, but only at a very high and probably pharmacologically irrelevant concentration of 100 μmol/mL (25.823 mg/mL) (Quach et al., 2010). Thalidomide has also been involved in many types of *in vitro* cancer cell studies. As reported from Costa with co-workers in 2005, the anti-proliferative effects of thalidomide have been studied in leukemia cells (HL-60), colon cells (HCT-8), melanoma cells (MDA/MB-435), glioblastoma (SF-295) and sarcoma 180 (S180) with treatment concentrations of 100 μg/mL. Unfortunately, IC_{50} values for all these types of cancer cell could not be achieved (da Costa et al., 2015). For types of non-small cell lung cancers (including NCI-HI1299, NCI-H460, A549, NCI-H661, NCI-H520, NCI-H596 and NCI-H522), these types of cell were reduced to about 60% confluence with treatment from thalidomide for eight (8) continuous days (DeCicco *et al.*, 2004). El-Aarag with co-workers in 2014 reported that metastatic breast cancer cell MDA-MB-231 cells proliferation was not significantly decrease by any concentration of thalidomide (6.25-100 μM) in 24 hours treatment (El-Aarag et al., 2014). Therefore, anti-proliferative agents of thalidomide in all in vitro studies did not generate the significant inhibitory effects. These results were consistent with the current study as described in the following section.

As Figure 86 shows, an anti-proliferative effect of thalidomide was found by MTT assay within the treatment concentrations ranging from 0.04 μg/mL to 100 μg/mL. Thus, an anti-proliferative effect of pure thalidomide was found in MDA-MB-231 cells in dose- and time-dependent manners (P-value < 0.05). After three days' treatment with thalidomide, the cell viability decreased to around 80% even with the treatment concentration at 100 μg/mL. Thus, the IC_{50} for MDA-MB-231 cells from treatments with thalidomide could not be reached. But, the trends of cell viability showed a gradual decrease, possibly indicating that if the treatment concentration kept increasing, this could lead to a continuous decrease in cell viability. As observed under an inverted microscope after treatment with thalidomide for 72 hours, the cell morphology looks the same as the control group (without treatment from thalidomide). Additionally, cell density could not be identified as having any difference between treatment groups in the highest concentration and those having non-treatment condition. The difference could only be determined by application of MTT assays. This possibly indicated that the anti-proliferative effects of thalidomide were quite low in this type of breast cancer MDA-MB-231 cell line. This result was consistent with a previous study (El-Aarag et al., 2014). In fact,

anti-proliferative effect from thalidomide could not be found in many types of tumour cell lines such as breast cancer cell line MCF-7, prostate cancer cell lines PC-3, DU-145 and LNCaP, colon cancer cell line HT-29, bladder cancer cell line TCCSUP and Burkitt's lymphoma Hs Sultan respectively (Li et al., 2006). Actually, thalidomide shows a modest cytotoxic effect, due to the need for its liver conversion from a pro-drug into an active metabolite (Ortiz de Montellano, 2013). Thus, cytotoxic effects of thalidomide are not high. In addition, El-Aarag with co-workers reported that cell viability of MDA-MB-231 gradually decreased after treatment with thalidomide for 72-hours, then when treatments were removed, cell viability increased back to their normal conditions. This result indicated that thalidomide inhibited the growth of MDA-MB-231 cells through a cytostatic effect and not a cytotoxic effect (El-Aarag et al., 2014).

3.6.3.1.3 Anti-proliferative Effect from All Thalidomide Analogues

From Figure 91 to Figure 94, the cytotoxic effect of all thalidomide analogue was found by MTT assay within the treatment concentrations ranging from 0.04 µg/mL to 100 µg/mL. Thus, the cytotoxic effect of thalidomide analogues was found in MDA-MB-231 cells in dose- and time-dependent manners (P-value < 0.05). The overall trend of MDA-MB-231 cell viability tended to decrease, although thalidomide analogues including Compound **3** and compound **4** could promote cell viability after 24 hours of treatment. Also, an IC_{50} value was not reached after treatment concentrations of 100 µg/mL for 72 hours for compound **2**, compound **3** and compound **4**. These results suggested that these three thalidomide analogues, at concentrations of 0.04 µg/mL to 100 µg/mL, could not generate significant inhibitory effects in MDA-MB-231 cells. As observed under an inverted microscope, cell morphology did not change after three days treatment with these thalidomide analogues compared with the control group (without treatment from thalidomide analogues). In addition, the cell density differences between treatment groups and non-treatment group were not easy to visually identify, indicating cytotoxic effects from those thalidomide analogues were not significant.

For compound **5**, however, a cytotoxic effect was determined in MDA-MB-231 cells in dose- and time-dependent manners (P-value < 0.05). Also, IC_{50} values for treatment of these cancer

cells was determined within the treatment concentrations ranging from 0.04 µg/mL to 100 µg/mL. This result suggested that breast cancer cell line MDA-MB-231 is sensitive to treatment with compound **5**. As treatment concentrations increased to 25 µg/mL, the cell viability sharply decreased in 24 hours treatment, suggesting that MDA-MB-231 cells responded to treatment once the concentration was higher than 10 µg/mL. This result was also verified by observations under the microscope, in that cell morphology was immediately altered to small rounded shapes once treatment was added to cells at the concentration of 25 µg/mL.

3.6.3.1.4 Intra- & Inter-comparison of Cytotoxic Effects from Thalidomide and its Analogues

The mechanism of action for thalidomide, as described in detail above, is a regulator in the immune system. It mainly suppresses monocyte/macrophage functions and thereby TNF-α and IFN-γ secretion, both of which upregulate endothelial cell integrin expression, a process crucial for new vessel formation. It suggested the major effect of thalidomide contributes to clinical treatments as an anti-angiogenic agent and through immune modulation, especially in treatments of multiple myeloma. This is the main reason that thalidomide, as a type of immunomodulatory drug, has a modest cytotoxic effect in treatments of cancer cells in *in vitro* studies. Of particular note, in this study, the cytotoxic effect towards breast cancer (MDA-MB-231) cells was not significant, and this result was reported from in a previous study. Similarly, for compound **2**, 2-(2,6-dioxopiperidin-3-yl)-phthalimidine (EM-12), a carbonyl group on C-2 of the phthalimide ring (Figure 1) has been removed, and this structure of EM-12 is similar to lenalidomide. Based on previous studies, lenalidomide, as another type of immunomodulatory drug, had no effect on breast cancer cells growth including MCF-7, MCF-12A and MDA-MB-231 cells, respectively (Brosseau *et al.*, 2012). Its mechanism is to mainly alter the production of the inflammatory cytokines TNF-α, IL-1, IL-6, IL-12, as well as anti-inflammatry cytokine IL-10. Therefore this type of drug generates an anti-tumour effect though interfering with the tumour microenvironment and enhancing the host's anti-tumour immune response rather than just directly causing cytotoxic effects. Compound **2** (EM-12) contributes to an increase in bioavailability of the substance because of its stability. Based on animal studies, EM-12 was reported to be an even more potent teratogenic agent than thalidomide in rats, rabbits and monkeys. For compound **3** and compound **4**, the

difference in the molecular structures between thalidomide and compound **2** are found on C-2 of the phthalimide ring (Figure 1). A methyl group and a hydroxyl group have been placed in that position instead of a carbonyl group (as found on thalidomide's C-2). However, both compound 3 and compound **4** are still potentially immunomodulatory drugs, since the cytotoxic effect from both compounds are similar to the cytotoxic effects from thalidomide and compound **2**. As shown in Figure 91 and Figure 92 , MDA-MB-231 cell viability was not siginicantly different after treatment with thalidomide or its analogues at the treatment concentrations of 25 µg/mL and 100 µg/mL. Even when the treatment concentration was increased 4 times from 25 µg/mL to 100 µg/mL, the cell viability after treatment with thalidomide and compound **2**, compound **3** and compound **4** was merely reduced no more than 5 %. All discussions above have suggested the biological activity relative to cytotoxic effects in cancer cells has remained although the structures of the phthalic ring of thalidomide or its analogues have changed. This result is consistent with a previous study that immunomodulatory drugs inhibited MDA-MB-231 cell proliferation though cytostatic effects rather than cytotoxic effects (El-Aarag et al., 2014).

Notably, for compound **5**, a significant drop in cell viability was found. From as treatment concentrations of 25 µg/mL at 24 hours, the cell viability was remarkably decreased based on time consumed or increasing concentration of the treatment. Consequently, the result suggested a greater inhibitory activity of this analogue over thalidomide, and was attributed to the presence of the substitution on the imide position (Figure 1) of the glutarimide ring of the thalidomide analogues. As discussed about compound **5**, chloromethyl substitution on imide position of glutarimide ring (Figure 1) as a type of alkylating agent contributed to cytotoxic effect, and this was one of the possible reason that cell viability was significantly decreased as compared with other thalidomide analogues. However, only chloromethyl group as a substitution in this study was added on the imide position of glutarimide ring of thalidomide analogue. Thus, the relationship cannot be determined between cytotoxic effects and *N*-substitution of glutarimide ring in structure of thalidomide analogues. As compared with thalidomide and other structural analogues, the highest anti-proliferative effect was found in treatment of compound **5**, it can confirm that *N*-substitution of thalidomide may still retain the original biological activity as well as improve its overall biological activity.

3.6.3.2 Cell Cycle Distribution

Many researchers have proposed various mechanisms for explaining the cytotoxic activity agents used as treatments against cancer cells. Induction of apoptosis, cell cycle arrest , and inhibition of angiogenesis, inhibition of various growth factors and inhibition of metastasis are all mechansms which are used as reference points to describe the effects of drug treatments. The cell cycle or cell division cycle is a set of events that result in cell growth and division into two daughter cells. The cell cycle is a orderly progression strictly following the sequence of G1-S-G2-M. The proportion of sub-G1 hypodiploid cells is proportional to cell death, so that sub-G1 was indicated as cells in apoptotic pathway. Thus, a cell cycle assay focuses on determination of differences in the change of phases in the cell cycle as a way to describe a mechanism of a particular drug treatment in the cell cycle.

Flow cytometry is an important technique applied in cell cycle studies. Cellular DNA is often the single parameter measured by flow cytometry for cell cycle studies. Once fluorescent molecules are specially and stoichiometrically used to bind DNA, a linear relationship between cellular fluorescence intensity and DNA amount can be measured. The emitted fluorescence of the DNA specific dyes is proportional to DNA content present in different phases of the cell cycle. PI is the most commonly used dye to quantitatively assess DNA content. PI binds to DNA by intercalating between the bases with little or no sequence preference. Because PI also bonds to RNA, nucleases such as Ribonclease (RNAse) are necessary to distinguish between RNA and DNA (Götte et al., 1995). To explore the possible mechanisms of action for thalidomide or its structural analogues, the compounds were analysed for cell cycle alterations by staining with PI.

3.6.3.2.1 Effects of Thalidomide on Breast Cancer Cell Cycle Distribution

Thalidomide as the first type of immunomodulatory drug has been involved in many areas of anti-cancer research. The mechanism of action for treatment of thalidomide mainly relies on at least two properties including anti-angiogenesis and immune modulation. Also, immunomodulatory drugs possess anti-proliferative effects to directly inhibit growth of cancer cells (Quach et al., 2010). In addition, it has been reported that thalidomide as a type of immunomodulatory drug generates anti-proliferative effects through arrest in the G0-G1

phase of the cell cycle of multiple myeloma (Quach et al., 2010). Due to use of immunomodulatory drugs in anti-angiogenic therapy as a novel type of treatment in cancer, most studies reported thalidomide or its analogues as a single anti-cancer treatment or combination of thalidomide as a supplement with other treatments to be involved in *in vitro* or *in vivo* analysis. It also has been reported that drugs with anti-neoplastic, immunomodulatory, and anti-angiogenic properties can induced G0-G1 growth arrest and apoptosis, and increases expression of genes found on the 5q locus, including genes involved in cell adhesion (Wilkes, 2010). El-Aarag with co-workers in 2014 reported that thalidomide and two novel analogues treated a metastatic breast cancer cell line MDA-MB-231, with resulting anti-proliferation effects from thalidomide determined to be not significant. Another in vitro breast cancer cell study reported that thalidomide as a single treatment could alter breast cancer cells MCF-7 and MDA-MB-231 as seen in the apparent apoptotic peaks (sub-G1) DNA histogram analysis by flow cytometry (Yang et al., 2010).

In the present study, thalidomide was found to act dose-dependently, arresting the metastatic breast cancer cells (MDA-MB-231) in G0-G1 phase after treatment of thalidomide for 72 hours exposure. This is because, as Figure 96 shows the percentage of G0-G1 phase was slightly and statistically increased with increasing concentrations of treatments, suggesting that fluorescent PI, which bound to DNA fragmentation, was accumulated in the G0-G1 phase after treatment with thalidomide at all concentrations ranging from 1 μg/mL to 500 μg/mL. Moreover, the percentages of G0-G1 phase were significantly higher than G0-G1 phase in non-treatment cells, even at treatment concentrations of 1 μg/mL (P-value < 0.05), suggesting breast cancer cell line MDA-MB-231 was quite sensitive to treatment with thalidomide even at lower concentrations of treatments. This result was consistent with results from literature reporting that thalidomide as a type of immunomodulatory drug contributes to generate anti-proliferative effects in cancer cells, with arrest at G0-G1 phase. As shown in figure, after exposure to treatment for 72 hours, the accumulations of cells decreased and the percentage of sub-G2 increased in a dose-dependent manner. Sub-G1 is an index of the apopotic DNA fragmentation. Once treatment concentrations increased to 500 μg/mL for 72 hours, the significant effect on cell apoptosis was determined with an increased percentage of sub-G1. The dose-dependent increase in apoptosis is definitely shown after treatment with thalidomide. This result is also consistent with previous results shown, and

suggested cell distribution arresting in G0-G1 phase undergoes cell death through the apoptotic pathway.

Progression of the eucaryotic cell through the four phases of the cell cycle is mediated by sequential activation and inactivation of cyclin-dependent kinases (CDKs) (Hunter *et al.*). The cyclin area family of cell cycle oscillator proteins, repeatedly express and degrade during the cell cycle process (Pucci *et al.*, 2000). Cyclins binding with CDKs act as theengines of the cell cycle. CDK inhibitors are able to bind complexes of cyclins and CDKs and inhibit their cell cycle accelerator function (Arora *et al.*, 2017). In this study thalidomide block the cells in G0-G1phase, and this is the reason that thalidomide has been demonstrated to induce cyclin-dependent kinase (CDK) inhibitors: p21, p27 and p15, which resultin inhibition of CDK activity, thereby causing cell cycle arrest in the G0-G1 phase of the cell cycle.

3.6.3.2.2 Comparison of (Intra- & Inter-) Thalidomide Analogues with Parent Compound on Breast Cancer Cell Cycle Distribution

All thalidomide analogues in this study, including compound **2**, compound **3**, compound **4** and compound **5** are classified as immunomodulatory drugs. It has been reported that immunomodulatory drugs exert direct anti-proliferative effects through inhibition of the cyclin-dependent kinase pathway, activation of Fas-mediated cell death, and down regulation of anti-apoptotic proteins (Hideshima et al., 2000). Thus, these thalidomide analogues were expected to arrest the cell distribution in G0-G1 phase, also apoptotic rate was potentially increased by the treatment of immunomodulatory drugs compared with non-treatment.

As Figure 103 shows, the percentage of sub-G1 has been increased after treatment with all compounds at concentrations of 500 μg/mL, suggesting all thalidomide analogues are the members of immunomodulatory drugs, and can increase the percentage of sub-G1 as the apoptotic rate in the treatment after 72 hours. Comparisons of thalidomide with compound **2**, compound **3**, compound **4**, indicate that the structure for these four compounds is only different in the phthaloyl ring, and the apoptotic rate was not changed to a great degree, even though treatment concentrations increased dramatically from 1 μg/mL to 100 μg/mL. These results suggest that breast cancer cell line MDA-MB-231 was not sensitive to an anti-proliferative effect from treatments with these compounds. For compound **2** and compound

4 especially, anti-proliferative effects from these compounds were the lowest compared to all other treatments from thalidomide and thalidomide analogues. In addition, for compound **5**, its structural difference was found on both the phthalimide ring and the imide position of the glutarimide ring compared with thalidomide. Anti-proliferative effects from this compound **5** were higher than other compounds' treatments. The apoptotic rate for MDA-MB-231 after treatment of compound **5** for 72 hours was signficantly increased, but also notable, compound **5** within this concentration range could immediately change the morphology of cells. This result suggests that there are greater inhibitory effects, able to increase apoptotic effects beyond those determined with thalidomide or other analogues, and may be attributed to the presence of substitutions in the chemical structures.

For changes observed in the G0-G1 phase values, the percentage of G0-G1 was shown to have a negative relationship with treatment concentrations for thalidomide, compound **2**, compound **3** and compound **4**, suggesting that these compounds are immunomodulatory thalidomide analogues, capable of cell cycle arrest at the G0-G1 phase. Regarding compound **2**, compund **3** and compound **4**, the percentage of G0-G1 phase values were higher than relative values from treatments of thalidomide. The outcome proposes that compound **2**, compound **3** and compound **4** generated more anti-proliferative effects than treatment with thalidomide, and higher anti-proliferative effects will arrest more cell cycle distributions to accumulate in G0-G1 phase. This results is consistent with the expectation that immunomodulatory thalidomide analogues could generate the effects necessary to arrest cell distribution in G0-G1 phase, and then cause the cells to undergo cell death.

For compound **5** as an immunomodulatory thalidomide analogue, the percentage of G0-G1 phase in treatment concentrations at both 100 μg/mL and 500 μg/mL was lower than its values after treatment for 72 hours at a concentration of 10 μg/mL and 1 μg/mL, suggesting that cell cycle distribution was not blocked after treatment with compound **5** at concentrations ranging from 1 μg/mL to 500 μg/mL. However, the percentage of both S phase and G2-M phase showed to an increase in a dose-dependent manner, proposing the cell cycle distribution was blocked by the treatment with compound **5** in S and G2-M phases. This results was not consistent with previous demonstrations that the type of immunomodulatory analogues generated anti-proliferative effects through arresting in the G0-G1 phase of the cell cycle of multiple myeloma (Quach et al., 2010). In fact, as results have shown, the

percentage of G0-G1 phase after treatment with concentrations of 1 μg/mL and 10 μg/mL was higher than percentage values from treatments with compound **5** at concentrations of 100 μg/mL and 500 μg/mL (*P*-value < 0.01). Also the percentage values after treatment with concentrations at 1 μg/mL and 10 μg/mL were higher than the percentage of G0-G1 phase from treatments with thalidomide at all concentrations ranging from 1 μg/mL to 100 μg/mL. In addition, the cell morphology as observed from Figure 102-C1 & Figure 102-D1 shown was not changed after treatment with compound **5** at treatment concentrations of 1 μg/mL and 10 μg/mL. Comparing the chemical structure of compound **5** with thalidomide and other compounds, these results propose the cytotoxic effects from compound **5** arise from substitution on the amide position of the glutarimide ring.

As discussed above, the orginal biological activity of an anti-proliferative effect increased from immunomodulatory analogues compound **2**, compound **3** and compound **4** when compared with their parent compound thalidomide. For compound **5** as another thalidomide analogue, its anti-proliferative effect was significantly higher than its parent compound, however the mechanism of action for treatments with compound **5** was completely changed compared to the parent compound thalidomide. The observed changes were all due to structural modifications from thalidomide, and will be discussed in detail in the following section.

3.6.3.2.3 Overall Comparison (Intra- & Inter-) about Structural Relationship of Anti-proliferative effects for Thalidomide & Its Analogues

As discussed, the structure of thalidomide contains two ring systems including a phthalimide ring and a glutarimide ring (Figure 1). The structure of thalidomide is a centrosystemmetic structure due to the presence of two carbonyl groups on the phthaloyl ring. Compared with thalidomide, the only differences in compound **2**, compound **3** and compound **4** are found on the carbonyl group on the C-2 carbon (Figure 1). However, results from anti-proliferative assays and apopotic rates of cell cycle analysis have shown that this difference in the chemical structure does not lead to increase in the anti-proliferative effect, suggesting that the original anti-proliferative effect compared to the parent compound thalidomide was not changed remarkably. A higher percentage of G0-G1 blockage would have suggested that

more cells would subsequently undergo cell death via the apoptosis pathway. However, higher apoptotic rates after treatments with compound **2**, compound **3** and compound **4** could also possibly be achieved thereby prolonging the period of treatment beyond 72 hours.

Compound **5**, as discussed, contains a chloromethyl substitution on imide position of glutarimide ring (Figure 1). This type of substitution makes the whole molecule more reactive and contributes to cytotoxic effect as a type of alkylation agent. As all results from anti-proliferative assays and mechanism studies have shown, the significant cytotoxic effect was found starting with the treatment concentration of 100 µg/mL. As observed under inverted microscopes, and in size *vs*. internal structure results, the cell morphology changed after treatments with compound **5**. Based on this new biologial effect, the mechanism of action on cell cycle distribution has changed as follows. As reported from previous literature, a compound with similar structure, *N*-hydroxymethylthalidomide (CPS11) demonstrated a wider activity spectrum and higher potency against cancer cells such as multiple myloma cell lines (Kumar et al., 2005). However, the relationship was not determined between *N*-substitution and cytotoxicity although many studies focused on the development of *N*-substitution thalidomide analogues (El-Aarag *et al.*, 2014; Talaat *et al.*, 2014). Thus, it can be concluded that chloromethyl substitution on imide position of glutarimide ring made the whole structure as a type of alkylating agent to generate cytotoxic effect, also this substitution on the compound **5** contributes to increase its orignial biological anti-proliferative effect by applying a new mechansim of action.

Chapter IV: Overall Discussion

Thalidomide, as compound 1, and other structural analogues including 2-(2,6-dioxopiperidin-3-yl)-phthalimidine (EM-12) (compound **2**), and two isomers 3-[(1*R*)-1-hydroxy-1-methyl-3-oxo-1,3-dihydro-2*H*-isoindol-2-yl]piperidine-2,6-dione (compound **3**) & 3-[(1*S*)-1-hydroxy-1-methyl-3-oxo-1,3-dihydro-2*H*-isoindol-2-yl]piperidine-2,6-dione (compound **4**), and 2-(1-Chloromethyl-2,6-dioxopiperidin-3-yl)phthalimidine (compound **5**) were successfully synthesised as presented in Chapter II. For all existing compounds, the synthetic methods were referenced from literature. Structural characteristics for these existing compounds have been confirmed with literature report including ^{1}H NMR, ^{13}C NMR, melting point, IR, and retention factor. The most interesting part in section of organic synthesis is to develop structures of compound **3** and compond **4**. After searching function of the SciFinder Scholar, no exact match was found from any literature report, so that compound **3** and compound **4** as novel thalidomide analogues have been developed in this study. All studies about development of thalidomide analogues mainly focused on the substitution on aromatic benzene ring of phthalimide structure. The relationship between biological activities and structure was determined on C-2 position of five-membered ring on the phthalimide structure (Figure 1). Another interesting aspect of those novel compounds development was to add a hydroxyl group at C-2 position on the structure, and activate this position to replace by more functional structures.

In Chapter III, thalidomide and all analogues have been placed in three *in vitro* analysis studies including the study of TNF-α modulation activity, the study of anti-tube activity, and metastastic breast cancer cells' anti-proliferative study, respectively. Results from the study of TNF-α modulation activity, indicated that compound **3** and compound **4** could generate higher TNF-α modulation activities compared with compound **2** and thalidomide, suggesting that substitutions on the phthalimide ring of thalidomide analogues contribute to an increase in its orignal biological activity. In addition, *N*-substitution could increase the original biological activity when compared with thalidomide as the parent compound. Additionally, *N*-substitution on the glutarimide ring of thalidomide analogues could generate the higher efficacy of biological effects rather than substitutions on the phthalidimide ring.

Discussions relative to the mechanism of thalidomide analogues, present that thalidomide inhibits angiogenesis in several experimental assay systems, such as in vivo suppression of vessel proliferation in a rabbit micropocket assay (D'Amato *et al.*, 1994), and in vitro against rat and human vascular endothelial cells in culture (Bauer *et al.*, 1998; Moreira *et al.*, 1999). Suppression of TNF-alpha and interferon γ (IFN-γ) secretion, are also presented, both of which upregulate endothelial cell integrin experssion (McCarty), a process crucial for a new vessel formation. Thalidomide inhibits secretion of basic fibroblast growth factor (bFGF), an angiogenic factor factor secreted by human tumours (Neubert *et al.*, 1995). The present study was consistent with the proposed mechanism of thalidomide analogues. As determined from anti-angiogenic assays, compound **3** and compound **4** (with substitutions instead of carbonyl groups at C-2) generate negative effects in preventing interaction between tubes. Thus, treatment from compound **3** and compound **4** could relatively reduce the size of tubes, contributing to prevention of tube aggregation to larger sizes of tubes. This activity could potentially contribute to reduce the overall tube formation. Additionally, from anti-proliferative studies, the results indicate that anti-proliferative effects from the parent compound of thalidomide were statistically similar to effects from treatments with compound **2**, compound **3** and compound **4**. Cell morphology seemed to remain unchanged after treatment with compound **2**, compound **3** and compound **4**, compared with thalidomide. The analyses and discussions from this study demonstrate that these substitutions applied in this study on the phthalimide ring contributes to an increase in relative biological activity while still preserving the original mechanism of action.

For compound **5**, moreover, its imide substitution (Figure 1) contributed to an increase in the original biological activity through anti-proliferative effects to reduce numbers of cells. This possible explanation are consistent with all *in vitro* observations and experimental results that cell morphology was changed depending on the dose of treatments, and relative numbers of cells are directly induced to undergo the apoptotic pathway in order to reduce numbers of cells present. The capillary tube *in vitro* measurements were also reduced based on concentrations of treatments. Thus, these imide substitutions on glutarimide ring of thalidomide analogues applied in this study contributes to an increase in relative biological activity while also adding a different mechanism of action. Another possible explanation is

about chloromethyl substitution added (Figure 1) on the imide position of glutarimide structure, and this substitution as a type of alkylating agents contribute to cytotoxic effects.

As results shown (Figure 94), compound **5** could decrease viability of breast cancer cell line MDA-MB-231 in treatment concentration of 10 µg/mL. HUVEC cells are a type of human normal healthy cells, and are cells derived from the endothelium of veins from the umbilical cord. Human normal primary cells such as HUVEC cells are commonly used as a laboratory model system for the study of the function and pathology of endithelial cells such as angiogenesis, also used as an *in vitro* model to determine the toxicity and selectivity for potential drugs. As results from anti-angiogenic effect shown (Figure 87), in this study, compound **5** in treatment concentration of 10 µg/mL did not contribute to reduce capability of tube formation, and more tube formation was found with treatment of compound **5** in concentration of 10 µg/mL. This results potentially suggested compound **5** in concentration of 10 µg/mL did not generate strong effect to function of cells, and possibly indicated to selectively reduce cell viability of cancer cells, although anti-proliferative assay for compound **5** did not perform to determine the toxicity by appling with HUVECs and other human normal primary cells.

Chapter V: Conclusion & Future Direction of Study

Thalidomide has attracted renewed interest in the treatment of cancer since late 1990s. Due to its famous teratogenic toxicity, many thalidomide analogues in recent years have been developed, attempting to avoid its teratogenicity and increase its efficacy. In this study, C-2 position of phthalimide ring and *N*-substitution of glutarimide ring (Figure 1) have been modified in an attempt to create novel analogues and determine the relationship between the substitution of those positions and resulting biological activities.

In this study, I have synthesized two novel compounds compound **3** (3-[(1*R*)-1-hydroxy-1-methyl-3-oxo-1,3-dihydro-2*H*-isoindol-2-yl]piperidine-2,6-dione, see Figure 111-A) and compound **4** (3-[(1*S*)-1-hydroxy-1-methyl-3-oxo-1,3-dihydro-2*H*-isoindol-2-yl]piperidine-2,6-dione, see Figure 111-B).

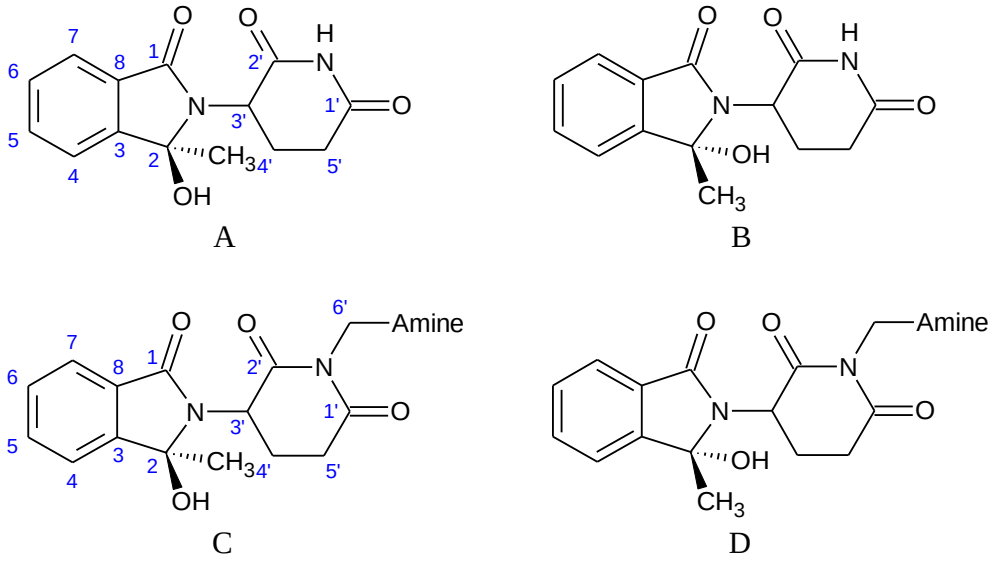

Figure 111: Structure of novel compounds & Potential novel compound in further studies; A: Compound **3**: 3-[(1*R*)-1-hydroxy-1-methyl-3-oxo-1,3-dihydro-2H-isoindol-2-yl]piperidine-2,6-dione;B: Compound **4**: 3-[(1*S*)-1-hydroxy-1-methyl-3-oxo-1,3-dihydro-2H-isoindol-2-yl]piperidine-2,6-dione; C & D: Conjugation structures

The main reactions for synthesis were (1) to activate the hydroxyl group to a good leaving group chloride on structure of 2-Acetylbenzoic acid to generate a reactive intermediate; and (2) to add the primary amine of glutarimide ring to carbonyl group to remove chloride to form a close ring structure. The strcutures for those novel compounds have been confirmed using with its characteristics of structure including 1H NMR, 13C NMR, IR, and high and low resolution of mass spectra. Also, compound **2** (Figure 23) without substitution in position of C-2 and compound **5** (Figure 31) with substitution in imide position of glutarimide ring was synthesised and confirmed with their structures. Then, all those synthesised compounds were used to test and compare their biological activities in terms of TNF-alpha inhibition, anti-angiogenesis and anti-proliferation to metastatic breast cancer cells MDA-MB-231.

Compared with parent compound thalidomide, novel analogues compound **3** and **4** may have better efficacy in inducing biological activities, such as cytokine modulation and tube formation inhibition. All these biological improvements were generated from two different substitutions (methyl group and hydroxyl group) on C-2 of phthalimide ring as compared to the parent compound thalidomide. For compound **5**, the substitution on imide position of glutarimide ring render it with higher cytotoxicity compared with the parent compound thalidomide using *in vitro* breast cancer cell line test. This suggests that *N*-substitution on glutarimide ring potentially can increase the biological activities of thalidomide. The substitution of chloromethyl group may contribute to higher cytotoxic effect, and this substitution may make the whole molecule more like alkylating agent. In future studies, a number of substitutions will be required to be added onto the imide position of the glutarimide ring to assess biological effects, which will reveal the relationship between the type of inhibition effect and the substitution group.

In conclusion, two novel compounds with better biological effects have been synthesised. Also, it is suggested that *N*-substitution on glutarimide ring may increase the biological effects as well. Thus, in future study, combining *N*-substitution of glutarimide ring and modification at C-2 position may generate even better biological effects. According to the literature, polyamine may facilitate drug to be delivered into cells via polyamine transport. Therefore, it is possible that a polyamine backbone can be added onto the imide position of glutarimide ring of the two novel compounds developed in this study (Figure 111-C and Figure 111-D) to gain better biological activities.

Reference:

Aeed PA, Nakajima M, Welch DR (1988). The role of polymorphonuclear leukocytes (PMN) on the growth and metastatic potential of 13762NF mammary adenocarcinoma cells. *International journal of cancer* **42**(5)**:** 748-759.

Aguilera KY, Brekken RA (2014). Recruitment and retention: factors that affect pericyte migration. *Cellular and molecular life sciences : CMLS* **71**(2)**:** 10.1007/s00018-00013-01432-z.

Alexanian R, Weber D, Anagnostopoulos A, Delasalle K, Wang M, Rankin K (2003). Thalidomide with or without Dexamethasone for Refractory or Relapsing Multiple Myeloma. *Seminars in Hematology* **40**(4 SUPPL. 4)**:** 3-7.

Ali D, Le Scodan R (2011). Treatment of the primary tumor in breast cancer patients with synchronous metastases. *Annals of Oncology* **22**(1)**:** 9-16.

Anders CK, Carey LA (2009). Biology, Metastatic Patterns, and Treatment of Patients with Triple-Negative Breast Cancer. *Clinical breast cancer* **9**(Suppl 2)**:** S73-S81.

Armaghany T, Wilson JD, Chu Q, Mills G (2012). Genetic Alterations in Colorectal Cancer. *Gastrointestinal Cancer Research : GCR* **5**(1)**:** 19-27.

Arora M, Moser J, Phadke H, Basha AA, Spencer SL (2017). Endogenous replication stress in mother cells leads to quiescence of daughter cells. *Cell reports* **19**(7)**:** 1351-1364.

Atra E, Sato EI (1993). Treatment of the cutaneous lesions of systemic lupus erythematosus with thalidomide. *Clinical and Experimental Rheumatology* **11**(5)**:** 487-493.

Avorn J (2011). Learning about the Safety of Drugs — A Half-Century of Evolution. *New England Journal of Medicine* **365**(23)**:** 2151-2153.

Awan FT, Johnson AJ, Lapalombella R, Hu W, Lucas M, Fischer B*, et al.* (2010). Thalidomide and lenalidomide as new therapeutics for the treatment of chronic lymphocytic leukemia. *Leukemia & lymphoma* **51**(1)**:** 27-38.

Badowska-Kozakiewicz AM, Budzik MP (2016). Immunohistochemical characteristics of basal-like breast cancer. *Contemporary Oncology* **20**(6)**:** 436-443.

Baidas SM, Winer EP, Fleming GF, Harris L, Pluda JM, Crawford JG*, et al.* (2000). Phase II Evaluation of Thalidomide in Patients With Metastatic Breast Cancer. *Journal of Clinical Oncology* **18**(14)**:** 2710-2717.

Baillie CT, Winslet MC, Bradley NJ (1995). Tumour vasculature a potential therapeutic target. *British Journal of Cancer* **72**(2)**:** 257-267.

Barlogie B, Zangari M, Spencer T, Fassas A, Anaissie E, Badros A*, et al.* (2001). Thalidomide in the management of multiple myeloma. *Seminars in Hematology* **38**(3)**:** 250-259.

Bartlett JB, Dredge K, Dalgleish AG (2004). The evolution of thalidomide and its IMiD derivatives as anticancer agents. *Nature reviews. Cancer* **4**(4)**:** 314-322.

Bauer KS, Dixon SC, Figg WD (1998). Inhibition of Angiogenesis by Thalidomide Requires Metabolic Activation, Which Is Species-dependent. *Biochemical Pharmacology* **55**(11)**:** 1827-1834.

Baz RC, Shain KH, Hussein MA, Lee J-H, Sullivan DM, FinleyOliver E*, et al.* (2014). Phase II study of pegylated liposomal doxorubicin, low-dose dexamethasone, and lenalidomide in patients with newly diagnosed multiple myeloma. *American journal of hematology* **89**(1)**:** 62-67.

Benazzi C, Al-Dissi A, Chau CH, Figg WD, Sarli G, de Oliveira JT*, et al.* (2014). Angiogenesis in Spontaneous Tumors and Implications for Comparative Tumor Biology. *The Scientific World Journal* **2014:** 919570.

Benjamin LE, Golijanin D, Itin A, Pode D, Keshet E (1999). Selective ablation of immature blood vessels in established human tumors follows vascular endothelial growth factor withdrawal. *Journal of Clinical Investigation* **103**(2)**:** 159-165.

Bergers G, Benjamin LE (2003). Tumorigenesis and the angiogenic switch. *Nature reviews. Cancer* **3**(6)**:** 401-410.

Bicknell R, Harris AL (1992). Anticancer strategies involving the vasculature: Vascular targeting and the inhibition of angiogenesis. *Seminars in Cancer Biology* **3**(6)**:** 399-407.

Brana MF, Cacho M, Garcia MA, de Pascual-Teresa B, Ramos A, Dominguez MT*, et al.* (2004). New analogues of amonafide and elinafide, containing aromatic heterocycles: synthesis, antitumor activity, molecular modeling, and DNA binding properties. *J Med Chem* **47**(6)**:** 1391-1399.

Brana MF, Fernandez A, Garrido M, Rodriguez MLL, Morcillo MJ, Sanz AM (1989). Synthesis, Structure and Cytostatic Activity of a Series of N-Substituted 3, 4-Diphenyl-1H-pyrrole-2, 5-diones. *CHEMICAL & PHARMACEUTICAL BULLETIN* **37**(10)**:** 2710-2712.

Brosseau C, Colston K, Dalgleish AG, Galustian C (2012). The immunomodulatory drug lenalidomide restores a vitamin D sensitive phenotype to the vitamin D resistant breast cancer cell line MDA-MB-231 through inhibition of BCL-2: potential for breast cancer therapeutics. *Apoptosis* **17**(2)**:** 164-173.

Brown RD, Pope B, Murray A, Esdale W, Sze DM, Gibson J*, et al.* (2001). Dendritic cells from patients with myeloma are numerically normal but functionally defective as they fail to up-regulate CD80 (B7-1) expression after huCD40LT stimulation because of inhibition by transforming growth factor-β1 and interleukin-10. *Blood* **98**(10)**:** 2992-2998.

Capitosti SM, Hansen TP, Brown ML (2003). Facile Synthesis of an Azido-Labeled Thalidomide Analogue. *Org. Lett.* **5**(Copyright (C) 2017 American Chemical Society (ACS). All Rights Reserved.)**:** 2865-2867.

Catlett-Falcone R, Landowski TH, Oshiro MM, Turkson J, Levitzki A, Savino R*, et al.* (1999). Constitutive activation of Stat3 signaling confers resistance to apoptosis in human U266 myeloma cells. *Immunity* **10**(1)**:** 105-115.

Cébe-Suarez S, Zehnder-Fjällman A, Ballmer-Hofer K (2006). The role of VEGF receptors in angiogenesis; complex partnerships. *Cellular and Molecular Life Sciences* **63**(5)**:** 601-615.

Chang H, Brown CW, Matzuk MM (2002). Genetic Analysis of the Mammalian Transforming Growth Factor-β Superfamily. *Endocrine Reviews* **23**(6)**:** 787-823.

Chaudary MM, Girling A, Girling S, Habib F, Millis RR, Hayward JL (1988). New lumps in the breast following conservation treatment for early breast cancer. *Breast Cancer Research and Treatment* **11**(1)**:** 51-58.

Ching L-M, Goldsmith D, Joseph WR, Körner H, Sedgwick JD, Baguley BC (1999). Induction of Intratumoral Tumor Necrosis Factor (TNF) Synthesis and Hemorrhagic Necrosis by 5,6-Dimethylxanthenone-4-Acetic Acid (DMXAA) in TNF Knockout Mice. *Cancer Research* **59**(14)**:** 3304-3307.

Ching LM, Xu ZF, Gummer BH, Palmer BD, Joseph WR, Baguley BC (1995). Effect of thalidomide on tumour necrosis factor production and anti-tumour activity induced by 5,6-dimethylxanthenone-4-acetic acid. *British Journal of Cancer* **72**(2)**:** 339-343.

Coelho AL, Gomes MP, Catarino RJ, Rolfo C, Lopes AM, Medeiros RM*, et al.* (2017). Angiogenesis in NSCLC: is vessel co-option the trunk that sustains the branches? *Oncotarget* **8**(24)**:** 39795-39804.

Contino-Pépin C, Parat A, Patinote C, Roscoe WA, Karlik SJ, Pucci B (2010). Thalidomide derivatives for the treatment of neuroinflammation. *ChemMedChem* **5**(12)**:** 2057-2064.

Conway EM, Collen D, Carmeliet P (2001). Molecular mechanisms of blood vessel growth. *Cardiovascular Research* **49**(3)**:** 507-521.

Corral LG, Haslett PAJ, Muller GW, Chen R, Wong L-M, Ocampo CJ*, et al.* (1999). Differential Cytokine Modulation and T Cell Activation by Two Distinct Classes of Thalidomide Analogues That Are Potent Inhibitors of TNF-α. *The Journal of Immunology* **163**(1)**:** 380-386.

Corral LG, Muller GW, Moreira AL, Chen Y, Wu M, Stirling D*, et al.* (1996). Selection of novel analogs of thalidomide with enhanced tumor necrosis factor alpha inhibitory activity. *Molecular Medicine* **2**(4)**:** 506-515.

Coussens LM, Werb Z (2002). Inflammation and cancer. *Nature* **420**(6917)**:** 860-867.

Cristofanilli M, Charnsangavej C, Hortobagyi GN (2002). Angiogenesis modulation in cancer research: novel clinical approaches. *Nat Rev Drug Discov* **1**(6)**:** 415-426.

Crown J, O'Shaughnessy J, Gullo G (2012). Emerging targeted therapies in triple-negative breast cancer. *Annals of Oncology* **23**(suppl_6)**:** vi56-vi65.

D'Amato RJ, Loughnan MS, Flynn E, Folkman J (1994). Thalidomide is an inhibitor of angiogenesis. *Proceedings of the National Academy of Sciences of the United States of America* **91**(9)**:** 4082-4085.

da Costa PM, da Costa MP, Carvalho AA, Cavalcanti SMT, de Oliveira Cardoso MV, de Oliveira Filho GB*, et al.* (2015). Improvement of in vivo anticancer and antiangiogenic potential of thalidomide derivatives. *Chemico-Biological Interactions* **239:** 174-183.

Dai X, Li T, Bai Z, Yang Y, Liu X, Zhan J*, et al.* (2015). Breast cancer intrinsic subtype classification, clinical use and future trends. *American Journal of Cancer Research* **5**(10)**:** 2929-2943.

Daly ME, Makris A, Reed M, Lewis CE (2003). Hemostatic Regulators of Tumor Angiogenesis: A Source of Antiangiogenic Agents for Cancer Treatment? *JNCI: Journal of the National Cancer Institute* **95**(22)**:** 1660-1673.

Damia G, D'Incalci M (1998). Mechanisms of resistance to alkylating agents. *Cytotechnology* **27**(1-3)**:** 165-173.

Davies FE, Raje N, Hideshima T, Lentzsch S, Young G, Tai Y-T*, et al.* (2001). Thalidomide and immunomodulatory derivatives augment natural killer cell cytotoxicity in multiple myeloma. *Blood* **98**(1)**:** 210-216.

DeCicco KL, Tanaka T, Andreola F, De Luca LM (2004). The effect of thalidomide on non-small cell lung cancer (NSCLC) cell lines: possible involvement in the PPARγ pathway. *Carcinogenesis* **25**(10)**:** 1805-1812.

Denekamp J (1992). Inadequate vasculature in solid tumours: consequences for cancer research strategies. *BJR supplement / BIR* **24:** 111-117.

Dimopoulos MA, Zervas K, Kouvatseas G, Galani E, Grigoraki V, Kiamouris C*, et al.* (2001a). Thalidomide and dexamethasone combination for refractory multiple myeloma. *Annals of Oncology* **12**(7)**:** 991-995.

Dimopoulos MA, Zervas K, Kouvatseas G, Galani E, Grigoraki V, Kiamouris C*, et al.* (2001b). Thalidomide and dexamethasone combination for refractory multiple myeloma. *Annals of oncology : official journal of the European Society for Medical Oncology* **12**(7)**:** 991-995.

Dmoszyńska A, Bojarska-Junak A, Domański D, Roliński J, Hus M, Soroka-Wojtaszko M (2002). Production of Proangiogenic Cytokines During Thalidomide Treatment of Multiple Myeloma. *Leukemia & Lymphoma* **43**(2)**:** 401-406.

Domenico R (2009). The Discovery of Antiangiogenic Molecules: A Historical Review. *Current Pharmaceutical Design* **15**(4)**:** 345-352.

Dunzendorfer S, Herold M, Wiedermann CJ (1999). Inducer-specific bidirectional regulation of endothelial interleukin-8 production by thalidomide. *Immunopharmacology* **43**(1)**:** 59-64.

Durie BGM, Jacobson J, Barlogie B, Crowley J (2004). Magnitude of Response With Myeloma Frontline Therapy Does Not Predict Outcome: Importance of Time to Progression in Southwest Oncology Group Chemotherapy Trials. *Journal of Clinical Oncology* **22**(10)**:** 1857-1863.

Eisen T, Boshoff C, Mak I, Sapunar F, Vaughan MM, Pyle L*, et al.* (2000). Continuous low dose Thalidomide: a phase II study in advanced melanoma, renal cell, ovarian and breast cancer. *British Journal of Cancer* **82**(4)**:** 812-817.

El-Aarag BYA, Kasai T, Zahran MAH, Zakhary NI, Shigehiro T, Sekhar SC*, et al.* (2014). In vitro anti-proliferative and anti-angiogenic activities of thalidomide dithiocarbamate analogs. *International Immunopharmacology* **21**(2)**:** 283-292.

Ellis IO (2010). Intraductal proliferative lesions of the breast: morphology, associated risk and molecular biology. *Mod Pathol* **23**(S2)**:** S1-S7.

Eriksson T, Bjorkman S, Lyon AW, Raisys VA (1997). Handling of blood samples for determination of thalidomide [3] (multiple letters). *Clinical Chemistry* **43**(6)**:** 1094-1095.

Eriksson T, Björkman S, Roth B, Björk H, Höglund P (1998). Hydroxylated metabolites of thalidomide: Formation in-vitro and in-vivo in man. *Journal of Pharmacy and Pharmacology* **50**(12)**:** 1409-1416.

Fife K, Phillips RH, Howard MR, Bower M, Gracie F (1998). Activity of thalidomide in AIDS-related Kaposi's sarcoma and correlation with HHV8 titre. *International Journal of STD & AIDS* **9**(12)**:** 751-755.

Figg WD, Arlen P, Gulley J, Fernandez P, Noone M, Fedenko K*, et al.* (2001a). A randomized phase II trial of docetaxel (taxotere) plus thalidomide in androgen-independent prostate cancer. *Seminars in Oncology* **28**(4 SUPPL. 15)**:** 62-66.

Figg WD, Dahut W, Duray P, Hamilton M, Tompkins A, Steinberg SM*, et al.* (2001b). A Randomized Phase II Trial of Thalidomide, an Angiogenesis Inhibitor, in Patients with Androgen-independent Prostate Cancer. *Clinical Cancer Research* **7**(7)**:** 1888-1893.

Fine HA, Figg WD, Jaeckle K, Wen PY, Kyritsis AP, Loeffler JS*, et al.* (2000). Phase II Trial of the Antiangiogenic Agent Thalidomide in Patients With Recurrent High-Grade Gliomas. *Journal of Clinical Oncology* **18**(4)**:** 708-708.

Folkman J (1995). Angiogenesis in cancer, vascular, rheumatoid and other disease. *Nat Med* **1**(1)**:** 27-30.

Folkman J (2007). Angiogenesis: an organizing principle for drug discovery? *Nat Rev Drug Discov* **6**(4)**:** 273-286.

Folkman J (1971). Tumor Angiogenesis: Therapeutic Implications. *New England Journal of Medicine* **285**(21)**:** 1182-1186.

Folkman J, Ingber D (1992). Inhibition of angiogenesis. *Seminars in Cancer Biology* **3**(2)**:** 89-96.

Fuhrmann-Benzakein E, Ma, M. N., Rubbia-Brandt, L., Mentha, G., Ruefenacht, D., Sappino, A.-P. and Pepper, M. S. (2000). Elevated levels of angiogenic cytokines in the plasma of cancer patients. *Int. J. Cancer* **85:** 40–45.

Fulmer GR, Miller AJM, Sherden NH, Gottlieb HE, Nudelman A, Stoltz BM*, et al.* (2010). NMR Chemical Shifts of Trace Impurities: Common Laboratory Solvents, Organics, and Gases in Deuterated Solvents Relevant to the Organometallic Chemist. *Organometallics* **29**(9)**:** 2176-2179.

Gao M, Gao L, Yang G, Tao Y, Hou J, Xu H*, et al.* (2014). Myeloma cells resistance to NK cell lysis mainly involves an HLA class I-dependent mechanism. *Acta Biochimica et Biophysica Sinica* **46**(7)**:** 597-604.

González-Barca E, Canales MA, Salar A, Ferrer S, Domingo-Domenech E, Vidal MJ*, et al.* (2016). Long-Term Follow-Up of a Phase II Trial of Six Cycles of Dose-Dense R-CHOP-14 for First-Line Treatment of Diffuse Large B-Cell Lymphoma in Young and Elderly Patients. *Acta Haematologica* **136**(2)**:** 76-84.

Goosen C, Laing TJ, Plessis Jd, Goosen TC, Flynn GL (2002). Physicochemical Characterization and Solubility Analysis of Thalidomide and Its N-Alkyl Analogs. *Pharmaceutical Research* **19**(1)**:** 13-19.

Götte M, Fackler S, Hermann T, Perola E, Cellai L, Gross HJ*, et al.* (1995). HIV-1 reverse transcriptase-associated RNase H cleaves RNA/RNA in arrested complexes: implications for the mechanism by which RNase H discriminates between RNA/RNA and RNA/DNA. *The EMBO Journal* **14**(4)**:** 833-841.

Grabstald H, Golbey R (1965). Clinical experiences with thalidomide in patients with cancer. *Clinical Pharmacology and Therapeutics* **6**(3)**:** 298-300.

Guirgis AA, Zahran MAH, Mohamed AS, Talaat RM, Abdou BY, Agwa HS (2010). Effect of thalidomide dithiocarbamate analogs on the intercellular adhesion molecule-1 expression. *International Immunopharmacology* **10**(7)**:** 806-811.

Gupta GP, Massagué J (2006). Cancer Metastasis: Building a Framework. *Cell* **127**(4)**:** 679-695.

Gutiérrez‐Rodríguez O (1984). Thalidomide a promising new treatment for rheumatoid arthritis. *Arthritis & Rheumatism* **27**(10)**:** 1118-1121.

Gutman M, Szold A, Ravid A, Lazauskas T, Merimsky O, Klausner JM (1996). Failure of thalidomide to inhibit tumor growth and angiogenesis in vivo. *Anticancer Research* **16**(6 B)**:** 3673-3678.

Hallek M, Bergsagel PL, Anderson KC (1998). Multiple Myeloma: Increasing Evidence for a Multistep Transformation Process. *Blood* **91**(1)**:** 3-21.

Hamza MH (1986). Treatment of Behçet's disease with thalidomide. *Clinical Rheumatology* **5**(3)**:** 365-371.

Han QW, Wen-ju; Hu, Jin-guo (2009). Synthesis of 1-hydroxy-1-methyl-3-oxo-isoindole derivatives. *Chinese Journal of Synthetic Chemistry* **17**(4)**:** 483-485.

Haslett P, Hempstead M, Seidman C, Diakun J, Vasquez D, Freedman VH*, et al.* (1997). The metabolic and immunologic effects of short-term thalidomide treatment of patients infected with the human immunodeficiency virus. *AIDS research and human retroviruses* **13**(12)**:** 1047-1054.

Helfrich I, Schadendorf D (2011). Blood vessel maturation, vascular phenotype and angiogenic potential in malignant melanoma: One step forward for overcoming anti-angiogenic drug resistance? *Molecular Oncology* **5**(2)**:** 137-149.

Hideshima T, Chauhan D, Podar K, Schlossman RL, Richardson P, Anderson KC (2001). Novel therapies targeting the myeloma cell and its bone marrow microenvironment. *Seminars in Oncology* **28**(6)**:** 607-612.

Hideshima T, Chauhan D, Shima Y, Raje N, Davies FE, Tai Y-T*, et al.* (2000). Thalidomide and its analogs overcome drug resistance of human multiple myeloma cells to conventional therapy. *Blood* **96**(9)**:** 2943-2950.

Hillen F, Griffioen AW (2007). Tumour vascularization: sprouting angiogenesis and beyond. *Cancer Metastasis Reviews* **26**(3-4)**:** 489-502.

Hunter T, Pines J Cyclins and cancer II: Cyclin D and CDK inhibitors come of age. *Cell* **79**(4)**:** 573-582.

Inic Z, Zegarac M, Inic M, Markovic I, Kozomara Z, Djurisic I*, et al.* (2014). Difference between Luminal A and Luminal B Subtypes According to Ki-67, Tumor Size, and Progesterone Receptor Negativity Providing Prognostic Information. *Clinical Medicine Insights. Oncology* **8:** 107-111.

Jin-Guo H (2008). Synthesis of o-acetylbenzamide derivatives. *Journal of Applied Chemistry Industry* **37**(12)**:** 1468-1471.

Johnson KE, Wilgus TA (2014). Vascular Endothelial Growth Factor and Angiogenesis in the Regulation of Cutaneous Wound Repair. *Advances in Wound Care* **3**(10)**:** 647-661.

Judah F (2003). Fundamental Concepts of the Angiogenic Process. *Current Molecular Medicine* **3**(7)**:** 643-651.

Keller H, Kunz W, Muckter H (1956). [N-phthalyl-glutamic acid imide; experimental studies on a new synthetic product with sedative properties]. *Arzneimittel-Forschung* **6**(8)**:** 426-430.

Kenyon BM, Browne F, D'Amato RJ (1997). Effects of Thalidomide and Related Metabolites in a Mouse Corneal Model of Neovascularization. *Experimental Eye Research* **64**(6)**:** 971-978.

Kim Y-K, Sohn S-K, Lee J-H, Yang D-H, Moon J-H, Ahn J-S*, et al.* (2010). Clinical efficacy of a bortezomib, cyclophosphamide, thalidomide, and dexamethasone (Vel-CTD) regimen in patients with relapsed or refractory multiple myeloma: a phase II study. *Annals of Hematology* **89**(5)**:** 475-482.

Klein CA (2009). Parallel progression of primary tumours and metastases. *Nature reviews. Cancer* **9**(4)**:** 302-312.

Komorowski J, Jerczyńska H, Siejka A, Barańska P, Ławnicka H, Pawłowska Z*, et al.* (2006). Effect of thalidomide affecting VEGF secretion, cell migration, adhesion and capillary tube formation of human endothelial EA.hy 926 cells. *Life Sciences* **78**(22)**:** 2558-2563.

Kortüm KM, Zhu YX, Shi CX, Jedlowski P, Stewart AK (2015). Cereblon binding molecules in multiple myeloma. *Blood Reviews* **29**(5)**:** 329-334.

Kotoh T, Dhar DK, Masunaga R, Tabara H, Tachibana M, Kubota H*, et al.* (1999). Antiangiogenic therapy of human esophageal cancers with thalidomide in nude mice. *Surgery* **125**(5)**:** 536-544.

Kruse FE, Joussen AM, Rohrschneider K, Becker MD, Volcker HE (1998). Thalidomide inhibits corneal angiogenesis induced by vascular endothelial growth factor. *Graefe's archive for clinical and experimental ophthalmology = Albrecht von Graefes Archiv fur klinische und experimentelle Ophthalmologie* **236**(6)**:** 461-466.

Kumar S, Raje N, Hideshima T, Ishitsuka K, Roccaro A, Shiraishi N*, et al.* (2005). Antimyeloma activity of two novel N-substituted and tetraflourinated thalidomide analogs. *Leukemia* **19**(7)**:** 1253-1261.

Langley RR, Fidler IJ (2011). The seed and soil hypothesis revisited - the role of tumor-stroma interactions in metastasis to different organs. *International journal of cancer. Journal international du cancer* **128**(11)**:** 2527-2535.

Larkin M (1999a). Low-dose thalidomide seems to be effective in multiple myeloma. *Lancet* **354**(9182)**:** 925.

Larkin M (1999b). Low-dose thalidomide seems to be effective in multiple myeloma. *The Lancet* **354**(9182)**:** 925.

Lepoittevin J-P (2006). Molecular Aspects of Allergic Contact Dermatitis. In: Frosch PJ, Menné T, Lepoittevin J-P (ed)^(eds). *Contact Dermatitis*, edn. Berlin, Heidelberg: Springer Berlin Heidelberg. p^pp 45-68.

Li J, Luo SK, Hong WD, Zhou ZH, Zou WY (2003). [Influence of thalidomide on bone marrow microenvironment in refractory and relapsed multiple myeloma]. *Ai zheng = Aizheng = Chinese journal of cancer* **22**(4)**:** 346-349.

Li P-K, Pandit B, Sackett DL, Hu Z, Zink J, Zhi J*, et al.* (2006). A thalidomide analogue with in vitro antiproliferative, antimitotic, and microtubule-stabilizing activities. *Molecular cancer therapeutics* **5**(2)**:** 450-456.

Lin AY, Brophy N, Fisher GA, So S, Biggs C, Yock TI*, et al.* (2005). Phase II study of thalidomide in patients with unresectable hepatocellular carcinoma. *Cancer* **103**(1)**:** 119-125.

List A, Kurtin S, Roe DJ, Buresh A, Mahadevan D, Fuchs D*, et al.* (2005). Efficacy of Lenalidomide in Myelodysplastic Syndromes. *New England Journal of Medicine* **352**(6)**:** 549-557.

Liu C-C, Shen Z, Kung H-F, Lin MCM (2006). Cancer gene therapy targeting angiogenesis: An updated Review. *World Journal of Gastroenterology : WJG* **12**(43)**:** 6941-6948.

Liu WM, Henry JY, Meyer B, Bartlett JB, Dalgleish AG, Galustian C (2009). Inhibition of metastatic potential in colorectal carcinoma in vivo and in vitro using immunomodulatory drugs (IMiDs). *British Journal of Cancer* **101**(5)**:** 803-812.

Lohbeck J, Miller AK (2016). Practical synthesis of a phthalimide-based Cereblon ligand to enable PROTAC development. *Bioorg. Med. Chem. Lett.* **26**(Copyright (C) 2017 American Chemical Society (ACS). All Rights Reserved.)**:** 5260-5262.

Luo W, Yu QS, Salcedo I, Holloway HW, Lahiri DK, Brossi A*, et al.* (2011). Design, synthesis and biological assessment of novel N-substituted 3-(phthalimidin-2-yl)-2,6-dioxopiperidines and 3-substituted 2,6-dioxopiperidines for TNF-α inhibitory activity. *Bioorganic and Medicinal Chemistry* **19**(13)**:** 3965-3972.

Luzzio FA, Mayorov AV, Ng SSW, Kruger EA, Figg WD (2003). Thalidomide metabolites and analogues. 3. Synthesis and antiangiogenic activity of the teratogenic and TNFα-modulatory thalidomide analogue 2-(2,6-dioxopiperidine-3-yl)phthalimidine. *J. Med. Chem.* **46**(18)**:** 3793-3799.

Lyon AW, Duran G, Raisys VA (1995). Determination of thalidomide by high performance liquid chromatography: Methodological strategy for clinical trials. *Clinical Biochemistry* **28**(4)**:** 467-470.

Ma X, Dong W, Su Z, Zhao L, Miao Y, Li N*, et al.* (2016). Functional roles of sialylation in breast cancer progression through miR-26a/26b targeting ST8SIA4. *Cell Death Dis* **7:** e2561.

Makki J (2015). Diversity of Breast Carcinoma: Histological Subtypes and Clinical Relevance. *Clinical Medicine Insights. Pathology* **8:** 23-31.

Makonkawkeyoon S, Limson-Pobre RN, Moreira AL, Schauf V, Kaplan G (1993). Thalidomide inhibits the replication of human immunodeficiency virus type 1. *Proceedings of the National Academy of Sciences of the United States of America* **90**(13)**:** 5974-5978.

Malhotra GK, Zhao X, Band H, Band V (2010). Histological, molecular and functional subtypes of breast cancers. *Cancer Biology & Therapy* **10**(10)**:** 955-960.

Man H-W, Corral LG, Stirling DI, Muller GW (2003). α-Fluoro-substituted thalidomide analogues. *Bioorganic & Medicinal Chemistry Letters* **13**(20)**:** 3415-3417.

Marlind J F16-IL2: a novel immunocytokine for the therapy cancer. Doctor of Science, Chalmers University of Technology, 2008.

Marriott JB, Muller G, Dalgleish AG (1999). Thalidomide as an emerging immunotherapeutic agent. *Immunology Today* **20**(12)**:** 538-540.

McBride WG THALIDOMIDE AND CONGENITAL ABNORMALITIES. *The Lancet* **278**(7216)**:** 1358.

McBride WG (1961). THALIDOMIDE AND CONGENITAL ABNORMALITIES. *The Lancet* **278**(7216)**:** 1358.

McCarty MF Thalidomide may impede cell migration in primates by down-regulating integrin β-chains: potential therapeutic utility in solid malignancies, proliferative retinopathy, inflammatory disorders, neointimal hyperplasia, and osteoporosis. *Medical Hypotheses* **49**(2)**:** 123-131.

Miller MT, Strömland K (1999). Teratogen update: Thalidomide: A review, with a focus on ocular findings and new potential uses. *Teratology* **60**(5)**:** 306-321.

Minuk L, Sibbald R, Peng J, Bejaimal S, Chin-Yee I (2010). Access to thalidomide for the treatment of multiple myeloma in Canada: physician behaviours and ethical implications. *Current Oncology* **17**(4)**:** 11-19.

Miyachi H, Azuma A, Ogasawara A, Uchimura E, Watanabe N, Kobayashi Y*, et al.* (1997). Novel biological response modifiers: phthalimides with tumor necrosis factor-alpha production-regulating activity. *J Med Chem* **40**(18)**:** 2858-2865.

Moller DR, Wysocka M, Greenlee BM, Ma X, Wahl L, Flockhart DA*, et al.* (1997). Inhibition of IL-12 production by thalidomide. *The Journal of Immunology* **159**(10)**:** 5157-5161.

Moreira AL, Friedlander DR, Shif B, Kaplan G, Zagzag D (1999). Thalidomide and a Thalidomide Analogue Inhibit Endothelial Cell Proliferation in vitro. *Journal of Neuro-Oncology* **43**(2)**:** 109-114.

Moreira AL, Sampaio EP, Zmuidzinas A, Frindt P, Smith KA, Kaplan G (1993). Thalidomide exerts its inhibitory action on tumor necrosis factor alpha by enhancing mRNA degradation. *The Journal of Experimental Medicine* **177**(6)**:** 1675-1680.

Mosmann T (1983). Rapid colorimetric assay for cellular growth and survival: Application to proliferation and cytotoxicity assays. *Journal of Immunological Methods* **65**(1)**:** 55-63.

Motzer RJ, Berg W, Ginsberg M, Russo P, Vuky J, Yu R*, et al.* (2002). Phase II Trial of Thalidomide for Patients With Advanced Renal Cell Carcinoma. *Journal of Clinical Oncology* **20**(1)**:** 302-306.

Mu N (2007). Study of anticancer effect in vivo and function mechanisms of paradise rain injection.,. *Shijia Zhuang, Hebei Medical University*.

Mückter H (1965). Thalidomide and tumor. *Antimicrobial Agents and Chemotherapy* **5:** 531-538.

Mückter H, Frankus E, More E (1969). Experimental Therapeutic Investigations with l-(Morpholinomethyl)-4-phthalimido-piperidindione-2,6 on Dimethylhenzanthracene-induced Tumors of Sprague-Dawley Rats. *Cancer Research* **29**(6)**:** 1212-1217.

Neubert R, Hinz N, Thiel R, Neubert D (1995). Down-regulation of adhesion receptors on cells of primate embryos as a probable mechanism of the teratogenic action of thalidomide. *Life Sciences* **58**(4)**:** 295-316.

Neufeld G, Tessler S, Gitay-Goren H, Cohen T, Levi BZ (1994). Vascular endothelial growth factor and its receptors. *Progress in Growth Factor Research* **5**(1)**:** 89-97.

Ng SSW, Gütschow M, Weiss M, Hauschildt S, Teubert U, Hecker TK*, et al.* (2003). Antiangiogenic Activity of N-substituted and Tetrafluorinated Thalidomide Analogues. *Cancer Research* **63**(12)**:** 3189-3194.

Nguyen M, Tran C, Barsky S, Sun JIR, McBride W, Pegram M*, et al.* (1997). Thalidomide and chemotherapy combination: Preliminary results of preclinical and clinical studies. *International Journal of Oncology* **10**(5)**:** 965-969.

Nishida N, Yano H, Nishida T, Kamura T, Kojiro M (2006). Angiogenesis in Cancer. *Vascular Health and Risk Management* **2**(3)**:** 213-219.

Nishimura K, Hashimoto Y, Iwasaki S (1994). Enhancement of Phorbol Ester-Induced Production of Tumor Necrosis Factor α by Thalidomide. *Biochemical and Biophysical Research Communications* **199**(2)**:** 455-460.

Niwayama S, Turk BE, Liu JO (1996). Potent inhibition of tumor necrosis factor-alpha production by tetrafluorothalidomide and tetrafluorophthalimides. *J Med Chem* **39**(16)**:** 3044-3045.

Nystedt S, Ramakrishnan V, Sundelin J (1996). The Proteinase-activated Receptor 2 Is Induced by Inflammatory Mediators in Human Endothelial Cells: COMPARISON WITH THE THROMBIN RECEPTOR. *Journal of Biological Chemistry* **271**(25)**:** 14910-14915.

Obermair A, Bancher-Todesca D, Bilgi S, Kaider A, Kohlberger P, Müllauer-Ertl S*, et al.* (1997). Correlation of Vascular Endothelial Growth Factor Expression and Microvessel Density in Cervical Intraepithelial Neoplasia. *JNCI: Journal of the National Cancer Institute* **89**(16)**:** 1212-1217.

Ogata A, Chauhan D, Teoh G, Treon SP, Urashima M, Schlossman RL*, et al.* (1997). IL-6 triggers cell growth via the Ras-dependent mitogen-activated protein kinase cascade. *Journal of immunology (Baltimore, Md. : 1950)* **159**(5)**:** 2212-2221.

Ogawara H, Handa H, Yamazaki T, Toda T, Yoshida K, Nishimoto N*, et al.* (2005). High Th1/Th2 ratio in patients with multiple myeloma. *Leukemia Research* **29**(2)**:** 135-140.

Olson KB, Hall TC, Horton J, Khung CL, Hosley HF (1965). Thalidomide (N - phthaloylglutamimide> in the treatment of advanced cancer. *Clinical Pharmacology and Therapeutics* **6**(3)**:** 292-297.

Olszewski AJ, Grossbard ML, Kozuch PS (2005). The horizon of antiangiogenic therapy for colorectal cancer. *ONCOLOGY* **19**(3)**:** 297-306.

Onitilo AA, Engel JM, Greenlee RT, Mukesh BN (2009). Breast Cancer Subtypes Based on ER/PR and Her2 Expression: Comparison of Clinicopathologic Features and Survival. *Clinical Medicine & Research* **7**(1-2)**:** 4-13.

Ortiz de Montellano PR (2013). Cytochrome P450-activated prodrugs. *Future medicinal chemistry* **5**(2)**:** 213-228.

Paget S (1889). THE DISTRIBUTION OF SECONDARY GROWTHS IN CANCER OF THE BREAST. *The Lancet* **133**(3421)**:** 571-573.

Palumbo A, Giaccone L, Bertola A, Pregno P, Bringhen S, Rus C*, et al.* (2001). Low-dose thalidomide plus dexamethasone is an effective salvage therapy for advanced myeloma. *Haematologica* **86**(4)**:** 399-403.

Périno S, Contino-Pépin C, Satchi-Fainaro R, Butterfield C, Pucci B (2004). Inhibition of angiogenesis by THAM-derived cotelomers endowed with thalidomide moieties. *Bioorganic & Medicinal Chemistry Letters* **14**(2)**:** 421-425.

Pollard M (1996). Thalidomide promotes metastasis of prostate adenocarcinoma cells (PA-III) in L-W rats. *Cancer Letters* **101**(1)**:** 21-24.

Pucci B, Kasten M, Giordano A (2000). Cell Cycle and Apoptosis. *Neoplasia (New York, N.Y.)* **2**(4)**:** 291-299.

Quach H, Ritchie D, Neeson P, Harrison S, Tai T, Tainton K*, et al.* (2008). Regulatory T Cells (Treg) Are Depressed in Patients with Relapsed/Refractory Multiple Myeloma (MM) and Increases towards Normal Range in Responding Patients Treated with Lenalidomide (LEN). *Blood* **112**(11)**:** 1696-1696.

Quach H, Ritchie D, Stewart AK, Neeson P, Harrison S, Smyth MJ*, et al.* (2010). Mechanism of action of immunomodulatory drugs (IMiDS) in multiple myeloma. *Leukemia* **24**(1)**:** 22-32.

Rafiee P, Stein DJ, Nelson VM, Otterson MF, Shaker R, Binion DG (2010). Thalidomide inhibits inflammatory and angiogenic activation of human intestinal microvascular endothelial cells (HIMEC). *American Journal of Physiology - Gastrointestinal and Liver Physiology* **298**(2)**:** G167-G176.

Rajkumar SV, Hayman S, Fonseca R, Dispenzieri A, Lacy MQ, Geyer S*, et al.* (2000). Thalidomide plus dexamethasone (thal/dex) and thalidomide alone (thal) as first line therapy for newly diagnosed myeloma (mm). *Blood* **96**(11 PART I).

Rajkumar SV, Hayman S, Gertz MA, Dispenzieri A, Lacy MQ, Greipp PR*, et al.* (2002). Combination therapy with thalidomide plus dexamethasone for newly diagnosed myeloma. *Journal of clinical oncology : official journal of the American Society of Clinical Oncology* **20**(21)**:** 4319-4323.

Reshetnikova G, Barkan R, Popov B, Nikolsky N, Chang L-S (2000). Disruption of the Actin Cytoskeleton Leads to Inhibition of Mitogen-Induced Cyclin E Expression, Cdk2 Phosphorylation, and Nuclear Accumulation of the Retinoblastoma Protein-Related p107 Protein. *Experimental Cell Research* **259**(1)**:** 35-53.

Ribatti D, Vacca A (2005). Therapeutic renaissance of thalidomide in the treatment of haematological malignancies. *Leukemia* **19**(9)**:** 1525-1531.

Richardson P, Mitsiades C, Schlossman R, Ghobrial I, Hideshima T, Chauhan D*, et al.* (2007). The treatment of relapsed and refractory multiple myeloma. *Hematology. American Society of Hematology. Education Program***:** 317-323.

Sampaio EP, Sarno EN, Galilly R, Cohn ZA, Kaplan G (1991). Thalidomide selectively inhibits tumor necrosis factor alpha production by stimulated human monocytes. *The Journal of Experimental Medicine* **173**(3)**:** 699-703.

Samson D, Gaminara E, Newland A, Van de Pette J, Kearney J, McCarthy D*, et al.* (1989). Infusion of vincristine and doxorubicin with oral dexamethasone as first-line therapy for multiple myeloma. *Lancet* **2**(8668)**:** 882-885.

Saudi M, Zmurko J, Kaptein S, Rozenski J, Gadakh B, Chaltin P*, et al.* (2016). Synthetic strategy and antiviral evaluation of diamide containing heterocycles targeting dengue and yellow fever virus. *European Journal of Medicinal Chemistry* **121:** 158-168.

Schmielau J, Teschendorf C, Konig M, Schmiegel W, Graeven U (2005). Combination of bortezomib, thalidomide, and dexamethasone in the treatment of relapsed, refractory IgD multiple myeloma. *Leuk Lymphoma* **46**(4)**:** 567-569.

Schulz M (2001). Dark Remedy: The Impact of Thalidomide and its Revival as a Vital Medicine. *BMJ* **322**(7302)**:** 1608.

Schumacher H, Smith RL, Williams RT (1965). THE METABOLISM OF THALIDOMIDE: THE SPONTANEOUS HYDROLYSIS OF THALIDOMIDE IN SOLUTION. *British Journal of Pharmacology and Chemotherapy* **25**(2)**:** 324-337.

Schutt P, Ebeling P, Buttkereit U, Brandhorst D, Opalka B, Hoiczyk M*, et al.* (2005). Thalidomide in combination with vincristine, epirubicin and dexamethasone (VED) for previously untreated patients with multiple myeloma. *European journal of haematology* **74**(1)**:** 40-46.

Schützenberger WG, Kolassa N, Wiener H, Kraupp O, Tuisl E (1979). Pharmacological properties of taglutimide, a new sedative-hypnotic drug. *Arzneimittel-Forschung/Drug Research* **29**(8)**:** 1146-1150.

Seneviratne S, Lawrenson R, Harvey V, Ramsaroop R, Elwood M, Scott N*, et al.* (2016). Stage of breast cancer at diagnosis in New Zealand: impacts of socio-demographic factors, breast cancer screening and biology. *BMC Cancer* **16:** 129.

Sheskin J (1965). Further observation with thalidomide in lepra reactions. *Leprosy Review* **36**(4)**:** 183-187.

Shibuya M (2003). Vascular endothelial growth factor receptor-2: Its unique signaling and specific ligand, VEGF-E. *Cancer Science* **94**(9)**:** 751-756.

Siegel RL, Miller KD, Jemal A (2016). Cancer statistics, 2016. *CA: A Cancer Journal for Clinicians* **66**(1)**:** 7-30.

Silva APC, Meneghini LZ, Bajerski L, Carini JP, Fialho SL, Mayorga P*, et al.* (2013). Discriminatory dissolution test for tablets containing α-and β-thalidomide polymorphs. *Dissolution Technologies* **20**(1)**:** 19-25.

Singhal S, Mehta J (2002a). Thalidomide in cancer. *Biomedicine & pharmacotherapy = Biomedecine & pharmacotherapie* **56**(1)**:** 4-12.

Singhal S, Mehta J (2002b). Thalidomide in cancer. *Biomedicine and Pharmacotherapy* **56**(1)**:** 4-12.

Singhal S, Mehta J, Desikan R, Ayers D, Roberson P, Eddlemon P*, et al.* (1999). Antitumor activity of thalidomide in refractory multiple myeloma. *The New England journal of medicine* **341**(21)**:** 1565-1571.

Solaini G, Sgarbi G, Baracca A (2011). Oxidative phosphorylation in cancer cells. *Biochimica et Biophysica Acta (BBA) - Bioenergetics* **1807**(6)**:** 534-542.

Somers GF (1960). PHARMACOLOGICAL PROPERTIES OF THALIDOMIDE (α - PHTHALIMIDO GLUTARIMIDE), A NEW SEDATIVE HYPNOTIC DRUG. *British Journal of Pharmacology and Chemotherapy* **15**(1)**:** 111-116.

Somers GF (1962). Thalidomide and abnormalities of development. *Orvosi hetilap* **103:** 2456-2459.

Song G, Li Y, Jiang G (2012). Role of VEGF/VEGFR in the pathogenesis o leukemias and as treatment targets (Review). *Oncology Reports* **28**(6)**:** 1935-1944.

Spector JA, Mehrara BJ, Greenwald JA, Saadeh PB, Steinbrech DS, Bouletreau PJ*, et al.* (2001). Osteoblast expression of vascular endothelial growth factor is modulated by the extracellular microenvironment. *American Journal of Physiology - Cell Physiology* **280**(1)**:** C72-C80.

Staton CA, Lewis CE (2005). Angiogenesis inhibitors found within the haemostasis pathway. *Journal of Cellular and Molecular Medicine* **9**(2)**:** 286-302.

Stebbing J, Benson C, Eisen T, Pyle L, Smalley K, Bridle H*, et al.* (2001). The treatment of advanced renal cell cancer with high-dose oral thalidomide. *British Journal of Cancer* **85**(7)**:** 953-958.

Stewart SG, Spagnolo D, Polomska ME, Sin M, Karimi M, Abraham LJ (2007). Synthesis and TNF expression inhibitory properties of new thalidomide analogues derived via Heck cross coupling. *Bioorganic & Medicinal Chemistry Letters* **17**(21)**:** 5819-5824.

Sung B, Kunnumakkara AB, Sethi G, Anand P, Guha S, Aggarwal BB (2009). Curcumin Circumvents Chemoresistance in vitro and Potentiates the Effect of Thalidomide and Bortezomib against Human Multiple Myeloma in Nude Mice Model. *Molecular cancer therapeutics* **8**(4)**:** 959-970.

Syamantak M, Sree Rama Chaitanya S, Santanu B, Suvro C (2012). TNF α Signaling Beholds Thalidomide Saga: A Review of Mechanistic Role of TNF-α Signaling Under Thalidomide. *Current Topics in Medicinal Chemistry* **12**(13)**:** 1456-1467.

Talaat R, El-Sayed W, Agwa H, Gamal-Eldeen A, Moawia S, Zahran M (2014). Novel thalidomide analogs: Anti-angiogenic and apoptotic effects on Hep-G2 and MCF-7 cancer cell lines. *Biomedicine & Aging Pathology* **4**(3)**:** 179-189.

Tarrado-Castellarnau M, de Atauri P, Cascante M (2016). Oncogenic regulation of tumor metabolic reprogramming. *Oncotarget* **7**(38)**:** 62726-62753.

Teo SK, Stirling DI, Zeldis JB (2005). Thalidomide as a novel therapeutic agent: New uses for an old product. *Drug Discovery Today* **10**(2)**:** 107-114.

Terpos E, Kastritis E, Roussou M, Heath D, Christoulas D, Anagnostopoulos N*, et al.* (2008). The combination of bortezomib, melphalan, dexamethasone and intermittent thalidomide is an effective regimen for relapsed/refractory myeloma and is associated with improvement of abnormal bone metabolism and angiogenesis. *Leukemia* **22**(12)**:** 2247-2256.

Therapontos C, Erskine L, Gardner ER, Figg WD, Vargesson N (2009). Thalidomide induces limb defects by preventing angiogenic outgrowth during early limb formation. *Proceedings of the National Academy of Sciences of the United States of America* **106**(21)**:** 8573-8578.

Torre LA, Bray F, Siegel RL, Ferlay J, Lortet-Tieulent J, Jemal A (2015). Global cancer statistics, 2012. *CA: A Cancer Journal for Clinicians* **65**(2)**:** 87-108.

Turk BE, Jiang H, Liu JO (1996). Binding of thalidomide to alpha1-acid glycoprotein may be involved in its inhibition of tumor necrosis factor alpha production. *Proceedings of the National Academy of Sciences* **93**(15)**:** 7552-7556.

Ucuzian AA, Gassman AA, East AT, Greisler HP (2010). Molecular Mediators of Angiogenesis. *Journal of burn care & research : official publication of the American Burn Association* **31**(1)**:** 158.

Vacca A, Di Loreto M, Ribatti D, Di Stefano R, Gadaleta-Caldarola G, Iodice G*, et al.* (1995). Bone marrow of patients with active multiple myeloma: angiogenesis and plasma cell adhesion molecules LFA-1, VLA-4, LAM-1, and CD44. *American journal of hematology* **50**(1)**:** 9-14.

Vacca A, Ribatti D, Presta M, Minischetti M, Iurlaro M, Ria R*, et al.* (1999). Bone marrow neovascularization, plasma cell angiogenic potential, and matrix metalloproteinase-2 secretion parallel progression of human multiple myeloma. *Blood* **93**(9)**:** 3064-3073.

Vacca A, Ribatti D, Roncali L, Ranieri G, Serio G, Silvestris F*, et al.* (1994). Bone marrow angiogenesis and progression in multiple myeloma. *British journal of haematology* **87**(3)**:** 503-508.

van Zijl F, Krupitza G, Mikulits W (2011). Initial steps of metastasis: Cell invasion and endothelial transmigration. *Mutation Research/Reviews in Mutation Research* **728**(1–2)**:** 23-34.

Varala R, Adapa SR (2005). A practical and efficient synthesis of thalidomide via Na/liquid NH 3 methodology. *Organic Process Research and Development* **9**(6)**:** 853-856.

Vargesson N (2015). Thalidomide‐induced teratogenesis: History and mechanisms. *Birth Defects Research* **105**(2)**:** 140-156.

Vargesson N (2013). Thalidomide Embryopathy: An Enigmatic Challenge. *ISRN Developmental Biology* **2013:** 18.

Verbon A, Juffermans NP, Speelman P, van Deventer SJH, ten Berge IJM, Guchelaar H-J*, et al.* (2000). A Single Oral Dose of Thalidomide Enhances the Capacity of Lymphocytes to Secrete Gamma Interferon in Healthy Humans. *Antimicrobial Agents and Chemotherapy* **44**(9)**:** 2286-2290.

Vogelsang GB, Farmer ER, Hess AD, Altamonte V, Beschorner WE, Jabs DA*, et al.* (1992). Thalidomide for the treatment of chronic graft-versus-host disease. *New England Journal of Medicine* **326**(16)**:** 1055-1058.

Wang S, Hasham MG, Isordia-Salas I, Tsygankov AY, Colman RW, Guo Y-L (2003). Upregulation of Cdc2 and cyclin A during apoptosis of endothelial cells induced by cleaved high-molecular-weight kininogen. *American Journal of Physiology - Heart and Circulatory Physiology* **284**(6)**:** H1917-H1923.

Ward SP (1962). Thalidomide and Congenital Abnormalities. *British Medical Journal* **2**(5305)**:** 646-647.

Weber D (2003). Thalidomide and Its Derivatives: New Promise for Multiple Myeloma. *Cancer Control* **10**(5)**:** 375-383.

Weber D, Rankin K, Gavino M, Delasalle K, Alexanian R (2003). Thalidomide Alone or With Dexamethasone for Previously Untreated Multiple Myeloma. *Journal of Clinical Oncology* **21**(1)**:** 16-19.

Wilkes GM (2010). *Targeted Cancer Therapy: A Handbook for Nurses*. edn. Jones & Bartlett Learning.

Wnendt S, Finkam M, Winter W, Ossig J, Raabe G, Zwingenberger K (1996). Enantioselective inhibition of TNF-alpha release by thalidomide and thalidomide-analogues. *Chirality* **8**(5)**:** 390-396.

Wong CC, Cheng K-W, Rigas B (2012). Preclinical Predictors of Anticancer Drug Efficacy: Critical Assessment with Emphasis on Whether Nanomolar Potency Should Be Required of Candidate Agents. *The Journal of Pharmacology and Experimental Therapeutics* **341**(3)**:** 572-578.

Xue H-x, Fu W-y, Cui H-d, Yang L-l, Zhang N, Zhao L-j (2015). High-dose thalidomide increases the risk of peripheral neuropathy in the treatment of ankylosing spondylitis. *Neural Regeneration Research* **10**(5)**:** 814-818.

Yakoub-Agha I, Mary JY, Hulin C, Doyen C, Marit G, Benboubker L*, et al.* (2012). Low-dose vs. high-dose thalidomide for advanced multiple myeloma: a prospective trial from the Intergroupe Francophone du Myelome. *European journal of haematology* **88**(3)**:** 249-259.

Yang Y, Yan L-N, Zhao J-C, Ma Y-K, Huang B, Li B*, et al.* (2010). Microsurgical reconstruction of hepatic artery in A-A LDLT: 124 consecutive cases without HAT. *World Journal of Gastroenterology : WJG* **16**(21)**:** 2682-2688.

Yuichi H (2002). Structural Development of Biological Response Modifiers Based on Retinoids and Thalidomide. *Mini-Reviews in Medicinal Chemistry* **2**(6)**:** 543-551.

Zahran MAH, Salem TAR, Samaka RM, Agwa HS, Awad AR (2008). Design, synthesis and antitumor evaluation of novel thalidomide dithiocarbamate and dithioate analogs against Ehrlich ascites carcinoma-induced solid tumor in Swiss albino mice. *Bioorganic & Medicinal Chemistry* **16**(22)**:** 9708-9718.

Zhong H, Deng F, Kong X (1996). Expression of basic fibroblast growth factor and its receptor in renal cell carcinoma. *Zhonghua wai ke za zhi [Chinese journal of surgery]* **34**(11)**:** 651-654.

Zhu X, Giordano T, Yu QS, Holloway HW, Perry TA (2003). Thiothalidomides: Novel Isosteric Analogues of Thalidomide with Enhanced TNF-α Inhibitory Activity. *J. Med. Chem.* **46**(24)**:** 5222-5229.

Ziyad S, Iruela-Arispe ML (2011). Molecular Mechanisms of Tumor Angiogenesis. *Genes & Cancer* **2**(12)**:** 1085-1096.

Zwingenberger K (1995). Immunomodulation by thalidomide: Systematic review of the literature and of unpublished observations. *Journal of Inflammation* **46**(4)**:** 177-211.

Zwingenberger K, Wnendt S (1995). Immunomodulation by thalidomide: systematic review of the literature and of unpublished observations. *J Inflamm* **46**(4)**:** 177-211.

Appendix I: Chemicals ordered from commercial for organic synthesis

Table 14: Chemicals ordered from commercial for organic synthesis

Number	Chemicals	Catalogue Number	Suppliers
1	N-(*tert*-butoxycarbonyl)-L-glutamine, Boc-Gln-OH 98%	408441	Sigma Aldrich, NZ
2	1,1'-Carbonyldiimidazole,CDI. ≥97.0%	21860	Sigma Aldrich, NZ
3	Tetrahydrofuran, THF, anhydrous 99.9%	401757	Sigma Aldrich, NZ
4	Trifluoroacetic acid, 99.0%	T6508	Sigma Aldrich, NZ
5	Triethylamine (≥99%)	T0886	Sigma Aldrich, NZ
6	Phthalic anhydride (≥99%)	320064	Sigma Aldrich, NZ
7	2-Acetylbenzoic Acid	A12801	Sigma Aldrich, NZ
8	Thionyl Chloride, (≥99%)	230464	Sigma Aldrich, NZ
9	N, N-Dimethylformamide, anhydrous, 99.8%	227056	Sigma Aldrich, NZ
10	Triethylenetetramine (≥97%)	90460	Sigma Aldrich, NZ
11	Ethyl trifluoroacetate	E50000	Sigma Aldrich, NZ
12	Magnesium Sulfate (Anhydrous, Reagent, ≥99.5)	M7506	Sigma Aldrich, NZ
13	Formaldehyde solution ACS reagent, 37% wt % in H2O	252549	Sigma Aldrich, NZ
14	Phthaldialdehyde for synthesis	8210270010	Merck, NZ
15	Di-tert-butyl decarbonate	8522610100	Merck, NZ
16	Dichloromethane HPLC grade	FSBD143	Thermo Scientific NZ
17	Ethyl acetate HPLC grade 4L	FSBE195	Thermo Scientific NZ
18	Hexane (98%) HPLC grade 2.5L	SCARH02372500	Global Science, NZ

Appendix II: Mass spectrometer results (High resolution & low resolution)

Compound 3: Mass spectrometer results (Low resolution)

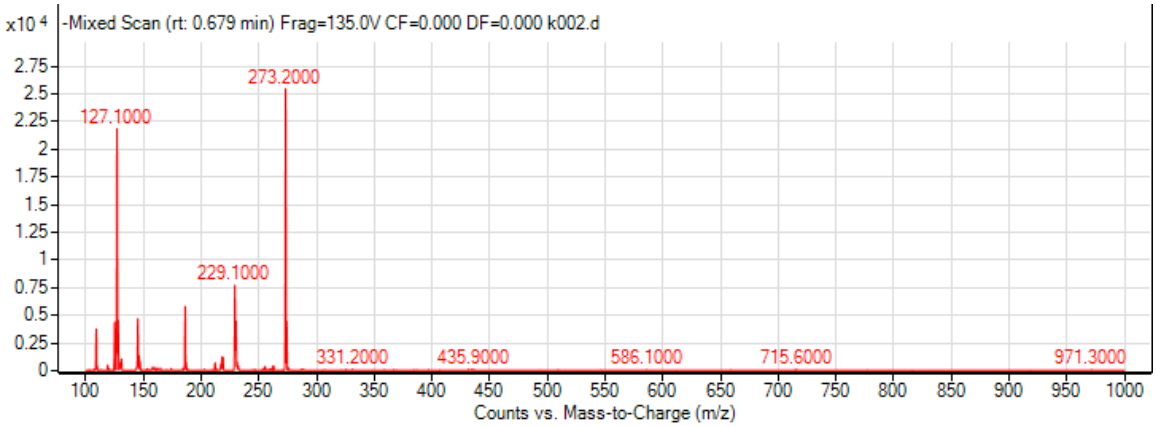

Compound 4: Mass spectrometer results (Low resolution)

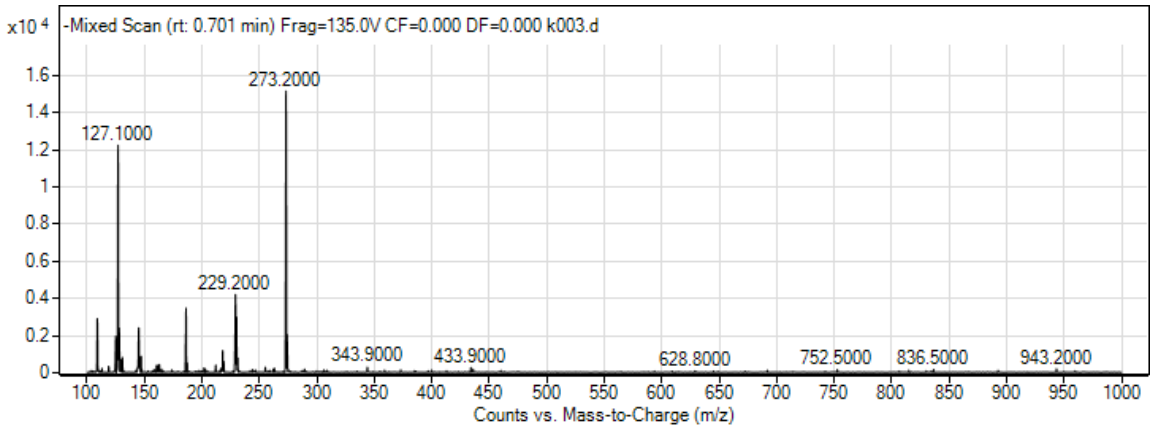

Appendix III: Doubling time calculation of HUVEC and MDA-MB-231

Doubling time of HUVEC

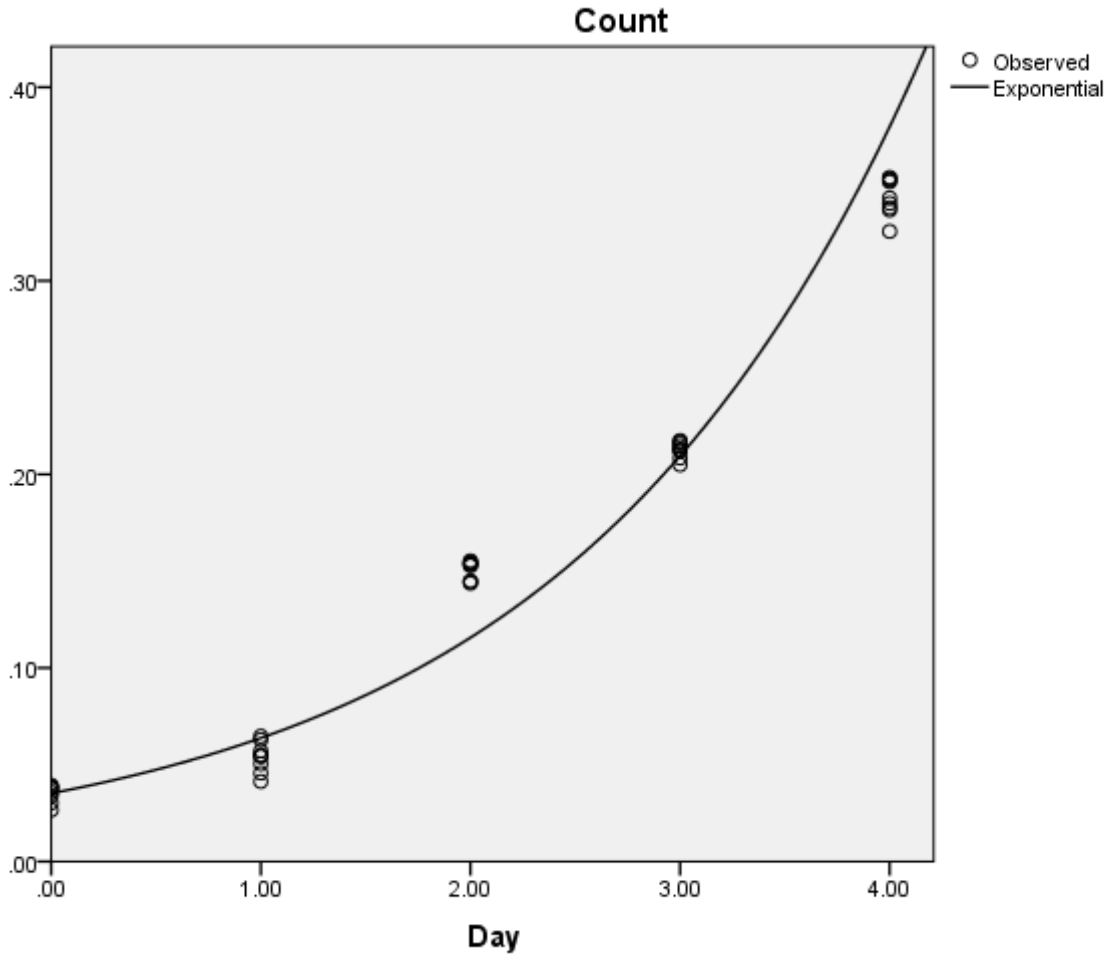

Figure 112: Cell Growth Fitting for HUVEC

Model Summary and Parameter Estimates

Dependent Variable: Count

	Model Summary					Parameter Estimates	
Equation	R Square	F	df1	df2	Sig.	Constant	b1
Exponential	.960	1034.090	1	43	.000	.035	.594

The independent variable is Day.

The doubling time of HUVEC cells: Td = (24/0.594) = 40.4 hrs

Doubling time of MDA-MB-231

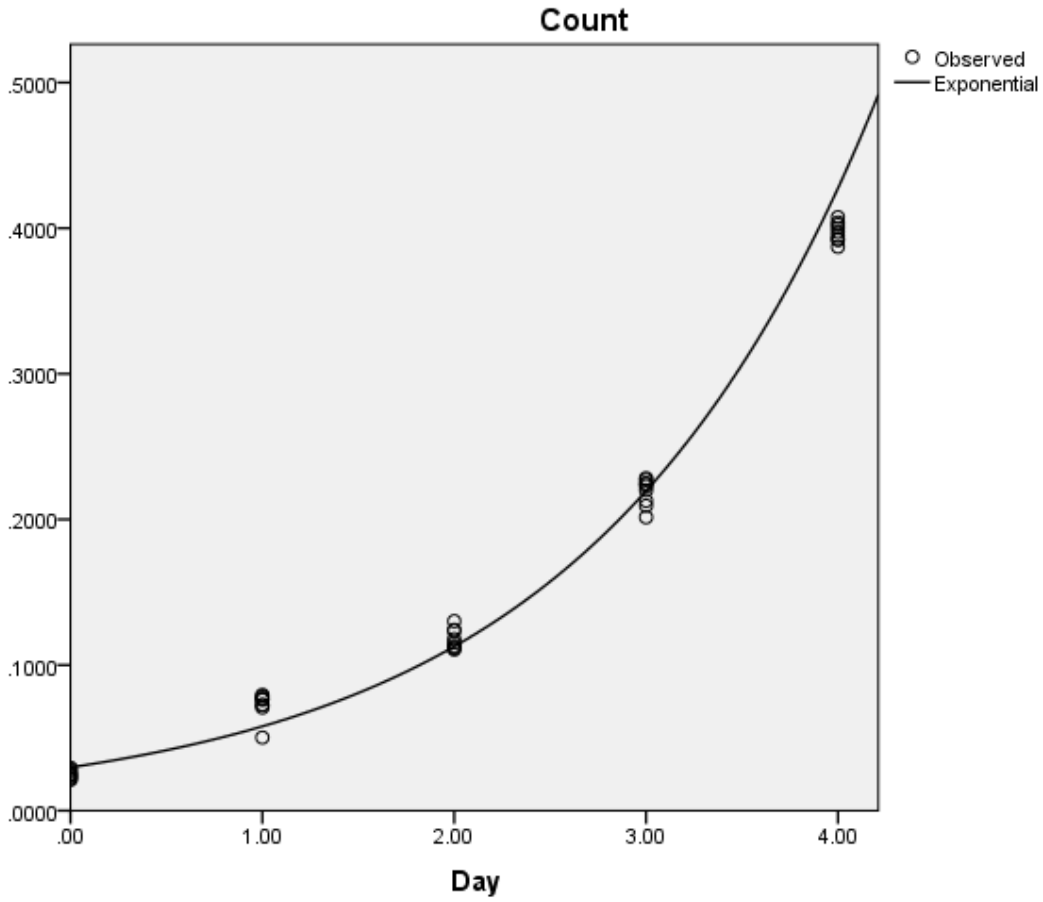

Figure 113: Cell Growth Fitting for MDA-MB-231

Model Summary and Parameter Estimates

Dependent Variable: Count

	Model Summary					Parameter Estimates	
Equation	R Square	F	df1	df2	Sig.	Constant	b1
Exponential	.973	1561.392	1	43	.000	.030	.666

The independent variable is Day.

The doubling time of MBA-MB-231 cells: Td = (24/0.666) = 36.04 hrs

Appendix IV: Tube formation of HUVEC cells in Matrigel from non-treatment, treatment of thalidomide and other analogues

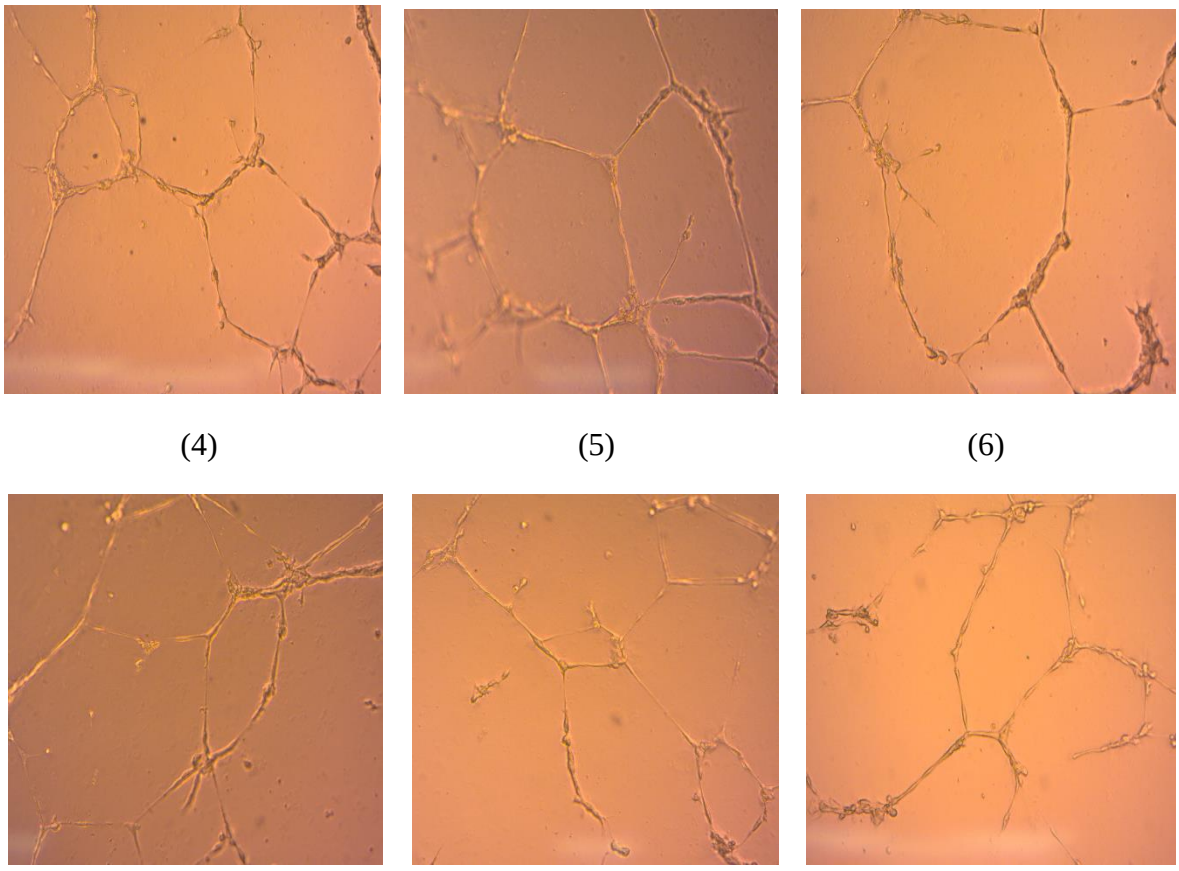

(4) (5) (6)

(7) (8) (9)

Figure 114: Tube Formation of HUVEC cells in Matrigel. Cells were treated with Medium only. There are nine viewing pictures that have been recorded.

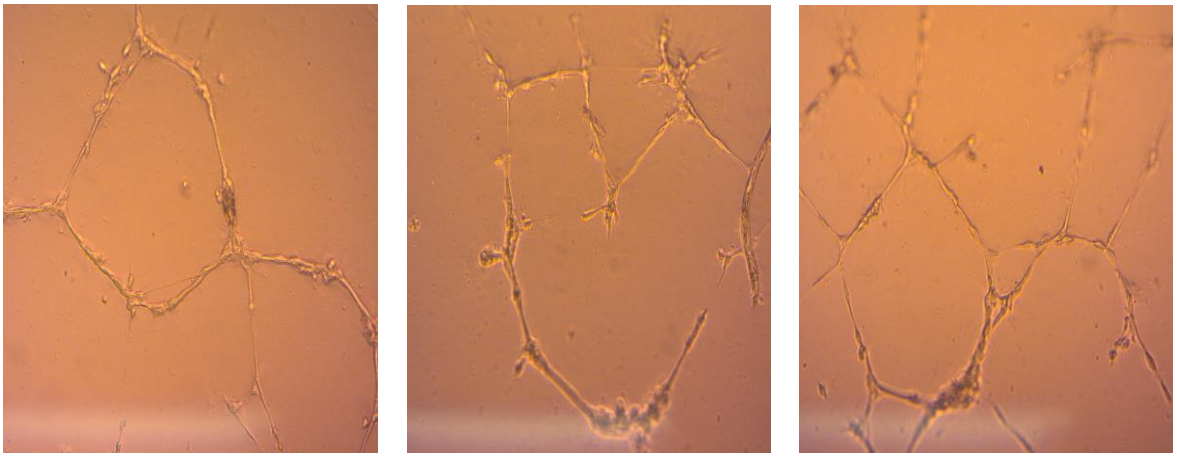

(4) (5) (6)

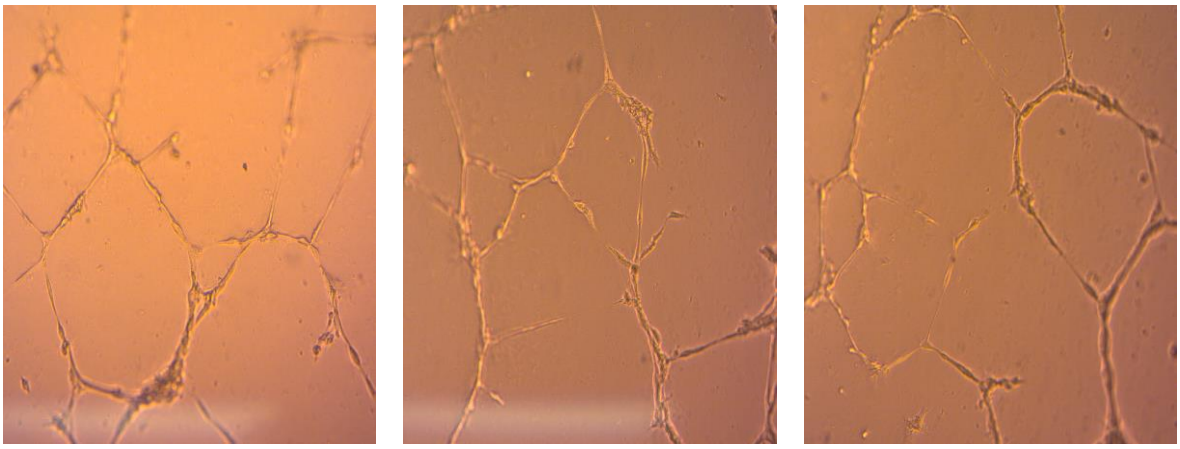

(7) (8) (9)

Figure 115: Tube Formation of HUVEC cells in Matrigel. Cells were treated with Medium with vehicle. There are nine viewing pictures that have been recorded.

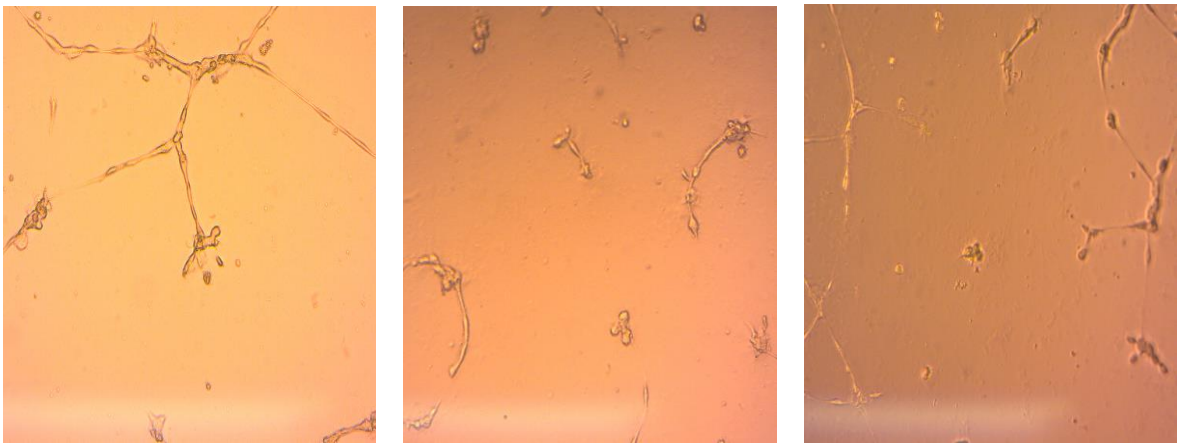

(4) (5) (6)

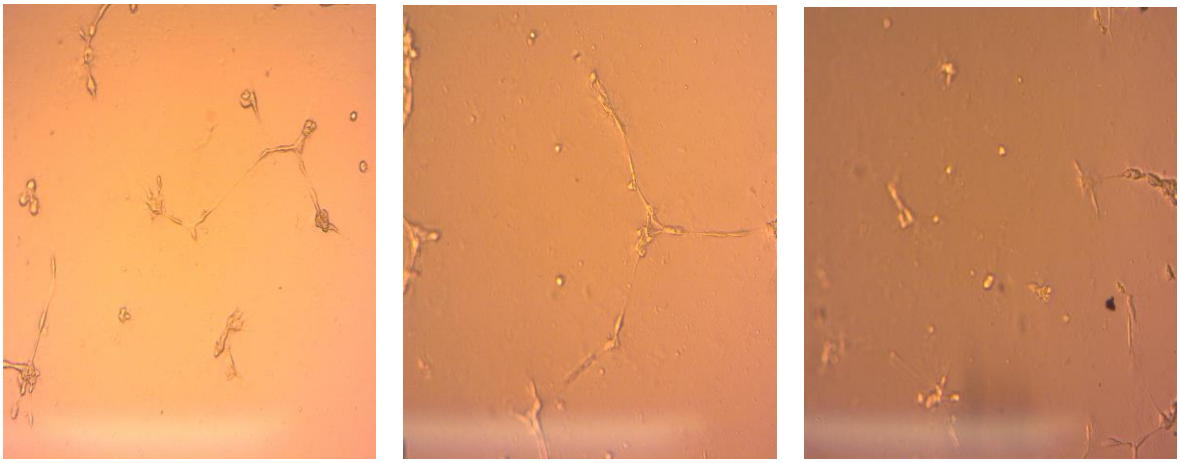

(7) (8) (9)

Figure 116: Tube Formation of HUVEC cells in Matrigel. Cells were treated with thalidomide in the concentration at 250 μg/mL. There are nine viewing pictures that have been recorded.

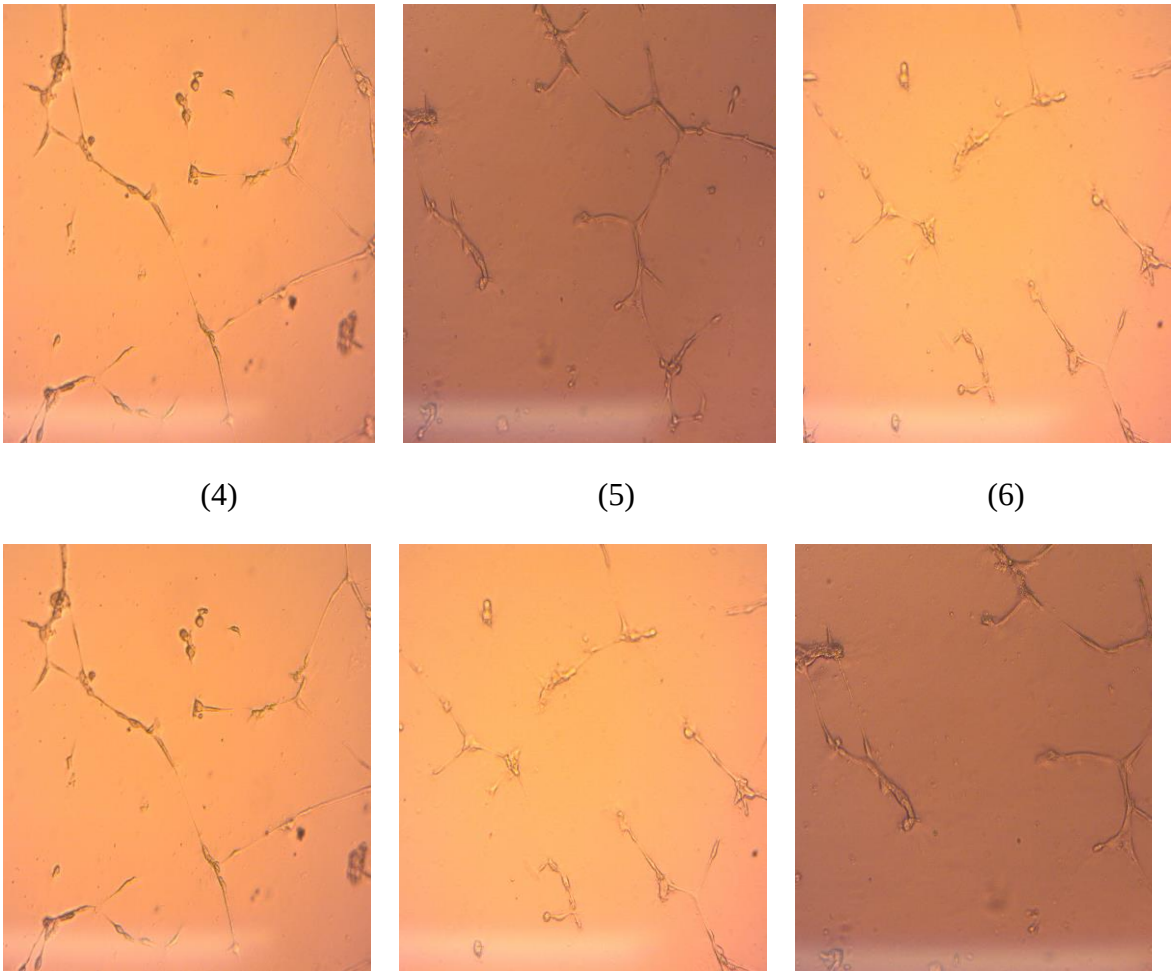

(4) (5) (6)

(7) (8) (9)

Figure 117: Tube Formation of HUVEC cells in Matrigel. Cells were treated with thalidomide in the concentration at 50 µg/mL. There are nine viewing pictures that have been recorded.

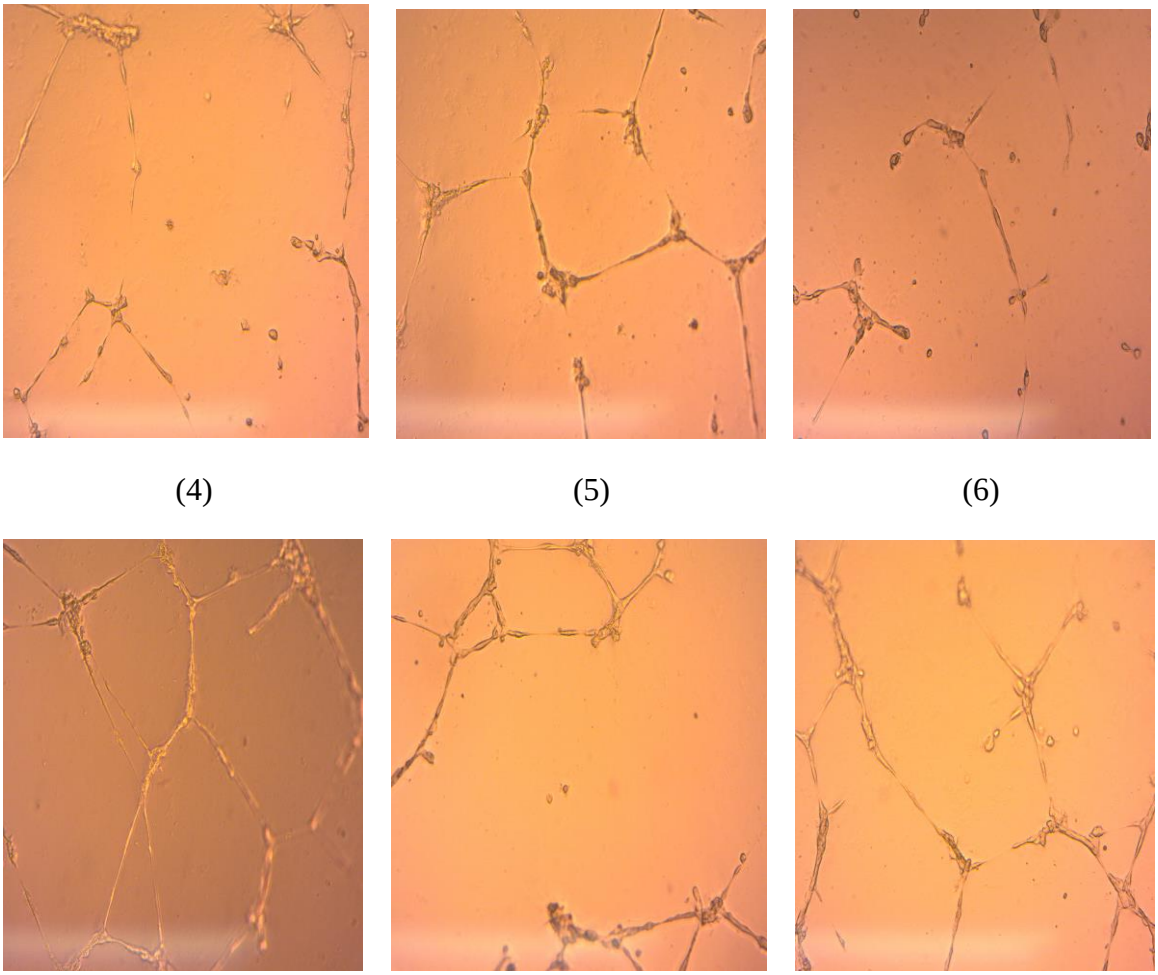

(4) (5) (6)

(7) (8) (9)

Figure 118: Tube Formation of HUVEC cells in Matrigel. Cells were treated with thalidomide in the concentration at 10 μg/mL. There are nine viewing pictures that have been recorded.

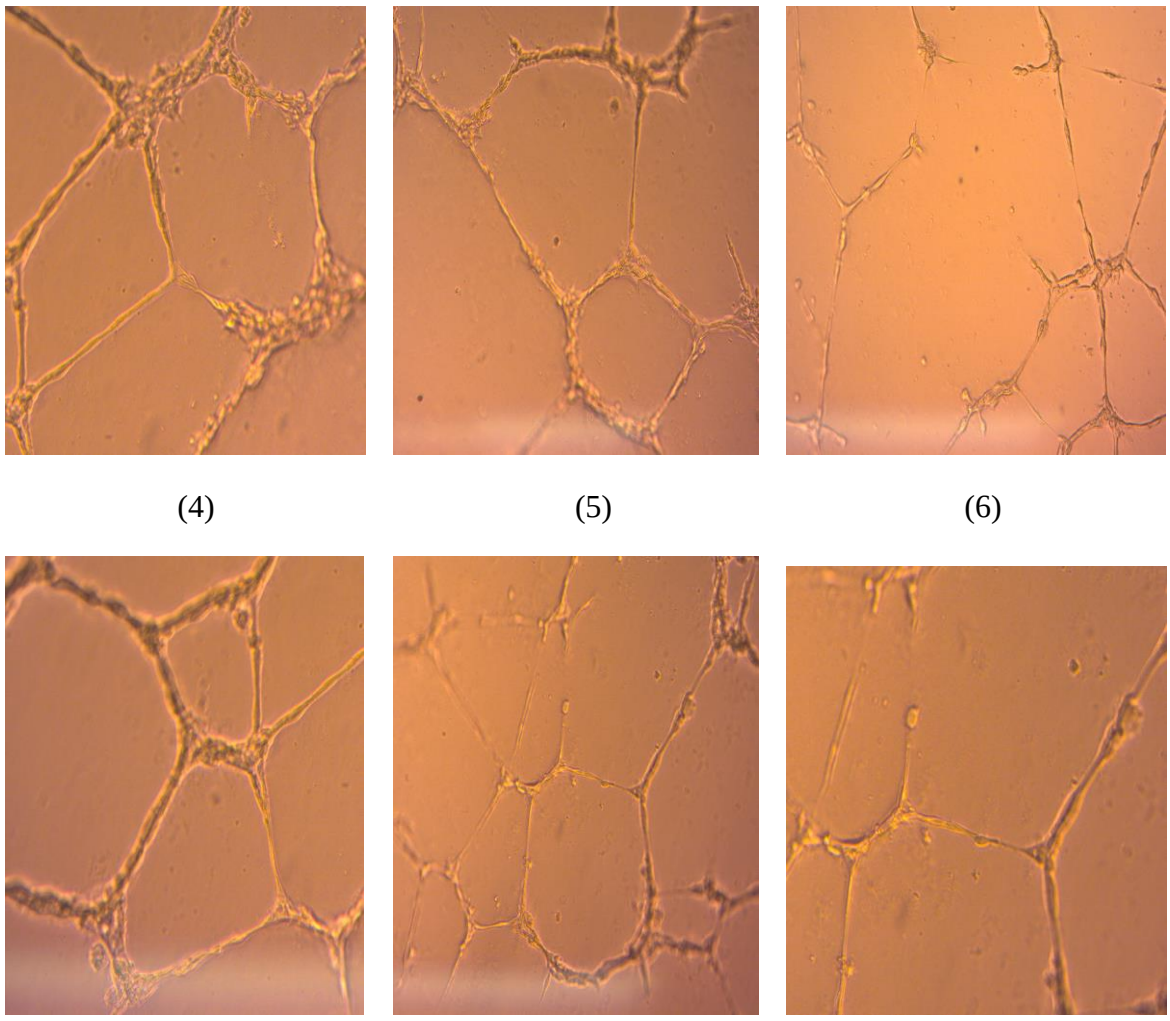

(4) (5) (6)

(7) (8) (9)

Figure 119: Tube Formation of HUVEC cells in Matrigel. Cells were treated with thalidomide in the concentration at 2 μg/mL. There are nine viewing pictures that have been recorded.

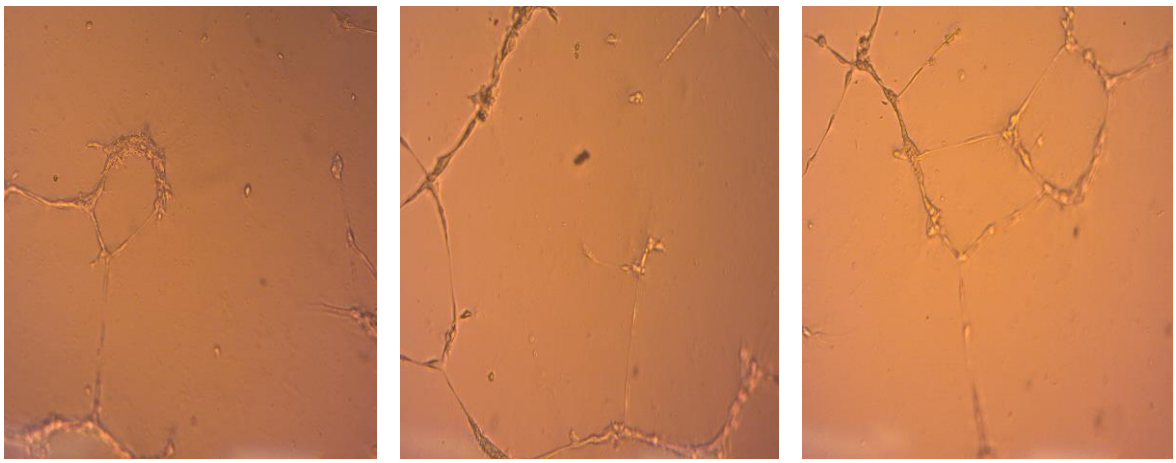

(4) (5) (6)

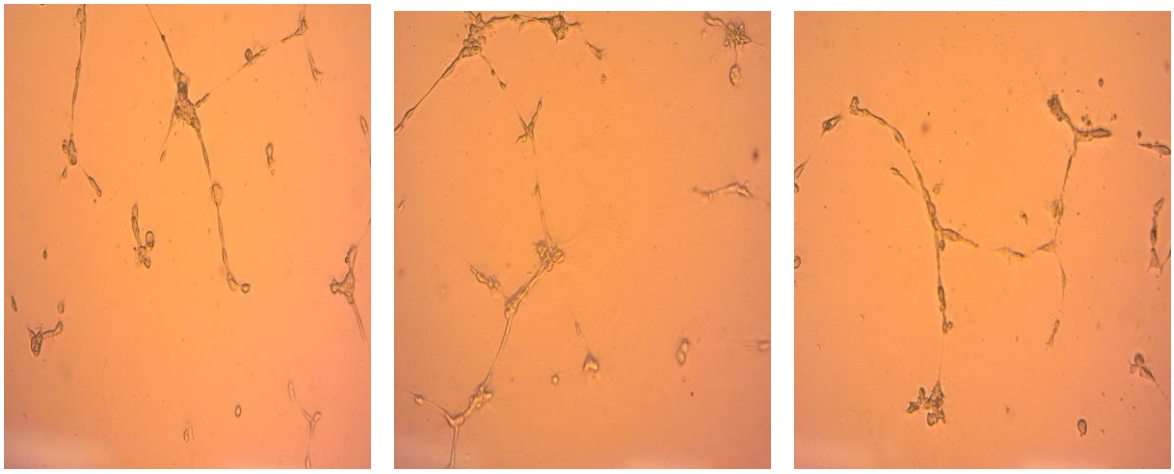

(7) (8) (9)

Figure 120: Tube Formation of HUVEC cells in Matrigel. Cells were treated with 2-(2, 6-dioxopiperidin-3-yl)-phthalimidine (EM-12) (Compound **2**) in the concentration at 250 µg/mL. There are nine viewing pictures that have been recorded.

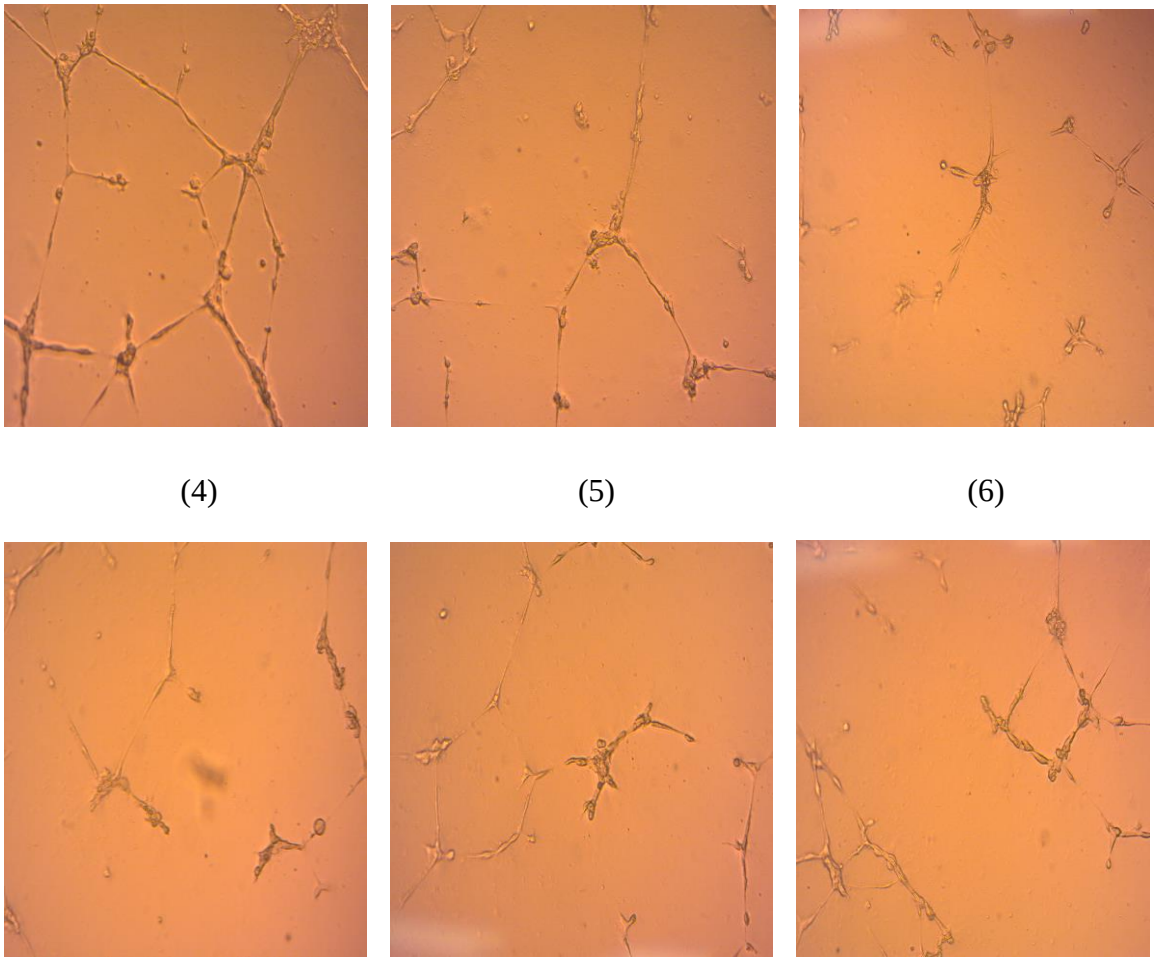

(4) (5) (6)

(7) (8) (9)

Figure 121: Tube Formation of HUVEC cells in Matrigel. Cells were treated with 2-(2, 6-dioxopiperidin-3-yl)-phthalimidine (EM-12) (Compound **2**) in the concentration at 50 µg/mL. There are nine viewing pictures that have been recorded.

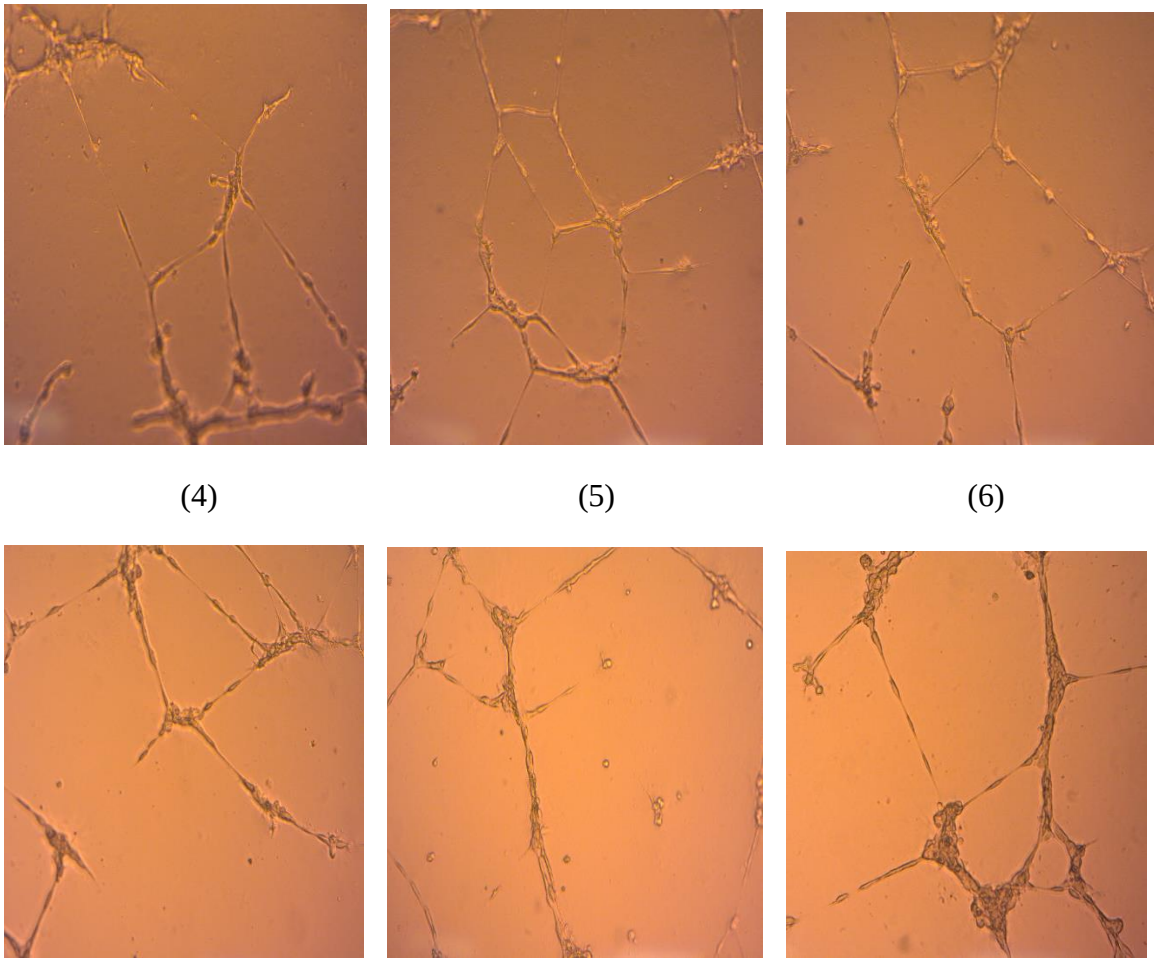

(4) (5) (6)

(7) (8) (9)

Figure 122: Tube Formation of HUVEC cells in Matrigel. Cells were treated with 2-(2, 6-dioxopiperidin-3-yl)-phthalimidine (EM-12) (Compound **2**) in the concentration at 10 μg/mL. There are nine viewing pictures that have been recorded.

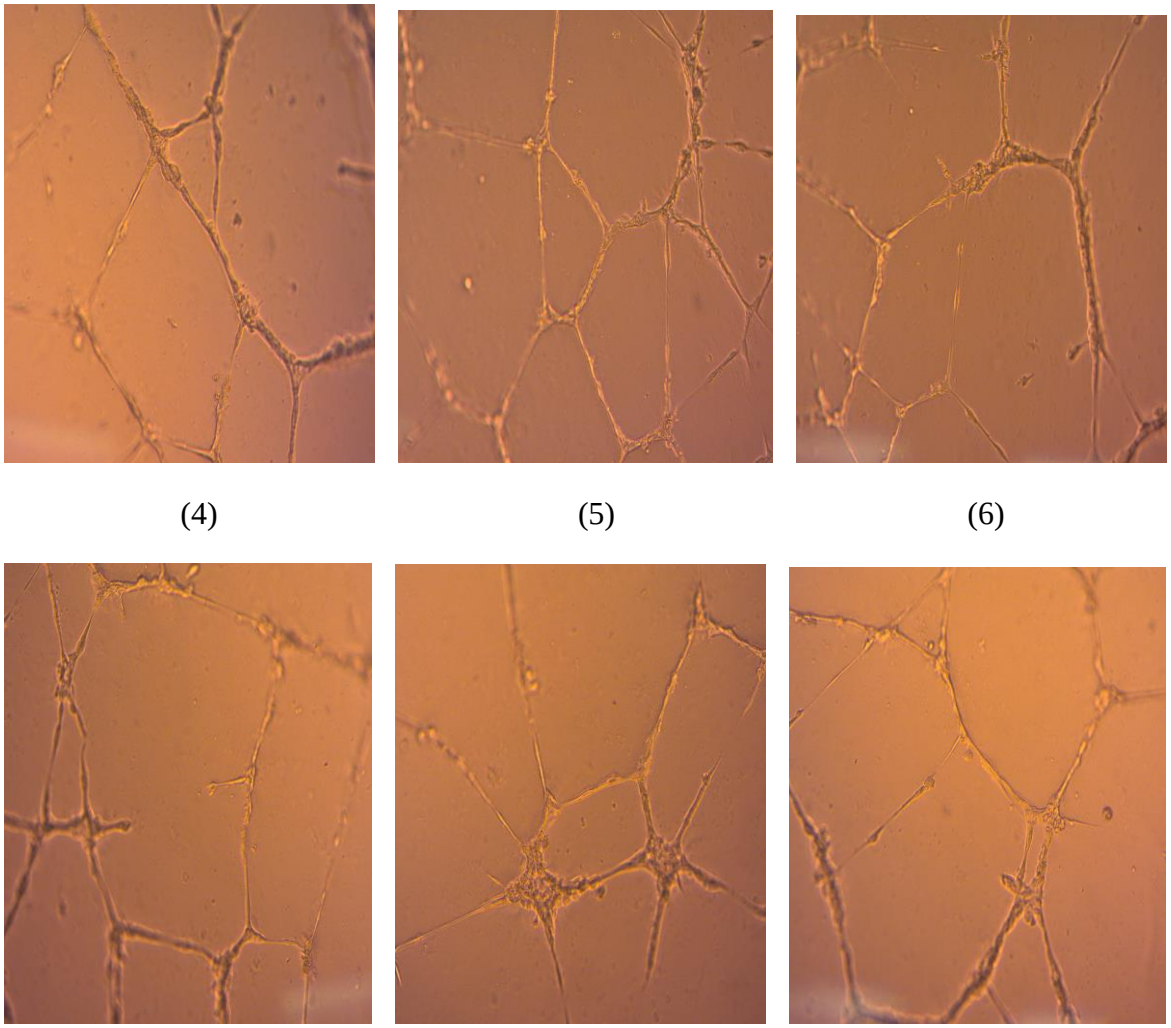

(4) (5) (6)

(7) (8) (9)

Figure 123: Tube Formation of HUVEC cells in Matrigel. Cells were treated with 2-(2, 6-dioxopiperidin-3-yl)-phthalimidine (EM-12) (Compound **2)** in the concentration at 2 μg/mL. There are nine viewing pictures that have been recorded.

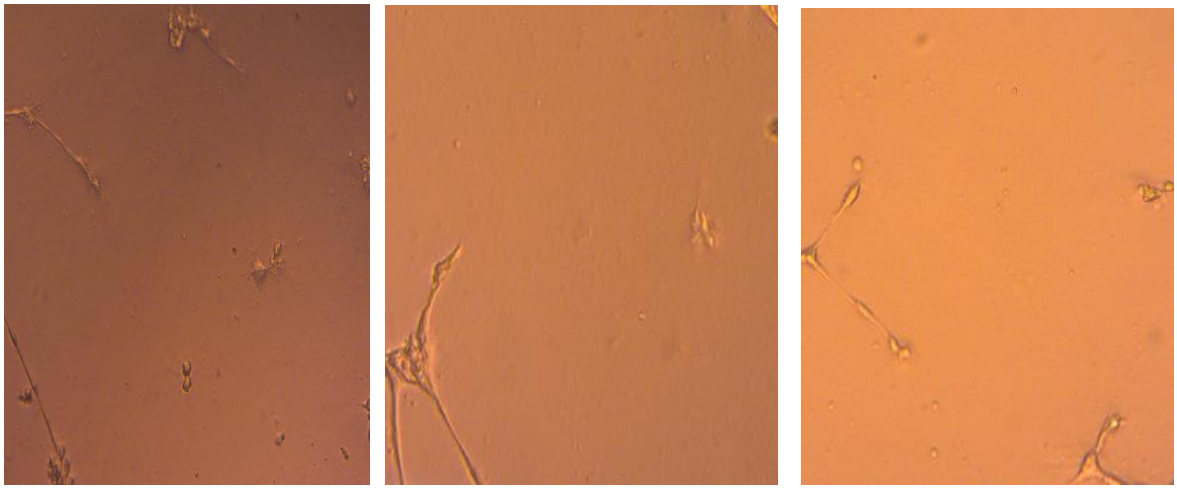

(4) (5) (6)

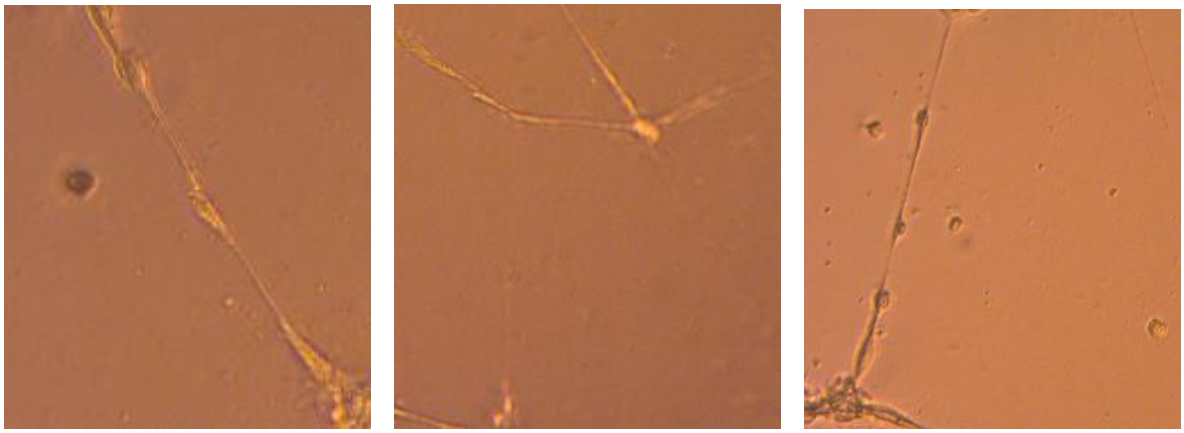

(7) (8) (9)

Figure 124: Tube Formation of HUVEC cells in Matrigel. Cells were treated with 3-[(1R)-1-hydroxy-1-methyl-3-oxo-1,3-dihydro-2H-isoindol-2-yl]piperidine-2,6-dione (Compound **3**) in the concentration at 250 μg/mL. There are nine viewing pictures that have been recorded.

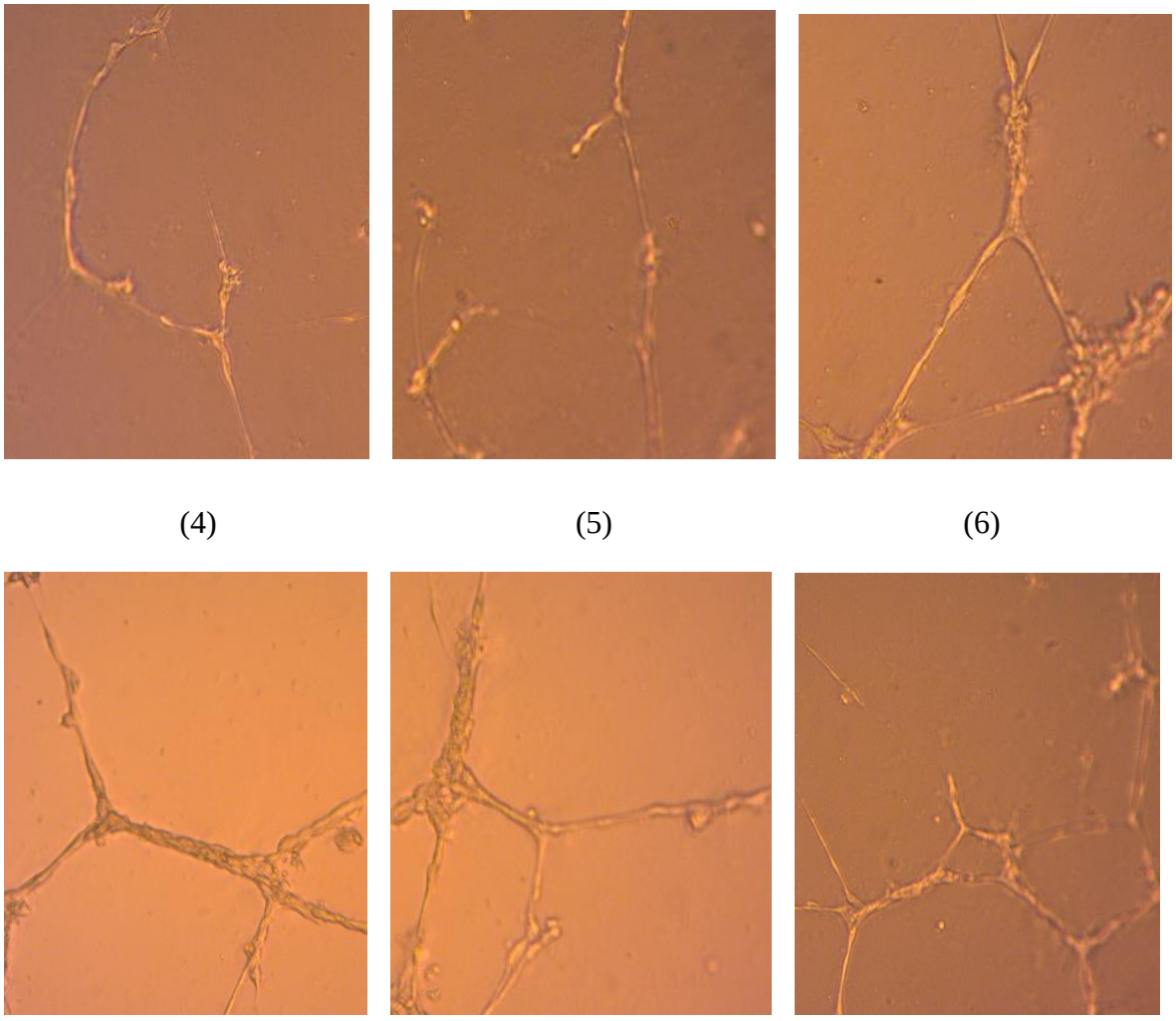

(4) (5) (6)

(7) (8) (9)

Figure 125: Tube Formation of HUVEC cells in Matrigel. Cells were treated with 3-[(1R)-1-hydroxy-1-methyl-3-oxo-1,3-dihydro-2H-isoindol-2-yl]piperidine-2,6-dione (Compound **3**) in the concentration at 50 μg/mL. There are nine viewing pictures that have been recorded.

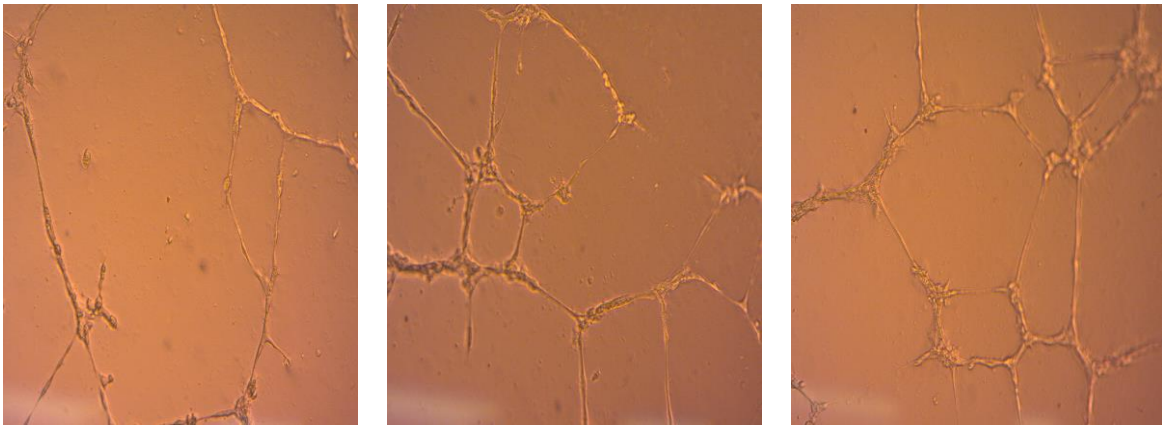

(4) (5) (6)

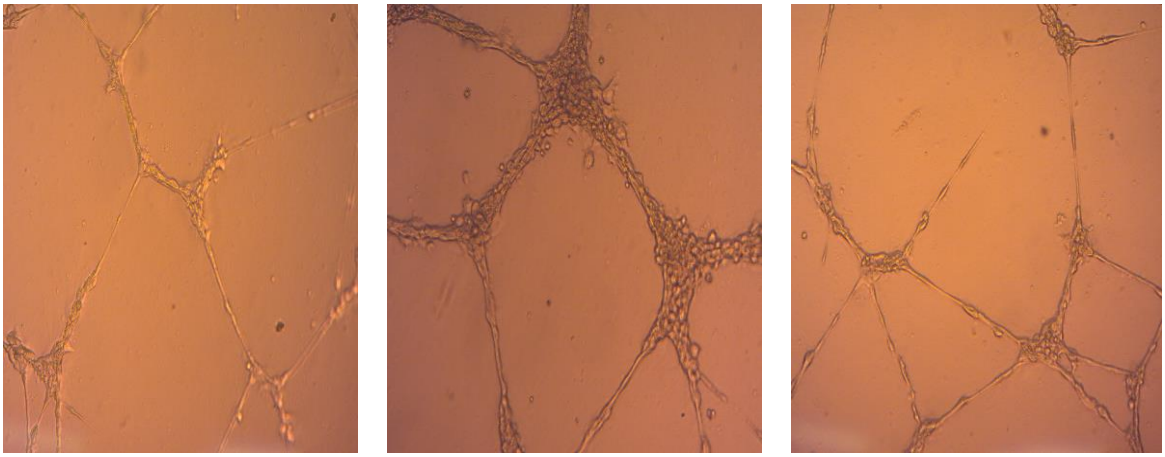

(7) (8) (9)

Figure 126: Tube Formation of HUVEC cells in Matrigel. Cells were treated with 3-[(1R)-1-hydroxy-1-methyl-3-oxo-1,3-dihydro-2H-isoindol-2-yl]piperidine-2,6-dione (Compound **3**) in the concentration at 10 μg/mL. There are nine viewing pictures that have been recorded.

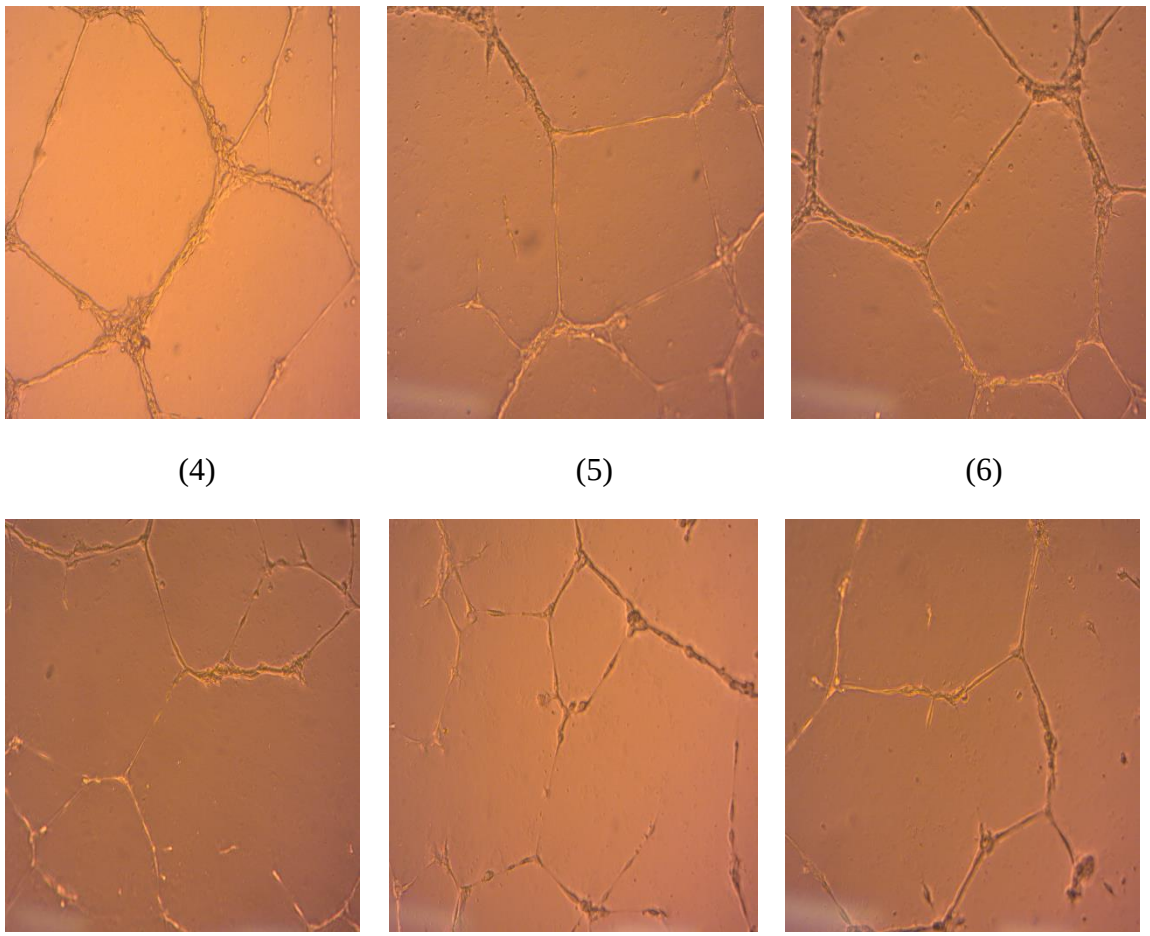

Figure 127: Tube Formation of HUVEC cells in Matrigel. Cells were treated with 3-[(1R)-1-hydroxy-1-methyl-3-oxo-1,3-dihydro-2H-isoindol-2-yl]piperidine-2,6-dione (Compound **3**) in the concentration at 2 μg/mL. There are nine viewing pictures that have been recorded.

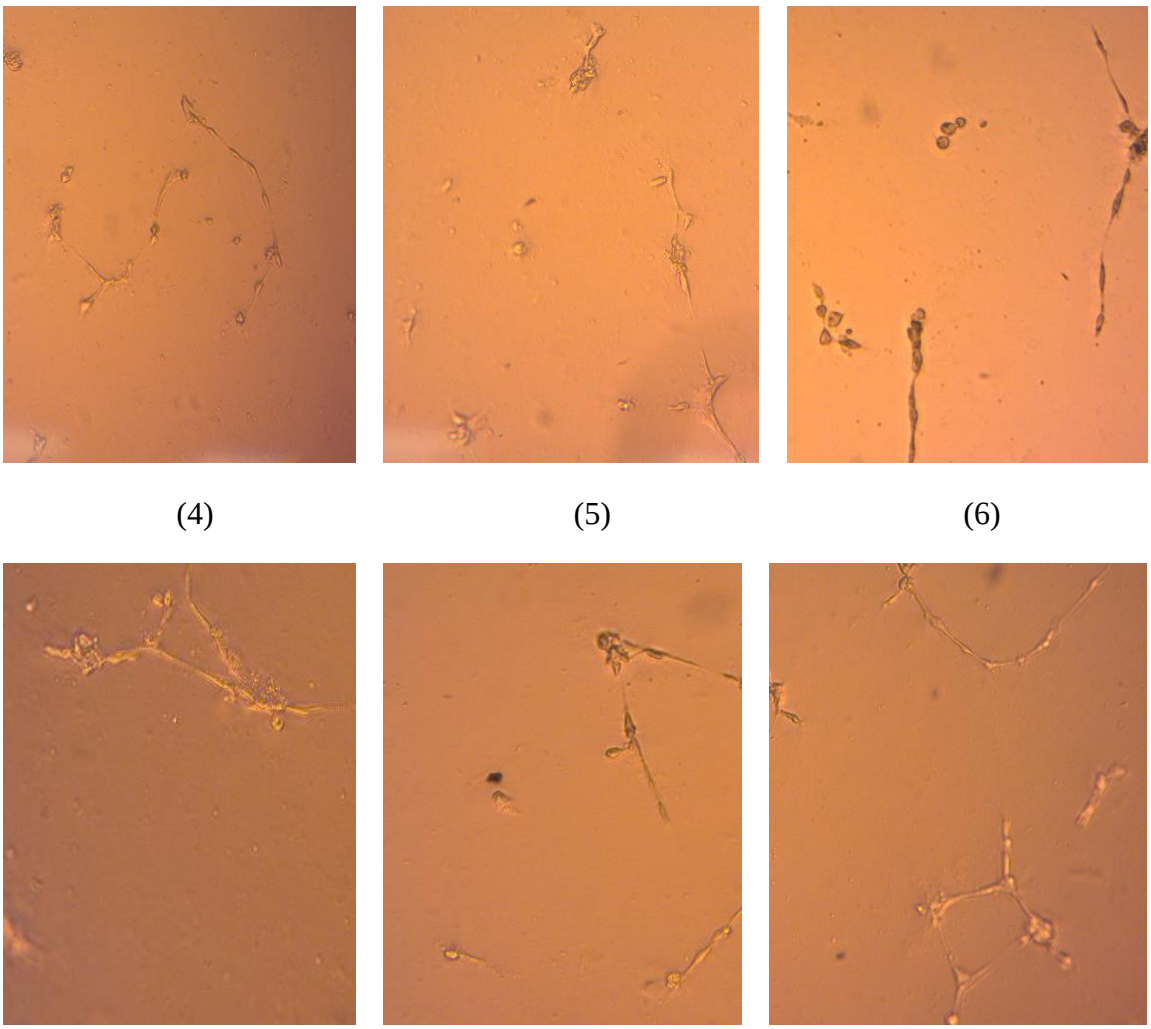

(4) (5) (6)

(7) (8) (9)

Figure 128: Tube Formation of HUVEC cells in Matrigel. Cells were treated with 3-[(1R)-1-hydroxy-1-methyl-3-oxo-1,3-dihydro-2H-isoindol-2-yl]piperidine-2,6-dione (Compound **3**) in the concentration at 2 μg/mL. There are nine viewing pictures that have been recorded.

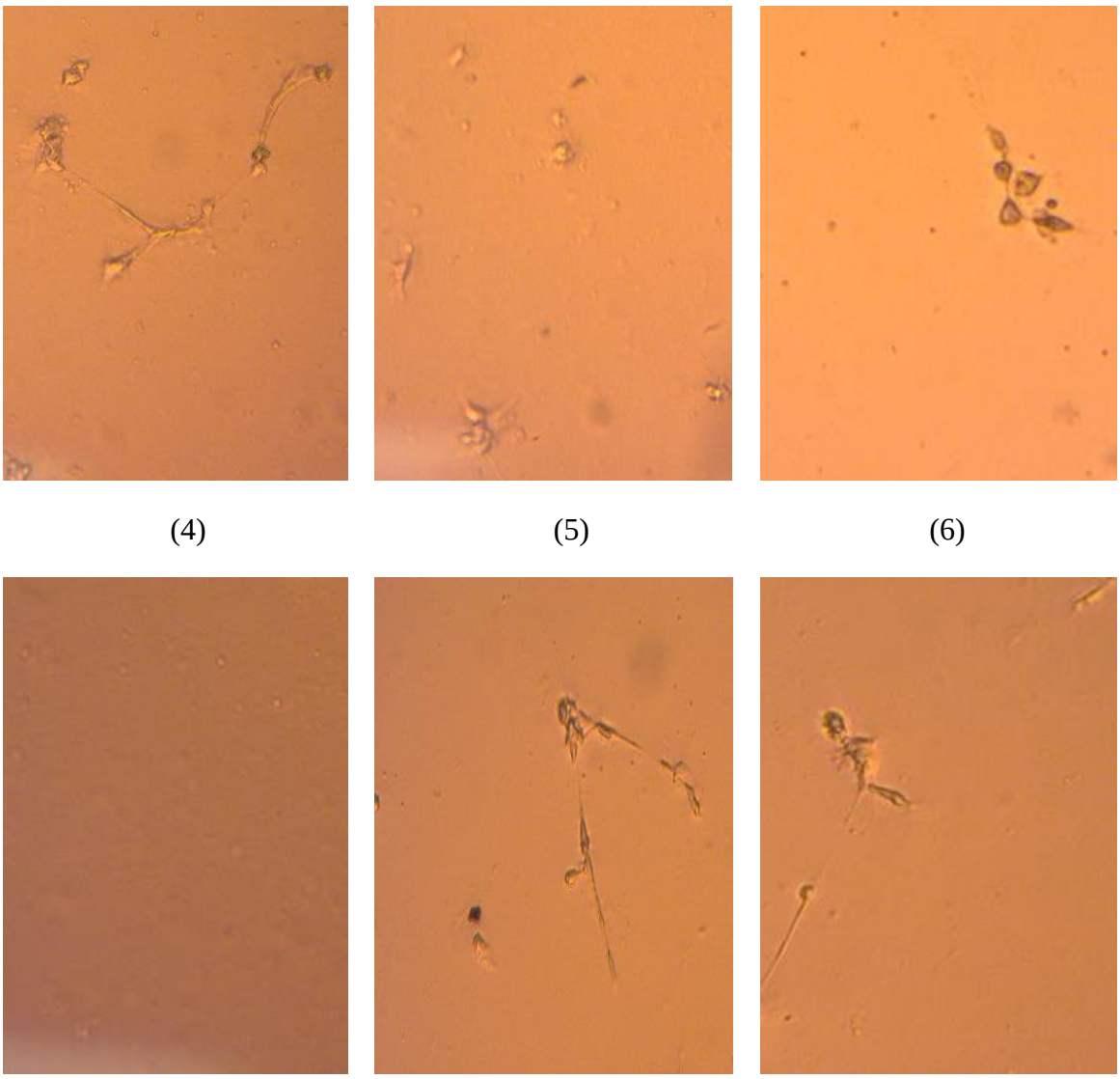

(4) (5) (6)

(7) (8) (9)

Figure 129: Tube Formation of HUVEC cells in Matrigel. Cells were treated with 3-[(1S)-1-hydroxy-1-methyl-3-oxo-1,3-dihydro-2H-isoindol-2-yl]piperidine-2,6-dione (Compound **4**) in the concentration at 250 μg/mL. There are nine viewing pictures that have been recorded.

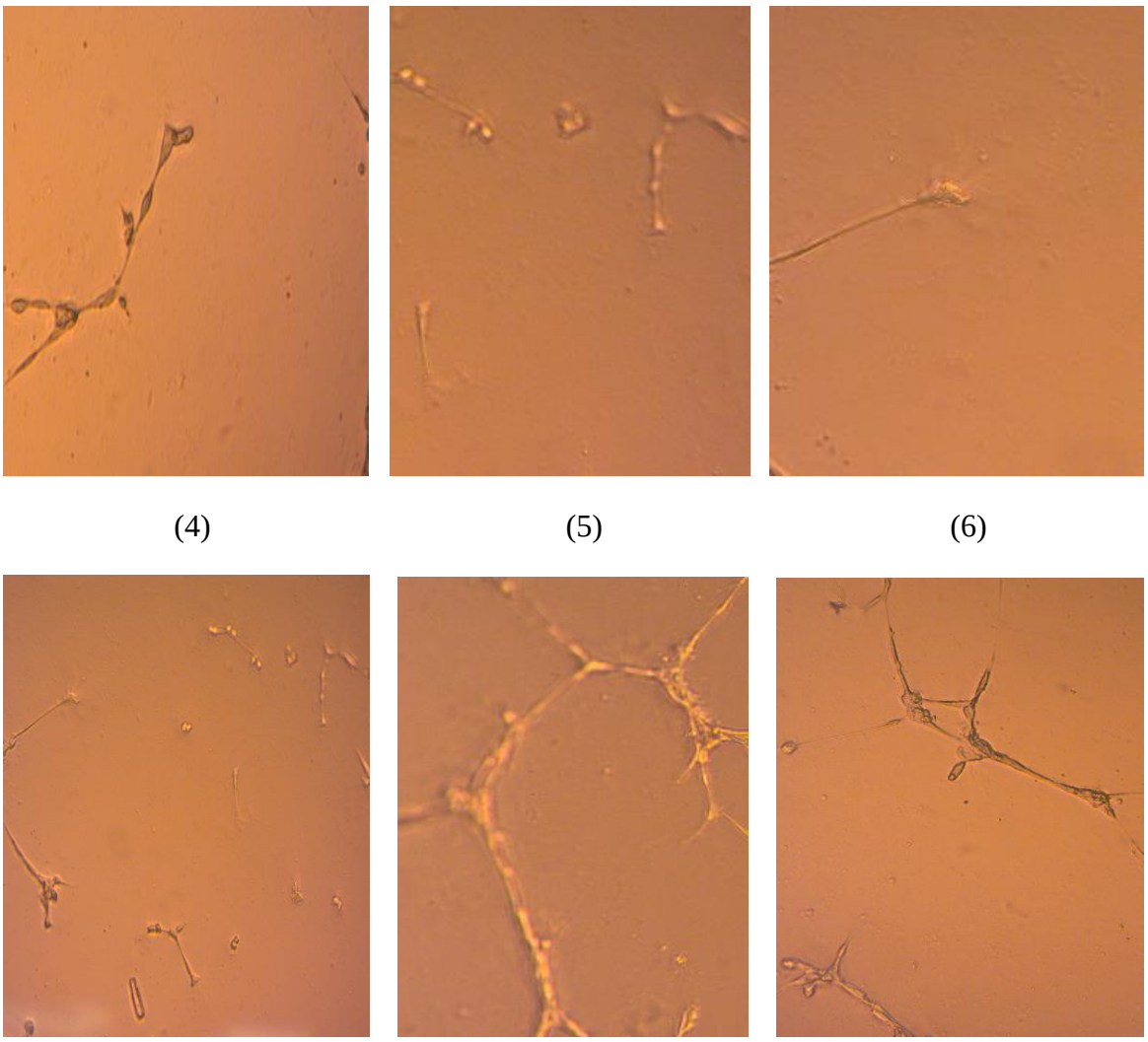

Figure 130: Tube Formation of HUVEC cells in Matrigel. Cells were treated with 3-[(1S)-1-hydroxy-1-methyl-3-oxo-1,3-dihydro-2H-isoindol-2-yl]piperidine-2,6-dione (Compound **4**) in the concentration at 50 μg/mL. There are nine viewing pictures that have been recorded.

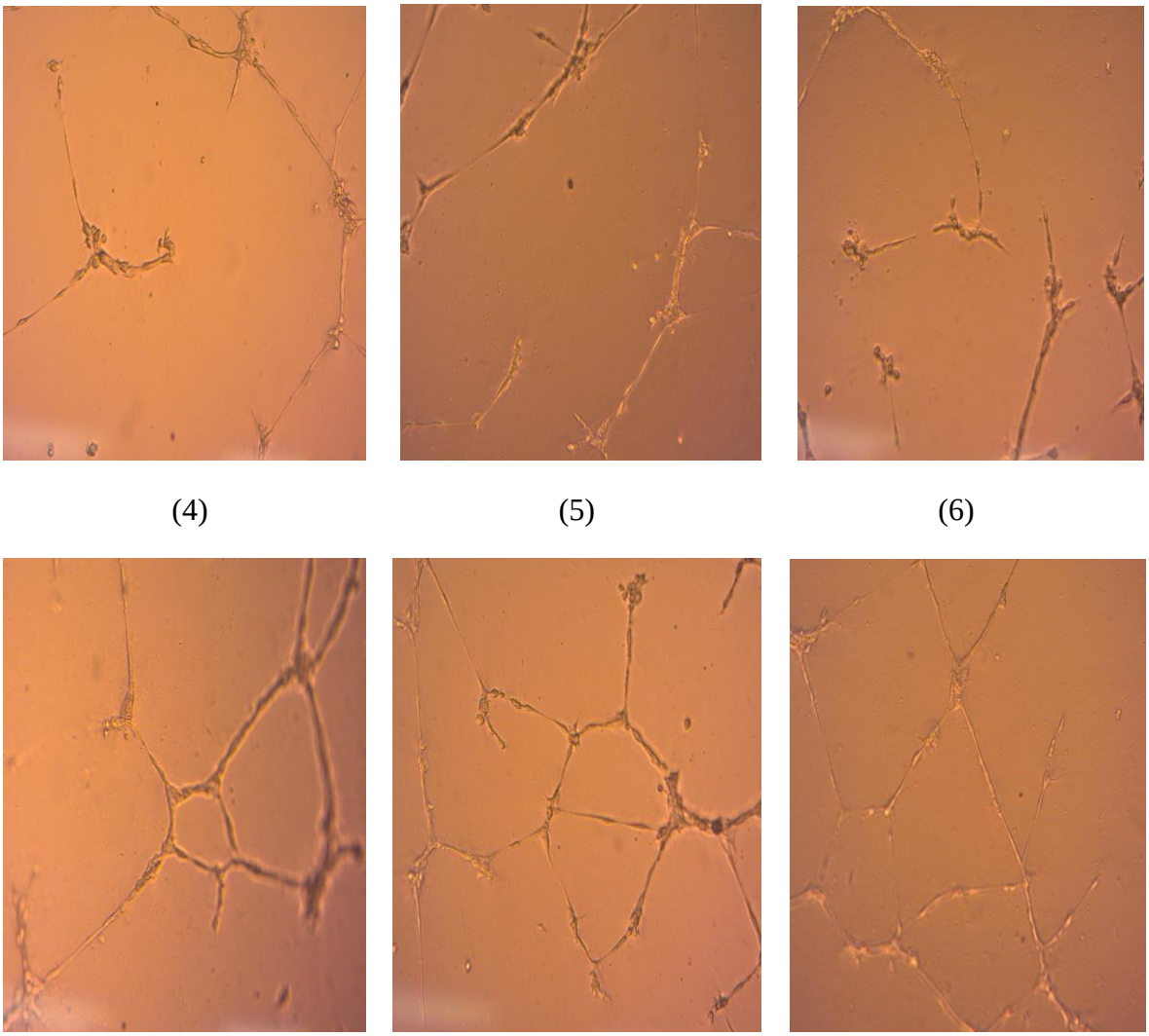

Figure 131: Tube Formation of HUVEC cells in Matrigel. Cells were treated with 3-[(1S)-1-hydroxy-1-methyl-3-oxo-1,3-dihydro-2H-isoindol-2-yl]piperidine-2,6-dione (Compound **4**) in the concentration at 10 μg/mL. There are nine viewing pictures that have been recorded.

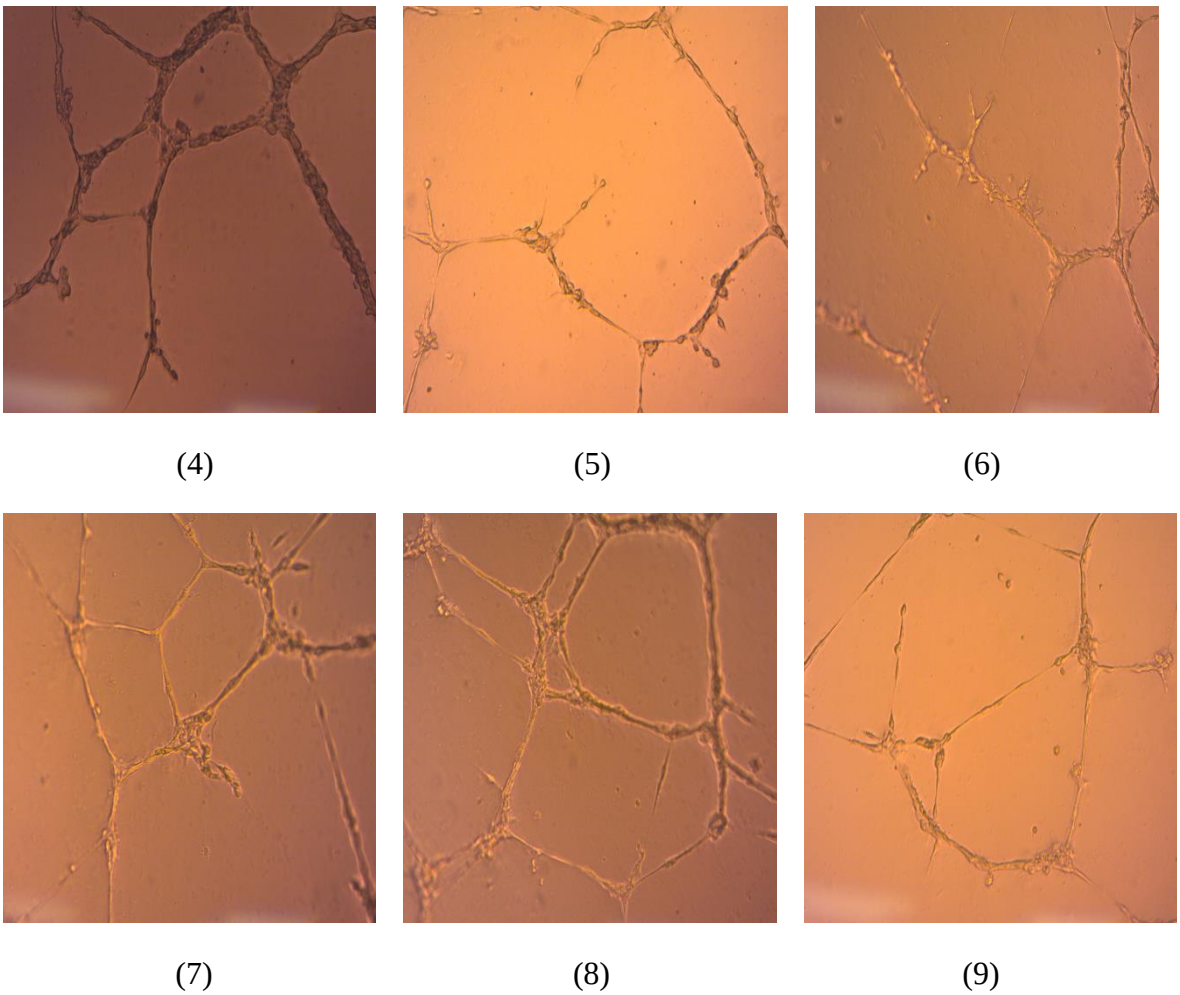

(4) (5) (6)

(7) (8) (9)

Figure 132: Tube Formation of HUVEC cells in Matrigel. Cells were treated with 3-[(1S)-1-hydroxy-1-methyl-3-oxo-1,3-dihydro-2H-isoindol-2-yl]piperidine-2,6-dione (Compound **4**) in the concentration at 2 μg/mL. There are nine viewing pictures that have been recorded

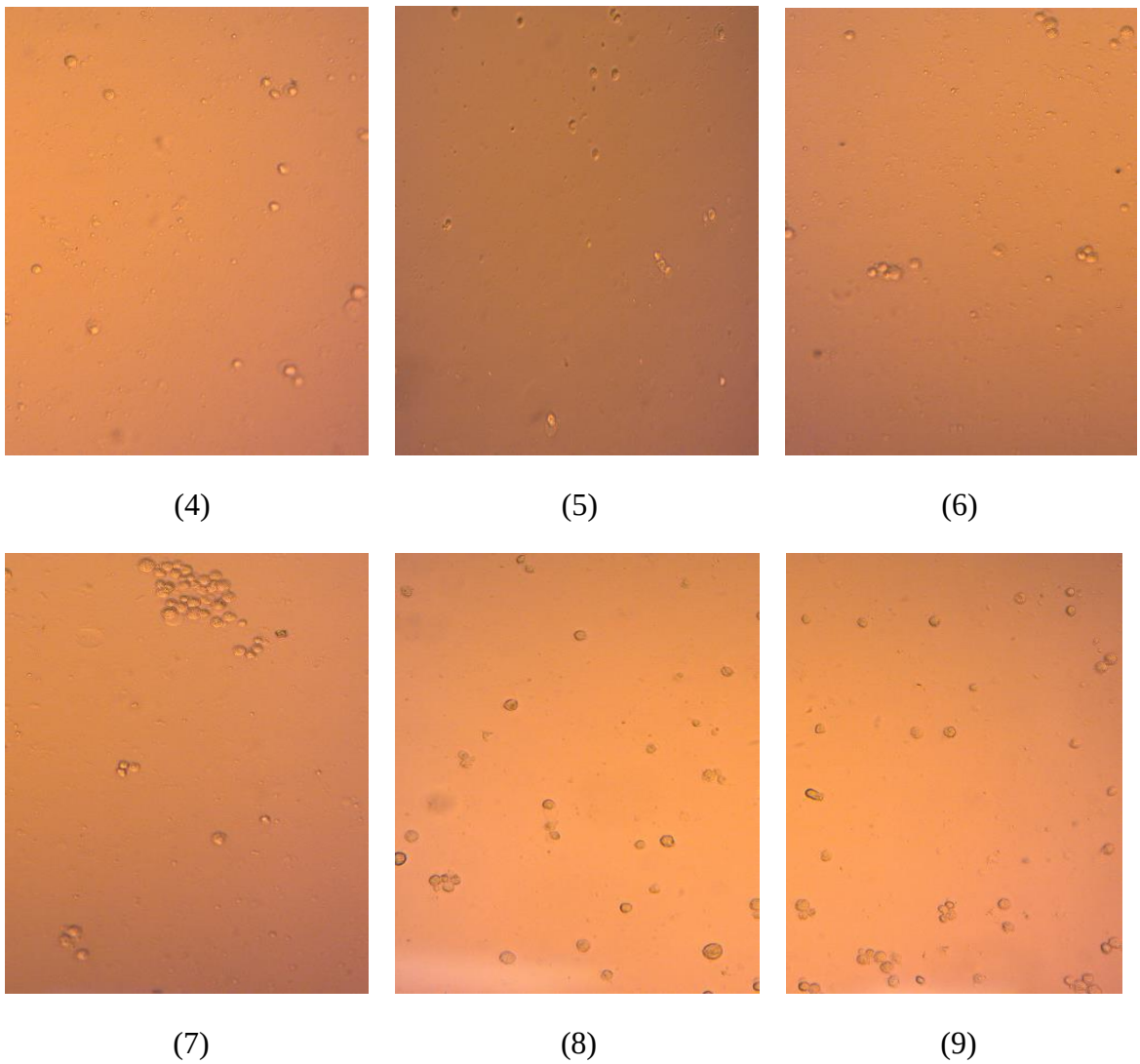

Figure 133: Tube Formation of HUVEC cells in Matrigel. Cells were treated with 2-(1-Chloromethyl-2,6-dioxopiperidin-3-yl)phthalimidine (Compound **5**) in the concentration at 250 μg/mL. There are nine viewing pictures that have been recorded.

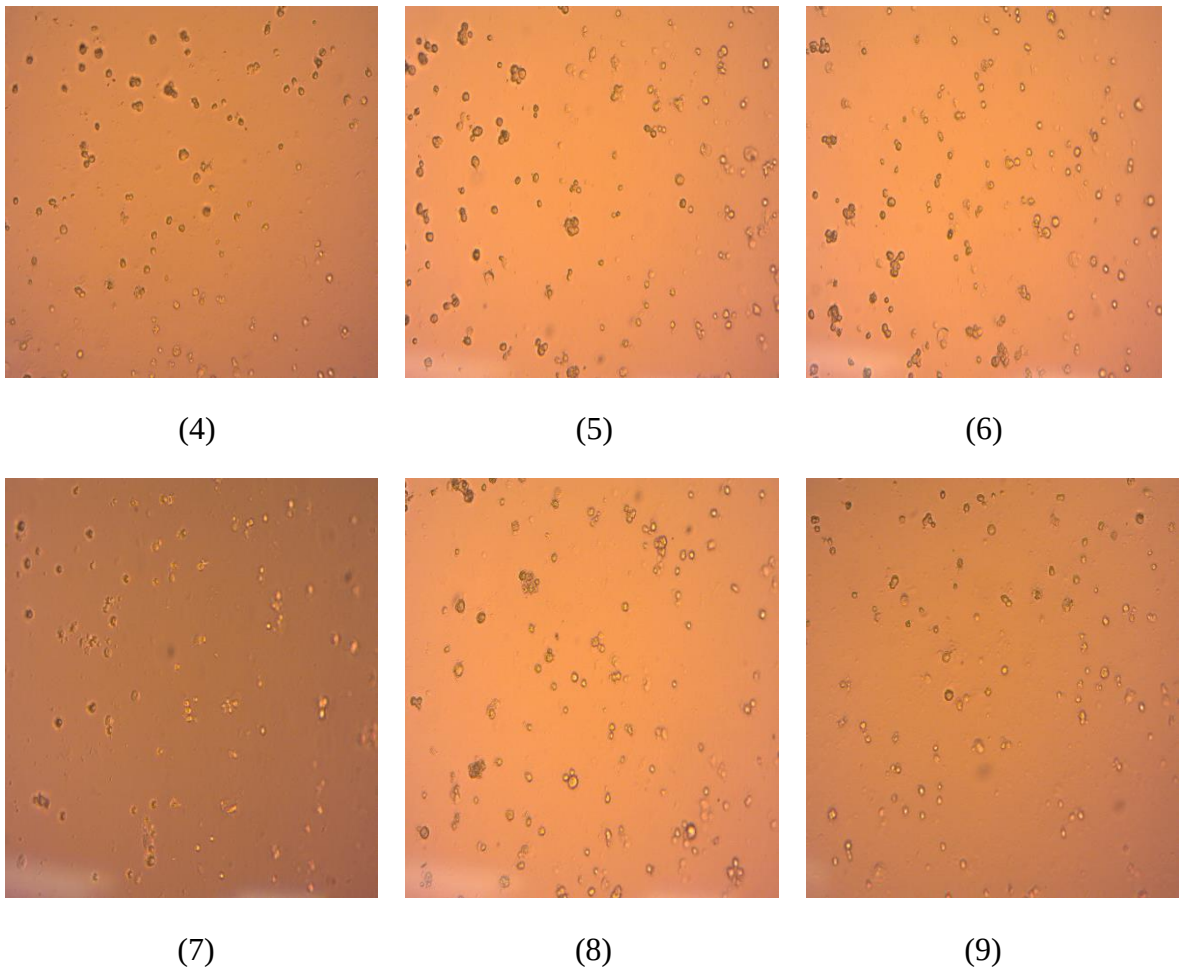

Figure 134: Tube Formation of HUVEC cells in Matrigel. Cells were treated with 2-(1-Chloromethyl-2, 6-dioxopiperidin-3-yl)phthalimidine (Compound **5**) in the concentration at 50 µg/mL. There are nine viewing pictures that have been recorded.

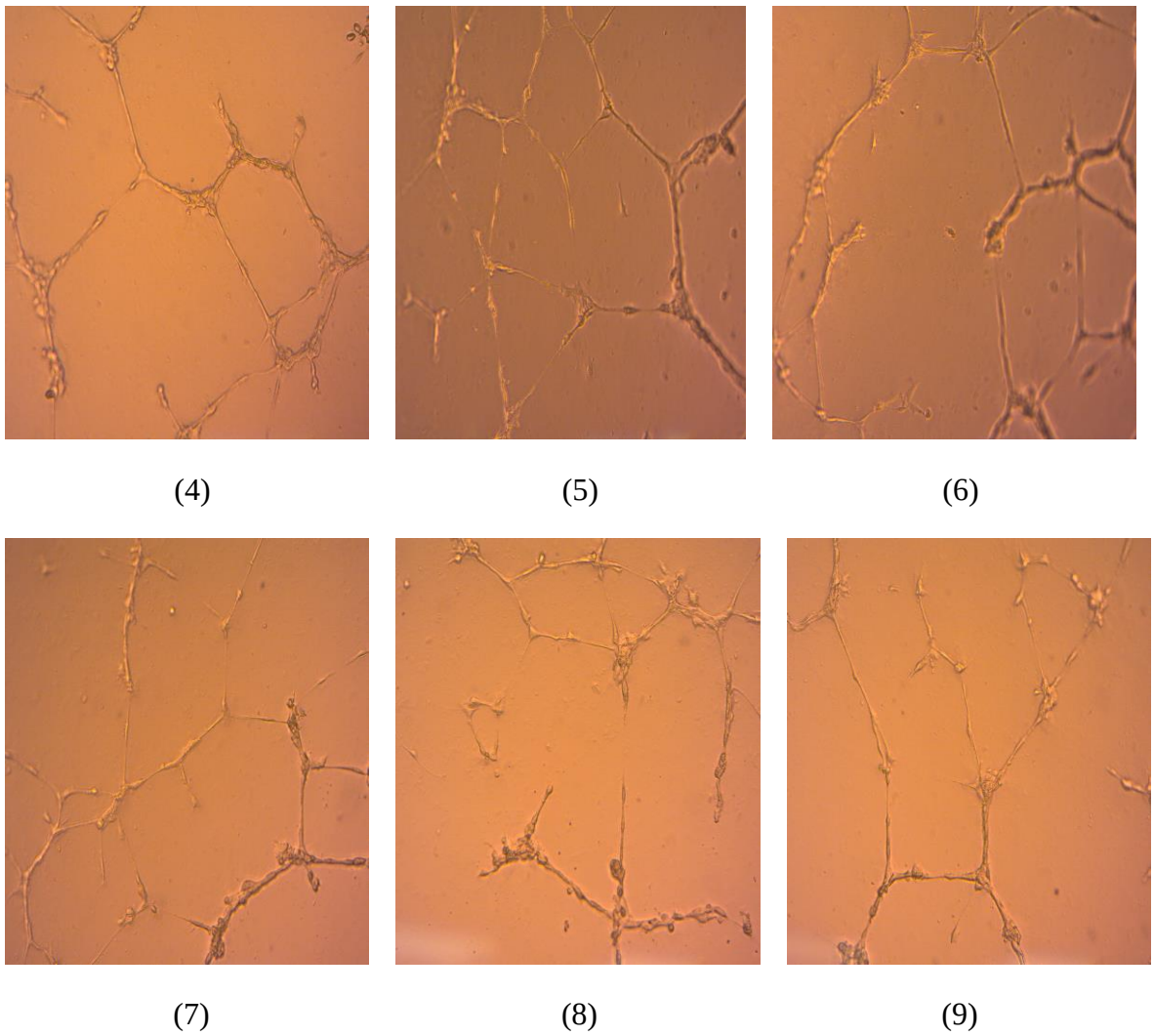

Figure 135: Tube Formation of HUVEC cells in Matrigel. Cells were treated with 2-(1-Chloromethyl-2, 6-dioxopiperidin-3-yl)phthalimidine (Compound **5**) in the concentration at 10 µg/mL. There are nine viewing pictures that have been recorded.

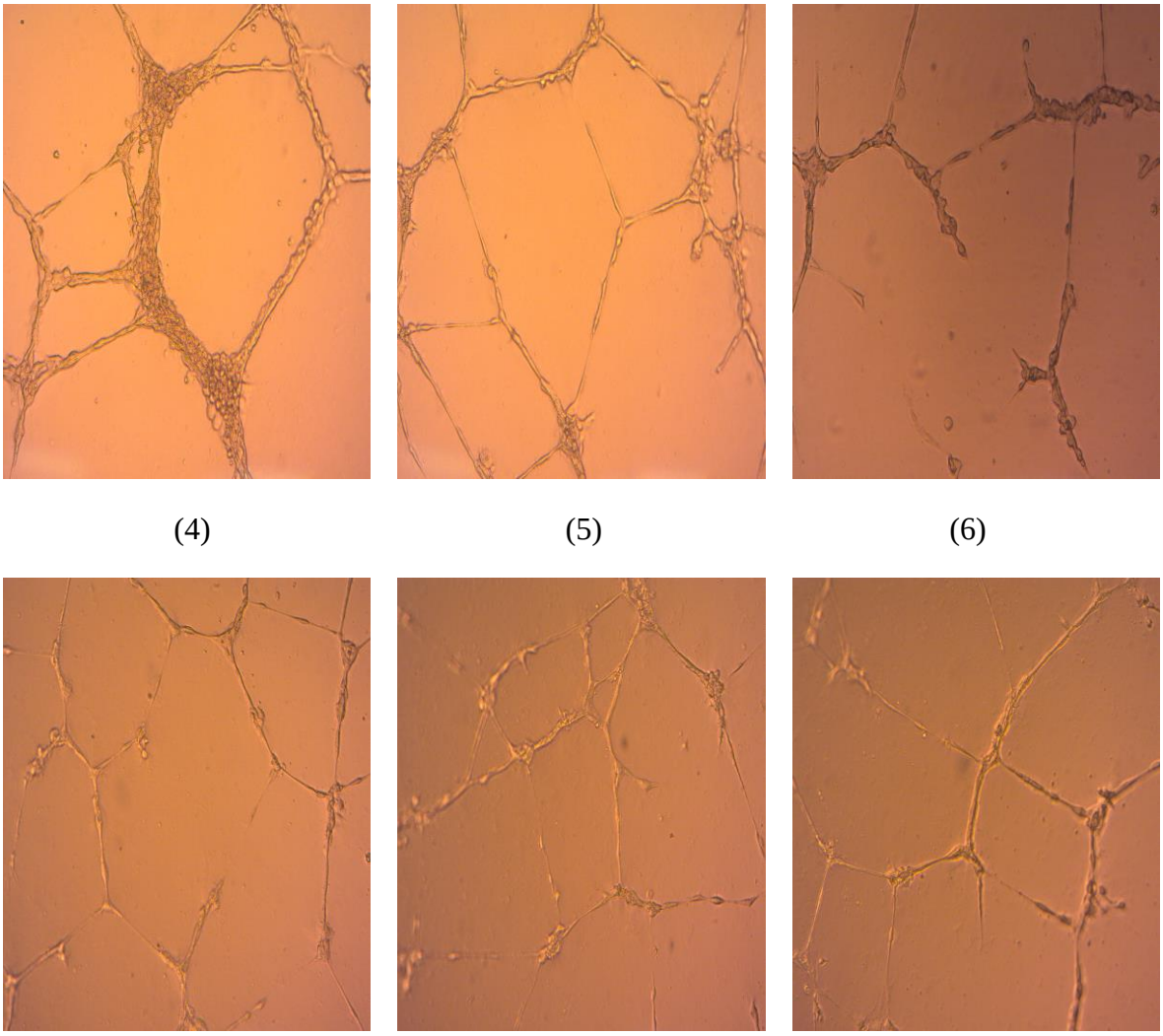

(4) (5) (6)

(7) (8) (9)

Figure 136: Tube Formation of HUVEC cells in Matrigel. Cells were treated with 2-(1-Chloromethyl-2, 6-dioxopiperidin-3-yl)phthalimidine (Compound **5**) in the concentration at 2 μg/mL. There are nine viewing pictures that have been recorded.

Appendix V: MDA-MB-231 Cell cycle distribution results from non-treatment, treatment of thalidomide and other analogues

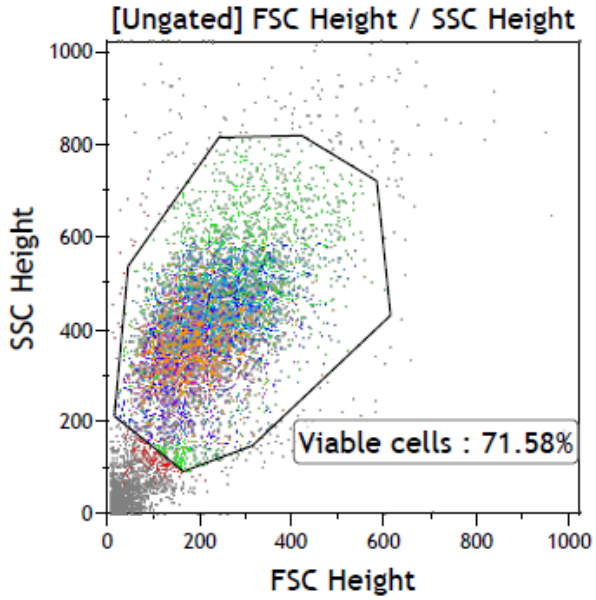

Figure 137: MDA-MB-231 Cell cycle distribution without any treatment at Day 0 & Cell Cycle Described in Dot Plot; FSC: Forward Scatter allows for the discrimination of cells by size & SSC: Side Scatter allows for the discrimination of cell about internal complexity.

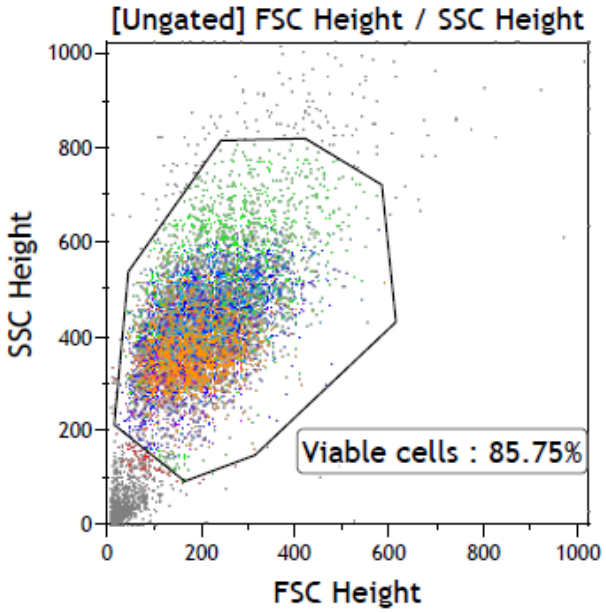

Figure 138: MDA-MB-231 Cell cycle distribution without any treatment at Day 3 at 72 hours & Cell Cycle Described in Dot Plot; FSC: Forward Scatter allows for the discrimination of cells by size & SSC: Side Scatter allows for the discrimination of cell about internal complexity.

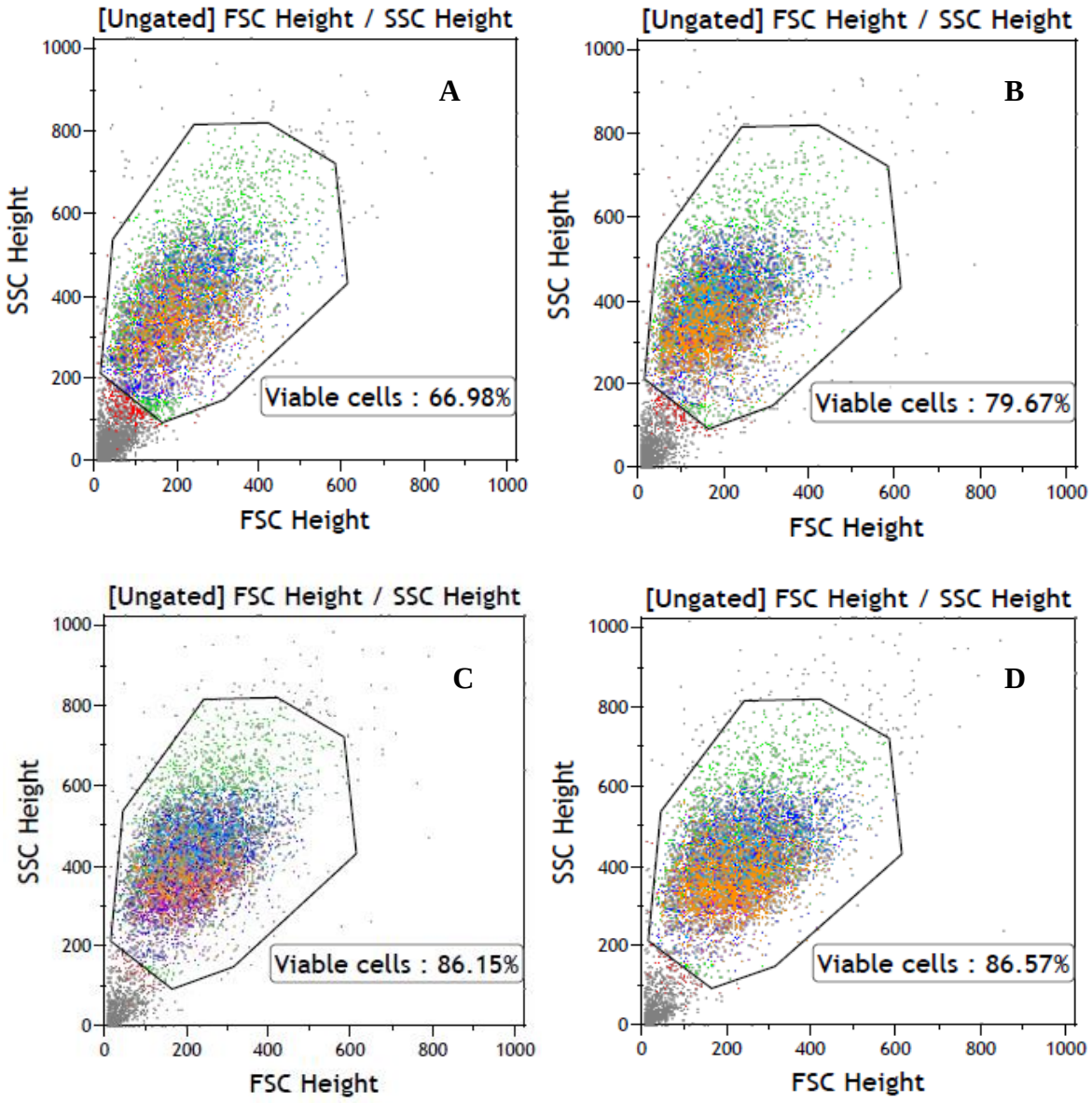

Figure 139: MDA-MB-231 Cell cycle distribution without any treatment of thalidomide on Day 3 at 72 hours & Cell Cycle Described in Dot Plot; The treatment concentration of thalidomide includes: 500 µg/mL (A); 100 µg/mL (B); 10 µg/mL (C) & 1 µg/mL (D). FSC: Forward Scatter allows for the discrimination of cells by size & SSC: Side Scatter allows for the discrimination of cell about internal complexity.

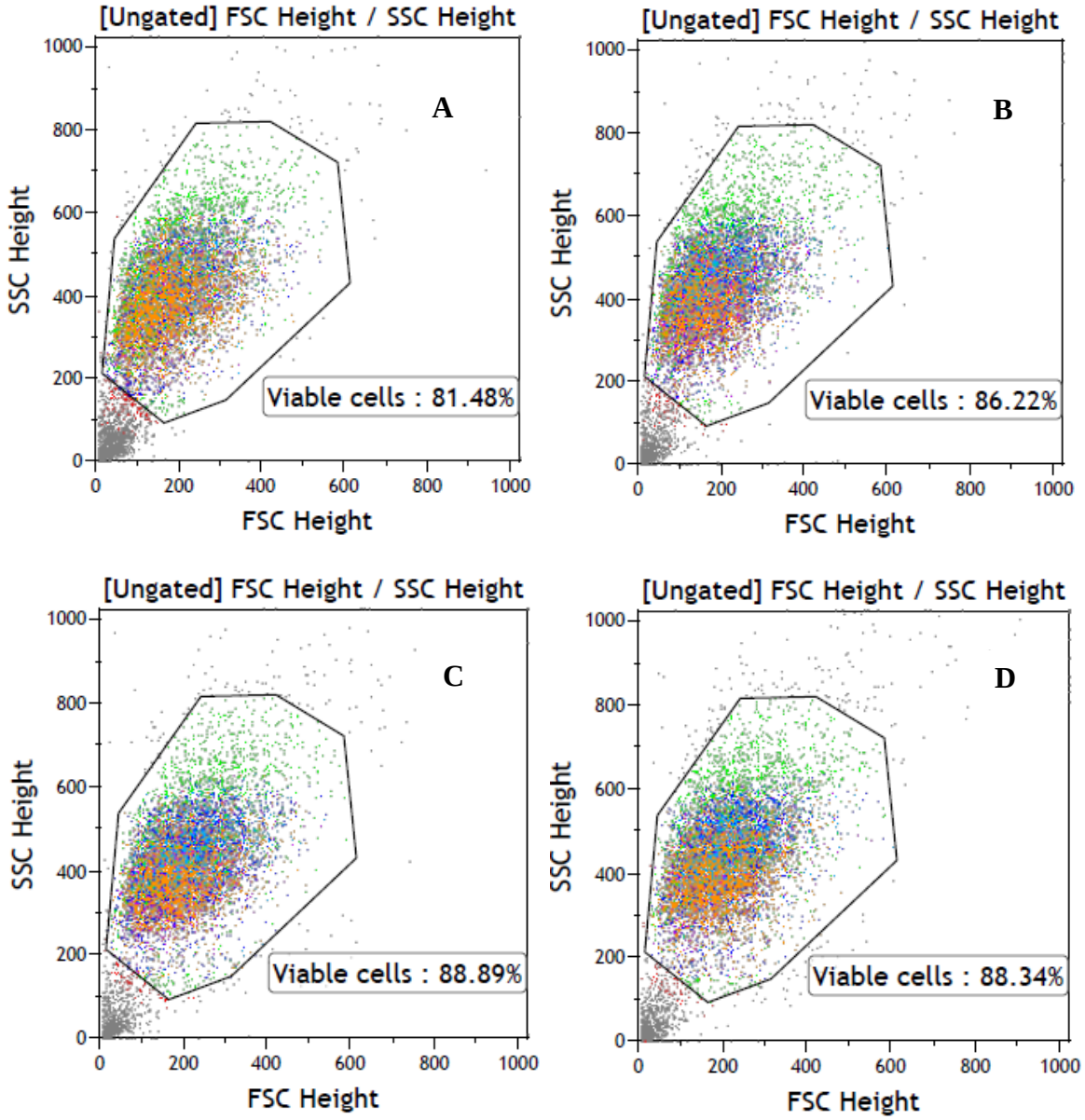

Figure 140: MDA-MB-231 Cell cycle distribution without any treatment of 2-(2,6-dioxopiperidin-3-yl)-phthalimidine (EM-12) (compound **2**) on Day 3 at 72 hours & Cell Cycle Described in Dot Plot; The treatment concentration of 2-(2,6-dioxopiperidin-3-yl)-phthalimidine (EM-12) (compound **2**) includes: 500 µg/mL (A); 100 µg/mL (B); 10 µg/mL (C) & 1 µg/mL (D). FSC: Forward Scatter allows for the discrimination of cells by size & SSC: Side Scatter allows for the discrimination of cell about internal complexity.

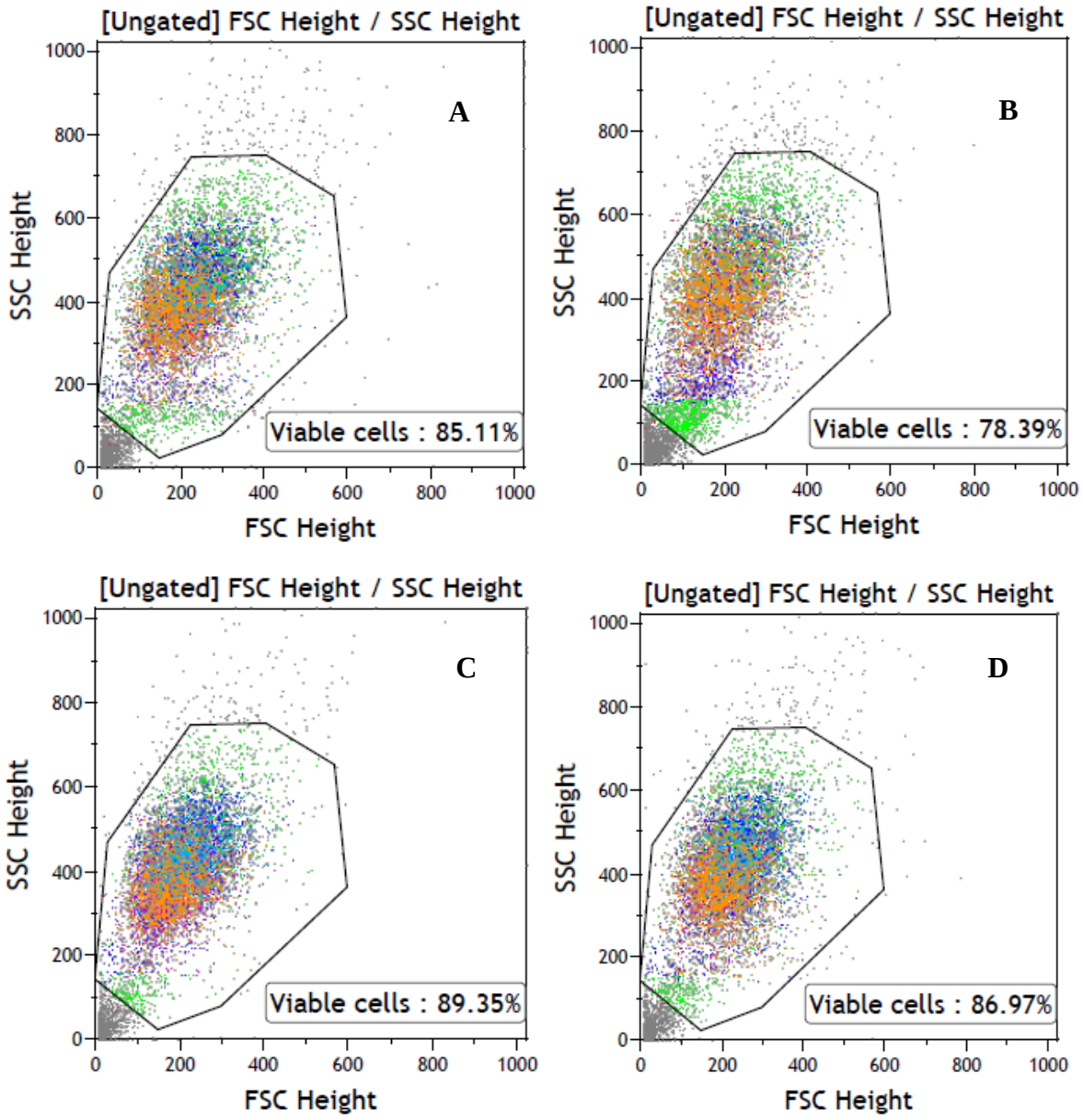

Figure 141: MDA-MB-231 Cell cycle distribution without any treatment of 3-[(1R)-1-hydroxy-1-methyl-3-oxo-1,3-dihydro-2H-isoindol-2-yl]piperidine-2,6-dione (compound **3**) on Day 3 at 72 hours & Cell Cycle Described in Dot Plot; The treatment concentration of 3-[(1R)-1-hydroxy-1-methyl-3-oxo-1,3-dihydro-2H-isoindol-2-yl]piperidine-2,6-dione (Compound **3**) includes: 500 µg/mL (A); 100 µg/mL (B); 10 µg/mL (C) & 1 µg/mL (D). FSC: Forward Scatter allows for the discrimination of cells by size & SSC: Side Scatter allows for the discrimination of cell about internal complexity.

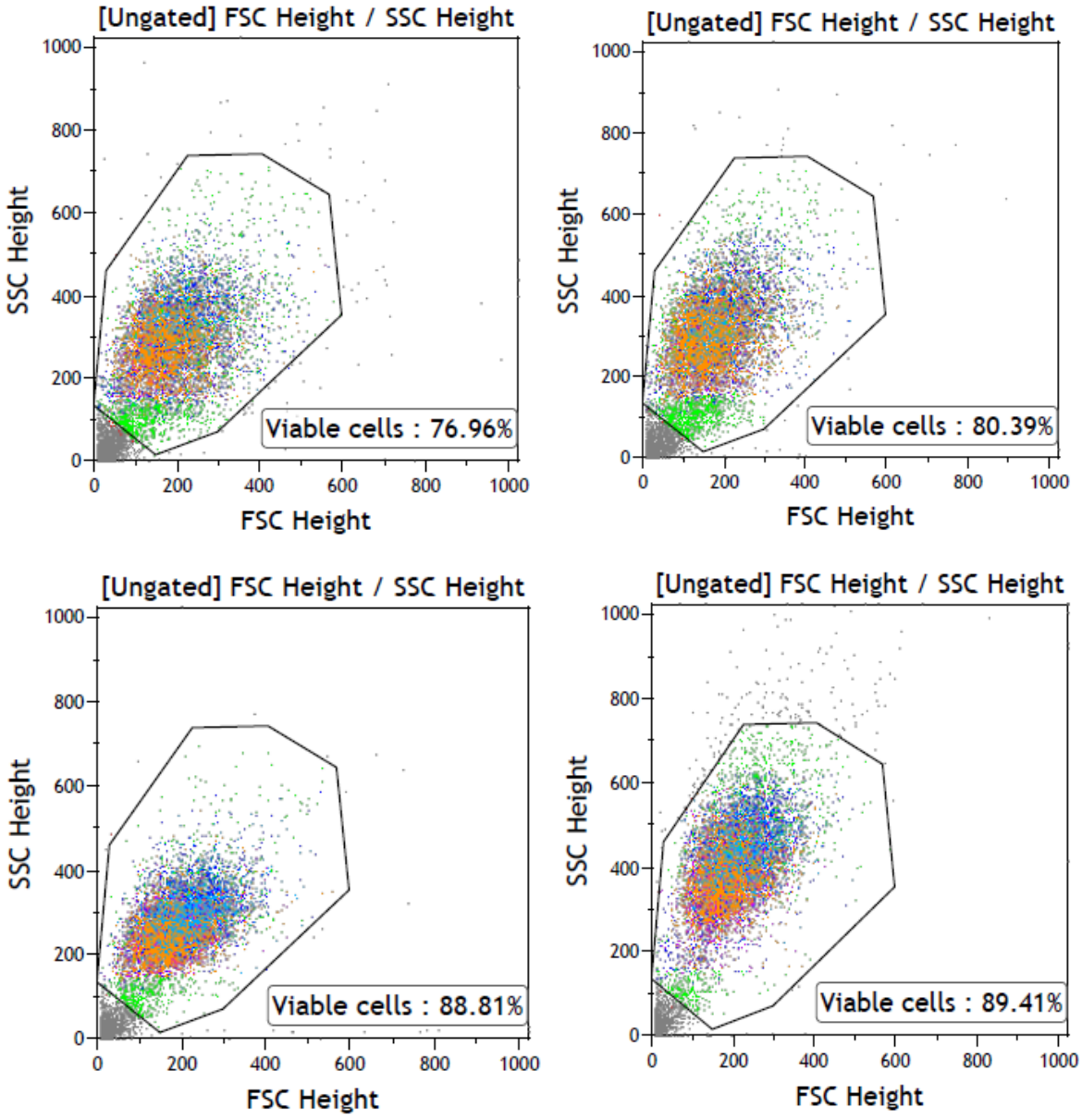

Figure 142: MDA-MB-231 Cell cycle distribution without any treatment of 3-[(1S)-1-hydroxy-1-methyl-3-oxo-1,3-dihydro-2H-isoindol-2-yl]piperidine-2,6-dione (Compound 4) on Day 3 at 72 hours & Cell Cycle Described in Dot Plot; The treatment concentration of 3-[(1S)-1-hydroxy-1-methyl-3-oxo-1,3-dihydro-2H-isoindol-2-yl]piperidine-2,6-dione (Compound 4) includes: 500 µg/mL (A); 100 µg/mL (B); 10 µg/mL (C) & 1 µg/mL (D). FSC: Forward Scatter allows for the discrimination of cells by size & SSC: Side Scatter allows for the discrimination of cell about internal complexity.

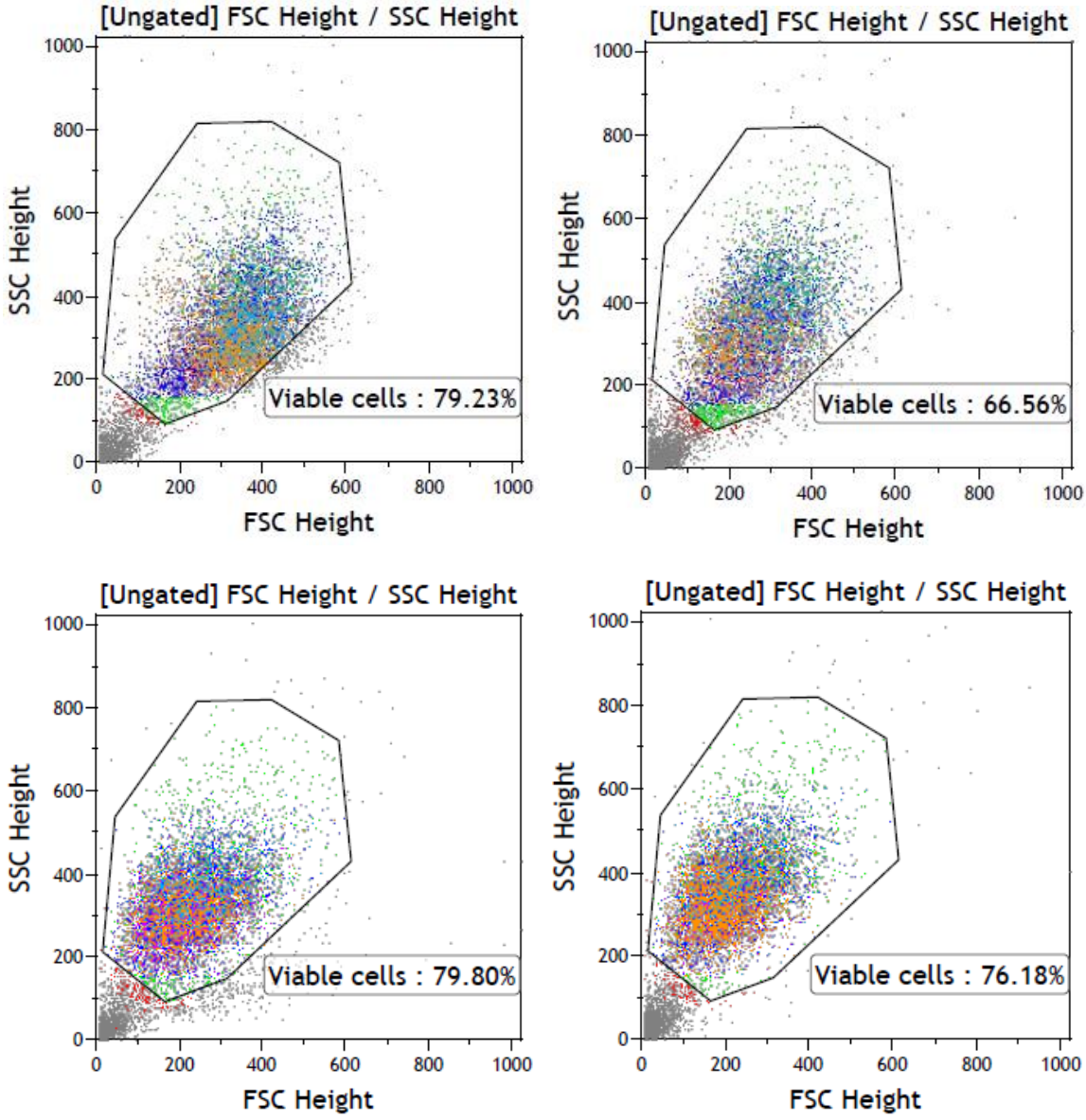

Figure 143: MDA-MB-231 Cell cycle distribution without any treatment of 4, 2-(1-Chloromethyl-2, 6-dioxopiperidin-3-yl)phthalimidine (Compound **5**) on Day 3 at 72 hours & Cell Cycle Described in Dot Plot; The treatment concentration of 2-(1-Chloromethyl-2,6-dioxopiperidin-3-yl)phthalimidine (Compound **5**) includes: 500 µg/mL (A); 100 µg/mL (B); 10 µg/mL (C) & 1 µg/mL (D). FSC: Forward Scatter allows for the discrimination of cells by size & SSC: Side Scatter allows for the discrimination of cell about internal complexity.